National Library of Canada

Acquisitions and Bibliographic Services Branch

395 Wellington Street
Ottawa, Ontario
K1A 0N4

Bibliothèque nationale du Canada

Direction des acquisitions et des services bibliographiques

395, rue Wellington
Ottawa (Ontario)
K1A 0N4

Your file Votre référence

Our file Notre référence

NOTICE

The quality of this microform is heavily dependent upon the quality of the original thesis submitted for microfilming. Every effort has been made to ensure the highest quality of reproduction possible.

If pages are missing, contact the university which granted the degree.

Some pages may have indistinct print especially if the original pages were typed with a poor typewriter ribbon or if the university sent us an inferior photocopy.

AVIS

La qualité de cette microforme dépend grandement de la qualité de la thèse soumise au microfilmage. Nous avons tout fait pour assurer une qualité supérieure de reproduction.

S'il manque des pages, veuillez communiquer avec l'université qui a conféré le grade.

La qualité d'impression de certaines pages peut laisser à désirer, surtout si les pages originales ont été dactylographiées à l'aide d'un ruban usé ou si l'université nous a fait parvenir une photocopie de qualité inférieure.

Canada

CHAR PARTICLE REACTION AND ATTRITION IN FLUIDIZED BED COMBUSTORS: MODELLING AND MEASUREMENT

by

Ivan T. Lau

A thesis submitted to the School of Graduate Studies and Research in partial fulfillment of the requirements for the degree of

DOCTOR OF PHILOSOPHY

IN THE

DEPARTMENT OF CHEMICAL ENGINEERING

UNIVERSITY OF OTTAWA

1995

ISBN 0-612-04965-5

Canada

UNIVERSITÉ D'OTTAWA
UNIVERSITY OF OTTAWA

ABSTRACT

Two slightly different models for predicting combustion efficiency for burning coal chars in bubbling fluidized bed combustors are developed. The models proposed assume that char particles are consumed simultaneously by combustion reaction and attrition with the rates of both processes following the shrinking particle model. To solve the gas-solid reaction problem, an approach quite different from the traditional method has been attempted. Characteristic times are introduced based on mean residence time concepts to characterize the reaction and attrition kinetics and particle size of different groups of char particles (ie original, attriated, elutriated, and withdrawal particles). Based on fundamental material balances and the proposed reaction-attrition mechanism, the models link combustion efficiency to some measurable paraneters, including a few of the introduced characteristic times.

Experimental techniques employing two types of batch experiments to determine the model parameters were developed. The first type experiments involve burning char particles to completion, while the second type experiments involve freezing the char combustion reaction, separating attrited particles from the original mother chars, and subsequently burning off attrited fines. With experimental records of exit gas

concentrations of carbon oxides vs time for first type experiments as input, the models can be used to evaluate the parameters which characterize the reaction of burning char particles. When similar records for second type experiments are used, other parameters characterizing the attrited and elutriated particles can be obtained. The method also allows carbon losses from both types of experiments to be estimated. The new developments give a way to estimate the attrition rate and the elutriation fraction of post-attrition combustion char fines in fluidized beds, problems not previously solved.

Experiments were performed with a bench-scale fluidized bed combustor to demonstrate the model parameter measuring techniques and to test the model features. The results show that the measured parameters are within reasonable ranges and generally agree well with the model assumptions. On the other hand, probably due to secondary fragmentation effects and the difficulty of precise burnout time measurement, most results evaluated for the power of dependence of fractional conversion on time are lower than expected, and discrepancies exist between the results of carbon loss estimated from the two types of experiments. The influences of coal type and operating conditions on the model parameters are also investigated. The results shown generally agree with past experience and are interpreted with the proposed model of the reaction-attrition mechanism.

ACKNOWLEDGEMENT

The author is greatly indebted to Professor William Hallett for his guidance, advice and constant encouragement throughout the development of this work.

Partially financial assistance from the Department of Natural Resources Canada is gratefully acknowledged.

NOMENCLATURE

The units given are those used throughout the text unless otherwise stated.

A	bed cross-sectional area, m^2
$A_a(t)$	total surface area of char particles at time t, m^2
A_{ao}	initial total surface area of char particles, m^2
C_{ca}	concentration of carbon dioxide in the inlet gas, $kg\text{-}mol/m^3$
C_p	concentration of oxygen in particulate phase, $kg\text{-}mol/m^3$
C_s	concentration of oxygen at the surface of a burning particle, $kg\text{-}mol/m^3$
C_{CO}	concentration of carbon monoxide, $kg\text{-}mol/m^3$
C_{CO2}	concentration of carbon dioxide, $kg\text{-}mol/m^3$
C_{CO+CO2}	concentration of carbon monoxide and carbon dioxide, $kg\text{-}mol/m^3$
C'_{CO2}	concentration of carbon dioxide in the flue gas, $kg\text{-}mol/m^3$
C'_{CO+CO2}	concentration of carbon monoxide and carbon dioxide in the flue gas, $kg\text{-}mol/m^3$
C_{O2}	concentration of oxygen, $kg\text{-}mol/m^3$
$C'_{O2}(t)$	tracer gas O_2 concentration at the exit of the gas sampling system, $kg\text{-}mol/m^3$
$C''_{O2}(t)$	tracer gas O_2 concentration at the bed entrance,

	$kg\text{-}mol/m^3$
C_{H2O}	concentration of moisture, $kg\text{-}mol/m^3$
d_a	diameter of attrited particles at the time of attrition, m
d_c	diameter of char particles, m
d''_c	diameter of burning char particles with inlet gas dispersion, m
d_e	diameter of char particles to be elutriated, m
d_i	diameter of withdrawn char particles, m
d_{ia}	diameter of attrited particles during re-burning in sub-tests, m
d_l	lower size limit of char particles, m
d_o	diameter of initial fuel particles, m
d_s	diameter of char particles at final split, also the largest size of attrited particles, m
d_u	upper size limit of char particles, m
d_{30}	mass mean diameter of char particles, m
d_{32}	Sauter mean diameter of fuel particles, m
$\bar{d}_a$	number mean diameter of attrited particles, m
D_g	molecular diffusivity of oxygen, m_2/s
E_{ai}	age distribution function of withdrawn carbon, s^{-1}
$E_a(t')$	age distribution function of tracer gas, see p.108, s^{-1}
E_{bi}	particle burnout time distribution function of withdrawn carbon, s^{-1}
E_{da}	particle size distribution function of attrited

carbon, m^{-1}

E_{df} particle size distribution function of fed carbon, m^{-1}

E_{dia} particle size distribution function of retrieved attrited carbon, m^{-1}

E_{dio} original attrition size distribution of retrieved attrited carbon, m^{-1}

E_{ti} ideal MCRT distribution function of withdrawn carbon, s^{-1}

E_{tia} MCRT distribution function of retrieved attrited particles from steady state mono-sized attrition, s^{-1}

$E_{\lambda a}$ dimensionless MCRT distribution function of attrited carbon

$E_{\lambda ac}$ dimensionless MCCT distribution function of attrited carbon

f_a carbon mass attrition fraction of char particles

f_{ai} carbon mass attrition fraction of withdrawn particles

f_{pw} withdrawal particle number fraction of mother particles

f_s carbon mass fraction remaining in the particle at the stage of final split

f_{so} carbon mass fraction remaining in the original char particle at the stage of final split

f_w carbon mass fraction remaining in the withdrawn

	particles
F	carbon feed rate, kg/s
F_w	withdrawal rate of bed materials, kg/s
$F'(t)$	step input tracer F curve (Levenspiel, 1972) measured at the exit of the sampling system
$F''(t)$	step input tracer F curve (Levenspiel, 1972) at the bed entrance
g	gravimetric constant, m/s^2
$G(t)$	combustion rate ratio defined by Equ.(5.24)
h	convective heat transfer coefficient, J/m^2sK
h_r	Stefan's radiative heat transfer coefficient, J/m^2sK^4
j	reaction regime dependent constant defined by Equ(3.26)
k	apparent first order reaction rate constant, m/s
k_a	attrition rate coefficient
k_g	mass transfer coefficient, m/s
k_h	mechanical attrition rate constant
k_o	frequency factor of carbon oxidation, m/s
k_{oco}	frequency factor of CO oxidation, m/s
k_r	chemical attrition rate constant, $m^2s/kg\text{-}mole$
k_α	apparent reaction rate constant, $kg\text{-}mol/m^2s(kg\text{-}mol/m^3)^\alpha$
$k_{1/2}$	apparent half order reaction rate constant, $kg\text{-}mol^{1/2}/m^{1/2}s$
k'	intrinsic reaction rate constant, m/s

[K1]	constant introduced by Equ.(5.54)
[K2]	constant introduced by Equ.(5.55)
[K3]	constant introduced by Equ.(5.56)
m_{po}	carbon mass of a char particle at t=0, kg
$m_p(t)$	carbon mass of a char particle at time t, kg
M_c	molecular weight of carbon, kg/kg-mole
n	reaction regime dependent constant defined in Table 2.1 and Equ.(3.20)
N	number of char particles after fragmentation
N_a	number of attrited char particles during re-burning at sub-tests
N_o	number of initial coal particles
P_{o2}	oxygen partial pressure, atm
P_{ai}	age distribution function of withdrawn char particles, s^{-1}
P_{aia}	age distribution function of retrieved attrited particles, s^{-1}
P_{da}	size distribution function of attrited particles, m^{-1}
P_{dia}	size distribution function of retrieved attrited particles, m^{-1}
q_a	specific attrition rate, s^{-1}
q_s	oxygen flux at fuel particle surface, kg-mol/m^2 s
Q_a	carbon attrition rate, kg/s
Q_e	carbon elutriation rate, kg/s

Q_{ea}	carbon elutriation rate of attrited particles, kg/s
Q_{pa}	numerical attrition rate, particle/s
Q_w	carbon withdrawal rate, kg/s
Q_{wa}	carbon withdrawal rate of attrited particles, kg/s
r	carbon reaction rate, kg-mole/m^2s
r_{co}	carbon monoxide oxidation rate, kg-mol/m^2s
r_m	reaction rate of a mother char particle, kg-mole/m^2s
R	universal gas constant, J/kg-molK
R_a	combustion rate of attrited particles, kg/s
R_c	combustion rate, kg/s
R_m	combustion rate of mother particles, kg/s
$R_{ia}(t)$	actual combustion rate of retrieved attrited particles, kg/s
$R'_{ia}(t)$	detected combustion rate of retrieved attrited particles, kg/s
t	time, s
t'	age of the detected gas element, s
t_κ	time of the data signal detected at index κ, s
$t_{\kappa'}$	age of the gas element detected at index κ', s

For the following characteristic time nomenclatures, the first subscript uses lower case letters for a mean time based on carbon mass, while capital letter subscripts represent

characteristic times for individual char particles. Also, the first subscript characterizes the time, while the second subscript characterizes the char particle in question. A superscript * represents the ideal case of no elutriation or withdrawal carbon losses, and an overline represents the mean value for a distribution of multi-size particles.

t_B	burnout time, s
t_B^*	ideal burnout time, s
t_{Ba}^*	ideal burnout time of attrited particles, s
t_{Be}^*	ideal burnout time of elutriable size particles, s
t_{Bo}^*	ideal burnout time of original char particles, s
t_{Bu}	burnout time of the largest char particle, s
$t"_B^*$	ideal burnout time of burning a char particle with inlet gas dispersion, s
t_c	mean carbon conversion time, s
t_{ca}	mean carbon conversion time of attrited particles, s
t_{cm}	mean carbon conversion time of mother particles, s
t_c^*	ideal mean carbon conversion time, s
t_d	MCRT associated with mother particles, s
t_{di}	MCRT associated with withdrawn mother particles, s
t_d^*	ideal MCRT associated with mother particles, s
t_{de}^*	ideal MCRT associated with an elutriable sized particle, s
t_{di}^*	ideal MCRT associated with a withdrawn mother

particle, s

t_{do}^* ideal MCRT associated with an original char particle, s

t_E residence time of char particles before elutriation, s

t_{Ea} residence time of attrited fines before elutriation, s

t_q a time corresponding to t_q'' for the same conversion but without inlet gas dispersion, s

t_q'' a time at which inlet gas dispersion becomes insignificant, s

t_r mean carbon residence time of char particles, s

t_{ra} MCRT of attrited particles, s

t_{ri} MCRT of withdrawn particles, s

t_{ro} MCRT of original char particles, s

t_r^* ideal MCRT of char particles, s

t_{ra}^* ideal MCRT of attrited particles, s

t_{re}^* ideal MCRT of elutriable sized particles, s

t_{ria*} ideal MCRT of retrieved attrited particles, s

t_{rs}^* ideal MCRT of particles of largest attrition size, or char particles at the stage of final split, s

$t''_r{}^*$ ideal MCRT of burning char particles with inlet gas dispersion, s

$t'_{ria}{}^*$ ideal MCRT of burning retrieved attriated fines estimated from data of experiments with product gas dispersion, s

t_s	residence time of a char particle at the stage of final split, s
T_b	bed temperature, K
T_s	temperature at fuel particle surface, K
u	superficial gas velocity, m/s
u_{mf}	minimum fluidization velocity, m/s
u_t	particle terminal velocity, m/s
W	in bed carbon inventory, kg
W_a	carbon inventory of attrited fines, kg
W_b	inventory of bed materials, kg
W_c	total carbon burnt, kg
W_{da}	carbon inventory of attrited fines having an initial size d_a, kg
W_m	carbon mass of mother char particles, kg
W_o	carbon mass of original char particles, kg
x	fraction of carbon conversion or detachment of char particles
x''	fractional carbon conversion for burning chars with inlet reactant gas dispersion
x_c	fractional conversion of carbon burnt
y	elutriation fraction of a char particle or mono-sized char particles
y_a	elutriation fraction of an attrited particle
y_m	elutriation fraction of a mother particle
y_{mi}	elutriation fraction of a withdrawn mother particle

y_{mo} elutriation fraction of an original mother particle

y_o elutriation fraction of a char particle in case of no withdrawal

$\underline{y}$ elutriation fraction of multi-sized char particles

y_a elutriation fraction of attrited particles

y_m elutriation fraction of multi-sized mother particles

y_w elutriation fraction of particles to be withdrawn at times before its exit

Z withdrawal fraction of char particles

Greek letters

α reaction order

β correction factor defined by Equ(2.10)

γ stoichiometric constant

ϕ exponential function defined by Equ.(3.38)

ϵ_{mf} bed void fraction at minimum fluidization

κ index of the detected data signal

κ' index of the data signal for the measurement of the age of the detected gas element in the bed and the gas sampling system

λ MCRT ratio defined by Equ.(3.37)

λ_e MCRT ratio defined by Equ.(3.41)

η combustion efficiency

ρ_c carbon density, kg/m^3

μ	gas viscosity, kg/m s
σ	population standard deviation, m
τ	mean residence time of bed materials, s
ξ	activation energy of carbon oxidation, J/mol
ξ_{CO}	activation energy of CO oxidation, J/mol
ΔH_r	heat of combustion of Equ.(2.4), J/kg-mol
Δt_k	data taking time interval, s
Δt_r	residence time deviation due to dispersion of product gas in bed and sampling system, s
$\Delta t"_r$	residence time deviation due to dispersion of inlet reactant gas, s
$\Delta t"_{r,mono}$	$\Delta t"_r$ for mono-sized char particles, s
ω_i	fraction of the total batch mass represented by a single particle
ω_u	fraction of the total batch mass represented by the largest particle

Dimensionless groups

Re	Reynolds number, $Re = d_c u \rho / \mu$
Sc	Schmidt number, $Sc = \mu / \rho D_g$
Sh	Sherwood number, $Sh = k_g d_c / D_g$

Acronyms

FBC	Fluidized Bed Combustion
FSI	Free Swelling Index
MCRT	Mean Carbon Residence Time

CONTENTS

		p
1.	INTRODUCTION	1
1.1	FBC of Coals	4
1.1.1	Operating conditions	5
1.1.2	Fuel properties	6
1.13	Combustion efficiency	7
1.2	Objectives and Scope	9
2.	LITERATURE SURVEY - MECHANISM OF IN-BED PROCESSES	11
2.1	Gas and Solid Mixing	11
2.2	Char Combustion	12
2.2.1	Rate controlling steps	12
2.2.2	Reaction kinetics	17
2.2.3	External mass transfer	22
2.2.4	Overall burning rate	23
2.3	Fragmentation and Attrition	24
2.3.1	Fragmentation	25
2.3.2	Attrition	27
2.3.3	Particle size distribution	30
2.4	Concluding Remarks	33
3.	THEORETICAL DEVELOPMENT	35
3.1	Basic Concepts and Assumptions	35
3.2	Carbon Balance	41
3.2.1	Overall balance	41

3.2.2 Balance for attrited fines 42
3.2.3 Attrited and elutriated fractions with negligible withdrawal 42
3.2.4 Effect of withdrawal 46
3.3 Mean Carbon Characteristic Times..... 47
3.3.1 Ideal combustion - no carbon loss 48
3.3.1.1 Combustion without attrition 48
3.3.1.2 Combustion with attrition 50
3.3.2 Combustion with elutriation 51
3.3.2.1 Combustion without attrition 52
3.3.2.2 Combustion with attrition 54
3.3.3 Combustion with elutriation and withdrawal 63
3.4 Combustion Efficiency 70
3.4.1 Combustion without carbon withdrawal 70
3.4.2 Combustion with carbon withdrawal 74
3.4.3 Multi-size particles 79
3.5 Concluding Remarks 82

4. EXPERIMENTAL 85
4.1 Equipment 85
4.1.1 Combustor systems 85
4.1.2 Gas sampling, analyzing, and recording 88
4.2 Materials 90
4.3 Procedure 91
4.3.1 Combustion studies 93
4.3.2 Fragmentation and attrition studies 94

5. EVALUATION OF MODEL PARAMETERS FROM EXPERIMENTAL DATA 98
5.1 Evaluation of t_c 98
5.2 Evaluation of Attrition Related Variables 99
5.2.1 Attrition rate and inventory 99
5.2.2 Evaluation of MCRTs for attrited and elutriated particles 102
5.3 Correction of Attrition Related Variables 107
5.3.1 Error introduced by exit gas dispersion 107
5.3.2 Error introduced by inlet gas dispersion 117
5.3.2.1 Correction to MCRT 120
5.3.2.2 Correction to CO_2 data 128
5.3.2.3 Correction to reaction rate 128
5.4 Evaluation of n and j 132

6. RESULTS AND DISCUSSIONS 136
6.1 First Series Experiments 136
6.1.1 Comparison of the combustion of various coal chars 137
6.1.2 Particle size and operating condition effects .. 143
6.1.3 Evaluation of the exponent n 147
6.2 Second Series Experiments 149
6.2.1 Shrinking particle model 151
6.2.2 Particle size distribution and fragmentation ... 152
6.2.3 Attrition characteristics 163
6.2.3.1 Particle size and extent of conversion effect .. 165

6.2.3.2 Comparison among various coals 169
6.2.3.3 Operation condition effects 180

7. CONCLUSIONS AND RECOMMENDATIONS 186
7.1 Conclusions 186
7.2 Recommendations 189

8. REFERENCES 191

9. APPENDICES 204
9.1 First series experimental results 204
9.2 Second series experimental results 223

TABLES

2.1 Expressions for shrinking spherical particles ... 16
4.1 Coal analysis 92
4.2 Operating conditions 96
6.1 Evaluation of n values 150
6.2 Comparison of various burning stages 167
6.3 Standard deviation in percentage of the measured attrition-elutriation parameters 176

FIGURES

1.1 Schematic diagram of FBC 3

2.1 Fragmentation and attrition effect on particle size distribution 32

3.1 Carbon balance without withdrawal 44

3.2 1-x and E_{ai} vs t/t_B^* or t/t_{di}^* 53

3.3 Calculation of y from parameters - no withdrawal 73

3.4 Calculation of η from parameters - with withdrawal 75

3.5 Carbon balance with withdrawal 77

4.1 Schematic diagram of bench-scale fluidized bed combustor 86

4.2 Schematic diagram of sampling gas flow 89

5.1 Exit age distribution E_a for gas flowing through the fluid bed and the sampling system combined, together with fractional concentration curves, in response to a step input, at the fluid bed inlet (F") and at the gas analyzer (F') 109

5.2 Comparison of carbon concentration profiles with and without product gas dispersion 112

5.3 Comparison of carbon inventories with and without inlet gas dispersion 121

6.1 Schematic CO_2 concentration and carbon conversion curves 138

6.2 Comparison of t_c for various coal chars 139

6.3 Comparison of combustion efficiency for various coal chars 142
6.4 Particle size effect on t_c and combustion efficiency 144
6.5 Bed temperature effect on t_c and combustion efficiency 147
6.6 Oxygen concentration effect on t_c and combustion efficiency 148
6.7 Carbon conversion vs weight loss 153
6.8 Effect of coal size on fragmentation 155
6.9 Primary and secondary fragmentation (7.2 mm coal size) 156
6.10 Primary and secondary fragmentation (13 mm coal size) 157
6.11 Particle size distributions of char fragments at the end of coal devolatilization 160
6.12 Increase in particle numbers by fragmentation .. 162
6.13 Typical flue gas CO_2 concentration curves 164
6.14 Particle size effect on attrition characteristics 168
6.15 Characteristic times comparison of various coal chars 170
6.16 Comparison of Y_a for various coal chars 173
6.17 Comparison of attrition % of various coas chars 175
6.18 Carbon loss comparison of various coal chars ... 179
6.19 Bed temperature effect on characteristic times . 181

6.20 Bed temperature effect on carbon loss 182

6.21 Oxygen concentration effect on characteristic times 184

6.22 Oxygen concentration effect on carbon loss 185

1. INTRODUCTION

With projections of diminishing crude oil production in the future, coal is by far the most reliable fossil fuel resource to supply the high energy consumption of our society. To burn coal efficiently and cleanly is one of the more pressing goals of engineering in recent decades.

Fluidized Bed Combustion (FBC) offers an attractive method of burning coal and other fuels in a clean manner. Lower temperatures than those in conventional pulverized coal furnaces result in less NO_x formation. Limestone or dolomite added to a fluidized bed captures SO_2 in-situ during combustion. Recently developed FBC technologies, such as the combined cycle, a process producing steam for a steam turbine and high pressure hot flue gas for a gas turbine, offer efficiencies much higher than conventional steam cycle power plants.

A FBC system feeds fuel into a preheated bed of inert particles which are fluidized by air from a gas distributor at the bottom of the combustion chamber. The air agitates the bed, and also supplies the oxygen requirement for the oxidation reaction. Usually limestone is added to capture SO_2 from sulphur bearing fuels, but sand or other solid materials may also be used. Bed temperature is controlled by heat

removal, usually by inserted heat exchanger tubes or water-cooled walls. Combustion flue gas usually exits the system with a certain amount of fine solids entrained, including unburnt combustibles. Cyclones and stand pipes are frequently installed to recycle these solids to allow them to burn more completely. In most cases, a continuous withdrawal of bed solids is required to maintain a constant bed inventory as fresh fuel and limestone are fed in. A schematic diagram of a FBC is given by Fig. 1.1.

Two types of fluidized bed combustors are most commonly used. The bubbling bed combustor requires a minimum amount of gas which flows through the interstices between the particles to suspend the entire bed solids. The superficial gas velocity of this minimum required gas flow is called the minimum fluidization velocity u_{mf}. Any excess amount of gas forms voids, or bubbles, which agitate the bed materials and mix them thoroughly while rising through the bed. Bubbles entrain particles in their wakes and throw them up into the freebcard, the space above the bed, when bubbles burst at the bed surface. Large entrained particles with terminal velocities higher than the superficial velocity have a chance to fall back into the bed, while the rest of the particles are elutriated out of the combustor. Details of the fundamentals of the bubbling bed regime can be found in the text book of Kunii and Levenspiel (1969).

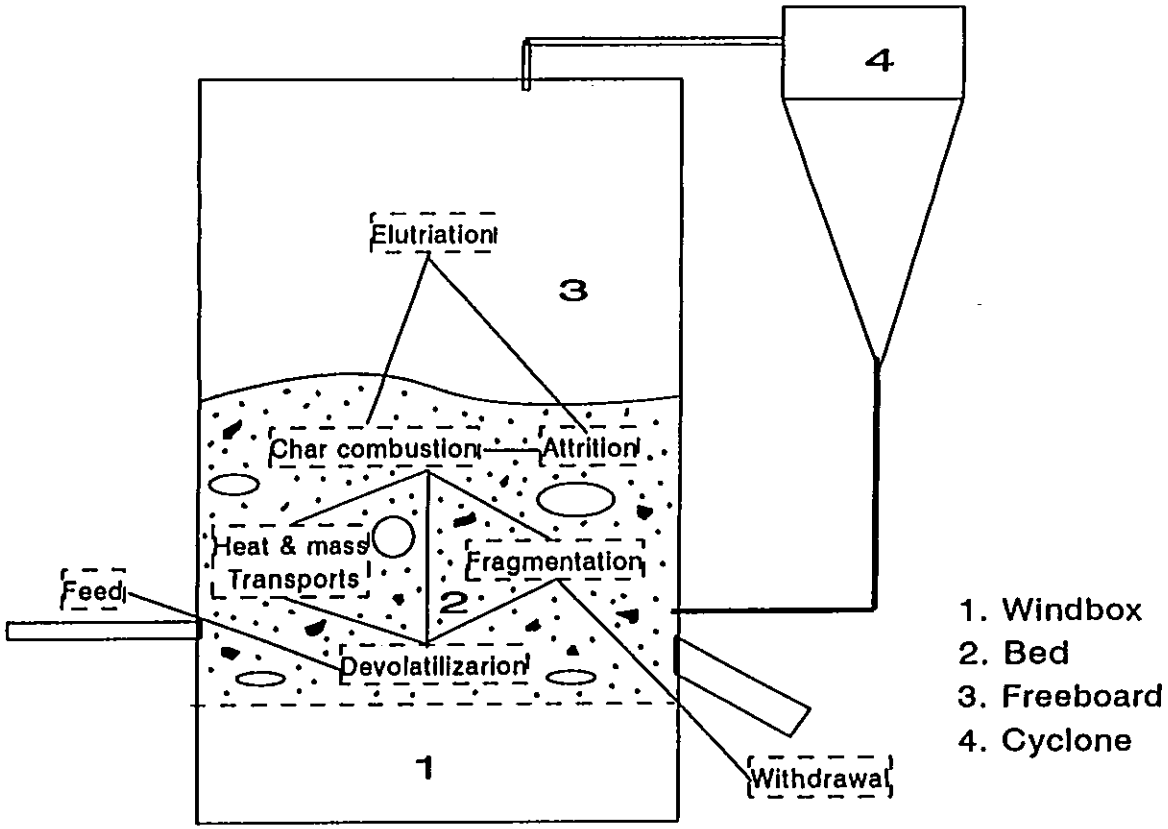

Fig. 1.1: FBC schematic diagram

The circulating bed combustor uses finer solid bed materials and higher superficial gas velocities, exceeding the particle terminal velocity. The result is a bed of different behaviour with formation of clusters and a high rate of entrainment of bed solids. The bed surface becomes indistinct with porosity increasing along the combustion chamber. A continuous supply of bed materials, provided by recirculating the elutriated solids, is required to maintain a constant bed inventory. Because of the finer particle size and longer residence time, the SO_2 sorbent utilization is higher than that of the bubbling mode.

This thesis is concerned with combustion processes in bubbling beds.

1.1 FBC of Coals

When coal is fed into a hot fluidized bed, the particle temperature rises rapidly by absorption of heat from the surrounding inert (usually limestone). Gaseous and tarry components (volatiles) are released by thermal decomposition, leaving behind carbon-rich solid residues (char). The reaction mechanisms of the combustion of volatiles and char are different and complex. Combustion performance depends on the coal type and the operating conditions.

1.1.1 Operating conditions

The air flow rate is desired to be as high as possible to maximize the energy output per unit bed surface area, but is restricted by elutriation. Superficial gas velocities for bubbling and circulating FBC systems are usually from 1 to 2.5 m/s and 5 to 7 m/s respectively.

Bed solids used in FBC systems are coarser than in most other industrial applications of fluidization to minimize materials loss through elutriation. Also, coarse bed solids allow more air to enter the particulate phase where heterogeneous gas-solid reaction between solid fuel and oxygen takes place. However, large bed particles reduce heat transfer rates (Botterill, 1975) and increase attrition (Arena et al., 1983), which in turn increases elutriated carbon loss. In general, the mean size of bed materials is between 0.5 to 1 mm for bubbling beds and about 0.3 mm for circulating bed combustors respectively.

Coal can be fed underbed using a screw feeder or overbed using a spreader. Because combustion is fast, the carbon inventory is low, usually 0.5 to 2% of the bed material; this depends on the burning rate or burnout time of the coal. Elutriation in general is the dominant process of carbon loss. Large freeboard sections and recycling of elutriated fines are

commonly used to promote complete burnout of fines. Coal particle size has been found to have little effect on combustion efficiency (Becker and Code, 1983, 1985; Hirama et al., 1984), defined as the percentage of carbon conversion. Coal feed particle sizes up to 30 mm are commonly used in FBC systems.

Combustion efficiency usually increases with higher bed temperature but so does NO_x emission. For burning high sulphur fuels, a bed temperature of about 1123°K is always used to optimize the sorbent's sulphur capture.

1.1.2 Coal properties

Coals are ranked according to their degree of geological aging from lignite to subbituminous to bituminous to anthracite, with further subclassification into groups (Stach et al., 1982). Coal type has been shown by many workers to be an important factor in determining the combustion efficiency of FBC systems (Beér et al., 1980, Hampartsoumiam and Gibbs, 1983). Therefore, understanding the coal's combustion characteristics and their effect on FBC processes is highly desirable in design calculations and operation optimization. To date, such correlations are seldom available, as it has not been possible to successfully predict the combustion performance of any coal simply on the basis of its properties.

For conventional pulverized coal firing, fuel residence time in the reaction zone is short. Coal reactivity in general is the dominant factor affecting combustion performance, and is often expressed adequately by rank or volatile content, perhaps with some corrections for ash content or maceral count. For FBC systems, however, attrition and elutriation also affect combustion efficiency, so that coal properties such as hardness and swelling are important.

1.1.3 Combustion efficiency

Perhaps the most important element of combustor performance is the combustion efficiency. Besides its obvious benefit in economics and conservation of energy, burning coal efficiently has a high impact on the environment because of the reduction of CO, CO_2, NO_x, SO_2 and other pollutant emissions. Combustion efficiency is influenced by a number of previously mentioned controllable conditions, such as bed temperature, fuel and bed material particle sizes, and fluidizing gas velocity. It also depends on a number of uncontrollable properties of the coal.

Combustion of both volatiles and char involves a number of chemical and physical processes. Many of these processes directly or indirectly influence the combustion efficiency. It has been suggested that the combustion efficiency of an FBC

system depends on the competing particle size reduction processes of combustion and attrition (Beér et al., 1980). The most important combustion efficiency related processes are labelled in Fig. 1.1. For high volatile coals, volatiles contribute a major fraction of the total heat release, and their evolution process may be critical to the subsequent char's combustion characteristics, since particle swelling and fragmentation during devolatilization determine the resulting char structure and size. On the other hand, volatiles burn readily and contribute little to the total combustible loss.

For char combustion, transport processes and char properties determine the reaction rate, which in turn determines the carbon inventory; this in turn is the main factor in the carbon loss due to withdrawal of material from the bed. Carbon inventory, together with particle size distribution, is also important in determining the rates of attrition and elutriation, the latter being the main source of carbon loss in FBC operations. Attrition of fuel particles is a major source of elutriable fines; the attrition rate depends on char structure and hardness, and on bed hydrodynamics. Also, the processes of attrition and combustion enhance each other through the weakening of porous bridges within the particle and creation of reacting surface.

1.2 Objectives and Scope

The complexity of the many interrelated processes makes it difficult to develop a mathematical model for predicting FBC efficiency. Since the pioneering work of Avedesian and Davidson (1973), many FBC models have been developed, with most following the same route of determining the oxygen diffusion and reaction rates based on the two-phase model (Davidson and Harrison, 1963). While some predict well the carbon burnout time or the combustion rate of certain fuels, they generally have little capability in efficiency evaluation. Few previous works take into account the important size altering processes such as fragmentation and attrition, or handle them as minor effects to be neglected. Probably due to the difficulty of experimental measurement, data in this area are rare, and the development of proper measuring techniques is essential. Another problem area is that reliable data on key parameters such as mass transfer coefficients and reaction rate constants are difficult to obtain. Despite considerable research on the reaction kinetics of coal in the FBC, certain areas remain unresolved or subject to controversy. As a result, most designs depend on practical experience or data from experiments on large scale units. From the economic point of view, the development of a semi-empirical model, which can employ data from bench-scale units to predict combustion efficiency, is highly

desirable.

The main objective of this work is to develop, with a new approach, a semi-empirical model for FBC efficiency evaluation. Since volatiles usually burn nearly to completion, only char combustion is considered here. The model includes char combustion efficiency related processes such as attrition, C-O_2 reaction, elutriation, and withdrawal. Efforts are made to ensure that all model parameters can be measured by experiments in a batchwise bench-scale fluidized bed unit. Another objective is to develop appropriate experimental techniques and apply them in demonstrating the measurement of the parameters.

The present work will concentrate on in-bed (bubbling bed) combustion of coal, in other words excluding freeboard burning, while the FBC efficiency evaluation considers char combustion only. Not considered are FBC reactions involved in the formation and destruction of pollutant gases, such as SO_2 and NO_x.

2. LITERATURE SURVEY - MECHANISMS OF IN-BED PROCESSES

Many proposed mechanisms and experimental findings for FBC have been presented in the literature. In this work, only those related to the processes influencing the combustion efficiency of the in-bed combustion of char are studied.

2.1 Gas and Solid Mixing

The performance of a fluidized bed combustor is strongly influenced by the fluid mechanics of the bed. On the other hand, owing to the low fuel inventory in the bed, combustion has little effect on the fluidizing flow pattern. Most of the early theories developed (Avedesian and Davidson, 1973; Campbell and Davidson, 1975; Gibbs, 1975; Gordon and Amundson, 1976; Gordon et al., 1978; Fan et al., 1979; Saxena and Rehmat, 1980; Bukur and Amundson, 1981) employed Davidson and Harrison's (1963) two-phase theory. This assumes that the excess gas flow beyond that required for minimum fluidization passes through the bed in bubbles. In recent years the differences between large and small size particle fluidization have been noted (Catipovic et al., 1978). Fluidized beds of large size bed materials, like most bubbling FBC systems, operate practically in the so-called slow bubble regime where the bubble rise velocity is slow relative to the interstitial gas velocities. The interstitial gas uses the bubbles as a

by-pass, thus a higher interphase (bubble-particulate) exchange is expected.

Solid particles are in general considered to be well mixed, whereas gases in bubble and particulate phases are regarded as being in either plug flow or mixed flow, as shown in model reviews by Park et. al (1980) and La Nauze (1985).

2.2 Char Combustion

2.2.1 Rate controlling steps

The heterogeneous reaction between oxygen and devolatilized char in general occurs in the particulate phase only. Within this region, oxygen transfers through the interstices of the bed materials to the burning char particle, where reaction may take place on the surface and inside pores. Therefore, reaction kinetics may involve steps such as mass transfer to the solid surface, diffusion through the pore structure, and chemical reaction. Depending on which steps are rate-controlling, one of these standard models may be used to describe particle consumption: the progressive-conversion model (constant diameter/decreasing density), the shrinking particle model (constant density/decreasing diameter), or the shrinking core model (ash layer enveloping a shrinking size unreacted core).

The relative importance of each of the various processes is a complicated function of bed temperature, fluid mechanics, oxygen concentration, particle size and char reactivity. At low temperature or for chars of low reactivity, oxygen penetrates into the interior of the highly porous char particle before it reacts with carbon; most combustion is then internal rather than at the surface. In extreme cases, when the resistance of diffusion is negligible compared to that of reaction, the internal oxygen concentration may reach a flat profile with its value equal to that of the exterior surface. Char particles will then burn with constant diameter but deplete in density until the whole particle structure collapses.

Except when highly porous and unreactive feedstocks are used, char combustion under common FBC conditions usually shows the other extreme to that described above. Penetration of oxygen into the unburnt char is limited to a short distance compared to the particle dimensions, so that reaction is confined to the outer thin layer of the particle. If the ash layer surrounding the unburnt core is preserved, reaction closely follows the shrinking core model (Yagi and Kunii, 1955; Levenspiel, 1972). This model describes solid reaction in a way that a thin reaction zone continuously moves inward into the solid leaving behind an outer ash layer. Judging from experimental findings (Hustad et al., 1991; Khraisha and

Dugwell, 1992), it is only for very fine, elutriable size char particles, usually under 150 μm, that intra-particle diffusion and reaction need to be considered.

Because of the vigorous agitation in a fluidized combustor, the residue of ash on the burning char surface is usually flaked off and presents no resistance to diffusion. Only for a few exceptions, probably due to a low softening temperature for the ash of the coal used, was it found that the ash layer adhered to the unburnt core without collapse and oxygen had to diffuse through it in order to contact the unreacted carbon (Andrei et al., 1985; Abdel-Hafez, 1988; Durão et al., 1990). The shrinking particle model rather than the shrinking core model is therefore generally applied in FBC theoretical works, although a few have used the shrinking core model to deal with the ash diffusion problem (Saxena and Rehmat, 1977).

With the simplification of a shrinking particle model, the reaction rate controlling steps of char combustion within the particulate phase of a fluidized bed are reduced to only two, external mass transfer and surface reaction. In order to determine which one is more important, extensive experimental studies have been carried out. Most works measured the particle burnout time, t_B, or burning rate, R_C, since understanding their relations with particle size may shed

light on the combustion mechanism. These relationships under different controlling regimes have been given by Levenspiel (1972) and are illustrated in Table 2.1. The table gives three reaction regimes for the shrinking particle model: kinetic, Stokes diffusion, and convection regimes.

Kinetic Regime. Here the rate of the reactant gas diffusing onto the solid surface is much faster than its reaction rate at the surface. Since the diffusion resistance is negligible, the gas reactant concentration at the solid surface can be considered equal to that of the surrounding environment, and the reaction is controlled by chemical kinetics alone.

Stokes Diffusion Regime. Here, in contrast to the kinetic regime, the reaction rate is fast enough to consume all the gas reactant diffused onto the solid surface. Thus the concentration of the gas reactant at the surface is nearly zero, and the reaction is controlled by gas diffusion. For this regime, stagnant gas is assumed so that only molecular diffusion is considered.

Convection Regime. This regime is similar to the last one, except that mass transfer is dominated by convection rather than molecular diffusion.

The exponents appearing in the expressions in Table 2.1

Table 2.1 : Expressions for shrinking spherical particles

(Extracted from Levenspiel, 1972)

SHRINKING PARTICLE MODEL		
Kinetic Regime	**Stokes Diffusion Regime**	**Convection Regime**
$1-x = (1-t/t_B)^3$	$1-x = (1-t/t_B)^{3/2}$	$1-x = (1-t/t_B)^2$
$t_B \propto d_o$	$t_B \propto d_o^2$	$t_B \propto d_o^{3/2}$
$R_c \propto d_c^2$	$R_c \propto d_c$	$R_c \propto d_c^{3/2}$
$dd_c/dt = \text{const.}$	$dd_c/dt \propto 1/d_c$	$dd_c/dt \propto d_c^{-1/2}$

indicate in which regime the reaction occurred. The results, operating conditions and fuel type used in many previous experiments have been summarized by different researchers (La Nauze, 1985; Zhang, 1987; Jia, 1991). As mass transfer coefficient decreases with increasing particle size, most agree that the combustion of large char particles (say > 2 mm) is dominated by mass transfer control, whereas chemical kinetics become important for the burning of smaller diameter particles (Ross and Davidson, 1981; Daw and Krishnan, 1983).

2.2.2 Reaction kinetics

Three reactions have been considered to occur on burning char surfaces:

$$C+\frac{1}{2}O_2 \rightarrow CO \qquad (2.1)$$

$$C+O_2 \rightarrow CO_2 \qquad (2.2)$$

$$CO_2+C \rightarrow 2CO \qquad (2.3)$$

The pioneering model of Avedesian and Davidson (1973) assumed that char oxidation follows the double-film scheme (Spalding, 1955), in which no oxygen reaches the particle surface, where only Equ.(2.3) of the C-CO_2 reaction occurs. The CO produced then burns in a diffusion flame surrounding the particle. However, the CO_2 reduction reaction was found

to be too slow at FBC temperatures to give a significant contribution to the overall reaction (Patel, 1979). Arthur (1951) has shown that both CO and CO_2 are produced on the char surface, and their proportions of formation depend on temperature. That Equ.(2.1) and (2.2) instead of (2.3) are the surface reactions was further verified by Basu et al. (1975). Recent studies show that CO rather than CO_2 is the primary product at the char surface and that the CO diffuses away from the particle and is then converted to CO_2 (Olander et al., 1981; Ross and Davidson, 1981):

$$CO+\frac{1}{2}O_2-CO_2 \qquad (2.4)$$

The distance from the surface at which the $CO-CO_2$ conversion occurs depends on fluid mechanics, heat transfer and particle size. Different researchers have concluded that for large particles, > 1 mm, CO burns close to the surface, while for small particles, < 0.5 mm, CO escapes the boundary layer before being consumed (Caram and Amundson, 1977; Ross and Davidson, 1981). Hayhurst (1991) concluded that CO combustion only occurs either above the bed or in the ascending bubbles. He suggested that Equ.(2.1) takes place inside the pores and Equ.(2.4) has no effect on the particle burning.

Experimental measurements of the reaction order and the

rate constant are very difficult and are often influenced by the effect of mass transfer outside the particle as well as through the pores. Often researchers have lumped the processes of pore diffusion and internal chemical reaction together and given the apparent rate constant and order based on external surface area. The rate of carbon oxidation reaction per unit surface area can then be expressed as

$$r=k_{\alpha}C_s^{\alpha} \qquad (2.5)$$

where C_s is the oxygen concentration at the char surface, and k_{α} and α are the apparent rate coefficient and reaction order respectively. Units used for the expressions are given in Nomenclature Section. For simplicity, first order is frequently assumed.

Field et al. (1967) assumed the reaction to be first order in O_2 and correlated the apparent rate data in Arrhenius form,

$$k=k_o e^{-\xi/RT_s} \qquad (2.6)$$

obtaining frequency factors k_0 and activation energies ξ for different coals.

When chemical reaction is fast compared to pore diffusion, however, Young and Smith (1981) found that the apparent order of the reaction is 0.5. The apparent rate constant, which incorporates the pore diffusional effect, is

given by

$$k_{\frac{1}{2}}=7\,e^{82400/RT_s} \tag{2.7}$$

Smith (1978) has correlated intrinsic rates (ie the true chemical reaction rate at the pore internal surface) for various coal chars and presented them in terms of the oxygen partial pressure to the first order. The intrinsic rate coefficient k' is

$$k'=470\,T_s e^{-179400/RT_s} \tag{2.8}$$

By noting the influence of the particle diameter on the apparent rate coefficient, Daw and Krishnan (1983) wrote their correlation in terms of oxygen partial pressure to include the particle size effect as

$$r=-6.459\times10^{-2}(d_c/0.0708)\,e^{-11500/RT_s}p_{O_2}^{0.6} \tag{2.9}$$

Obviously, the kinetics of various chars are different. However, owing to the lack of reactivity data, models have employed different correlations, with most assuming first order apparent kinetics.

Calculating rate constants requires knowledge of the particle temperature, which is reported to be higher than the

bed temperature by up to 200°K by various measuring techniques (Basu, 1977; Chakraborty and Howard, 1978; Roscoe et al., 1980; Ross et al., 1981). An alternative way to obtain burning particle temperatures is by calculating them through a steady state heat balance equation (Turnbull and Davidson, 1984):

$$\beta \Delta H_r r = h(T_s - T_b) + h_r(T_s^4 - T_b^4) \qquad (2.10)$$

where ΔH_r is the heat of combustion of Equ.(2.4), β is a correction factor to give the net heat from the combustion reaction reaching the particle, and h and h_r are the convective and radiative heat transfer coefficients respectively. The value of β has been deduced by Turnbull (1983) to be 0.71 using data measured by Ross (1979).

The gas phase reaction of Equ.(2.4) takes place in the presence of moisture acting as a catalyst. Its rate is given by Howard et al. (1973) as

$$r_{CO} = k_{o_{CO}} e^{-\xi_{CO}/RT_b} C_{CO} C_{O_2}^{0.5} C_{H_2O}^{0.5} \qquad (2.11)$$

where r_{CO}, k_{oCO}, and ξ_{CO} are reaction rate, frequency factor, and activation energy respectively for the CO oxidation reaction. More recently, a radical mechanism is proposed to be responsible for CO oxidation in FBC (Bulewicz et. al., 1989; Anthony et. al., 1994). Since most assume that CO burns either on the char surface or outside of the boundary layer,

application of the above equation to FBC modelling is rare.

2.2.3 External mass transfer

To define mass transfer to the burning particle in a fluidized bed, the expression for the local Sherwood number, Sh, in the form developed by Frössling (1938) is commonly used. Rowe et al. (1965) have suggested a correlation equation

$$Sh=2+0.69Re^{1/2}Sc^{1/3} \tag{2.12}$$

where Sh, Re, and Sc are the Sherwood number, the Reynolds number, and the Schmidt number respectively. If the burning char particle in a fluidized bed is assumed to be surrounded by a stagnant film of gas, then Sh is constant and equal to 2, the minimum value. However, due to the fact that diffusion is hindered by surrounding inert particles, Avedesian and Davidson (1973) suggested Sh = $2\epsilon_{mf}$, the void fraction at minimum fluidization, so that

$$k_g=2\epsilon_{mf}\frac{D_g}{d_c} \tag{2.13}$$

where k_g is the mass transfer coefficient and D_g is the molecular diffusion coefficient of oxygen.

To interpret many experimental results, which gave reaction rates higher than estimated from Equ.(2.13), forced

convection was considered important in later FBC models (Chakraborty and Howard, 1980, 1981; Congalidis and Georgakis, 1981; Pillai, 1981; La Nauze and Jung, 1982). Also, as pointed out by Turnbull and Davidson (1984), many have used the Reynolds number, Re, based on the superficial velocity u rather than u_{mf} to evaluate the Sherwood number in more satisfactory agreement with their data (Chakraborty and Howard, 1981; Pillai, 1981, La Nauze and Jung, 1982). Sherwood number expressions developed by various researchers for FBC are given in the literature (La Nauze, 1985; Zhang, 1987; Jia, 1991).

2.2.4 Overall burning rate

With combustion described by the shrinking particle model, the relative significance of the external diffusion and reaction processes may vary as conversion progresses. Chemical kinetics may become progressively more important as the particle size shrinks. Since the controlling steps act in series, the individual resistances can be combined to give an overall equation. For simplicity, first order reaction is usually assumed, so that the overall reaction rate can be expressed in terms of particulate phase oxygen concentration, C_p

where γ is the stoichiometric constant, equal to 1 or 2 when CO_2 or CO is the effective surface product respectively.

$$r = \frac{C_p}{\frac{1}{\gamma k_g} + \frac{1}{k}} \qquad (2.14)$$

2.3 Fragmentation and Attrition

Particle size reduction due to attrition in fluidized bed systems was first investigated more than forty years ago (Forsythe and Hertwig, 1949). In fluidized bed combustors, breakage of particles of coal, char, limestone, or other bed materials may be caused by various mechanisms, including thermal, chemical, static mechanical, and kinetic stresses (Vaux and Keairns, 1980). The resulting size reduction and fines generation may affect fluidization properties as well as causing loss of fine material by elutriation, which has a large effect on both combustion efficiency and sulphur capture. It has been reported that the main source of elutriated carbon is the fines generated by the attrition of char surface by abrasion (Chirone et al., 1982).

Different terms and definitions are used in the literature to describe particles breaking down to smaller pieces (Bemrose and Bridgwater, 1987; Arastoopour and Chen, 1983). Most FBC studies, including this work, use the definitions of fragmentation and attrition adopted from an earlier paper presented by Chirone et al. (1982): Fragmentation is a process which leads to breakage of

particles into relatively large pieces with limited production of fines, while attrition is defined as the detachment of fines from particle surfaces as they rub against bed inert solids and walls and the internals of the combustor.

2.3.1 Fragmentation

There are two types of fragmentation in FBC. Primary fragmentation occurs during devolatilization and is mainly caused by the build-up of volatile pressure inside the coal particle under rapid heating conditions. Despite fast surface heating, thermal stress is not considered to have a significant effect (Chirone and Massimilla, 1991). Fragmentation occurring in devolatilized char particles is called secondary fragmentation. Combustion weakens the bridges connecting various elements of a char particle, which then breaks during collision.

The extent of fragmentation is commonly characterized by the ratio of particle numbers after and before fragmentation, N/N_o. For primary fragmentation, experimental results from various investigations show that this parameter depends on coal type and initial particle size (Chirone et al., 1982; Chirone and Massimilla, 1989; Dakic et al., 1989; Stubington and Linjewile, 1989). Coal properties such as volatile content, pore structure, and plasticity are obviously major

factors. For caking coals, particle softening and swelling during heating could ease the pressure built up by volatiles, thus reducing the degree of fragmentation. However, resolidification of the plastic material forms a thin shell on the particle surface which is fragile and easy to break into pieces.

A critical coal fragmentation diameter is defined as a particle size under which no fragmentation occurs. The value of the critical diameter was measured to be between 1 and 6 mm for various coals in one work (Chandran et al., 1989), and appears to be about 2 mm for another (Chirone et al., 1982, from Fig.3 of their paper). Peeler and Poynton (1992) defined a fragmentation index based on the apparent surface area instead of the number of particles, and little fragmentation was found with particles of various coals up to about 13 mm. Recently, Dakic et al. (1989) found that the critical diameter can be correlated to the ratio of volatiles and equilibrium moisture contents of the fuel, and has a minimum value of 3 mm. They developed a statistical model for primary fragmentation based on this relationship. Chirone and Massimilla (1988, 1989) present another statistical model for primary fragmentation, with four submodels accounting for the heat-up of coal particles, devolatilization kinetics, convective transport, and pressure inside the pore structure. Model development in this area is rare: the heterogeneity and

the complex nature of physical and chemical changes during devolatilization hinder accurate prediction of this phenomenon.

For secondary fragmentation, experimental data are rare but various techniques have been used (Andrei et al., 1985; Chirone at al., 1989; Sundback et al., 1984; Ragland and Pecson, 1988). Similar to primary fragmentation, the extent of secondary fragmentation depends on coal type and particle size. Because the process is difficult to handle mathematically and its scale is usually small, as far as is known, these phenomena have not been included in combustion models.

Fragmentation does not significantly contribute to the emission of carbon fines through an increased number of unburnt particles (Chirone et al., 1982). However, fragmentation and swelling of particles during devolatilization create more surface area for reaction. Thus, reaction kinetics are obviously complicated by fragmentation processes.

2.3.2 Attrition

Attrition in a fluidized bed without chemical reaction is dominated by abrasion upon collision of moving particles. The

instantaneous specific attrition rate q_a is defined as

$$q_a = \frac{1}{W_m} \frac{dW_m}{dt} \qquad (2.15)$$

where W_m is the mass of the mother particles in the bed at time t. The value of q_a usually has an initial peak, then falls rapidly towards a constant value. The sharp decay of the initial attrition rate is due to rounding off the corners and edges of particles. Experimental results have shown that q_a increases with fluidization velocity, bed height, and wall hardness (Arastoopour and Chen, 1983, Sishtla et al., 1989). Also, some researchers suggested that energy dissipated by jets near the distributor contributes the largest part of the attrition (Patel et al., 1986; Sishtla et al., 1988). On the other hand, a recent study (Shamlou et al., 1990) indicates that attrition is most likely to be caused by low energy impacts in the core of the bed.

For porous solids, reactant gas may diffuse through pores a certain depth into the particle, depending on diffusion and reaction rates. The reaction occurring in this surface layer weakens the local bonds and bridges and results in more extensive attrition upon collision. This phenomenon is called chemical attrition, and may have a different behaviour than purely mechanical attrition. Chirone et al. (1985) showed that attrition is enhanced by combustion and its rate is much higher during oxidation than during pyrolysis. Because the

detachable asperities are continuously renewed by the irregular movement of the combustion front, the attrition rate does not decay sharply.

Extensive work on attrition under FBC conditions has been carried out by the excellent research group led by Massimilla. They proposed that the attrition rate Q_a is proportional to the product of the excess of gas velocity above the minimum for fluidization, i.e. $(u-u_{mf})$, and the overall carbon surface exposed to attrition inside the bed (Arena et al., 1983):

$$Q_a=k_a(u-u_{mf})\frac{W}{d_{32}} \qquad (2.16)$$

where W is the carbon inventory, d_{32} is the Sauter mean diameter of the fuel particle, and k_a is the attrition constant, which is dependent on both char and inert bed material properties, but is insensitive to operating conditions. Some earlier works on mechanical attrition suggested that attrition rate depends on the superficial gas velocity u to a power instead of on $(u-u_{mf})$ (Blinichev et al., 1968; Kono, 1981). There are also arguments as to whether attrition rate depends on particle surface or volume. In the development of a mechanical attrition model, Ray et al. (1987) suggested that Equ.(2.16) is valid when the particle subjected to attrition is coarser than the fluidizing material, as is usually the case with FBC. Otherwise, the particle size affects the attrition rate only through its effects on u_{mf};

thus Q_a is proportional to particle volume, as suggested by Merrick and Highley (1972).

According to Beér et al. (1980), coals of higher reactivity burn faster and result in less carbon inventory in the bed. Consequently there is less carbon surface exposed to attrition and fewer elutriated combustible fines, hence better combustion efficiency. Arena et al. (1984) showed that some factors on which burning rate depends, such as feed particle size, bed temperature, and excess air, affect the attrition rate through the Sauter mean diameter and the bed carbon inventory as suggested by Equ.(2.16). On the other hand, the particle size distribution of the elutriated fines was found to be insensitive to changes in these operating factors. Since attrition is the major source of the elutriated fines, these authors therefore concluded that combustion of the attrited particles after attrition is negligible,most fines being immediately elutriated. Furthermore, the attrition rate constant k_a was found not to be significantly influenced by the combustor's scale, and can therefore be determined by means of a laboratory scale unit (Arena et al., 1986).

2.3.3 Particle size distribution

The effect of fragmentation and attrition is to reduce the particle size of the feed materials. Without chemical

reaction, mechanical attrition in a fluidized bed has been reported to generate particles of extremely fine size, most attrited material being below 50 μm (Salatino and Massimilla, 1985; Fuertes et al., 1989; Pis et al., 1991). Such fine particles will be elutriated under normal FBC conditions; thus attrition rate is normally estimated through the measurement of elutriated fines collected by a cyclone or a filter (Arena et al., 1983; Chirone et al., 1982, 1985). On the other hand, fragmentation produces a negligible amount of fines, but rather fragmented particles which are large enough to remain in the bed. The effect of fragmentation and attrition is therefore easily distinguished in this case, as the particle size distribution which is illustrated in Fig. 2.1b shows, with that of the initial particles given in Fig. 2.1a.

Chirone et al. (1985) found that attrited fines in fluidized combustors are coarser than those generated by mechanical attrition alone. Particles larger than 300 μm were collected in the filter as illustrated in Fig.9 of their paper. When an attrited char particle is larger than the elutriable particle size, it will burn until that size is attained. Freeboard combustion may also reduce its size further before it reaches the combustor exit. If significant amounts of attrited char particles are larger than the elutriable size, as illustrated in Fig. 2.1c, size reduction by post-attrition combustion cannot be neglected. Measurement

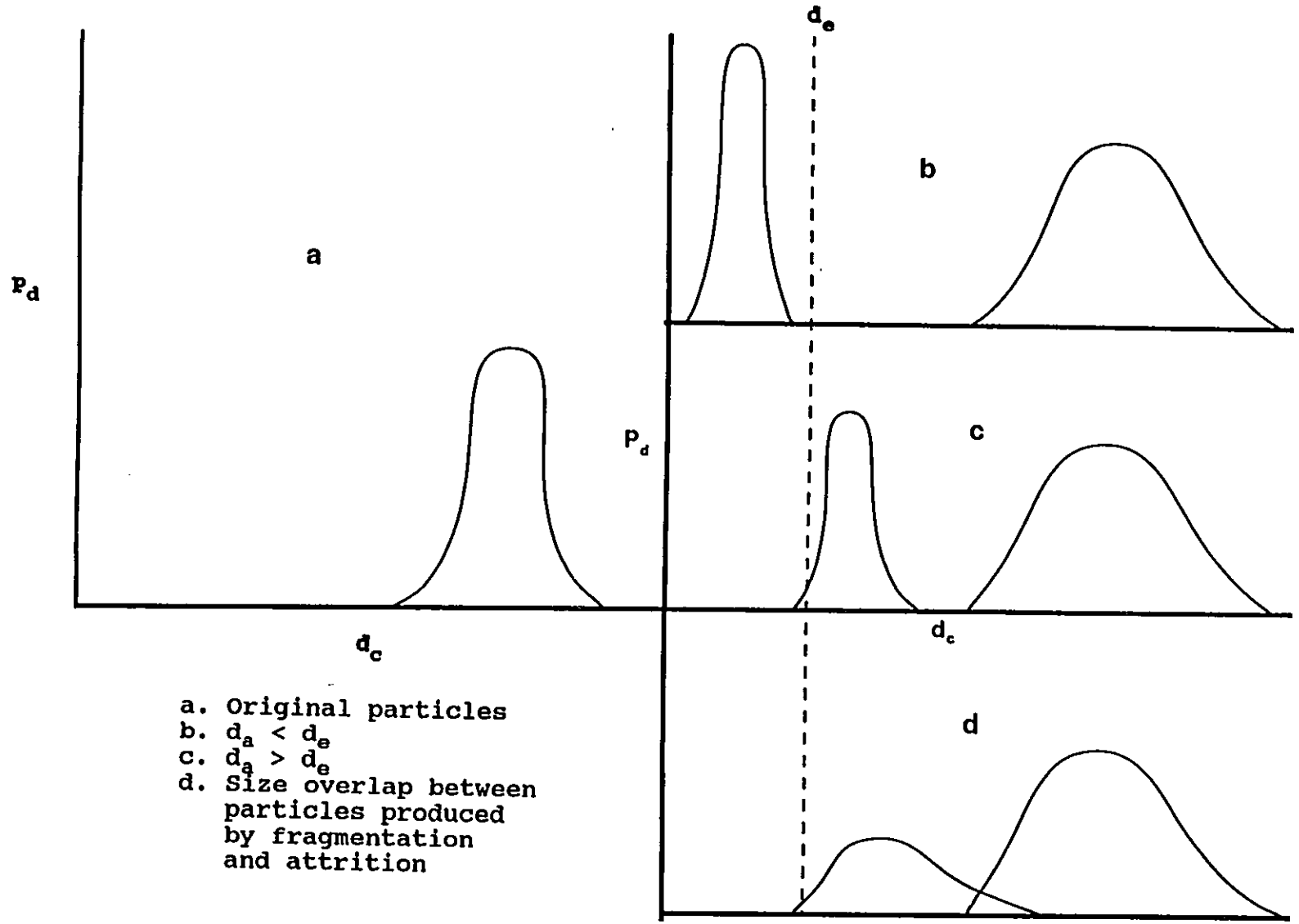

Fig. 2.1: Fragmentation and attrition effect on particle size distribution

from cyclone or filter collection will then underestimate the attrition rate. Since it is impossible to separate the freshly attrited particles from the rest of the bed right after their birth, direct measurement of the attrition rate is difficult. Furthermore, if the attrited particles are large enough so that their size distribution overlaps with that of the fragmented pieces (see Fig. 2.1d), measuring attrition rate will be complicated by the process of secondary fragmentation.

Little work has been done on the size of attrited particles in FBC and the post combustion effect on their size reduction. Experimental methods to measure the attrition rate for the large particle size attrition case require to be developed.

2.4 Concluding Remarks

The literature clearly indicates the complexity of the mechanism of coal char combustion in a fluidized combustor. Detailed knowledge of important processes such as reaction kinetics, mass and energy transport, fragmentation and attrition is still incomplete. In addition, despite the fact that attrition is the key process for combustion efficiency determination, there is still a lack of appropriate techniques for measuring the attrition rate and the degree of burnout of

the attrited particles. This hinders the development of a mathematical model as a tool for design and operation prediction.

Since the first FBC model (Avedesian and Davidson, 1973) appeared, many successful works have followed to present models more close to reality. Despite differences given in the mechanisms of certain processes, they all approach the problem in the same general manner. Because coals from different mines are never equal, coal chars have different structures after devolatilization and behave differently in various combustion processes. Usually a model may be modified to fit the data and predict one coal's performance well, in some cases by sacrificing the elegance of the fundamental concept, but it may not be successful for the others. It is hoped that a new approach in modelling may provide some advances in FBC performance prediction. With this objective, the present work develops two semi-empirical models approaching differently from those classical methods. Measuring techniques using only batch operating bench-scale FBC facilities for model parameters evaluation are also developed.

3. THEORETICAL DEVELOPMENT

FBC Models developed today generally follow the classical gas-solid reaction kinetics and fundamental fluidization theories. Because of the complexity of the mechanisms used, recent models approach closer to representing the true picture; however, they are also more complicated. Despite many research efforts, certain areas are still unclear. Also, reliable data on physical and chemical parameters, such as mass transfer coefficients, fuel reactivity, and attrition rate constants are seldom available. Therefore, FBC performance predictions from mathematical modelling are not yet satisfactory. In this work, a fresh approach is attempted, introducing certain new parameters to characterize both reaction and attrition kinetics instead of those classically used. Theory is developed to relate these parameters and ultimately to determine carbon losses from elutriation and withdrawal, a method no one has attempted before. Two novel models are developed with the purpose of searching out a new route to evaluate combustion, attrition, elutriation, and withdrawal from laboratory experiments and to use these quantities to predict combustion efficiency.

3.1 Basic Concepts and Assumptions

When coal is fed into a fluidized bed combustor,

particles larger than the critical size for fragmentation break into a number of fragments during volatiles evolution. In considering the coal size generally used in FBCs (minus 30 mm), the volatile flux is large enough to prevent oxygen from reaching the solid surface (Howard and Essenhigh, 1967; Atimtay, 1987). The combustion steps of volatiles burning and char combustion thus can be treated independently. This study concentrates on combustion of char, which is assumed uniform in property throughout the entire particle. Secondary fragmentation effects are assumed small and are not considered here.

Combustion reaction and attrition occur simultaneously on the surface of post-fragmented char particles. Because of the fast reaction, oxygen penetrates into a char particle only through the large pores at its surface. No significant amount of oxygen can possibly be present in the other micro pores. In general, O_2 penetration is short compared to the particle dimensions, and combustion is limited to a thin layer near the surface. The residual ash is usually flaked off due to the vigorous agitation in the fluidized bed. Therefore, the size reduction of char is assumed to follow the shrinking particle model. As pointed out in section 2.3.3, the attrited particle size is a few hundred microns and under, the size range in which chemical reaction is generally considered to play the dominant role under FBC conditions. The results of a recent

study (Flour, 1991) burning fine size char particles in a fluidized bed confirm this. Therefore, while mother char particles may burn under different reaction regimes, depending on reactivity, particle size, and operating conditions, attrited fines may be assumed to burn under kinetic control.

Combustion reaction inside the pores near the char surface weakens the bridges and bonds; this allows attrition to occur as char particles frequently contact other particles, container walls, and internals in a fluidized bed. Since it is chemical reaction which weakens the particle, this is referred to as chemical attrition. As the chemical mode dominates the attrition prccess, the attrited particle size distribution should be closely related to the effective gas penetration depth, since this depth is likely to be close to the size of the particles most frequently breaking off. A wide size distribution from zero to a maximum size, d_s, arbitrarily taken as double the most frequent size, is assumed in this study. This size distribution of the attrited fines is assumed to be independent of the size of the mother char particle. Because the attrited particle sizes in FBC systems are generally much larger than those produced by pure mechanical attrition as stated in section 2.3.3, only a small portion of the attrited carbon is immediately elutriable, unlike the case of pure mechanical attrition. The rest will be partially burnt until the attrited particles shrink to the

elutriable size, d_e. The elutriable size is assumed to be a single constant diameter for a given set of FBC operating conditions.

Attrition occurs along the walls of large pores in the surface of mother particles, but within attrited fines there is considered to be a lack of large pores. Therefore the attrited fines are unlikely to have further significant attrition. It may be argued that for very fine particles whose sizes are comparable to the effective O_2 penetration depth, internal combustion becomes important and the shrinking particle model is no longer valid. If the combustion of these particles approaches internal kinetic control (constant volume, decreasing density), the whole structure of the particle will be uniformly weakened and finally collapsed, disintegrating to a number of ultrafine particles. This process, called uniform percolation, is considered to have only a minor effect in FBC conditions, since most fines are generated by attrition, and internal combustion is not significant for attrited particles due to the lack of large pores. Also, as discussed in Section 2.2.1, only the micro-size char particles can reach the state of internal kinetic control. The majority of fines will be elutriated out of the bed before reaching this size.

In this study two slightly different models for chars

with sizes larger than the elutriable size d_e are proposed:

Model 1: - assumes that the mother particle shrinks continuously with combustion and attrition until elutriable.

Model 2: - assumes that when oxygen can effectively penetrate into the centre of the mother particle, a final attrition occurs to break it up into pieces. Thus the minimum size of the mother particle, at the time just before the final split, equals d_s. The size distribution of the particles resulting from the final split is assumed statistically identical to that of the normally attrited fines, which has a size range from zero to d_s. This means that in rare cases it could happen that no breakage occurs for a particle that has already shrunk to a size equal to or smaller than d_s. However, such a particle at this stage is considered to be an attrited rather than a mother particle according to this model. In other words, since d_s is larger than d_e, mother particles will never be elutriated.

Since the attrition of chars under FBC conditions is dominated by the combustion reaction, its rate can therefore

be assumed to be directly proportional to the combustion rate. A modification to Equ.(2.16) is proposed:

$$Q_a=(k_r r_m+k_h)\,(u-u_{mf})\,\frac{W}{d_{32}} \qquad (3.1)$$

where r_m is the reaction rate per unit surface area of the mother char particle, and k_r and k_h are chemical and mechanical attrition constants respectively. As stated in Section 2.3.2, the attrition rate is much higher during combustion than during pyrolysis (Chirone et al., 1985). With $k_r>>k_h$, the equation shows that the attrition rate may not necessarily be in proportion to the area of total char surface in the bed but rather may follow the size dependence of reaction rates. This simplifies the model development because both size reduction processes, combustion and attrition, act in the same manner, which allows the shrinking particle model to be used in the same way as for the combustion reaction alone.

In practical FBC boilers, bed materials are generally withdrawn continuously to maintain bed depth. Char particles may be withdrawn from the bed before they shrink to the elutriable size. Bed solids are considered perfectly mixed so that the carbon concentration in the withdrawn stream is no different to that of the bed. Thus carbon loss due to withdrawal depends on bed materials withdrawal rate and in-bed carbon inventory.

3.2 Carbon Balances

3.2.1 Overall balance

In a coal FBC system, carbon fed into the bed exits in three different streams: 1. conversion to CO or CO_2 which escapes above the bed; 2. elutriation; 3. withdrawal. From a material balance of fixed carbon (ie. char, excluding volatiles) at steady state, the carbon feed rate, F, equals the sum of these three exit rates:

$$F=R_c+Q_e+Q_w \tag{3.2}$$

Let Z be the fraction of carbon withdrawn and Y be the fraction of elutriated carbon in the remaining non-withdrawn portion, so that

$$Q_w=ZF \tag{3.3}$$

$$Q_e=Y(1-Z)F \tag{3.4}$$

$$R_c=(1-Y)(1-Z)F \tag{3.5}$$

The carbon combustion efficiency, η, is:

$$\eta=(1-Y)(1-Z) \tag{3.6}$$

The prediction of η by developing expressions for Y and Z is the main purpose of this chapter.

3.2.2 Balance for attrited fines

In addition to combustion of mother char particles, attrition produces fines which also contribute to all three exit streams. A material balance for the attrited carbons alone gives

$$Q_a = R_a + Q_{ea} + Q_{wa} \tag{3.7}$$

where R_a, Q_{ea}, and Q_{wa} are the rates of reaction, elutriation, and withdrawal of the attrited carbons respectively. Since the attrited particles are fine and have very short residence times, their inventory in a fluidized bed is small and therefore Q_{wa} can be neglected. Defining Y_a for attrited fines in the same manner as Y for the feed char particles, Equ.(3.7) can be written as:

$$Q_a = \frac{R_a}{1-Y_a} \tag{3.8}$$

3.2.3 Attrited and elutriated fractions with negligible withdrawal

In cases when coal reactivity is high and/or particle size is small, the in-bed carbon inventory would be low owing to the high combustion rate. The amount of carbon withdrawn is then small and can be neglected, in which case carbon efficiency depends on the elutriation loss fraction Y only.

Model 1: If the original size of a char particle is larger than the elutriable size, based on the first model, the fraction of the original carbon content which is elutriated for a given mother particle is

$$y=f_a Y_a+y_m \qquad (3.9)$$

where f_a and y_m are the fraction of attrition and the fraction of elutriation of the mother char particle. (Please note that lower case y is used in Eq.(3.9) for the elutriated fraction of a single particle, or of mono-sized particles, to distinguish it from that of the whole distribution of particle sizes or the whole carbon mass, which uses a capital letter Y). The fraction of attrition, of course, depends on the competition between attrition and reaction of the mother char particle:

$$f_a=\frac{Q_a}{Q_a+R_m}(1-y_m) \qquad (3.10)$$

where R_m is the reaction rate of the mother char particle. A schematic diagram of carbon "flow" of a char particle burning without withdrawal for model 1 is given in Fig. 3.1a.

Model 2: If the second model is assumed, based on the attrition phenomenon described in the previous

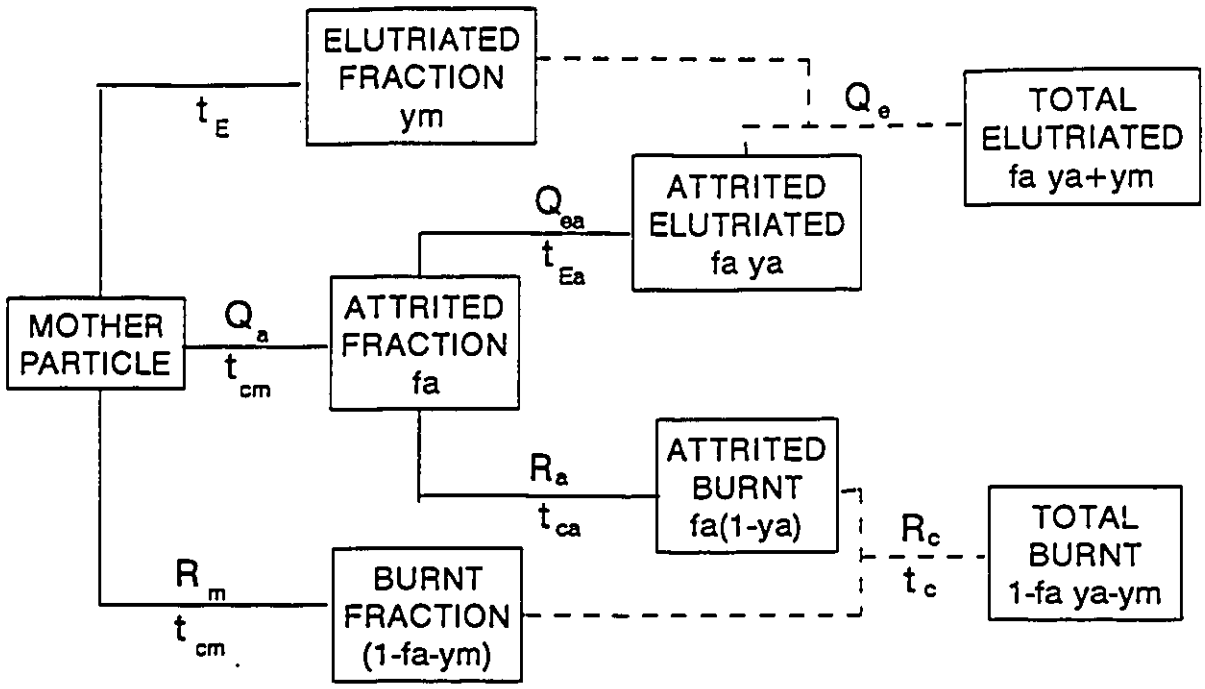

a: model 1

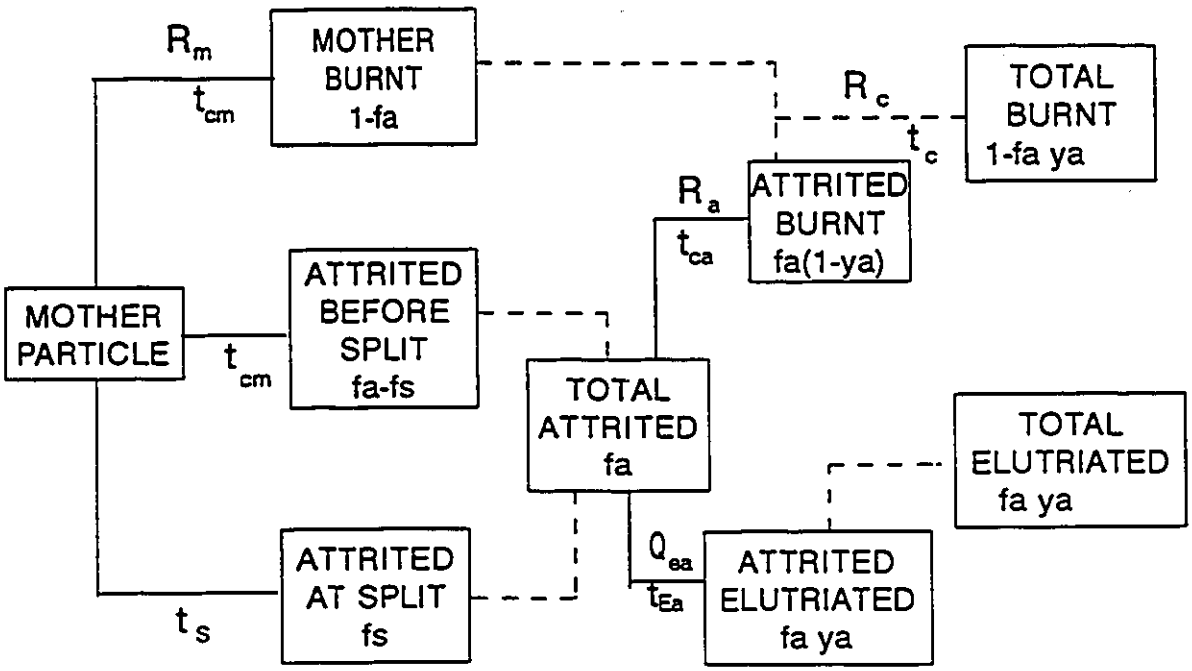

b: model 2

Fig. 3.1: Carbon balance without withdrawal

section, attrition is the sole source responsible for the elutriation loss, since a mother char particle breaks up before being elutriated (see Fig. 3.1b):

$$y=f_a Y_a \tag{3.11}$$

For this model, the attrited carbon mass includes that detached from the mother particle during its combustion and that resulting from the final split:

$$f_a=\frac{Q_a}{Q_a+R_m}(1-f_s)+f_s \tag{3.12}$$

where f_s is the fraction of the original carbon remaining in the mother particle at the time of its final split. Note that $y_m=0$ for model 2.

For large particles, both y_m and f_s are small and can be neglected, and the elutriation fraction y becomes identical for the two models:

$$y=\frac{Q_a}{Q_a+R_m}Y_a \tag{3.13}$$

By neglecting the mechanical attrition rate in Equ.(3.1), the rate competition ratio $Q_a/(Q_a+R_m)$ can be shown to be a constant for a given set of operating conditions:

$$\frac{Q_a}{Q_a+R_m}=\frac{k_r\rho_c(u-u_{mf})}{k_r\rho_c(u-u_{mf})+1}=Const. \qquad (3.14)$$

Note that lower case r is used to represent reaction rate per unit surface area, while capital R denotes total reaction rate in kg/s.

3.2.4 Effect of withdrawal

When the withdrawal carbon loss is significant, the withdrawal loss fraction Z can be calculated through the overall inventory and the withdrawal rate of a perfectly mixed bed:

$$Z=\frac{Q_w}{F}=\frac{F_w W}{W_b F} \qquad (3.15)$$

where F_w and W_b are the overall withdrawal rate and total inventory of bed material, including inert materials such as sand, ash and limestone, and W is the carbon inventory in the bed. Thus the ratio W/W_b is the mass fraction of carbon in the bed.

By applying the basic residence time concept to carbon instead of particles, the carbon inventory W in a fluidized bed is:

$$W=Ft_r \qquad (3.16)$$

where t_r is the mean carbon residence time, MCRT, for all

carbon mass in the three exit streams. Substituting Equ.(3.16) and the commonly defined mean residence time τ for the overall withdrawn material into Equ.(3.15) results in

$$Z=\frac{t_r}{\tau} \qquad (3.17)$$

where $\tau = W_b/F_w$.

The value of MCRT not only affects the carbon loss by material withdrawal; other factors determining the elutriation loss are also directly or indirectly related to one or the other form of mean residence time based on carbon mass as illustrated in the later sections.

3.3 Development of Characteristic Times - Single Particle

In the following sections, relations are developed for t_r and the fraction elutriated for progressively more complex cases of char combustion, beginning with combustion alone and then adding attrition, elutriation, and withdrawal. The development considers first the combustion of single char particles, or mono-sized particles fed in continuous operations, and is extended later to multi-sized particle systems.

The development introduces several characteristic time parameters. The nomenclature employed for the first subscript

uses lower case letters for a mean time based on carbon mass, while capital letter subscripts represent characteristic times for individual char particles. For example, t_r is the mean residence time of carbon mass as a whole, while t_E is the elutriation time of a single char particle. Also, the first subscript characterizes the time, while the second subscript characterizes the char particle in question, so that t_{ra} is the mean carbon residence time of an attrited particle. A superscript * represents the ideal case of no elutriation or withdrawal carbon losses, and an overline represents the mean value for a distribution of multi-size particles.

3.3.1 Ideal combustion - no carbon loss

This section describes the ideal case of a char particle burning to completion without the complication of elutriation and withdrawal.

3.3.1.1 Combustion without attrition

When a single char particle shrinks by the process of combustion alone, previous theories for gas-solid reaction kinetics can be applied directly. By definition the mean time for carbon conversion t_c^* is,

$$t_c^* = \int_0^1 t\,dx \qquad (3.18)$$

where x is the fractional conversion of carbon at time t, and subscript c in t_c^* stands for carbon conversion, so that only the burnt carbon mass is counted.

The area represented by Equ.(3.18) can be expressed alternatively as:

$$t_c^* = \int_0^{t_B^*} (1-x)\,dt \qquad (3.19)$$

where t_B^* is the ideal burnout time of the char particle, at which x=1. The relation between the fractional conversion and time depends on the regime in which the reaction occurred (see Table 2.1). Since for the ideal case no carbon loss is assumed, t_c^* represents the mean carbon conversion time of all carbon in the char particle. Thus t_c^* is equal to the mean carbon residence time t_r^* if all carbon is assumed to leave the bed as CO or CO_2 immediately after conversion, or

$$t_r^* = t_c^* = \int_0^{t_B^*} \left(1-\frac{t}{t_B^*}\right)^n dt \qquad (3.20)$$

where n=3 for the kinetically controlled regime, n=3/2 for the Stokes diffusion regime, and n=2 for the convection regime (Table 2.1). Integrating Equ.(3.20) gives the relationship between t_r^*, or t_c^*, and t_B^*:

$$t_B^* = (n+1)\, t_r^* \qquad (3.21)$$

3.3.1.2 Combustion with attrition

When combustion reaction and attrition occur simultaneously in a fluidized bed, both the attrited and the mother particles contribute to combustion products. For the attrited particles, all equations developed in the previous section can be directly applied to them, since no further attrition is assumed. Also, the assumption of reaction under kinetic control gives n=3 and $t_{ra}^* = t_{Ba}^*/4$, where t_{ra}^* and t_{Ba}^* are the ideal MCRT and the burnout time of the attrited particle respectively, counting from the time of detachment from the mother particle.

For the mother char particle, because the attrition rate is assumed to be directly proportional to the combustion rate, the mean age of the burnt carbon at the moment of conversion and that of the attrited carbon at the moment of detachment from the mother particle are equal. Here another ideal (i.e. no elutriation and withdrawal carbon loss) characteristic time called the mean carbon consumption time t_d^* is introduced, defined as the time at which carbon associated with the mother particle is removed by attrition or reaction. If we replace t_c^* or t_r^* with t_d^*, then the equations developed for the case of no attrition in section 3.3.1.1 can also be applied to this

case of complete carbon consumption of a mother char particle by simultaneous combustion and attrition processes. For example, Equ.(3.20) and (3.21) become:

$$t_d^* = \int_0^{t_B^*} (1 - \frac{t}{t_B^*})^n dt \qquad (3.22)$$

$$t_B^* = (n+1)\, t_d^* \qquad (3.23)$$

Note that the subscript d denotes the residence time of carbon prior to removal from the mother particle, not necessarily leaving the bed. Of course, x in this case represents the fraction of carbon mass removed from the mother particle by both reaction and attrition processes, and the value of t_B^*, due to the added removal rate by attrition, is shorter in this case than that with combustion alone.

Since the attrited fraction of carbon has an additional mean residence time equal to t_{ra}^*, the overall mean residence time for all carbons of the char particle is

$$t_r^* = t_c^* = t_d^* + f_a t_{ra}^* \qquad (3.24)$$

The above equation distinguishes the introduced characteristic times in the ideal case and shows their relationship.

3.3.2 Combustion with elutriation

3.3.2.1 Combustion without attrition

If a char particle shrinks to the elutriable size d_e, with combustion as the lone size reduction process, and then is entrained out of the bed at time t_E, Equ.(3.20) becomes:

$$t_r = \int_0^{t_E} (1 - \frac{t}{t_B^*})^n dt \qquad (3.25)$$

By integration, the result shows the relationship between t_r and t_{r*}, the mean carbon residence times with and without elutriation respectively:

$$t_r = (1 - y^j)\, t_r^* \qquad (3.26)$$

where j=1+1/n, or j=4/3 for the kinetic regime, j=5/3 for the Stokes diffusion regime, and j=3/2 for the convection regime. Since y, the elutriation fraction for a single particle, is the fraction of the original mass remaining at t_E, its value is (Table 1):

$$y = 1 - x(at\ t_E) = (1 - \frac{t_E}{t_B^*})^n \qquad (3.27)$$

The method described for evaluation of t_r is illustrated by Fig. 3.2, in which the shaded and the total areas under the (1-x) vs t curve represent the values of t_r and t_r^* respectively.

Unlike the ideal case in which all carbons are burnt,

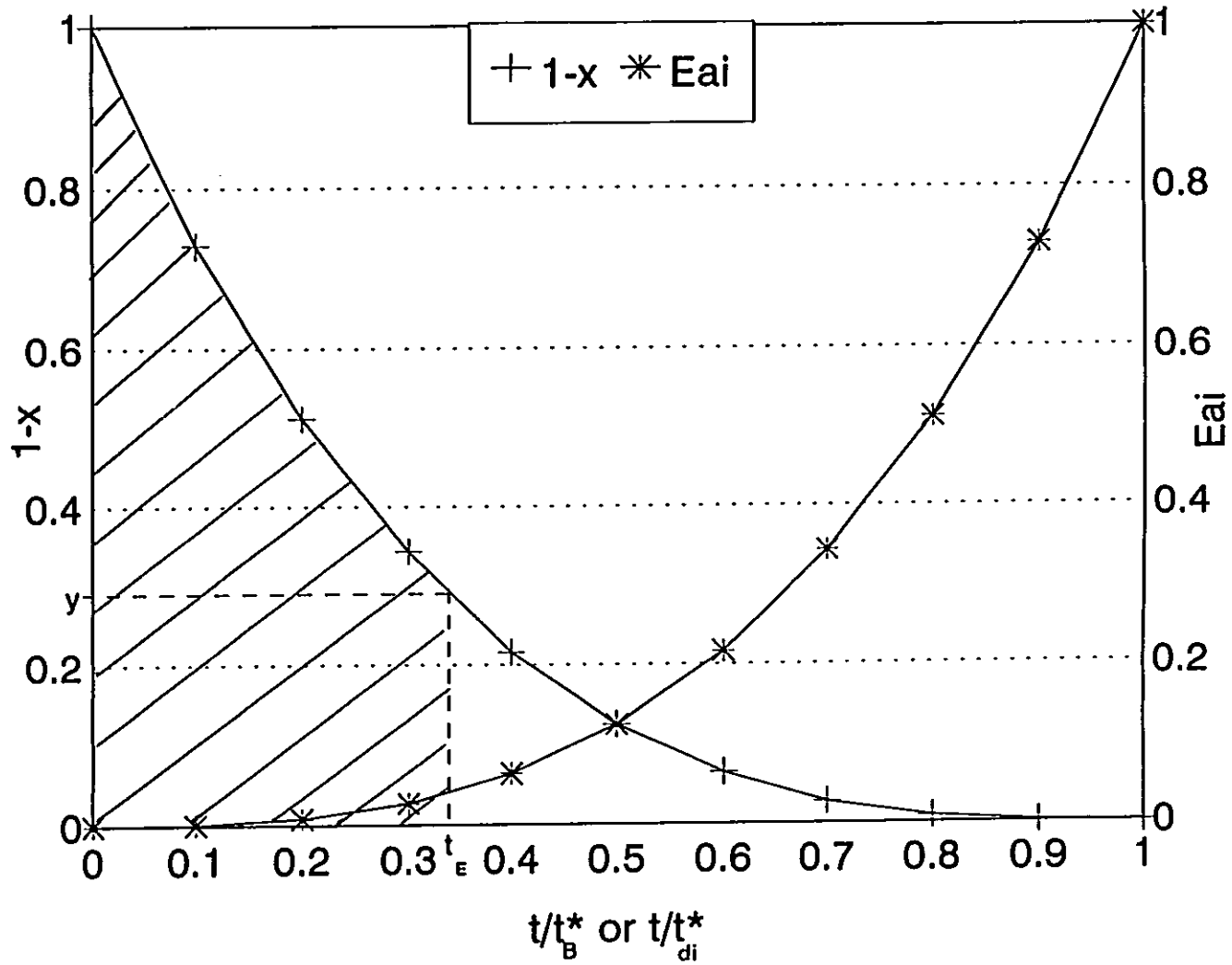

Fig. 3.2: 1-x and E_{ai} vs t/t_{di}^* or t/t_B^*

t_r*t_c in this case. If only the carbon which actually burns is counted, its mean conversion time is:

$$t_c=\frac{t_r-yt_E}{1-y} \qquad (3.28)$$

In Fig. 3.2, $(1-y)t_c$ is represented by the area under the 1-x curve and above the horizontal dotted line at 1-x=y, which is equal to the shaded area minus the area of the rectangle under the horizontal dotted line, t_r-yt_E, as given by Equ.(3.28).

3.3.2.2 Combustion with attrition

In this section, both combustion and attrition are considered to occur simultaneously. Residence times of carbon spent associated with the mother particle and with the attrited fines are analyzed separately. Following the argument stated in Section 3.3.1.2, the expression for the mean time at which carbon associated with mother particles is detached by reaction or attrition, t_d, can be developed equivalent to that for combustion alone, i.e Equs.(3.25) to (3.27).

Model 1: For model 1, which assumes that the mother char particle shrinks to d_e, this becomes:

$$t_d=\int_0^{t_E}(1-\frac{t}{t_B^*})^n dt=(1-y_m^j)\,t_d^* \qquad (3.29)$$

$$y_m = (1 - \frac{t_E}{t_B^*})^n \qquad (3.30)$$

Note that t_d represents the mean time for all carbon mass of the mother char particle, including the fraction elutriated, but y_m is the elutriation fraction for the mother particles only. Similar to t_B^* in Equ.(3.22), the value of t_E in this case is shorter than it is without attrition due to the added carbon removal rate by attrition.

Model 2: For model 2, one replaces t_E and y_m in the above equations with t_S, the time when the mother particle splits at the final stage, and f_s, the fraction of the original carbon remaining in the mother particle at t_S respectively.

After being detached from the mother particle, attrited fines burn under kinetic control to provide an additional residence time to the attrited carbon fraction. Without further attrition, an attrited particle of size larger than d_e shrinks by combustion alone as described in the previous section. Assuming combustion in the kinetic regime, the MCRT, irrespective of which of the two models used, is (cf. Equ.(3.26) and (3.27)):

$$t_{ra} = (1 - y_a^{4/3})\, t_{ra}^* \qquad (3.31)$$

and

$$y_a = (1 - \frac{t_{Ea}}{t_{Ba}^*})^3 \qquad (3.32)$$

where t_{Ea} is the time required for the attrited particle to reach the elutriable size measured from the time of detachment from the mother particle.

Because attrition generates fines in a wide range of particle sizes, it is more reasonable to assume a normal (Gaussian) size distribution for these particles. We define P_{da} as the number density distribution of the initial particle size d_a of the fines generated by attrition, so that

$$P_{da} = \frac{e^{\frac{1}{2}[(d_a - \bar{d}_a)/\sigma]^2}}{\sigma\sqrt{2\pi}} \qquad (3.33)$$

With the assumptions given in Section 3.1, the number mean size, $\bar{d}_a$, equals half of the maximum particle size, d_s. Assuming also that as the value $(d_a - \bar{d}_a)/\sigma$ approaches ±3 (99.7% confidence), P_{da} becomes negligibly small, the value σ is thus estimated to be $d_s/6$, and

$$P_{da} = \frac{6}{\sqrt{2\pi} d_s} e^{-18(\frac{d_a}{d_s} - \frac{1}{2})^2} \qquad (3.34)$$

The above size distribution function for particle diameter can be written in a form based on the mass of carbon, E_{da}, rather than the number of particles

$$E_{da}=\frac{d_a^3 P_{da}}{\int_0^{d_s} d_a^3 P_{da} dd_a} \tag{3.35}$$

Since the kinetic regime is assumed, t_{ra}^* is directly proportional to d_a (cf Table 1), and the ideal MCRT distribution function can be written in the same form as E_{da}. By introducing t_{rs}^* as the ideal MCRT of the largest attrited particle, the distribution function in dimensionless form is given as:

$$E_{\lambda a}=\frac{\lambda^3 \phi}{\int_0^1 \lambda^3 \phi d\lambda} \tag{3.36}$$

where λ and the exponential function ϕ are defined as:

$$\lambda=\frac{d_a}{d_s}=\frac{t_{ra}^*}{t_{rs}^*} \tag{3.37}$$

$$\phi=e^{-18(\lambda-\frac{1}{2})^2} \tag{3.38}$$

The MCRT of all attrited fines can be obtained by integrating the t_{ra}, given by Equ.(3.30), of all sizes,

$$\overline{t_{ra}}=\int_{d_e}^{d_s} (1-y_a^{4/3})\, t_{ra}^* E_{da} dd_a \tag{3.39}$$

Defining t_{re}^* to be the MCRT that the elutriated particles would have if they were to be put back in the bed and burnt completely under the kinetic regime, we have the fraction of

size d_a elutriated as

$$y_a=(\frac{d_e}{d_a})^3=(\frac{t^*_{re}}{t^*_{ra}})^3 \tag{3.40}$$

In dimensionless form:

$$\lambda_e=\frac{t^*_{re}}{t^*_{rs}} \tag{3.41}$$

Combining Equs.(3.36) to (3.41) gives

$$\overline{t_{ra}}=\frac{\int_{\lambda_e}^{1}(\lambda^4-\lambda_e^4)\phi d\lambda}{\int_0^1\lambda^3\phi d\lambda}t^*_{rs} \tag{3.42}$$

Note that all carbon of the char has a mean residence time associated with the mother particle of t_d, and the fraction attrited has an additional mean residence time of $\overline{t_{ra}}$ after detaching from the mother particle. Therefore, the overall MCRT is:

$$t_r=t_d+f_a\overline{t_{ra}} \tag{3.43}$$

In estimation of the mean carbon conversion time t_c, as opposed to the residence time t_r, only the carbon which burns, from both the mother and the attrited particles, is considered. This is calculated as follows:

Model 1: Since the attrition rate is assumed proportional to the combustion rate, the mean time for the attrited carbon mass at the moment of detachment from the mother particle equals the mean conversion time for the carbon burnt associated with the mother particle. In other words, all the carbon which burns, irrespective of whether it comes from the mother or from the attrited particles, has a mean residence time associated with the mother particle equal to t_{cm}, the mean carbon conversion time of the mother particle. Again, the fraction attrited has an additional mean conversion time $\bar{t}_{ca}$ after detachment from the mother particle (see Fig. 3.1a). Thus the overall mean carbon conversion time can be expressed in analogy to Equ.(3.43), with the attrition fraction of the converted carbon equal to the fraction attrited and burnt divided by the total fraction burnt:

$$t_c = t_{cm} + \frac{f_a(1-Y_a)}{1-y_m-f_aY_a}\overline{t_{ca}} \qquad (3.44)$$

The difference between t_{cm} and t_d is that t_{cm} does not include the carbon mass of the final elutriated mother particle but t_d does. Since the elutriated fraction of the mother particle has a

residence time of t_E, thus, similar to Equ.(3.28), the relation between t_{cm} and t_d is:

$$t_{cm}=\frac{t_d-y_m t_E}{1-y_m} \tag{3.45}$$

Similarly, the value of t_{ca} for a single attrited particle is:

$$t_{ca}=\frac{t_{ra}-y_a t_{Ea}}{1-y_a} \tag{3.46}$$

The elutriation time t_{Ea} for an attrited particle of initial size d_a is the time difference between the moments of its attrition and elutriation, which can be expressed in terms of ideal MCRT's of the attrited and elutriated particles (cf 3.3.1.2):

$$t_{Ea}=t^*_{Ba}-t^*_{Be}=4\,(t^*_{ra}-t^*_{re}) \tag{3.47}$$

Substituting Equs.(3.31), (3.40) and (3.47) in Equ.(3.46) and dividing both the numerator and the denominator of the right hand side of the equation by t_{rs}^* results in

$$t_{ca}=\frac{\lambda^4-4\lambda_e^3\lambda+3\lambda_e^4}{\lambda^3-\lambda_e^3}\,t^*_{rs} \tag{3.48}$$

The mean value of t_{ca} for all attrited particles larger than the elutriable size can be obtained by

integration using the dimensionless ideal MCRT distribution function for the carbon which burns, $E_{\lambda ac}$:

$$\overline{t_{ca}}=\int_{\lambda_o}^{1} t_{ca}E_{\lambda ac}d\lambda \qquad (3.49)$$

The value of $E_{\lambda ac}$ is different from $E_{\lambda a}$ for all attrited carbons but can be developed in a similar way:

$$E_{\lambda ac}=\frac{(\lambda^3-\lambda_o^3)\phi}{\int_{\lambda_o}^{1}(\lambda^3-\lambda_o^3)\phi d\lambda} \qquad (3.50)$$

Substituting Equ.(3.48) and (3.50) into Equ.(3.49) and integrating,

$$\overline{t}_{ca}=\frac{\int_{\lambda_o}^{1}(\lambda^4-4\lambda_o^3\lambda+3\lambda_o^4)\phi d\lambda}{\int_{\lambda_o}^{1}(\lambda^3-\lambda_o^3)\phi d\lambda}t_{rs}^{*} \qquad (3.51)$$

If the original char particle is large, $y_m\approx 0$ and $t_{cm}\approx t_d\approx t_d^*$, and Equ.(3.44) can be simplified to:

$$t_c=t_d^*+\frac{f_a(1-Y_a)}{1-f_aY_a}\overline{t}_{ca} \qquad (3.52)$$

If the amount of attrition is very small, $f_a\approx 0$,

and Equs.(3.44) with (3.45) are reduced to Equ.(3.28), the case of combustion with elutriation only.

Model 2: In case model 2 is assumed, the MCRT for the amount of carbon burnt only is:

$$t_c=\frac{(1-f_a)\,t_{cm}+f_s(1-Y_a)\,t_S+(f_a-f_s)\,(1-Y_a)\,t_{cm}+f_a(1-Y_a)\,\overline{t_{ca}}}{1-f_aY_a} \quad (3.53)$$

Since the mother particle contributes no elutriation loss, the fraction of carbon burnt of the char particle equals $1-f_aY_a$ which is given as the denominator on the right hand side of the equation. Together with the denominator, the first, second, third, and fourth terms of the numerator represent the fractional MCRTs of the carbon burnt from the mother particle, from the particles attrited at the final split (time prior to their attrition), from the particles attrited before the split (time prior to their attrition), and from all attrited particles (time after their attrition) respectively (see Fig. 3.1b). By rearrangement, Equ.(3.53) becomes:

$$t_c=t_{cm}+\frac{1-Y_a}{1-f_aY_a}\,[f_s(t_S-t_{cm})+f_a\bar{t}_{ca}] \quad (3.54)$$

where t_{cm} and $\bar{t}_{ca}$ can use the same expressions

given for the first model except that y_m and t_E in Equ.(3.45) should be replaced by f_s and t_S respectively.

For large char particles such that $f_s \approx 0$, Equ.(3.54) simplifies to Equ.(3.52), indicating no difference between the two models for large particles.

3.3.3 Combustion with withdrawal

In this section, we consider that both elutriation and withdrawal carbon losses are significant, and the mother char particle is consumed by combustion and attrition processes. Consider first an FBC system that is continuously fed mono-size char particles at a constant rate. When the amount of carbon withdrawal is significant, the reduction of the value of MCRT due to withdrawal equals the fractional MCRT of the portion withdrawn:

$$t_r = t_{ro} - Z\overline{t_{ri}} \qquad (3.55)$$

where subscripts o and i denote values for the original char particle and the withdrawn particles respectively. The value for the withdrawn particles is the MCRT that they would have if they were fed back into the combustor, and does not include any time spent in the bed before withdrawal. Both t_{ro} and $\bar{t}_{Ri}$ represent the MCRT of burning the denoted particles without carbon withdrawal. Thus t_{ro} can be obtained directly from the

expressions of the last sections.

To develop expressions for $\bar{t}_{ri}$ one should include all withdrawn particles, both mother and attrited. However, the fine attrited particles have short residence times, hence present a low inventory. Therefore, the attrited fines are neglected and only the mother particles are considered in the withdrawn stream. Note that $\bar{t}_{ri}$ is then a mean value for all mother particles of various sizes reduced from the original size in the bed.

Similar to the development in the last section, the MCRT for a single withdrawn particle is equal to the mean residence time associated with the mother particle plus the fractional MCRT of the attrited fines. Note that the mother and attrited particles mentioned here refer to the particles which would result if the withdrawn particle was reburnt, not to be confused with those before withdrawal. Equivalent to Equ.(3.43),

$$t_{ri}=t_{di}+f_{ai}\overline{t_{ra}} \qquad (3.56)$$

Model 1: By applying Equ.(3.29), the value of t_{di} can be deduced from its ideal counterpart, t_{di}^*. Also, defining t_{de}^* to be the ideal mean consumption time for carbon associated with a particle of elutriable initial size (the mother particle) to be

consumed by combustion and attrition simultaneously, we have, equivalent to Equ.(3.40),

$$y_{mi}=\left(\frac{t_{de}^{*}}{t_{di}^{*}}\right)^{n} \qquad (3.57)$$

Substituting this into Equ.(3.29) written for d_i, and using the fact that nj=n+1 gives

$$t_{di}=t_{di}^{*}-y_{mi}t_{de}^{*} \qquad (3.58)$$

The mean value, $\bar{t}_{ri}$, is found by integration over all mother particles:

$$\overline{t_{ri}}=\int_{t_{de}^{*}}^{t_{do}^{*}} t_{ri}E_{ti}dt_{di}^{*} \qquad (3.59)$$

where E_{ti} is the ideal (no elutriation and withdrawal loss) mean carbon consumption time distribution function of the withdrawn particles; it represents the size distribution of these particles at the moment of withdrawal. Note that $E_{ti}dt_{di}^{*}$ is the fraction of carbon mass (not particles) represented by particles having a mean ideal time value between t_{di}^{*} and $t_{di}^{*}+dt_{di}^{*}$. By inserting Equs.(3.56) and (3.58) into (3.59) we obtain

$$\overline{t_{ri}} = \int_{t_{de}^*}^{t_{do}^*} t_{di}^* E_{ti} dt_{di}^* - t_{de}^* \int_{t_{de}^*}^{t_{do}^*} y_{mi} E_{ti} dt_{di}^* + \overline{t_{ra}} \int_{t_{de}^*}^{t_{do}^*} f_{ai} E_{ti} dt_{di}^* \qquad (3.60)$$

Please note that f_{ai} and y_{mi} are the fractions of the attrition and elutriation respectively that would occur if the withdrawn particles were reburnt - not the same as the attrition and elutriation that occurred before withdrawal. Both f_{ai} and y_{mi} vary with the size of the withdrawn particles while $\bar{t}_{ra}$ and t_{de}^* are constants. The value of $\bar{t}_{ra}$ can be obtained by Equ.(3.42), and that of f_{ai} can be found by Equ.(3.10), where the ratio $Q_a/(Q_a+R_m)$ is independent of the size of the withdrawn particles since Q_a is assumed proportional to R_m.

The method of obtaining the distribution function E_{ti} is by first obtaining the carbon age distribution function of the withdrawn particles and then transforming it to E_{ti}. Since perfect mixing is assumed, there is no difference between the distribution of the withdrawn particles and that of the remaining particles in the fluidized bed. The age distribution based on carbon fraction, E_{ai}, can be obtained from the age distribution based on the particle number fraction, P_{ai}:

$$E_{ai}dt=\frac{m_p(t)\,P_{ai}dt}{\int_0^{t_E} m_p(t)\,P_{ai}dt} \qquad (3.61)$$

where $m_p(t)$ is the carbon mass of a char particle at age t, which can be expressed in terms of m_{po}, the original carbon mass at t=0:

$$m_p(t)=(1-x)\,m_{po} \qquad (3.62)$$

Also, for a well-mixed reactor (Levenspiel, 1972),

$$P_{ai}=\frac{1}{\tau}e^{-t/\tau} \qquad (3.63)$$

where τ is the mean residence time for the bed (Equ.(3.17)). Combining Equ.(3.61) to (3.63),

$$E_{ai}=\frac{(1-x)\,e^{-t/\tau}}{\int_0^{t_E}(1-x)\,e^{-t/\tau}dt} \qquad (3.64)$$

Equ.(3.64) can be integrated and solved providing that the relation between x and t is given. However, in most FBC operations, the value of τ is much larger than t_E, since the concentration of carbon in the bed is low, in which case the term $e^{-t/\tau}$ is roughly equal to 1 and can be eliminated from both the numerator and the denominator. Integration of the simplified equation gives (see Equ.(3.29)),

$$E_{ai}=\frac{(n+1)\,(1-\frac{t}{t^*_{Bo}})^n}{t^*_{Bo}(1-y^j_{mo})} \qquad (3.65)$$

where $y_{mo} = (t_{de}^*/t_{do}^*)^n$.

Since the residence time left for a burning particle at any time equals the difference between its burnout time and its age, the withdrawn carbon residence time distribution should be a mirror image to that of the carbon age (see Fig. 3.2). By replacing t with $t_{Bo}^*-t_B^*$, where t_{Bo}^* and t_B^* are the ideal burnout times of the original char and the particle at age t respectively, the mean carbon burnout time distribution of the withdrawn particles is:

$$E_{bi}=\frac{(n+1)\,(t^*_B/t^*_{Bo})^n}{t^*_{Bo}(1-y^j_{mo})} \qquad (3.66)$$

Because $t_d^* \propto t_B^*$, the t_d^* distribution function, E_{ti} has the same form as E_{bi}, or

$$E_{ti}=\frac{(n+1)\,(t^*_{di}/t^*_{do})^n}{t^*_{do}(1-y^j_{mo})} \qquad (3.67)$$

The MCRT of the withdrawn particles can be obtained by substituting E_{ti} from Equ.(3.67) into Equ.(3.60) and integrating the three integrals (using

Equ.(3.57)). The integrals in the first, second, and third terms on the right hand side of the equation are the mean values of t_{di}^*, y_{mi}, and f_{ai} respectively of the withdrawn mother particles, and can be expressed, after integration, as:

$$\overline{t_{di}^*} = \frac{n+1}{n+2} \frac{(1-y_{mo}^{j+\frac{1}{n}})}{(1-y_{mo}^{j})} t_{do}^* \qquad (3.68)$$

$$\overline{y_{mi}} = (n+1)\, y_{mo} \frac{1-y_{mo}^{\frac{1}{n}}}{1-y_{mo}^{j}} \qquad (3.69)$$

$$\overline{f_{ai}} = \frac{Q_a}{Q_a+R_m} \left[1-(n+1)\, y_{mo} \frac{1-y_{mo}^{\frac{1}{n}}}{1-y_{mo}^{j}}\right] \qquad (3.70)$$

Model 2: Except for Equ.(3.70), the above developments for the first model can also be applied to the second model by replacing y_{mi}, y_{mo}, t_E, and t_{de}^* with f_{si}, f_{so}, t_S, and t_{ds}^* respectively in the equations. Similar to the introduction of t_{de}^* in model 1, t_{ds}^* is defined as the ideal mean carbon consumption time for carbon associated with a particle of maximum attrited particle size, (which is also the size of a mother particle at the stage of the final split), to be consumed by both attrition and combustion processes simultaneously. To obtain f_{ai}

for the second model, since Equ.(3.12) should be used instead of Equ.(3.10), the result is:

$$\overline{f_{ai}}=\frac{Q_a}{Q_a+R_m}-(n+1)\frac{1-f_{so}^{\frac{1}{n}}}{1-f_{so}^{j}}\left(\frac{Q_a}{Q_a+R_m}-1\right)f_{so} \qquad (3.71)$$

3.4 Combustion Efficiency

3.4.1 Combustion without carbon withdrawal

When carbon withdrawal is insignificant, the source of carbon loss is from elutriation alone. In order to evaluate carbon efficiency according to Equ.(3.6) and (3.9) or (3.11), knowledge of the attrition and elutriation fractions is required.

Model 1: When applying the first model for burning a char particle or mono-sized char particles, Equ.(3.10) represents f_a as a function of y_m. Equ.(3.44) also involves these two variables. If all the other variables in these equations can be found, including Y_a, they can be solved simultaneously. The resulting value of f_a can then be used in Equ.(3.9) to obtain y, the elutriation carbon loss. The following will identify the required parameters and the methods to evaluate them will be given in the

next section.

Attrition rate and combustion rate appear to be required from Equ.(3.10). Fortunately, we need only to know their ratio, which is assumed to be unaltered during combustion of char particles despite their shrinkage.

Equ.(3.44) is more complicated and involves more variables. In order for all variables to be measurable, the first term on the right hand side of the equation, t_{cm}, is expressed in terms of y_m and t_{re}^*. By applying the relationship of Equ.(3.29) and the equivalent of Equ.(3.57),

$$t_d = y_m^{-\frac{1}{n}} (1-y_m^j)\, t_{de}^* \tag{3.72}$$

Also, equivalent to Equ.(3.47),

$$t_E = (n+1)\,(t_d^*-t_{de}^*) = (n+1)\,(y_m^{-\frac{1}{n}}-1)\, t_{de}^* \tag{3.73}$$

Substituting Equ.(3.72) and (3.73) into (3.45),

$$t_{cm} = (n y_m \frac{1-y_m^{-\frac{1}{n}}}{1-y_m} + y_m^{-\frac{1}{n}})\, t_{de}^* \tag{3.74}$$

The parameter t_{de}^* can be transformed to the ideal MCRT of the particle shrinking by combustion alone,

$$t_{de}^{*}=\frac{R_m}{Q_a+R_m}t_{re}^{*} \qquad (3.75)$$

Equ.(3.51) presents another variable $\bar{t}_{ca}$ in terms of t_{re}^{*} and t_{rs}^{*}. To help easily follow the above described relations, a diagram which links combustion efficiency η to the parameters to be measured is given in Fig. 3.3. With equations represented by numbers within bracket, this figure shows that besides knowledge of the reaction regime to determine the values of n and j, the variables required to be measured are t_c, t_{re}^{*}, t_{rs}^{*}, Y_a, Q_a and R_m. Of course, the last two variables have to be measured at the same burning stage to give their ratio.

Model 2: In applying the second model, Equ.(3.12) and (3.54) are used to solve simultaneously for f_a and f_s. The same procedure as previously described for the first model can be used to represent t_{cm} in terms of t_{rs}^{*} and f_s. The result shows that the same variables are required for this model.

For large char particles, y_m and f_s are small and can be neglected. Equs.(3.9) and (3.10), or (3.11) and (3.12), show that y is determined by Y_a, Q_a, and R_m only; thus the number

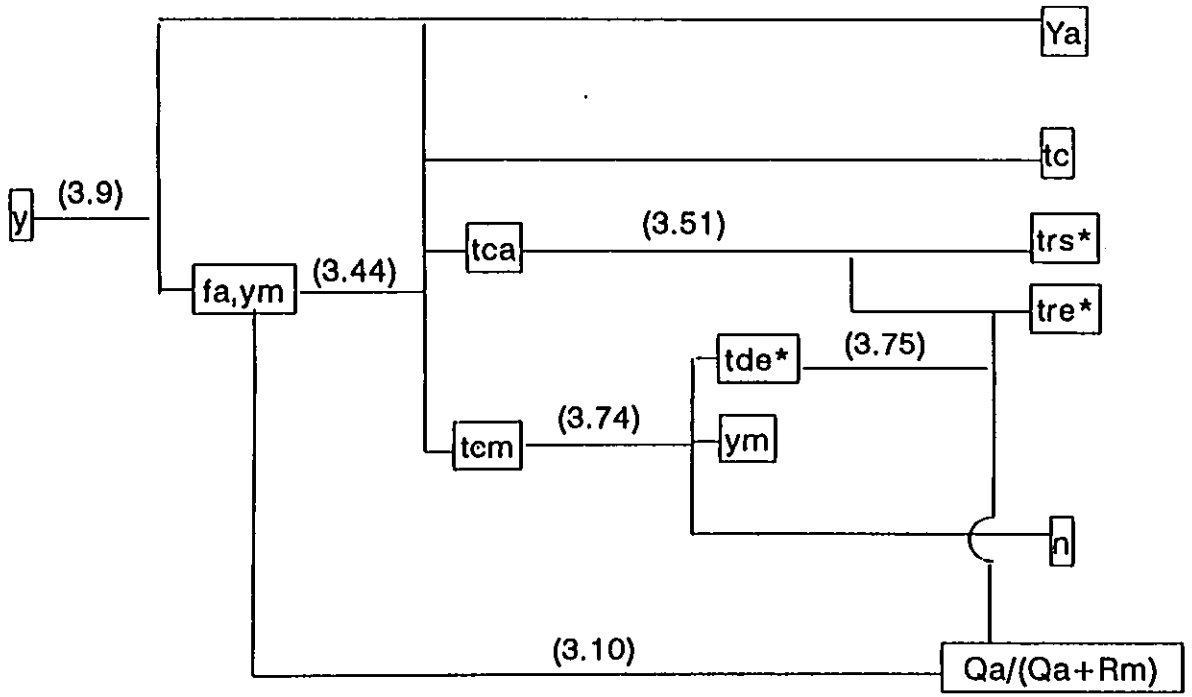

Fig. 3.3: Calculation of y from parameters - no withdrawal

of required variables is reduced. However, large particles are usually associated with high carbon withdrawal, and the same variables are still required for Z evaluation, as shown in the following section.

3.4.2 Combustion with carbon withdrawal

In this case both y and Z are important for evaluating combustion efficiency. If t_{ro}, $\bar{t}_{ri}$, and τ are known, the value of Z, together with t_r, can be obtained by solving Equs.(3.17) and (3.55) simultaneously. Equ.(3.43) can be used to represent t_{ro} in terms of t_{do}, f_a, and $\bar{t}_{ra}$, which in turn are determined by $Q_a/(Q_a+R_m)$, t_{re}^*, t_{rs}^*, and y_{mo} (for the first model) or f_{so} (for the second model) from Equs.(3.10) or (3.12), (3.42), (3.72), and (3.75). Similarly, $\bar{t}_{ri}$ can be found to be a function of the same parameters when examining Equs.(3.42), (3.60), (3.68) to (3.72), and (3.75). Fig. 3.4 shows how withdrawal loss fraction Z links with the parameters to be measured for model 1. The figure shows that, except for adding τ, the same parameters mentioned in the last section for evaluation of y when no carbon withdrawal are required to evaluate Z for the present case with carbon withdrawal. Note that the subscript o denotes the original char particle burning without carbon withdrawal; thus y_o and y_{mo} can be obtained through the development of the last section. The value of τ is determined by the size of the combustor, the

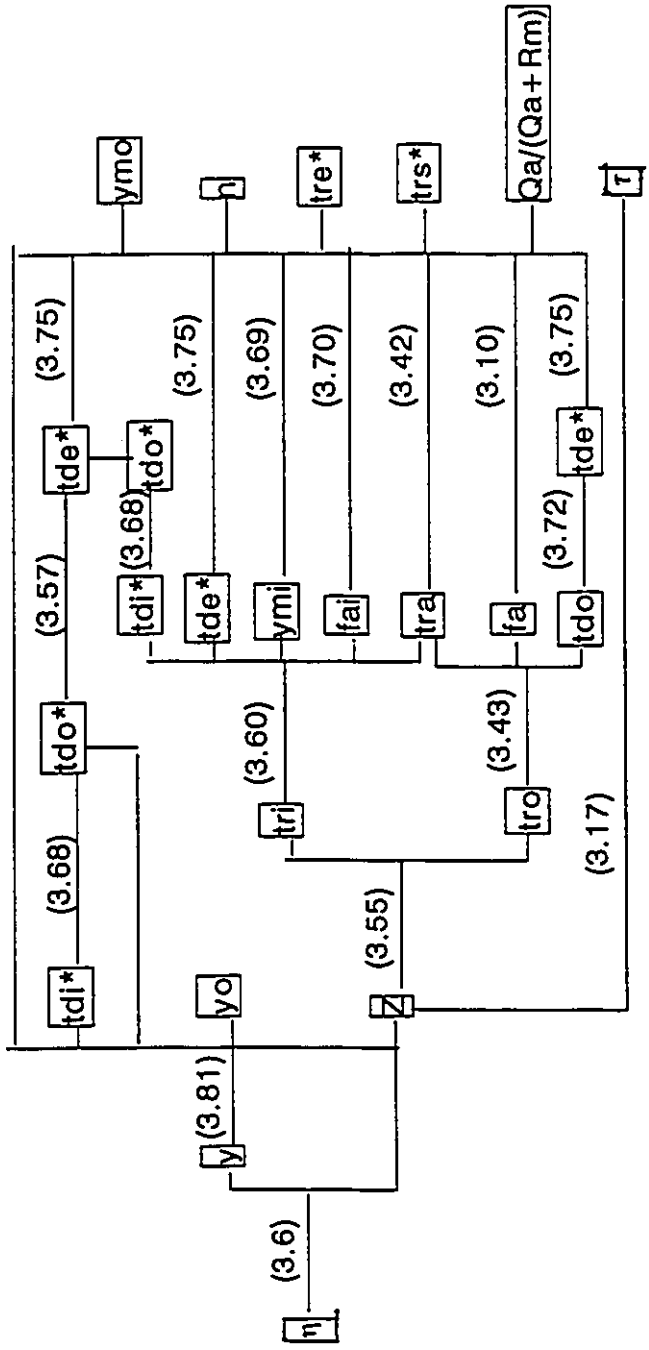

Fig. 3.4: Calculation of η from parameters - with withdrawal

operating conditions, the coal and limestone feed rates and the coal ash content.

In order to obtain the elutriation fraction y, we introduce the withdrawn particle fraction f_{pw}. (ie the number of mother particles withdrawn per number of particles fed), and f_w, the carbon fraction remaining in the withdrawn particles, so that,

$$y=\frac{(1-f_{pw})\,y_o+f_{pw}(1-f_w)\,Y_w}{1-f_{pw}f_w} \qquad (3.76)$$

where y_o and Y_w are the elutriation mass fractions of the burning char particles without carbon withdrawal and of the consumed carbon mass of the withdrawn particles prior to their withdrawal respectively. Since mono-sized feed is assumed, f_{pw} represents the mass as well as the number fraction of the original particles entering the bed. Note that y is based on the non-withdrawn portion, not on the total feed (cf. Equ.(3.4)). Since y_o represents non-withdrawn particles, its value is identical to the elutriation fraction y obtained from the case of combustion without carbon withdrawal given in Section 3.4.1. A schematic to illustrate the carbon balance for char combustion with withdrawal is given in Fig. 3.5.

The value of f_w can be obtained as:

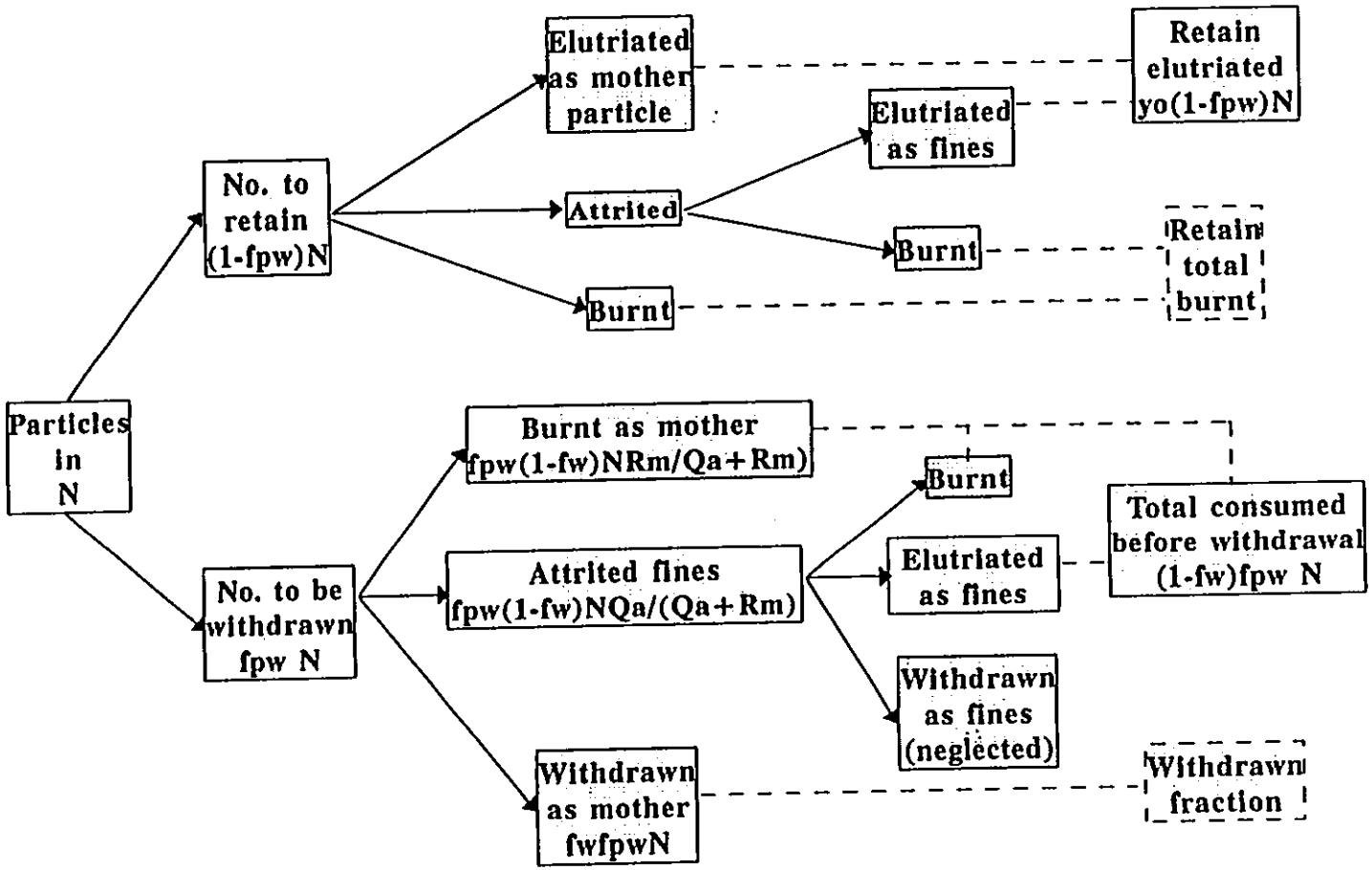

Fig. 3.5: Carbon balance with withdrawal

$$f_w=(\frac{\overline{d_i}}{d_o})^3=(\frac{\overline{t_{di}^*}}{t_{do}^*})^n \qquad (3.77)$$

The ratio $\bar{t}_{di}^*/t_{do}^*$ is given by Equ.(3.68) and is shown to be a function of y_{mo}. Also, f_{pw} is related to Z as:

$$f_{pw}=\frac{Z}{f_w}=\frac{Z}{(\frac{\overline{t_{di}^*}}{t_{do}^*})^n} \qquad (3.78)$$

Because the sizes of the withdrawn particles are larger than d_e or d_s, the elutriation loss of these particles prior to withdrawal is contributed by attrited fines only, or,

$$Y_w=\frac{Q_a}{Q_a+R_m}Y_a \qquad (3.79)$$

Model 1: For this model, the attrition-reaction ratio can be eliminated by using Equ.(3.10), thus Y_w is related to y_o as (cf. Equ.(3.9)):

$$Y_w=\frac{f_aY_a}{1-y_{mo}}=\frac{y_o-y_{mo}}{1-y_{mo}} \qquad (3.80)$$

Note that f_a is the attrition fraction of the material which is not withdrawn. Combining Equs.(3.76) to (3.80),

$$y=y_o-\frac{Z}{1-Z}[(\frac{t_{di}^*}{t_{do}^*})^{-n}-1][\frac{y_{mo}(1-y_o)}{1-y_{mo}}] \qquad (3.81)$$

Model 2: For the second model, combining Equs.(3.12) and (3.79) gives

$$Y_w=\frac{(f_a-f_s)\,Y_a}{1-f_s}=\frac{y_o-f_sY_a}{1-f_s} \qquad (3.82)$$

where $f_aY_a=y_o$ since no elutriation of mother particles occurs. The elutriation fraction y is,

$$y=y_o-\frac{Z}{1-Z}\left[\left(\frac{t^*_{di}}{t^*_{do}}\right)^{-n}-1\right]\left[\frac{f_s(Y_a-y_o)}{1-f_s}\right] \qquad (3.83)$$

The above equations show that irrespective of which of the two models is used to evaluate y, no additional variable requires to be measured. Applying model 1, Fig. 3.4 shows that y links to the same parameters required by the case of without withdrawal as given in the last section. In addition, for most FBC operations, the second term in Equ.(3.81) or (3.83), is small compared to y_o, and can be neglected. Then the elutriation fractions with and without carbon withdrawal are not significantly different.

3.4.3 Multi-size Particles

The developments so far describe only the case of a single char particle, or mono-size particle combustion. For burning multi-size particles, we first assume that they are all initially larger than the elutriable size.

Model 1: By examining Equs.(3.9) and (3.10) for the first model with no withdrawal it can be seen that y_m is the only variable which varies with particle size. Combining these two equations and integrating over all size fractions, the overall elutriation fraction is,

$$Y=\frac{Q_a}{Q_a+R_m}Y_a+(1-\frac{Q_a}{Q_a+R_m}Y_a)\int_{d_e}^{\infty}y_m E_{df}dd_c \qquad (3.84)$$

where $E_{df}dd_c$ is the carbon mass fraction of particles of size between d_c and d_c + dd_c. The integral part of the equation is the mean value of mother particle elutriation fraction Y_m. This mean value relates to the mass mean diameter, d_{30}, and the y_m value of any particle of size d_c, which is larger than d_e, as

$$Y_m=(\frac{d_e}{d_{30}})^3=(\frac{d_c}{d_{30}})^3 y_m \qquad (3.85)$$

In order to find Y_m, first substitute Equ.(3.10) into (3.43) and integrate over all size fractions,

$$\overline{t_c}=\overline{t_{cm}}+\frac{\frac{Q_a}{Q_a+R_m}(1-Y_a)}{1-\frac{Q_a}{Q_a+R_m}Y_a}\overline{t_{ca}} \qquad (3.86)$$

where $\bar{t}_c$ and $\bar{t}_{cm}$ are mean values for all char particles. The second term on the right hand side

of the equation is independent of particle size. The first term can be expressed in terms of Y_m by inserting Equ.(3.85) into (3.74) and integrating,

$$\bar{t}_{cm}=t^{*}_{de}\int_{d_*}^{\infty}[nY_m(\frac{d_{30}}{d_c})^3\frac{1-Y_m^{-\frac{1}{n}}(\frac{d_{30}}{d_c})^{-\frac{3}{n}}}{1-Y_m(\frac{d_{30}}{d_c})^3}+Y_m^{-\frac{1}{n}}(\frac{d_{30}}{d_c})^{-\frac{3}{n}}]E_{df}dd_c \quad (3.87)$$

Equs.(3.84),(3.86) and (3.87) show that the same previously stated variables for burning mono-size particles are required, except that t_c is replaced by $\bar{t}_c$, to evaluate Y_m and Y providing that the char particle size distribution is known. Alternatively, Y_m can be deduced from a pre-evaluated value of a single char particle size by using Equ.(3.85).

Model 2: For the second model, evaluation of Y requires determining the mean value of f_s. Combining Equs.(3.11) and (3.12)

$$Y=[\frac{Q_a}{Q_a+R_m}+(1-\frac{Q_a}{Q_A+R_m})\int_{d_*}^{\infty}f_sE_{df}dd_c]\,Y_a \quad (3.88)$$

The integral part of the equation can be obtained in a similar manner to Y_m of the first model, except that both terms on the right hand side of Equ.(3.54) are particle size dependent and require

to be integrated separately.

When withdrawal is significant, evaluating Z involves more complicated functions. However, equations (3.10), (3.12), (3.17), (3.42), (3.43), (3.55), (3.60), (3.68) to (3.72), and (3.75) illustrate that all size dependent variables involved can be expressed in terms of y_m or f_s. The value of Z can then be obtained by integration over all size fractions.

If a significant number of char particles are finer than the elutriable size, the elutriation fraction of that portion is equal to 1. On the other hand, if all char particles are quite large or y_m or f_s are negligible, carbon loss is independent of particle size and can be obtained the same way as for mono-sized particles.

3.5 Concluding Remarks

This chapter describes the model development for FBC combustion efficiency prediction. The development involves both combustion reaction and particle attrition kinetics, using only fundamental reaction engineering concepts, such as material balances, the shrinking particle model and reactor residence time, and simple mathematics. The result is two slightly different models with a very different approach from

"traditional" models.

It is well known that in order to predict combustion efficiency, information on reaction and attrition kinetics is required. In addition, the estimation of the fractional losses of both mother and attrited particles requires the knowledge of the particle sizes of these particles and those elutriated. To obtain the rate constant and the particle size information involved in these processes is extremely difficult if not impossible. The present models attempt an indirect method by introducing various mean time parameters to characterize the kinetics of the corresponding particles with sizes in question.

The model development starts with a simple case of burning a single char particle. In order to estimate combustion efficiency, a number of equations have been developed to link η to the parameters to be measured n, t_c, τ, t_{re}^*, t_{rs}^*, Y_a, and $Q_a/(Q_a+R_m)$ (Figs. 3.3 and 3.4). According to these models, except for n and t_c the parameters are independent of particle size and progress of conversion. Experimental techniques using bench-scale FBC facilities for measuring these model parameters are developed and are given in the next two chapters. For multi-size char feeding, the same parameter information is needed with the original particle size distribution of the char being the only

additional requirement. In general FBC of coal, this information can only be obtained by fragmentation studies.

The only difference between the two models results from the handling of the final combustion stage of char particles. For large char particles such that the end portion y_m or f_s can be neglected, the models become simpler and are identical.

4 EXPERIMENTAL

In order to evaluate the required model parameters stated in Section 3.4, novel experimental methods are developed. This chapter describes the experimental details, and the parameter evaluation techniques from experimental data are given in the next chapter.

4.1 Equipment

4.1.1 Combustor system

The bench-scale combustor is built specifically for FBC kinetic measurements and is shown schematically in Fig. 4.1. The rig is fabricated of no. 310 stainless steel to ensure adequate performance up to temperatures of 1000°C. Its dimensions are 0.1 m ID, enlarged to 0.2 m at the upper freeboard section, and 1.17 m high.

The combustor is heated externally by electrical elements divided into four individually controlled sections. The combustor is thermally insulated. Either air, nitrogen or a mixture of these can be supplied as the fluidizing gas into the combustor. An electrically operated three-way solenoid valve allows the sudden interchange of the inlet gas for rapid starting or to freeze the oxidation reaction in the combustor.

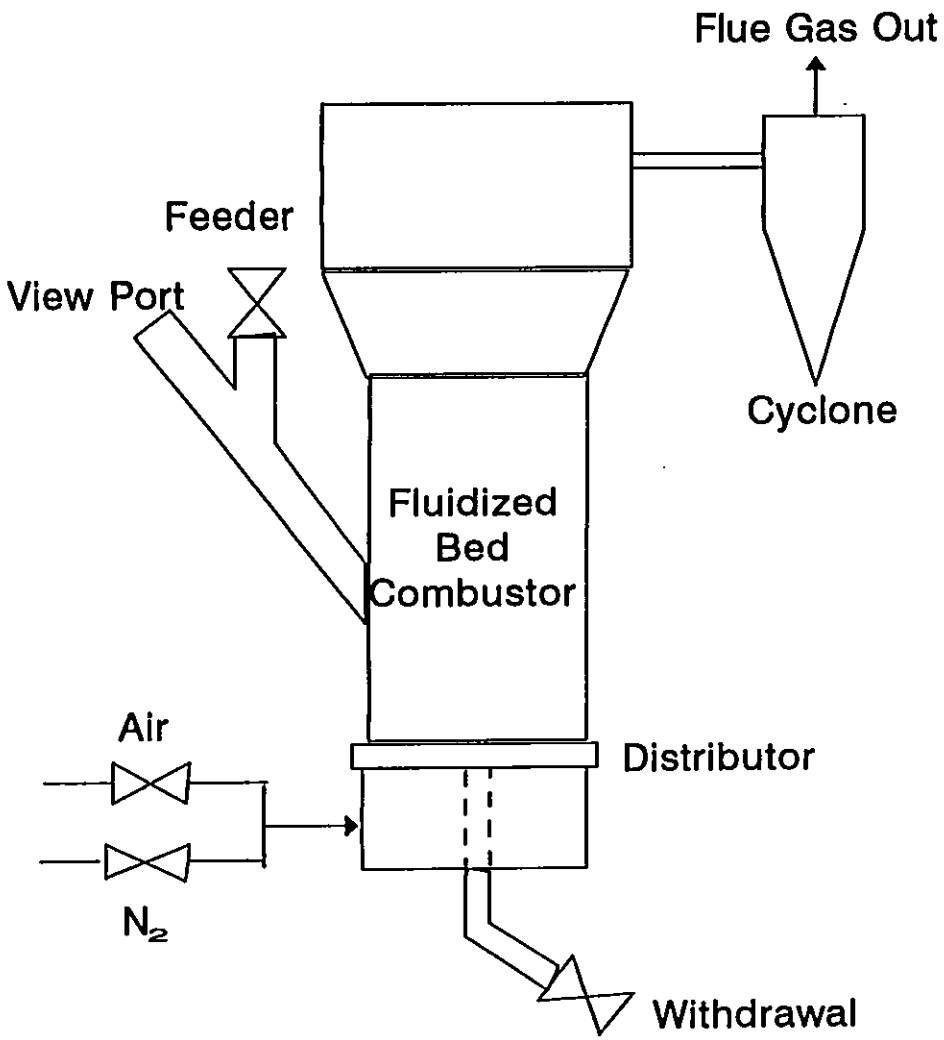

Fig. 4.1: Schematic diagram of bench-scale fluidized bed combustor

Inlet gas is preheated to about 600-700°C in tubing wrapped around the windbox before being passed through the distributor into the bed. Three Sierra Series 840 mass flow controllers are used to regulate the inlet and the feeder purging gas flows.

The gas distributor is a 6.35 mm thick stainless steel perforated plate with 14 holes 1.59 mm dia arranged in 25.4 mm triangular pitch. A 44 μm size stainless steel screen is attached underneath the distributor to prevent weeping of bed solids through the orifices.

Solid fuel is fed batchwise through a slanted pipe, at an angle of 60 degrees to the horizontal, with its lower end located just above the fluidized bed level. A viewport glass covering the other end of the pipe provides a clear view of the top of the bed during combustion operation, and permits verification of successful feeding and ignition. Above the pipe there is a vertically affixed feeder assembly which consists of two ball valves in series. The lower valve is operated electrically by a switch which has two other functions. When the switch is turned on, it actuates a solenoid valve to shift the direction of a pneumatic gas jet from sweeping the dust off the viewport glass to washing down solid fuel particles in the feeder. Simultaneously, a combustion experiment start signal is sent to a computer. The

time for valve opening and feeder purging is controlled by a timer adjusted from 1 to 10s. Alternatively, fine, potentially sticky solid fuels are fed by a water-cooled pneumatic jet feeder inserted through the slanted pipe.

Bed solids can be withdrawn into a cooling drum through a 19 mm dia down pipe which is welded near the centre of the distributor and passes vertically downward through the windbox. An in-line full port ball valve is used to control solid flow. Nitrogen as an inert cooling gas enters the drum at a flow rate equal to the minimum fluidization velocity or lower and exits through a top valve which provides pressure control.

Particles elutriated from the bed are collected by a cyclone, 63 mm dia, and a high temperature porous stainless steel filter in series. A graduated 12.7 mm dia glass tube, which is joined to the lower end of the cyclone, provides a qualitative indication of the amount elutriated.

4.1.2 Gas sampling, analyzing, and recording

The flue gas samples to be analyzed are continuously drawn during experiments from a point downstream of the porous metal filter by a vacuum pump. The sampling gas flow schematic is given in Fig. 4.2, which shows that the gas

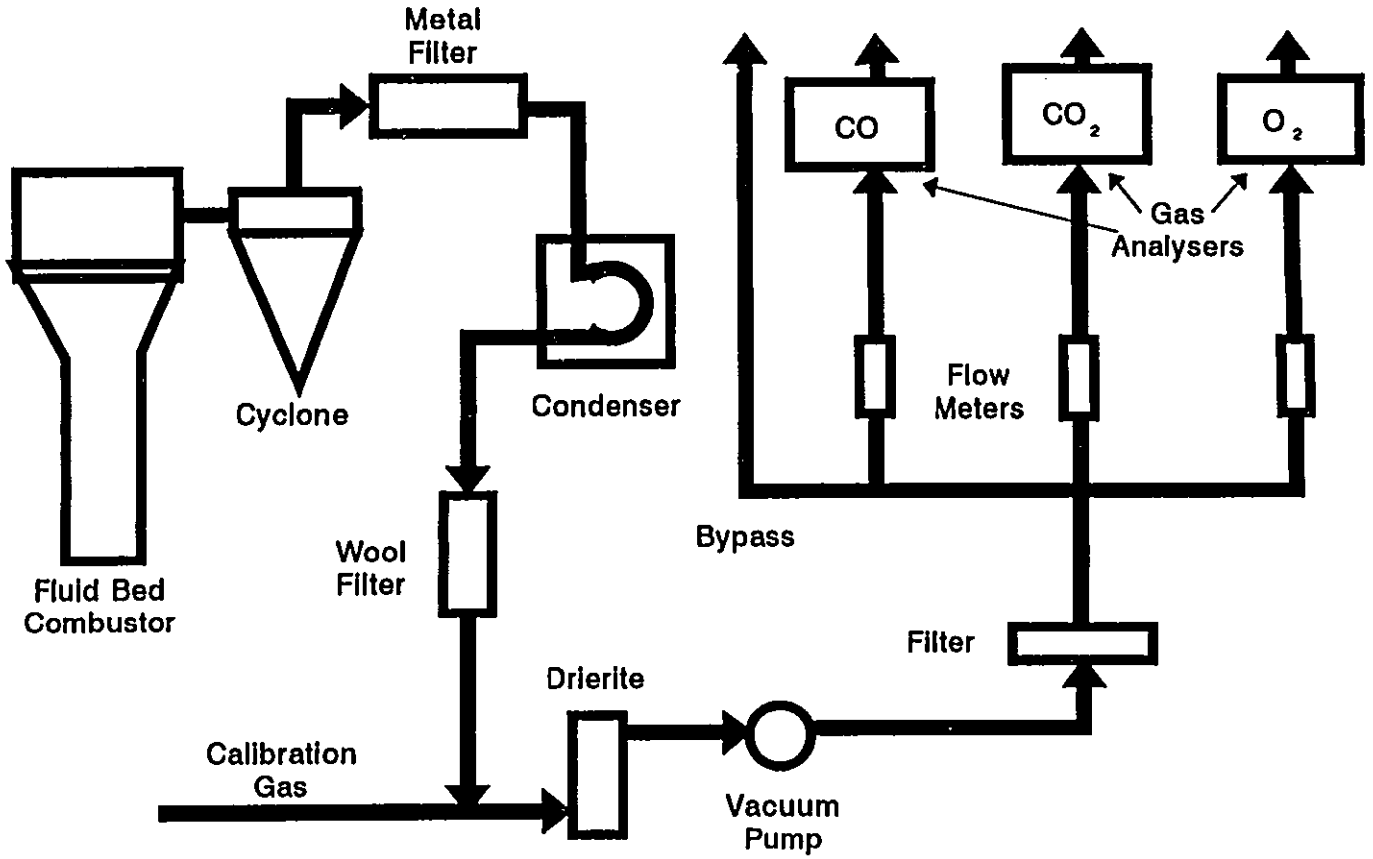

Fig. 4.2: Schematic diagram of sampling gas flow

sample is dried and cleaned by passing through a condenser, in-line filters, and a moisture absorber prior to entering various gas analyzers.

Two infrared analyzers are used for CO and CO_2 measurements and a paramagnetic analyzer for O_2. A flame ionization analyzer is also available for measuring the total concentration of hydrocarbons when required.

The analog signals generated from the gas analyzers, thermocouple, pressure transducers, and the fuel valve switch are converted to digital form by a data logging system, then stored and analyzed by a mini-computer.

4.2 Materials

The fluidized bed is composed of about 1.5 kg of silica sand with a density of 2600 kg/m^3 and an arithmetic mean size of 0.5 mm, with a narrow size range, which gives a static bed height of about 0.12 m in the combustor. Another 0.17 kg of sand is packed above the valve in the solids withdrawal pipe. This portion of sand does not participate in fluidization, but provides a cushion layer in the cooling drum for falling bed solids during the withdrawal operation.

Coals used in the present work, ranked from anthracite to

lignite, are listed in Table 4.1, where symbols used to represent them are bracketed. Raw mined coals are usually washed to reduce the ash and mineral content. In order to establish the effect of ash content without the complicating effect of other coal properties, samples of a freshly mined, high volatile coal (Prince coal) having the same origin but different cleaning histories were obtained. They are raw coal, coal washed by a deep cleaning process, and coal washed by a medium cleaning process. The coals were subjected to proximate analysis, i.e., volatile, ash, and fixed carbon contents, ultimate analysis, and the determination of the free swelling index, FSI. The analytical results presented in dry base (db%) are also given in Table 4.1.

Chars were prepared by devolatilizing the coals using the same bench-scale apparatus and under similar combustion conditions as most of the experiments (850°C and fluidized with air). Although only narrow range large sized coal particles (above 8 mm) were used, the product chars have a wide size distribution because of primary fragmentation. With a few exceptions, only particles larger than 4 mm were used in experiments.

4.3 Procedure

The required model parameters for predicting combustion

Table 4.1: Coal Analysis

Coal Type	Proximate Analysis (%db)			Carbon Content (%db)	FSI
	Volatile Matter	Fixed Carbon	Ash		
Quintette (B) (Medium-Vol. Bituminous)	22.28	71.71	6.01	81.60	0.5
Evans (C) (High-Vol. Bituminous B)	36.37	55.24	8.39	70.47	0.75
Coal Valley (G) (High Vol. Bituminous C)	35.14	56.44	8.42	70.47	-
Bienfait (E) (Lignite)	40.92	49.01	10.07	63.36	-
Mt. Clappan (H1) (Anthracite)	6.80	68.20	25.00	70.00	-
Prince (F2) (High Vol. Bituminous A) Raw	29.69	43.54	26.77	56.90	2.75
Prince (F3) Deep Cleaned	38.39	58.12	3.49	80.03	5.50
Prince (F4) Medium Cleaned	36.38	52.92	10.70	72.13	2.5

efficiency have been given in Section 3.4. Two experimental series with different procedures are required to provide the necessary data for their evaluation.

4.3.1 Combustion studies - 1st series

With the purpose of obtaining the mean carbon conversion time t_c and the exponent n, this series of experiments simply burns char particles batchwise to completion in the bench-scale fluidized combustor.

The bed of inert sand particles is fluidized with air and preheated electrically to the desired bed temperature condition. The windbox heater is controlled at 700°C to provide gas preheating, while temperatures at the upper and lower freeboard sections are controlled below 400°C and 600°C respectively. The freeboard is maintained at a low temperature to minimize combustion of particles elutriated from the bed.

After the bed reaches the desired temperature, the fluidizing gas is adjusted to the designated conditions of oxygen concentration and superficial gas velocity. When steady state approaches, a weighed solid fuel sample is fed overbed into the preheated bed zone. The flue gas compositions, bed and freeboard temperatures are recorded

continuously until CO and CO_2 concentrations return to zero. Specially written computer programs run on a mini-computer are then used to analyze data, calculate results, and plot appropriate combustion curves.

4.3.2 Fragmentation and attrition studies - 2nd series

The purpose of the second experimental series is to provide information for evaluating the parameters relating to attrition. The method is to first abruptly freeze the reaction of a batch of burning chars in the fluidized bed, following by separation of the attrited fines from the mother particles using proper screens. Finally, the attrited fines are returned to the bed and burnt to completion with a low superficial gas velocity to approximate ideal combustion conditions (ie no elutriation). Thus the second series experiments involve two kinds of sub-experiment. In order to avoid confusion between them, the experiments burning the original char particles (including mother and attrited particles) are called the maintests, and those later burning only the retrieved attrited fines are called sub-tests.

For the maintests, char burning operations are similar to those of the combustion studies experiments described in last section, except that the reaction is frozen at a pre-determined burning period by suddenly shifting to inert gas

(nitrogen) fluidization. The whole bed of hot solids is transferred out of the reactor into the cooling drum where it is cooled to near room temperature with a nitrogen stream. The system has been designed for gently transporting and cooling hot solids to avoid further significant particle breakage. The cooled char solids are separated from the sand and attrited fines by sifting using a specified screen. The screen size is determined by preliminary experiments which are designed to distinguish the size of mother particles from that of attrition. The solid fuel particles (excluding attrited fines) before and after combustion are counted and individually weighed. To avoid attrition effects being complicated by combustion, only particles of a size that would not shrink (due to reaction) to smaller than that of the screen during the combustion period are used. In the present work, this cut size is assigned to be 3.4 mm for a burning period of 2.5 min as given in Table 4.2, which also lists the other operating conditions of both experimental series. Note that oxygen concentration conditions were controlled by mixing air with nitrogen as inlet fluidizing gas; for simplicity, this operating condition is represented by the percentage of air in the gas mixture.

The attrited carbon inventory in the bed (the undersized fine char particles mixed with the sand) is retrieved from the sub-test. Similar operating conditions to that of the burning

Table 4.2: Operating conditions

Operating Conditions	1st Series	2nd Series	
		Main test	Sub-test
Particle Size (mm)	0.84 - 25.0	> 3.4	< 1.0
Sample Size (g)	2.2 - 6.5	3.1 - 5.9	-
Superficial Gas Velocity (m/s)	0.8 - 0.9	0.8 - 0.9	0.1 - 0.2
Bed Temperature (°C)	700 - 900	700 - 900	700 - 900
Inlet gas air %	25 - 100	25 - 100	25 - 100
Burning Time (min)	To End	2.5	To End

mother char particles are used except that gas flow rate is much lower, about one to two times the minimum fluidization velocity. The carbon inventory and the burning rate results of the attrited carbon combustion test are useful in calculating the attrition rate and related parameters with the techniques developed in the following chapter.

Some experiments designated to study fragmentation and attrition simultaneously under various carbon conversion stages were run consecutively using the same fuel particles. Large coal particles were used in the first experiment and the residual chars (larger than the cut size) were used in the following runs. As described previously, each experimental run includes a main-test and sub-test. The first experiment, with combustion of the main-test terminated at the end of devolatilization period, investigates the effect of primary fragmentation, while the remaining experiments study the secondary fragmentation and attrition behaviour at various stages of burnoff.

5. EVALUATION OF MODEL PARAMETERS FROM EXPERIMENTAL DATA

The required parameters for evaluating combustion efficiency have been given in Section 3.4. The following will present the methods to obtain them. The necessary data for these parameter evaluations are provided by two bench-scale FBC experimental series with different techniques as described in the last section.

5.1 Evaluation of t_c

Only the data from the first series experiments are required to evaluate the value of t_c. The burning rate at any time during combustion and the total carbon conversion, W_c, can be obtained from the CO and CO_2 concentrations as a function of time from the experimental flue gas analysis:

$$R_c = uAM_c(C_{CO}+C_{CO_2}) \tag{5.1}$$

$$W_c = \int_0^{t_B} R_c dt \tag{5.2}$$

where u is the superficial gas velocity, A is the cross-sectional area of the combustor, and M_c is the molecular weight of carbon. Note that t_B represents the burnout time of the batch of char particles, equal to that of the largest char particle in the bed.

To obtain t_c, the previously described concept is applied, in analogy to Equ.(3.19),

$$t_c = \int_0^{t_s} (1-x_c)\, dt \tag{5.3}$$

where x_c is the fractional conversion based on the amount of carbon which burns. The x_c value at any time can be estimated from the reaction rate using the relationship

$$x_c = \int_0^{t} R_c dt / W_c \tag{5.4}$$

5.2 Evaluation of Attrition-Elutriation Parameters

Four of the required model parameters for combustion efficiency evaluation are related to the attrition and/or the elutriation processes. They are t_{re}^*, t_{rs}^*, Y_a, and $Q_a/(Q_a+R_m)$.

5.2.1 Attrition rate and inventory

Information on the attrition-elutriation variables is supplied by the second series of experiments. During the maintests, fine chars generated from attrition in an FBC system are consumed by reaction and subsequent elutriation. Because of the small particle size, a much shorter in-bed life time is expected. In a batch FBC system, a pseudo-steady state for the attrited char particles can be assumed to be

reached after an initial period - the residence time of the largest fine particle generated. Since experiments operate batchwise, Equ.(3.8) for no carbon withdrawal is therefore applicable as a material balance of the attrited carbons in this case.

Also, in analogy to Equ.(3.16) for the original char particles, Q_a can be expressed by the carbon inventory of the attrited fines, W_a, and their MCRT, $\bar{t}_{ra}$:

$$Q_a = \frac{W_a}{\bar{t}_{ra}} \tag{5.5}$$

Combining Equ.(3.8) and (5.5) gives,

$$\frac{\bar{t}_{ra}}{1-Y_a} = \frac{W_a}{R_a} \tag{5.6}$$

For the left hand side of Equ.(5.6), $\bar{t}_{ra}$ is given by Equ.(3.42). In similar fashion to $\bar{t}_{ra}$ (Equ.3.39), $(1 - y_a)$ can be integrated with the same distribution function,

$$1-Y_a = \int_{d_e}^{d_s} (1-y_a)\, E_{da}\, dd_a \tag{5.7}$$

Substituting y_a and E_{da} from Equs.(3.40) and (3.35) respectively and transforming the equation to dimensionless form (using the previously introduced ratios $\lambda = t_{ra}^*/t_{rs}^*$ and $\lambda_e = t_{re}^*/t_{rs}^*$) yields

$$1-Y_a=\frac{\int_{\lambda_o}^{1}(\lambda^3-\lambda_o^3)\,\phi\,d\lambda}{\int_{0}^{1}\lambda^3\phi\,d\lambda} \tag{5.8}$$

Inserting Equs.(3.42) and (5.8) into (5.6) yields

$$\frac{\int_{\lambda_o}^{1}(\lambda^4-\lambda_o^4)\,\phi\,d\lambda}{\int_{\lambda_o}^{1}(\lambda^3-\lambda_o^3)\,\phi\,d\lambda}\,t_{rs}^{\bullet}=\frac{W_a}{R_a} \tag{5.9}$$

The values of W_a and R_a can both be obtained from the results of the sub-test. Since the same attrited fines from the main test are used in the later sub-test, the steady state burning rate R_a of the main test should equal the initial burning rate of the sub-test. Note that although different superficial gas velocities were used between the main test and the sub-test, this should not affect the reaction rate of the attrited fines, since these burn under the kinetically controlled regime.

The attrited carbon inventory W_a can be calculated by integration of the flue gas composition data from the sub-test, similar to the method used for char combustion in the first series experiments, Equs.(5.1) and (5.2),

$$W_a = uAM_c \int_0^{t_s} (C_{CO} + C_{CO_2})\, dt \qquad (5.10)$$

5.2.2 Evaluation of MCRTs for attrited and elutriated particles

The only unknown variables in Equ.(5.9) are t_{rs}^* and t_{re}^* (incorporated in λ_e), the MCRTs for ideal combustion of the largest attrited particles and of the elutriated particles. According to the previous assumptions, t_{rs}^* could be approximated from the burnout time for attrited particle combustion (sub-test), which operates under low superficial velocity condition. However, in practice, it is difficult to determine the burnout time precisely because the CO and CO_2 concentrations produced by burning the few ultra-fine particles at the final stage of combustion are extremely low. The combustion signals are unclear as complications from instrument noise become significant. Also, when a char particle shrinks to a certain small size, internal combustion becomes important and uniform fragmentation may occur. The fine fragments will be elutriated even with a low gas flow rate, since a certain minimum flow rate is necessitated by the requirement of simulating the combustion environment, the temperature and the oxygen concentration of the original char burning test (main test). For reaction under kinetic control, carbon mass and burnout time depend on particle diameter to

different powers, 3 and 1 respectively (Table 2.1), so that, although the carbon fraction of the attrited particles at the stage of internal combustion is small, the difference in burnout time may be significant.

A more accurate method for evaluating t_{rs}^*, also t_{re}^*, is therefore developed by relating the MCRT of the reburnt attrited particles to these parameters. Since post-attrition combustion (after detachment from the mother particle) reduces the attrited particle size, the ideal MCRT of the attrited particles retrieved from the maintest, $\bar{t}_{ria}^*$, is different from that of the original attrited particles at the time of detachment, $\bar{t}_{ra}^*$. For a simple case in which attrition produces only mono-sized char fines at a constant rate, the attrited particles in the bed during the main test will develop, upon reaching pseudo steady state, a size distribution ranging from d_e up to d_a, the initial attrited particle size with a corresponding MCRT t_{ra}^*. Thus the development of the MCRT expression for the reburnt particles is in analogy with that of the withdrawn char particles previously described in Section 3.3.4. Therefore, Equ.(3.68), with n=3 and j=4/3 for kinetic control, can be directly used to show the ideal MCRT of the reburnt attrited particles, t_{ria}^*,

$$t^*_{ria}=\frac{4}{5}\frac{1-y_a^{5/3}}{1-y_a^{4/3}}t^*_{ra} \qquad (5.11)$$

When a normal size distribution is assumed for the original attrited particles, the mean t_{ria}^* for all carbons is,

$$\overline{t^*_{ria}}=\int_{d_e}^{d_s} t^*_{ria}E_{dio}dd_a \qquad (5.12)$$

where $E_{dio}dd_a$ represents the fraction of the attrited carbon mass in the bed having an initial size between d_a and d_a+dd_a.

During the maintest, for any size fraction of the original attrited particles larger than the elutriable size the number of particles in the fluidized bed at steady state having an initial size range d_a to d_a+dd_a is $Q_{pa}(P_{da}dd_a)t_{Ea}$, where P_{da} is the number density distribution function of initial attrited particle sizes (Equ.3.33), Q_{pa} is the numerical attrition rate and t_{Ea} is the residence time of an attrited particle prior to elutriation. Defining P_{aia} as the age distribution function based on the number of particles in the bed having initial size d_a, the average mass of carbon per particle for particles of original size d_a is found by integrating $m_p(t)P_{aia}dt$ over a time period from 0 to t_{Ea}, where $m_p(t)$ is the particle carbon mass. Thus the carbon inventory of that size fraction w_{da} is,

$$w_{da}=Q_{pa}P_{da}dd_a t_{Ea}\int_0^{t_{Ea}} m_p(t)\,P_{aia}dt \qquad (5.13)$$

Since the attrition rate is assumed constant, P_{aia} is a constant equal to $1/t_{Ea}$, where t_{Ea} is a function of d_a. Substituting $m_p(t)$ from Equ.(3.62) and applying the x-t relationship from Table 1 to the integral part of the equation,

$$\int_0^{t_{Ea}} m_p(t)\,P_{aia}dt=\frac{m_{po}}{t_{Ea}}\int_0^{t_{Ea}}(1-\frac{t}{t_{Ba}^*})^3dt \qquad (5.14)$$

The integral part on the right hand side of Equ.(5.14) is the MCRT of an attrited particle t_{ra} as developed previously in section 3.3.2.1 (eg. Equ(3.25)). By inserting Equ.(5.14) into (5.13) and applying Equs.(3.31) and (3.40) to substitute for the integral part (t_{ra}) in terms of ideal MCRTs, we obtain

$$w_{da}=Q_{pa}\rho_c\frac{\pi}{6}d_a^3 t_{ra}^*[1-(\frac{t_{re}^*}{t_{ra}^*})^4]\,P_{da}dd_a \qquad (5.15)$$

Since attrited particles with size smaller than d_e are assumed to be elutriated immediately, the total attrited carbon inventory is obtained by integration of w_{da} for all size fractions from d_e to d_s. Thus the distribution function E_{dio} (simply w_{da} normalized) can be expressed in dimensionless form, using Equs.(3.34) and (3.38) for P_{da} and recalling that $t_{ra}^* \propto t_{Ba}^* \propto d_a$ (Table 2.1):

$$E_{dio}=\frac{(\lambda^4-\lambda_o^4)\,\phi}{\int_{d_o}(\lambda^4-\lambda_o^4)\,\phi\,dd_a} \tag{5.16}$$

Inserting Equs.(5.11) and (5.16) into (5.12), and using (3.40), one obtains

$$\frac{\int_{\lambda_o}^{1}(\lambda^5-\lambda_o^5)\,\phi\,d\lambda}{\int_{\lambda_o}^{1}(\lambda^4-\lambda_o^4)\,\phi\,d\lambda}\,\bar{t}_{rs}^{\,*}=\frac{5}{4}\,\overline{t_{ria}^{\,*}} \tag{5.17}$$

The value of $\bar{t}_{ria}^{\,*}$ can be evaluated from the attrited carbon reburn test (sub-test) data in analogy to the calculation of t_c described in the previous section by Equs.(5.1) to (5.4),

$$\overline{t_{ria}^{*\prime}}=\int_0^{t_{Be}}\left[1-\frac{uAM_c}{W_{ca}}\int_0^{t}(C_{CO}+C_{CO_2})\,dt\right]dt \tag{5.18}$$

The superscript ' here denotes the MCRT value being obtained from experimental data to distinguish from the corrected value to be given in the next section.

Since $t_{re}^{\,*}$ and $t_{rs}^{\,*}$ are the only unknown variables, they can be obtained by solving Equs. (5.9) and (5.17) simultaneously. The values of $t_{re}^{\,*}$ and $t_{rs}^{\,*}$ in turn can be used to obtain the values of $\bar{t}_{ra}$ and Y_a from Equs.(3.42) and (5.8) respectively. With these results, the attrition rate Q_a

can be evaluated either by Equ.(3.8) or (5.5). Finally, the reaction rate R_m of the mother particles can be obtained by subtracting R_a from the corresponding combustion rate, which is estimated as that at the time of freezing the reaction in the main-test:

$$R_m=R_c-R_a \qquad (5.19)$$

By using the values of Q_a and R_m evaluated from the same experiment, the attrited fraction of the mother particle, $Q_a/(Q_a+R_m)$ is readily obtained.

5.3 Correction for Attrition-Elutriation Parameters

5.3.1 Error introduced by exit gas dispersion

In the preceding MCRT development, converted carbons are assumed to leave the bed immediately. In reality, CO and CO_2 may disperse in the bed and in the sampling system before they reach the detector of the gas analyzer. The dispersion of gas affects the detected signal timing, which could cause an error in calculating the value of the MCRT's from experimental data. This error in general is too small, a few seconds, to be significant for tests burning large original char particles. However, when burning attrited fines alone, the particles are small and their residence times are short. The evaluation of the attrition-related parameters from the flue gas concentration data is more sensitive to deviations and

requires a correction. Thus the correction procedure described in the following is applied to the results of the sub-test of the second series experiments only.

To perform the correction, the residence time distribution function $E_a(t')$ of CO and CO_2 between conversion and the time when they are detected by the gas analyzers is first obtained by injecting a pulse of tracer gas (containing CO_2) into the bed under simulated operating conditions. Fig. 5.1 shows the tracer gas residence time distribution result of the present system together with two cumulative age distribution curves for inlet gas dispersion which will be discussed in the next sub-section.

Since the signal delay times are the same for the tracer and the actual experiments, they can both simply use the onset of the signal detection as the zero starting point. Thus the mean residence time increase due to gas dispersion, Δt_r, is

$$\Delta t_r = \int_0^\infty t E_a(t')\,dt \qquad (5.20)$$

The ideal MCRT of the reburnt particles $\bar{t}_{ria}^{*}$ can then be corrected by,

$$\overline{t_{ria}^{*}} = \overline{t_{ria}^{*'}} - \Delta t_r \qquad (5.21)$$

The tracer age distribution function is also applicable

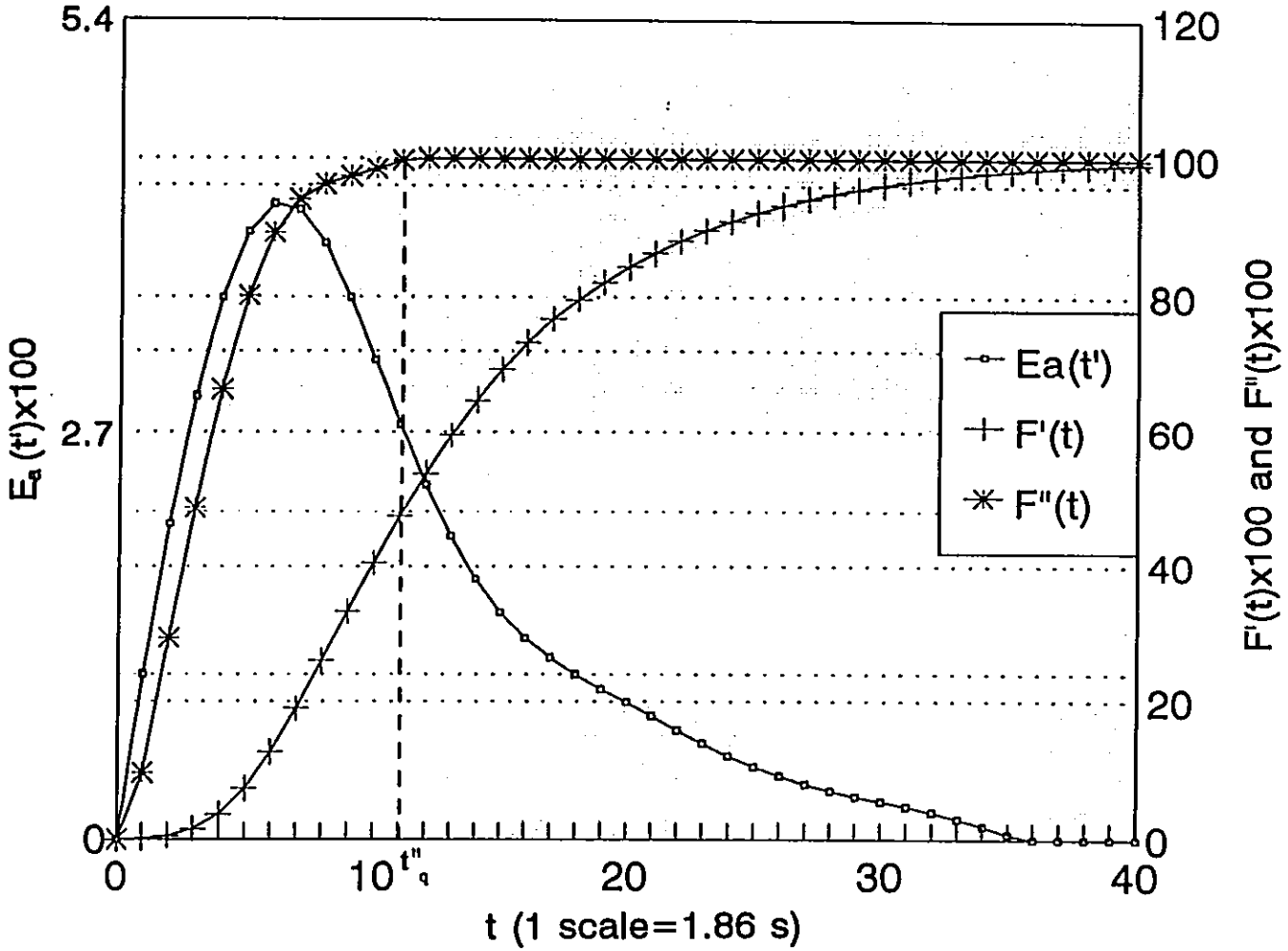

Fig. 5.1: Exit age distribution E_a for gas flowing through the fluid bed and the sampling system combined, together with fractional concentration curves, in reponse to a step input, at the fluid bed inlet (F'') and at the gas analyzer (F')

to two other data corrections for the attrited carbon reburn experiments (sub-test). The first one is to correct the CO_2 concentration data due to CO_2 present in the inlet fluidizing gas. This amount of CO_2 is very small, about 350 ppm (and rising!) if air is used, but so is the amount produced from the burning of the attrited fines (typically below 1000 ppm in the present experiments). In such experiments, the attrited fines have to be heated up in an inert environment to the original char combustion temperature conditions. A sudden shift to the reacting gas (air or air mixture) containing both O_2 and CO_2 starts the combustion of the attrited fines. Because of gas dispersion, the amount of combustion CO_2, especially during the early stage of the test, is not simply equal to the difference between the CO_2 amounts in the flue gas and in the fluidizing gas, but rather should be calculated by

$$C_{CO_2}=C'_{CO_2}-C_{Ca}\int_0^t E_a(t')\,dt \qquad (5.22)$$

where C'_{CO2} and C_{Ca} are the CO_2 concentrations of the flue gas and of the fluidizing gas respectively, and C_{CO2} and C'_{CO2} are functions of time.

Another application of the dispersion residence time distribution function is to correct the value of the reaction rate of the attrited fines. During the sub-test, the $C-O_2$ reaction rate decreases continuously from the initial maximum

value, R_a, to zero as the fines are consumed. Because of dispersion of gas in the bed and the sample line, the detected maximum value of the $CO+CO_2$ concentration signal will be later and lower. In analogy to the development for continuous systems (Levenspiel, 1972), the measured concentration history is the convolution integral of the input concentration with the residence time:

$$C'_{CO+CO_2}(t) = \int_0^t C_{CO+CO_2}(t-t') E_a(t') dt' \qquad (5.23)$$

where t is the time at which the concentration signal is detected, and t' is the age of the detected gas element. The total carbon concentration symbols with and without superscript ' denote the instrumental read-out and the local in-bed (no dispersion effect) values respectively. Fig. 5.2 illustrates both concentration-time relationships using the same origin as their starting point.

According to Equ.(5.1), the reaction rate is directly proportional to the total carbon concentration, so that the above equation expressing carbon concentrations can also be used to represent reaction rates. By introducing a time-dependent variable, G(t), which equals the ratio of the reaction rate at time t, $R_{ia}(t)$, to the reaction rate at time zero, R_a, the equation becomes

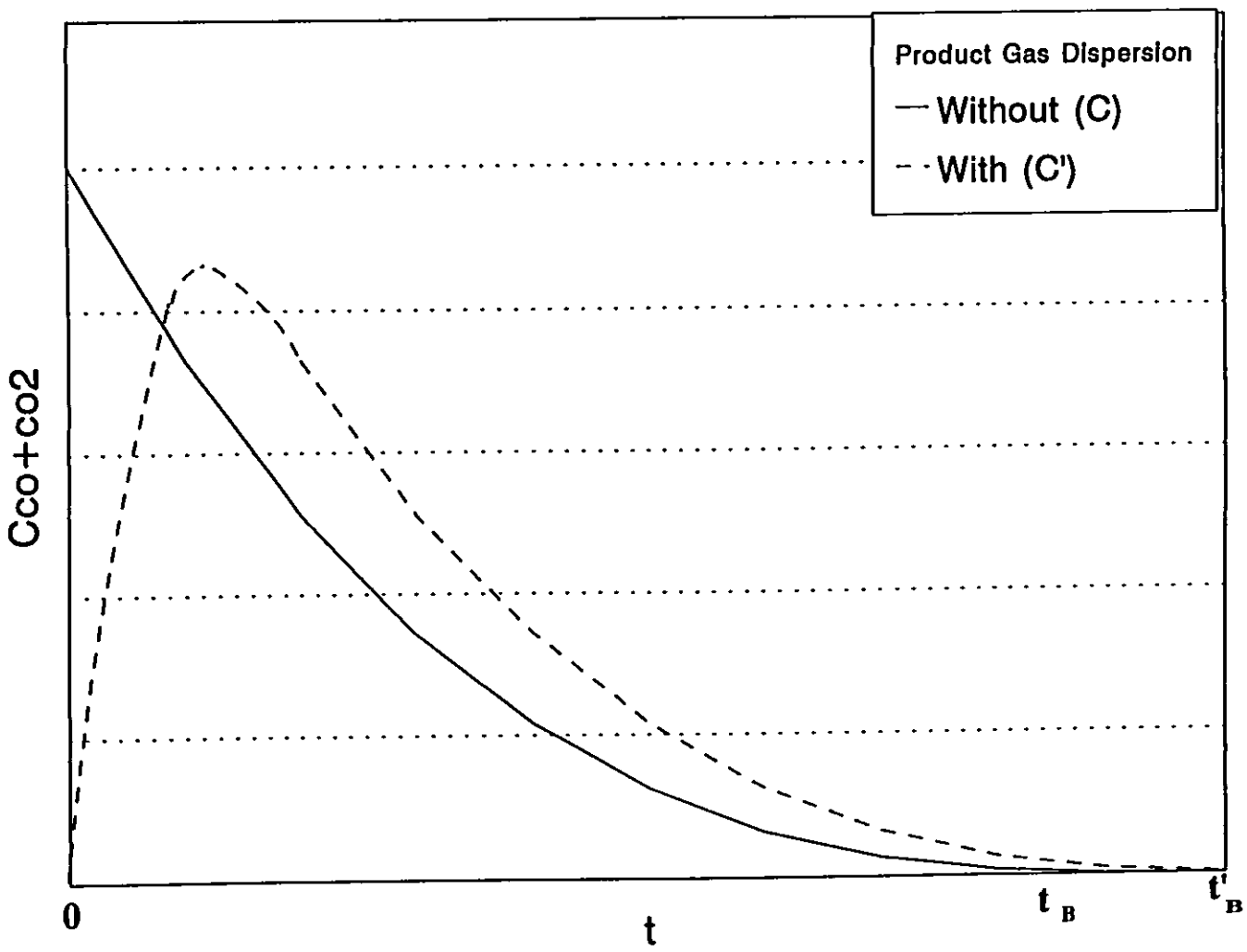

Fig. 5.2: Comparison of carbon concentration profiles with and without product gas dispersion

$$R'_{ia}(t) = R_a \int_0^t G(t-t')\, E_a(t')\, dt' \qquad (5.24)$$

where $R'_{ia}(t)$ refers to the reaction rate $R_{ia}(t)$ as it is measured after distortion by gas dispersion.

In order to solve Equ.(5.24), the relationship between G(t) and t is required. Since the kinetic regime of combustion is assumed, the reaction rate of a char particle is directly proportional to its surface area, so that

$$G(t) = \frac{R_{ia}(t)}{R_a} = \frac{A_a(t)}{A_{ao}} \qquad (5.25)$$

where $A_a(t)$ and A_{ao} are the total surface areas of attrited particles at time t and at time zero respectively. To evaluate $A_a(t)$ and A_{ao}, we again first consider mono-sized attrition and then introduce an attrited particle size distribution. If mono-size attrition is assumed during the maintest, since the number of attrited particles in the bed equals $Q_{pa}t_{Ea}$, A_{ao} is

$$A_{ao} = Q_{pa} t_{Ea} \int_{d_e}^{d_a} \pi d_c^2 P_{dia}\, dd_c \qquad (5.26)$$

where P_{dia} is the in-bed particle size distribution function based on particle number, and is a constant equal to $1/(d_a - d_e)$. When integrated, the above equation becomes,

$$A_{ao}=\frac{\pi}{3}Q_{pa}t_{Ea}\frac{d_a^3-d_e^3}{d_a-d_e} \qquad (5.27)$$

During the earlier period of combustion in the sub-test, when $t<t_{Be}^*$, the burnout time of the smallest particles (corresponding to the elutriable size in the main test), the sizes of the particles reduce but the number of particles in the bed remains unchanged. Therefore, their surface area can be integrated using the same equation but different integration limits. The upper and the lower limits, d_u and d_l, can be obtained from the fractional burnout relationship,

$$d_u=(1-\frac{t}{t_{Ba}^*})\,d_a \qquad (5.28)$$

$$d_l=(1-\frac{t}{t_{Be}^*})\,d_e \qquad (5.29)$$

With $P_{dia}=d_u-d_l$, integration results in

$$A_a(t)=\frac{\pi}{3}Q_{pa}t_{Ea}\frac{(1-\frac{t}{t_{Ba}^*})^3d_a^3-(1-\frac{t}{t_{Be}^*})^3d_e^3}{(1-\frac{t}{t_{Ba}^*})\,d_a-(1-\frac{t}{t_{Be}^*})\,d_e} \qquad (5.30)$$

When $t>t_{Be}^*$, the number of particles, N_a, reduces with time and the reduction ratio-time relationship is,

$$\frac{N_a}{Q_{pa}t_{Ea}}=\frac{t^*_{Ba}-t}{t^*_{Ba}-t^*_{Be}} \tag{5.31}$$

Also, in this case, the lower limit of the particle size becomes zero (assuming no elutriation), and $P_{dia} = d_u$. With these changes, and with N_a substituted for $Q_{pa}t_{Ea}$, the same equation is integrated to

$$A_a(t)=\frac{\pi}{3}Q_{pa}t_{Ea}\frac{(t^*_{Ba}-t)^3d_a^2}{(t^*_{Ba}-t^*_{Be})\,t^{*2}_{Ba}} \tag{5.32}$$

When a normal size distribution for attrited particles is assumed, the number of particles of any attrited size fraction in the bed during the main test equals $Q_{pa}t_{Ea}P_{da}dd_a$. The total surface area of the particles at the start of the sub-test is,

$$A_{ao}=\frac{\pi}{3}Q_{pa}\int_{d_e}^{d_a}t_{Ea}\frac{d_a^3-d_e^3}{d_a-d_e}P_{da}dd_a \tag{5.33}$$

For combustion at $t<t_{Be}^*$, replacing all burnout times with ideal MCRTs in Equ.(5.30) (cf. Equ.(3.21)) and integrating over all size fractions with $d>d_e$ results in

$$A_a(t)=\frac{\pi}{3}Q_{pa}\int_{d_e}^{d_a}t_{Ea}\frac{(t^*_{ra}-\frac{t}{4})^3\frac{d_a^3}{t^{*3}_{ra}}-(t^*_{re}-\frac{t}{4})^3\frac{d_e^3}{t^{*3}_{re}}}{(t^*_{ra}-\frac{t}{4})\frac{d_a}{t^*_{ra}}-(t^*_{re}-\frac{t}{4})\frac{d_e}{t^*_{re}}}P_{da}dd_a \tag{5.34}$$

The ratio G(t) can be obtained by dividing Equ.(5.34) by

Equ.(5.33) and substituting P_{da} from Equ.(3.34). The result can be simplified by using the relation $t_r^* \propto d_a$ as well as Equs.(3.37), (3.38), (3.41) and (3.47):

$$G(t)=\frac{\int_{\lambda_e}^{1}[(\lambda-\frac{t}{4t_{rs}^*})^3-(\lambda_e-\frac{t}{4t_{rs}^*})^3]\phi d\lambda}{\int_{\lambda_e}^{1}(\lambda^3-\lambda_e^3)\phi d\lambda} \qquad (5.35)$$

When $t>t_{Be}^*$, Equ.(5.32) is employed to give the total surface area,

$$A_a(t)=\frac{4\pi}{3}Q_{pa}\int_{d_{(t_B^*-t)}}^{d_a}(t_{ra}^*-\frac{t}{4})^3\frac{d_a^2}{t_{ra}^{*2}}P_{da}dd_a \qquad (5.36)$$

and the ratio G(t) is,

$$G(t)=\frac{\int_{\frac{t}{4t_{rs}^*}}^{1}(\lambda-\frac{t}{4t_{rs}^*})^3\phi d\lambda}{\int_{\lambda_e}^{1}(\lambda^3-\lambda_e^3)\phi d\lambda} \qquad (5.37)$$

As shown by the equation, besides time t, G(t) is a function of t_{re}^* and t_{rs}^* only.

With the value of G(t) as a known function of t, Equ.(5.24) can be solved at any time t for R_a by numerical integration. Since G(0) = 1, the value of R_a could be obtained simply from the first data read-out. However, it is

difficult to completely match the timing of data taking between the tracer experiments to measure $E_a(t')$ and the combustion experiments: the data logger samples concentrations at discrete times, and these times may not exactly correspond for the two different experiments. The time deviation may vary from zero up to the time between two consecutive samples but is constant for all data points within a single experiment. On the other hand, the percentage error in the data introduced by this time deviation is different from one point to another, and is dependent on the slope of the total carbon concentration curve and the quantity of the data. Less error is expected from a data point located at flatter slope and with larger value. Therefore, the data at the maximum point of the curve should be used for R_a evaluation.

5.3.2 Error introduced by inlet gas dispersion

With reasons similar to those given in the last section for the dispersion of the product gas, the reacting gas dispersed in the gas inlet system (inlet gas line, windbox, and distributor) can also cause significant error to the sub-test of the second series experiments. During these runs, the inlet fluidizing gas is suddenly shifted from inert gas to air or air mixture to commence combustion of attrited fines when the desired bed temperature has been reached. The gas switching solenoid valve is located upstream of the inlet line

and the windbox, in which dispersion between gases before and after switching occurs. The dispersion of the reacting gas into the inert gas influences the inlet gas concentration and the reaction rate during the early stage of combustion, which again results in another MCRT enlargement and R_a reduction.

Correction of such errors introduced by the inlet gas dispersion requires the knowledge of the residence time distribution of the gas in the gas inlet system. To conduct experiments with tracer gas flowing through the entire system, ie. including the bed and the sampling line, is much easier than to do it for the inlet gas system alone. With simulated operating conditions, a step input of tracer gas, using air here, allows the exit gas analyzer to detect the accumulated age distribution, or the F curve (Levenspiel, 1972), of the tracer flowing through the system. The system can be considered to be composed of two independent flow units in series, one before the gas enters the bed and one for the bed and sampling system. Similar to Equ.(5.23), the relationship between the tracer concentrations at the exits of the first and second flow units (C''_{O2} and C'_{O2} respectively) is

$$C'_{O_2}(t) = \int_0^t C''_{O_2}(t-t')\, E_a(t')\, dt' \qquad (5.38)$$

When dividing both sides by the input gas tracer concentration, the equation shows the dependence of the F values between both exit points,

$$F'(t) = \int_0^t F''(t-t') E_a(t')\, dt' \tag{5.39}$$

To evaluate F"(t), the cumulative age distribution function of the gas inlet system, from Equ.(5.39) is difficult, involving deconvolution of the distribution function under an integral. To simplify the problem, the convolution is approximated by using the average values between two consecutive data points in time similar to graphical integration. With data points taken at a fixed time interval, the relationship of Equ.(5.39) is transformed tc:

$$F'(t_\kappa) = \frac{1}{4}\Delta t_\kappa \sum_1^\kappa [F''(t_\kappa - t_{\kappa'}) + F''(t_\kappa - t_{\kappa'-1})]\,[E_a(t_{\kappa'}) + E_a(t_{\kappa'-1})] \tag{5.40}$$

where t_κ is the time of the data signal detected at index κ, $t_{\kappa'}$ is the age of the gas element in the bed and the gas sampling system detected at index κ', and $\Delta t_\kappa = t_\kappa - t_{\kappa-1} = t_{\kappa'} - t_{\kappa'-1}$, is the data taking time interval. Since F"(0)=0, the F"(t_κ) values can be estimated consecutively from the point κ=1 to the point that F"(t_κ) nearly equals 1 by using the experimentally found F'(t_κ) and $E_a(t_{\kappa'})$ function. The result, together with the two tracer curves F'(t) and $E_a(t')$, when plotted at the same origin, are given in Fig. 5.1.

5.3.2.1 **Correction to MCRT**

To find the MCRT gain due to the dispersion of the inlet gas, let us first consider the simple case of burning a single char particle. Assuming ideal combustion conditions (ie. no carbon loss), with reaction under kinetic control and first order, the rate of size reduction is directly proportional to oxygen concentration, so that

$$\frac{1-(1-x'')^{1/3}}{1-(1-x)^{1/3}}=\frac{d_o-d_c''}{d_o-d_c}=\frac{C_{O_2}\int_0^t F''(t)\,dt/t}{C_{O_2}} \qquad (5.41)$$

where C_{O2} is the inlet oxygen concentration, and symbols with and without superscript " denote values in cases with and without inlet gas dispersion respectively. According to Table 1, the denominator on the left hand side of Equ.(5.41) equals t/t_B^*, and the equation can be written as

$$1-x''=(1-\int_0^t F''(t)\,dt/t_B^*)^3 \qquad (5.42)$$

The effect on conversion of the inlet gas dispersion is illustrated in Fig. 5.3.

At $t=t_B"^*$, the ideal burnout time of the char particle with inlet gas dispersion, (1-x")=0, and the relationship between t_B^* and $t_B"^*$ is

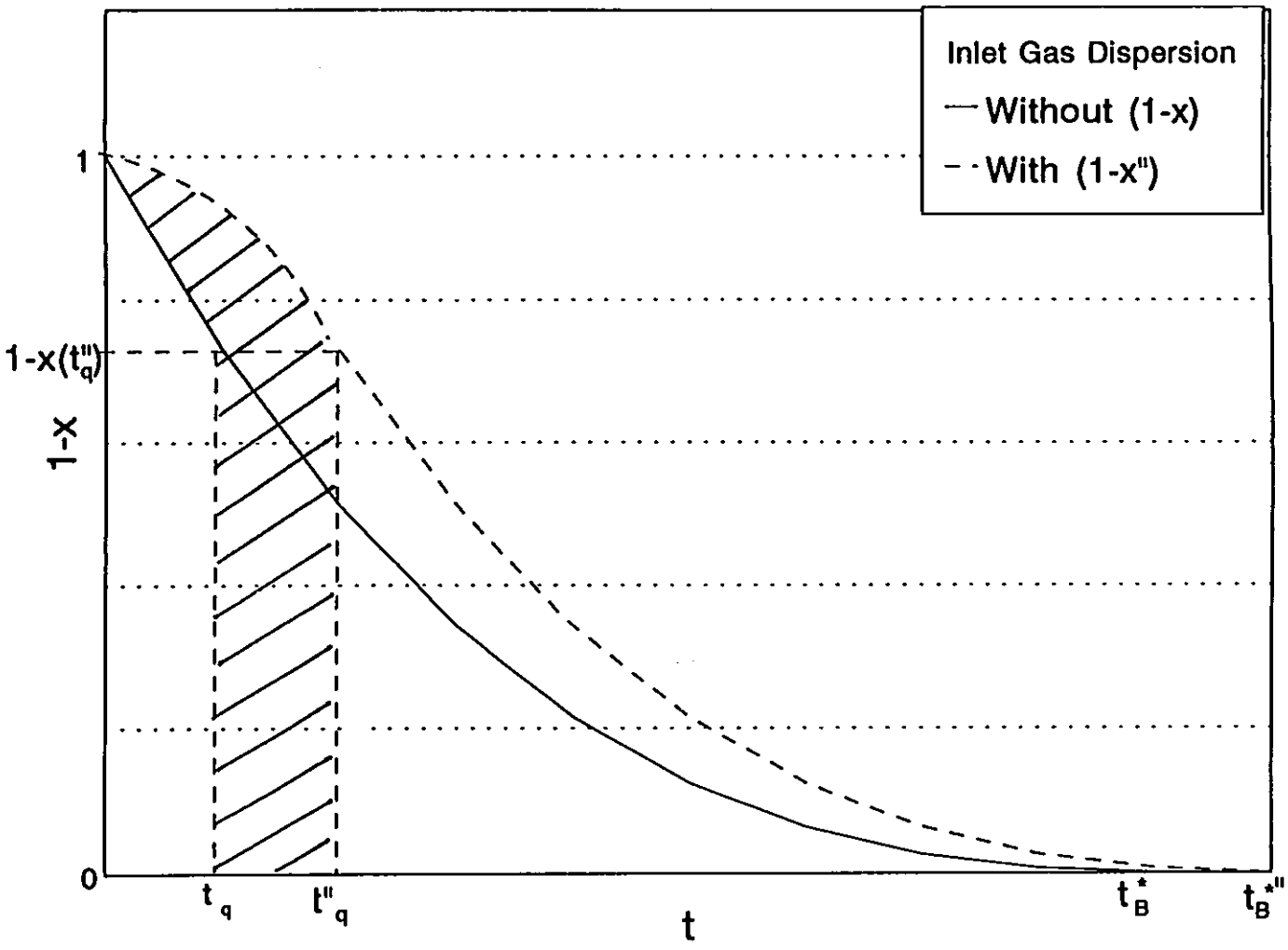

Fig. 5.3: Comparison of carbon inventories with and without inlet gas dispersion

$$t_B^* = \int_0^{t_B''^*} F''(t)\,dt \qquad (5.43)$$

The form of the above equation is not limited to the burnout time but can be applied to any other burning time as well. Using Equ.(5.42), the time required to burn a char particle with no inlet gas dispersion to a certain degree of conversion can be shown to equal integral of the F"(t) function from time 0 to the time when the same conversion is achieved during combustion with inlet gas dispersion, a relation similar to Equ.(5.43).

The mean time gain is given by the difference between the MCRT values with and without inlet gas dispersion, or

$$\Delta t_r'' = t_r''^* - t_r^* \qquad (5.44)$$

where

$$t_r''^* = \int_0^{t_B''^*} (1-x'')\,dt = \int_0^{t_B''^*} \left(1-\int_0^t F''(t)\,dt/t_B^*\right)^3 dt \qquad (5.45)$$

For the case of mono-sized attrition, the mean value of MCRT gain for the burning of extracted attrited particles in a second series sub-test experiment $\Delta\bar{t}''_{r,mono}$ is

$$\Delta \bar{t}''_{r,mono} = \int_{t^*_{re}}^{t^*_{ra}} \Delta t''_r E_{tia} dt^*_{ria} \tag{5.46}$$

The subscript mono here denotes the case of mono-sized attrition. As mentioned in Section 5.2.2, the MCRT distribution function of the attrited particles can be developed in similar fashion to that of withdrawn char particles, or, in analogy to Equ.(3.67) and using Equ.(3.40) to substitute for y_a,

$$E_{tia} = \frac{4\,(t^*_{ria}/t^*_{ra})^3}{t^*_{ra}(1-y_a^{4/3})} = \frac{4\,t^{*3}_{ria}}{t^{*4}_{ra}-t^{*4}_{re}} \tag{5.47}$$

For the case of a normal size distribution for attrited particles, the overall mean time gain $\Delta\bar{t}_r''$ is

$$\Delta \bar{t}''_r = \int_{d_e}^{d_a} \Delta \bar{t}''_{r,mono} E_{dio}\, dd_a \tag{5.48}$$

Substituting E_{dio} from Equ.(5.16), Equ.(5.48) becomes

$$\Delta \bar{t}''_r = \frac{\int_{\lambda_e}^{1} \Delta \bar{t}''_{r,mono} (\lambda^4 - \lambda_e^4)\, \phi\, d\lambda}{\int_{\lambda_e}^{1} (\lambda^4 - \lambda_e^4)\, \phi\, d\lambda} \tag{5.49}$$

The above evaluation method involves multiple integration through Equs.(5.44) to (5.49) and requires very long computing time. Fortunately, the calculation can be simplified and

shortened unless an exceptionally large gas inlet system causing excessively long gas residence time is used. As the F"(t) value approaches unity with time, a time will be reached, defined as t_q", after which F"(t)=1 can be assumed. This point can be chosen arbitrarily as long as the F"(t) value is considered close enough to its upper limit, say F"(t_q")=0.98, without introducing significant error in the subsequent correction calculations. In other words, inlet gas dispersion is effective only up to a conversion equal to x"(t_q"), after which the oxygen concentration becomes essentially the same as the case with no inlet gas dispersion. For a normal windbox and gas inlet system design, the mean residence time of the gas in it is small, so that t_q" is shorter than the ideal burnout time of even the smallest retrieved attrited particles, or $t_{Be}^*>t_q$". The value of Δt_r" of a burning particle can be obtained by the difference between the MCRTs with and without inlet gas dispersion (Equ.(5.44)), which are represented graphically by the areas under curves for (1-x") and (1-x) respectively in Fig. 5.3. As shown in the figure, the time corresponding to t_q" for the same conversion but without inlet gas dispersion is defined as t_q. Since reactions between the two cases are identical after conversion x"(t_q") is reached, Δt_r" is represented by the difference between areas below the curves prior to this conversion point (the shaded area in Fig. 5.3), or

$$\Delta t_r'' = \int_0^{t_q''} (1-x'')\,dt - \int_0^{t_q} (1-x)\,dt \qquad (5.50)$$

In analogy to the development in Section 3.3.2.1 for conversion with elutriation, the second term in the right hand side of the above equation equals t_r and can be expressed, using Equ.(3.26) with y replaced by $(1-x''(t_q''))$, as

$$\int_0^{t_q} (1-x)\,dt = [1-(1-x''(t_q''))^{4/3}]\, t_r^* \qquad (5.51)$$

By applying the above relationship and substituting 1-x" from Equ.(5.42), Equ.(5.50) becomes

$$\Delta t_r'' = \int_0^{t_q''} (1-\int_0^{t} F''(t)\,dt/t_B^*)^3 dt - [1-(1-\int_0^{t_q''} F''(t)\,dt/t_B^*)^4]\, t_r^* \qquad (5.52)$$

Equ.(5.52) can be expanded and rearranged, using Equ.(3.21) to

$$\Delta t_r'' = t_q'' - \int_0^{t_q''} F''(t)\,dt - 3\,[K1]/t_B^* + [K2]/t_B^{*2} - [K3]/t_B^{*3} \qquad (5.53)$$

where

$$[K1] = \int_0^{t_q''}\int_0^{t} F''(t)\,dt\,dt - \frac{1}{2}\left(\int_0^{t_q''} F''(t)\,dt\right)^2 \qquad (5.54)$$

$$[K2] = 3\int_0^{t_q''} \left(\int_0^{t} F''(t)\,dt\right)^2 dt - \left(\int_0^{t_q''} F''(t)\,dt\right)^3 \qquad (5.55)$$

$$[K3] = \int_0^{t_q''} \left(\int_0^t F''(t)\,dt \right)^3 dt - \frac{1}{4} \left(\int_0^{t_q''} F''(t)\,dt \right)^4 \qquad (5.56)$$

The above equations involve many integrations, and may appear complicated, but all integrals, including those in [K1], [K2], and [K3], depend on inlet gas dispersion only and not on combustion, thus only have to be evaluated once for all experiments. Evaluating the MCRT gain by Equ.(5.53) is actually simpler than by Equs.(5.43) to (5.45). If the burning particle is large or unreactive, so that its burnout time is much longer than t_q'', the mean time delay is a constant equal to the difference of the first two terms in the right hand side of Equ.(5.53). Thus in this case the correction does not depend on the characteristics of the burning particle and requires only the tracer experimental data. As illustrated by Fig. 5.3, the time difference between the two curves at same conversion level becomes a constant equal to $t_B^{*}''-t_B^{*}$, after $x''(t_q'')$ is reached. By applying the form of Equ.(5.43) to t_q'' instead of t_B^{*}'', the MCRT delay for large or unreactive particles can be shown to equal the difference between the burnout times with and without inlet gas dispersion:

$$\Delta t_r'' = t_q'' - \int_0^{t_q''} F''(t)\,dt = t_q'' - t_q = t_B^{*}'' - t_B^{*} \qquad (5.57)$$

By substituting Equs.(5.53), with (5.54) to (5.56), and (5.47) into Equ.(5.46) and integrating, the MCRT gain for the case of mono-sized attrition can be obtained. The result is represented in dimensionless form by using Equ.(3.37), (3.38) and (3.41),

$$\Delta \bar{t}''_{r,mono} = t''_q - \int_0^{t''_q} F(t)\,dt - \frac{[K1]}{t^*_{rs}} \frac{\lambda^3-\lambda_o^3}{\lambda^4-\lambda_o^4} + \frac{[K2]}{8\,t^{*2}_{rs}} \frac{1}{\lambda^2+\lambda_o^2} - \frac{[K3]}{16\,t^{*3}_{rs}} \frac{\lambda-\lambda_o}{\lambda^4-\lambda_o^4}$$

(5.58)

The above equation can be inserted into Equ.(5.49) to estimate $\Delta\bar{t}_r$" when normal size distribution attrition is assumed:

$$\overline{\Delta t''_r} = t''_q - \int_0^{t''_q} F''(t)\,dt - \frac{\int_{\lambda_o}^{1} \left[\frac{[K1]}{t^*_{rs}}(\lambda^3-\lambda_o^3) - \frac{[K2]}{8\,t^{*2}_{rs}}(\lambda^2-\lambda_o^2) + \frac{[K3]}{16\,t^{*3}_{rs}}(\lambda-\lambda_o)\right]\phi\,d\lambda}{\int_{\lambda_o}^{1} (\lambda^4-\lambda_o^4)\,\phi\,d\lambda}$$

(5.59)

With the parameters t_q", [K1], [K2], [K3}, and the integral of F"(t) from 0 to t_q", which are independent of combustion, being pre-determined, evaluating the MCRT gain by Equ.(5.59) involves much less integration operations and computing time than that from Equs.(5.43) through (5.49).

With the mean time gains due to both reacting and product gas dispersions estimated, the ideal MCRT of the retrieved attrited particles can be corrected as

$$\overline{t^{\bullet}_{ria}} = \overline{t^{\bullet\prime}_{ria}} - \Delta t_r - \overline{\Delta t''_r} \qquad (5.60)$$

5.3.2.2 **Correction to CO_2 data**

The CO_2 concentration data correction due to CO_2 present in the inlet gas is rather simple. Since gas dispersion in the entire system is considered, the overall distribution function should be used instead of that giving the product gas alone in Equ.(5.22), or,

$$C_{CO_2} = C'_{CO_2} - C_{Ca} F'(t) \qquad (5.61)$$

5.3.2.3 **Correction to reaction rate**

When correcting the combustion rate of the attrited fines, the main concern is the reduction of oxygen concentration available for reaction at the early stage of combustion of the second series experiments due to inlet gas dispersion. During this burning period, the increase in oxygen concentration with time will raise the reaction rate but the effect of shrinking particle size will do the opposite. Thus the value of $R_{ia}(t)$ increases from zero to a maximum and then decreases. Both Equ.(5.23) and (5.24) are applicable in this case; however, the value of G(t), which is the ratio of the reaction rate at time t to R_a, the initial

reaction rate without inlet gas dispersion, now depends on both oxygen concentration and particle surface area, or

$$G(t)=\frac{A_a(t)}{A_{ao}}F''(t) \qquad (5.62)$$

For the case of the burning particles which are retrieved from mono-size attrition, the original surface area A_{ao} is not affected by the oxygen concentration and is given by Equ.(5.27). However, the value of $A_a(t)$ depletes more slowly compared to that obtained from the case of no inlet gas dispersion, owing to the slower shrinking rate. Since the change in oxygen concentration does not alter the form of attrited particle size distribution (a constant), the relationship $P_{dia}=d_u-d_l$ can also be applied here. If both the upper and lower size limits are known, the value of $A_a(t)$ can be integrated over the surface area of all particles similar to the procedure described in the last section,

$$A_a(t)=\frac{\pi N_a}{d_u-d_l}\int_{d_l}^{d_u} d_{ia}^2 dd_{ia} \qquad (5.63)$$

When $t<t_{Be}"^*$, the particle number does not change and equals $Q_{pa}t_{Ea}$, but d_u and d_l become (cf. Equ.(5.28) to (5.29))

$$d_u=(1-\int_0^t F''(t)\,dt/t_{Ba}^*)\,d_a \qquad (5.64)$$

$$d_i=(1-\int_0^t F''(t)\,dt/t_{Be}^*)\,d_e \qquad (5.65)$$

Substituting Equ.(5.64) and (5.65) into (5.63) and integrating, the result is (cf. Equ.(5.30))

$$A_a(t)=\frac{\pi}{3}Q_{pa}t_{Ea}\frac{(1-\int_0^t F''(t)\,dt/t_{Ba}^*)^3d_a^3-(1-\int_0^t F''(t)\,dt/t_{Be}^*)^3d_e^3}{(1-\int_0^t F''(t)\,dt/t_{Ba}^*)\,d_a-(1-\int_0^t F''(t)\,dt/t_{Be}^*)\,d_e} \qquad (5.66)$$

When $t>t_{Be}''^*$, if also $t>t_q''$, indicating that the highest oxygen level has already been reached, the number of particles equals

$$N_a=\frac{t_{Ba}''^*-t}{t_{Ba}^*-t_{Be}^*}Q_{pa}t_{Ea} \qquad (5.67)$$

Since the time difference between curves with and without inlet gas dispersion for equal conversion at times larger than t_q'' is constant, applying the form of Equ.(5.43) to t shows

$$t_{Ba}''^*-t=t_{Ba}^*-\int_0^t F''(t)\,dt \qquad (5.68)$$

Also, the lower size limit equals zero, and $P_{dia}=d_u$, the upper size limit, which can be obtained from the same expression, Equ.(5.64), developed for $t<t_{Be}^*$". Applying these into Equ.(5.63) and integrating results in

$$A_a(t) = \frac{\pi}{3} Q_{pa} t_{ea} \frac{(t^*_{Ba} - \int_0^t F''(t)\,dt)^3 d_a^2}{(t^*_{Ba} - t^*_{Be})\, t^{*2}_{Ba}} \qquad (5.69)$$

On the other hand, if $t<t_q''$, a time period equal to $(t_q''-t)$ remains in which the attrited particles still burn under reduced oxygen conditions. The corresponding time period for combustion without inlet gas dispersion is obtained by integrating the F"(t) function within these times. The number of particles in this case is

$$N_a = \frac{t''^*_{Ba} - t''_q + \int_t^{t''_q} F''(t)\,dt}{t^*_{Ba} - t^*_{Be}} Q_{pa} t_{Ea} = \frac{t^*_{Ba} - \int_0^t F''(t)\,dt}{t^*_{Ba} - t^*_{Be}} Q_{pa} t_{Ea} \qquad (5.70)$$

Equ.(5.70) is identical to Equ.(5.67) with (5.68). Thus Equ.(5.69) can be used to estimate $A_a(t)$ irrespective of where t_q'' is located.

When a normal size distribution for attrited particles is assumed, the total surface area of the retrieved attrited particles is already given by Equ.(5.33). For combustion during $t<t_{Be}^*$, the difference between $A_a(t)$ results with and without the inlet gas dispersion effect can be seen by comparing Equs.(5.30) and (5.64). Since t is independent of particle size for these equations, the desired G(t) value in this case can be expressed by replacing t with the integral of the F curve from 0 to t in Equ.(5.35):

$$G(t)=\frac{\int_{\lambda_e}^{1}\left[\left(\lambda-\frac{\int_0^t F''(t)\,dt}{4t_{rs}^*}\right)^3-\left(\lambda_e-\frac{\int_0^t F''(t)\,dt}{4t_{rs}^*}\right)^3\right]\phi\,d\lambda}{\int_{\lambda_e}^{1}(\lambda^3-\lambda_e^3)\,\phi\,d\lambda} \qquad (5.71)$$

Similarly, for $t>t_{Be}^*$, the G(t) expression can be obtained by using Equ.(5.37),

$$G(t)=\frac{\int_{\frac{\int_0^t F''(t)\,dt}{4t_{rs}^*}}^{1}\left(\lambda-\int_0^t F''(t)\,dt/4t_{rs}^*\right)^3\phi\,d\lambda}{\int_{\lambda_e}^{1}(\lambda^3-\lambda_e^3)\,\phi\,d\lambda} \qquad (5.72)$$

With the exit gas residence time distribution function $E_a(t')$, the values of G(t) obtained from the above equations as a function of time can be used in Equ.(5.24) to evaluate R_a from the reaction rate data $R_{ia}'(t)$ resulted from sub-tests. As discussed previously in Section 5.3.1, the highest rate data point should be used.

5.4 Evaluation of n and j

The time resolution of conversion x_c also provides information on the regime in which the combustion reaction occurred. In general, FBC of coal is believed to occur in between the diffusion and the kinetic regimes. Also, the

reaction can change from one regime to another due to the shrinkage of the particles, so that the value of n may vary during the combustion of a char particle. For simplicity, it is assumed that an overall value of n, also of j, can be used to represent the entire combustion process.

The evaluation of these overall values requires results from both experimental series. The fractional carbon loss of the char burning in experiments of the first series can be obtained from the analytical data of the char:

$$Y=1-\frac{W_c}{W_o} \tag{5.73}$$

where W_o is the carbon content of the char particles fed. If model 1 is used for mono-size char particle combustion, combining Equs.(3.9) and (3.10) gives,

$$y_m=\frac{y-\frac{Q_a Y_a}{Q_a+R_m}}{1-\frac{Q_a Y_a}{Q_a+R_m}} \tag{5.74}$$

The first series experiments also result in t_c as described in section 4.1. By substituting t_{cm} from Equs.(3.74) and (3.75) and f_a from (3.10) into (3.44),

$$t_c = \left(n y_m \frac{1-y_m^{-\frac{1}{n}}}{1-y_m} + y_m^{-\frac{1}{n}}\right) \frac{R_m}{Q_a+R_m} t_{re}^* + \frac{\frac{Q_a}{Q_a+R_m}(1-Y_a)}{1-\frac{Q_a}{Q_a+R_m}Y_a} \overline{t_{ca}} \qquad (5.75)$$

All the attrition-related variables and R_m in Equ.(5.75), where $\bar{t}_{ca}$ is a function of t_{re}^* and t_{rs}^* and is given by Equ.(3.51), are obtained from the second series experiments. With the calculated value of y_m from Equ.(5.74), Equ.(5.75) can be solved to give the only unknown n. The values of j can then be deduced from n based on their relationship, given previously.

For large particles, $t_{cm} \approx t_d^*$, and the first term in the right hand side of Equ.(5.75) simplifies to $t_B/(n+1)$. Since attrition fractions and their residence times are usually small, the second term can be neglected, to a first approximation, and the equation is further simplified to,

$$n \approx \frac{t_B}{t_c} - 1 \qquad (5.76)$$

Similar procedures can be followed if the second model is applied.

It is difficult to have the particles in a char sample exactly similar both in size and shape. Even with hand-picked particles from a narrow size range, mono-sized combustion

experiments are rarely achieved. For experiments burning multi-sized char particles, the equations developed in section 3.4.3 can be used with the measured particle size distribution. If particles are large, approximate values of n can be estimated from the measured mean carbon conversion time, $\bar{t}_c$, and burnout time. By applying Equ.(5.76), the value of $\bar{t}_c$ for a batch of multi-sized particles is

$$\bar{t}_c=\sum \omega_i t_{ci}=\frac{1}{n+1}\sum \omega_i t_{Bi} \qquad (5.77)$$

where subscript i denotes an individual particle, and ω_i is the fraction of the total batch mass represented by a single particle. By applying the relationship between t_B and d_o given by Table 2.1, the above equation becomes

$$\bar{t}_c=\frac{t_{Bu}}{n+1}\sum \omega_i \left(\frac{\omega_i}{\omega_u}\right)^{\frac{1}{n}} \qquad (5.78)$$

where t_{Bu} and ω_u are the burnout time and the mass fraction of the largest particle respectively. Assuming no secondary fragmentation effect, t_{Bu} equals the measured burnout time, thus n can be evaluated from the values of $\bar{t}_c$ and t_B resulting from the first series experiments.

6. RESULTS AND DISCUSSION

Results of the two different experimental series, in which one measures t_c and n while the other measures the attrition-elutriation parameters, are given separately in the following sub-sections.

6.1 First Series Experiments

The main purpose of this series of experimental work is to measure the mean carbon conversion time t_c. Coal char was the fuel used and was burned to completion in all experiments. Except for those runs studying the effects of parameters, experiments were run at 850°C bed temperature and with pure air as the inlet gas using 4 to 8 mm diameter char samples.

The amount of carbon conversion at any time during the char combustion period can be easily deduced by adding the measured CO and CO_2 concentrations of the flue gas. With the present experimental conditions, no significant CO concentration was detected; therefore, the amount of burnt carbon was estimated from the concentration of CO_2 alone. Corrections due to gas dispersions are not necessary in this series of experiments since the combustion times are long and therefore the errors introduced are too small to be significant. A schematic CO_2 concentration profile is given

in Fig. 6.1. With the known superficial gas flow rate, the burning rate as a function of time can also be deduced, which has the identical shape as the CO_2 curve. By integrating the CO_2 concentration curve up to various burning times, the time profile of carbon conversion can be obtained and is also given schematically in Fig. 6.1. According to Equ.(5.3), the value of t_c can be represented by the shaded area in Fig. 6.1 which is equivalent to the area under the (1-x) vs t curve. The experimental results of this series, presented in similar graph form, are given in Appendix 1.

The value of t_c is a function of char particle size, operating conditions, and coal char properties. The following analyzes the results and shows the effects of these parameters on t_c and combustion efficiency. Also, results for the evaluation of the exponent n, which characterizes the order of the combustion reaction, are given. For repeated experimental runs, the results were averaged.

6.1.1 Comparison of the combustion of various coal chars

Perhaps the most important char properties are its reactivity and the attrition characteristics. Fig. 6.2 compares the t_c values of various coal chars, which are all measured from experiments using particles from 4 to 8 mm in size and burnt under 850°C and pure air inlet gas

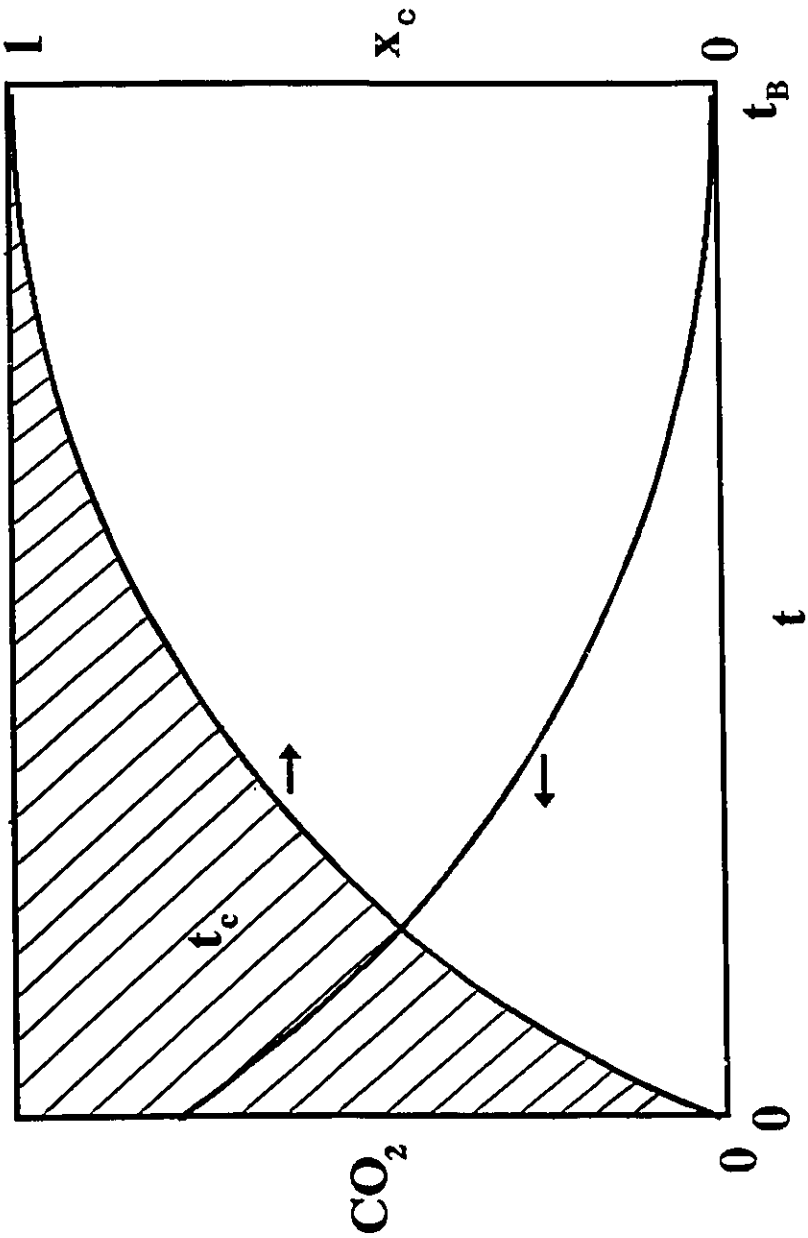

Fig. 6.1: Schematic CO_2 concentration and carbon conversion curves

850 C, Pure air inlet gas conditions
Particle size range: 4 to 8 mm

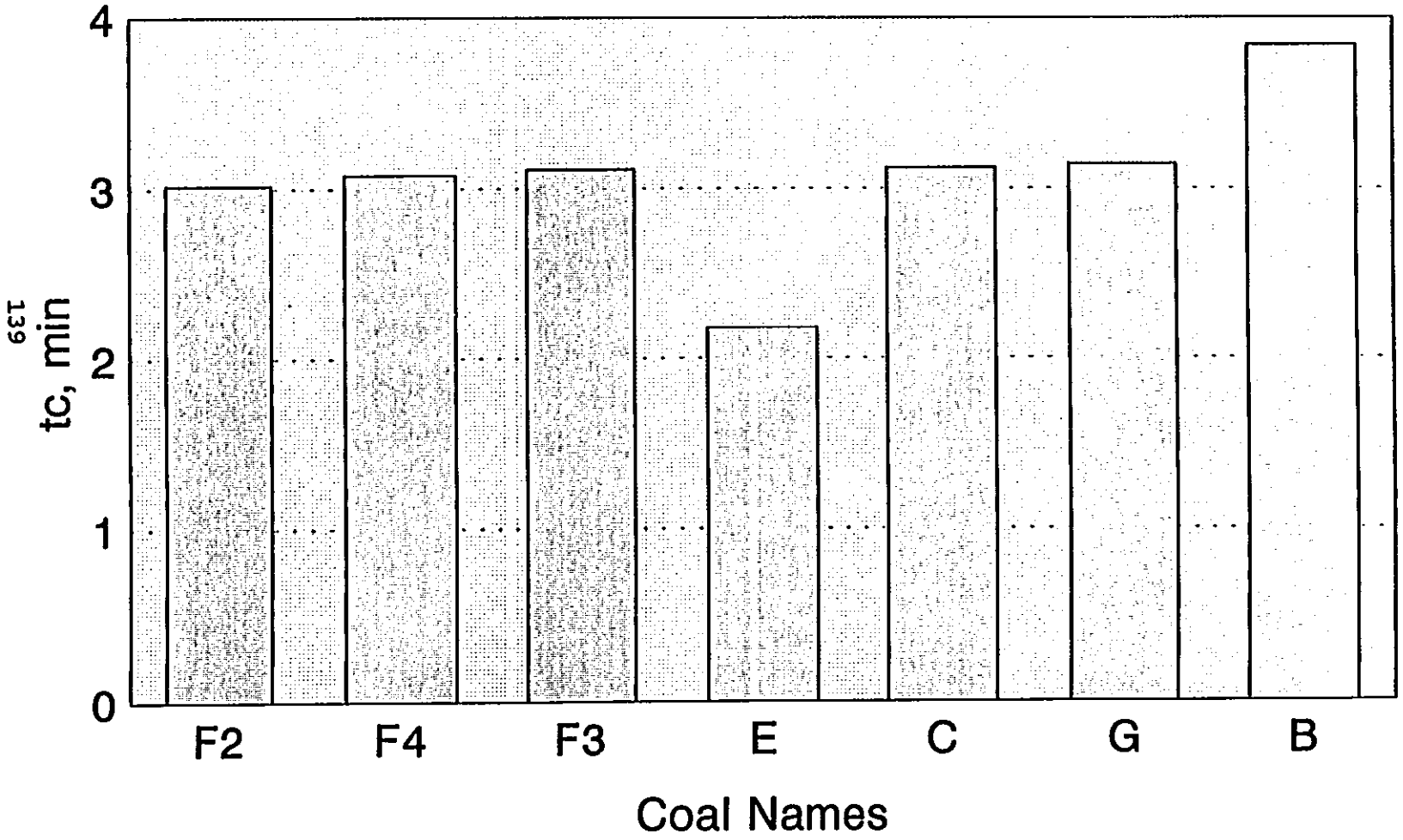

Fig. 6.2: Comparison of tc for various coal chars

conditions. As mentioned previously, uniform mono-sized char samples are not practical, but efforts were made to pick particles in as close a size range as possible.

Low rank coals like lignites are well known to be very reactive, while for bituminous coals, swelling and the amount of weight loss during devolatilization affect the porosity and reactivity of the char. The figure shows that the lignite, E, and the medium-volatile bituminous coal, B, produce the fastest and the slowest burning char respectively as expected. All high-volatile coal chars used in the present study show similar reactivity. However, the Evans, C, and the Coal Valley, G, coal samples are highly oxidized as shown by their swelling indexes (coal G shown no swelling at all). That these coal chars did not burn much more slowly than the chars produced from the fresh Prince, F, coal is surprising, since oxidation reduces plasticity and swelling of bituminous coals, which causes them to become less reactive. For the Prince coals, the raw and the washed coal chars show little variation in t_c despite a wide range in ash content. The results suggest, at least within the context of this experimental program, that ash forms no significant resistance to the reaction of the char.

The carbon combustion efficiency of the various coal chars can be obtained by carbon balance using the experimental

total conversion data with the carbon content of the char from chemical analysis. This reflects the elutriation loss. The results are given in Fig. 6.3, which shows that the medium-volatile bituminous coal, Quintette, and the washed Prince coal chars suffer higher carbon loss than the others. When comparing the various Prince coal chars, the result shows that the raw Prince coal char having higher ash content burned with better efficiency. Although the more reactive Bienfait lignite char burned much better than the unreactive Quintette coal char, reactivity does not appear to be the dominant factor in determining combustion efficiency when comparing the results given by the two figures (Figs. 6.2 and 6.3). For the case that attrition is dominated by chemical mode, the general idea that less reactive chars burn with longer residence time, and therefore allow more attrition and elutriation, is questionable.

In this work, only a small number of repeated experiments were performed to test the reproducibility. For the first series, they all used the raw Prince coal running under 850°C and 100% air inlet gas conditions. The repeated runs were operated on different days; in other words, the apparatus was shut down and restarted. The standard deviation of the population was calculated using the data of two experiments for the largest size coal range (5.7 to 12.7 mm) to be 15.1% for t_c and 2.44% for η. When using the data of three runs for

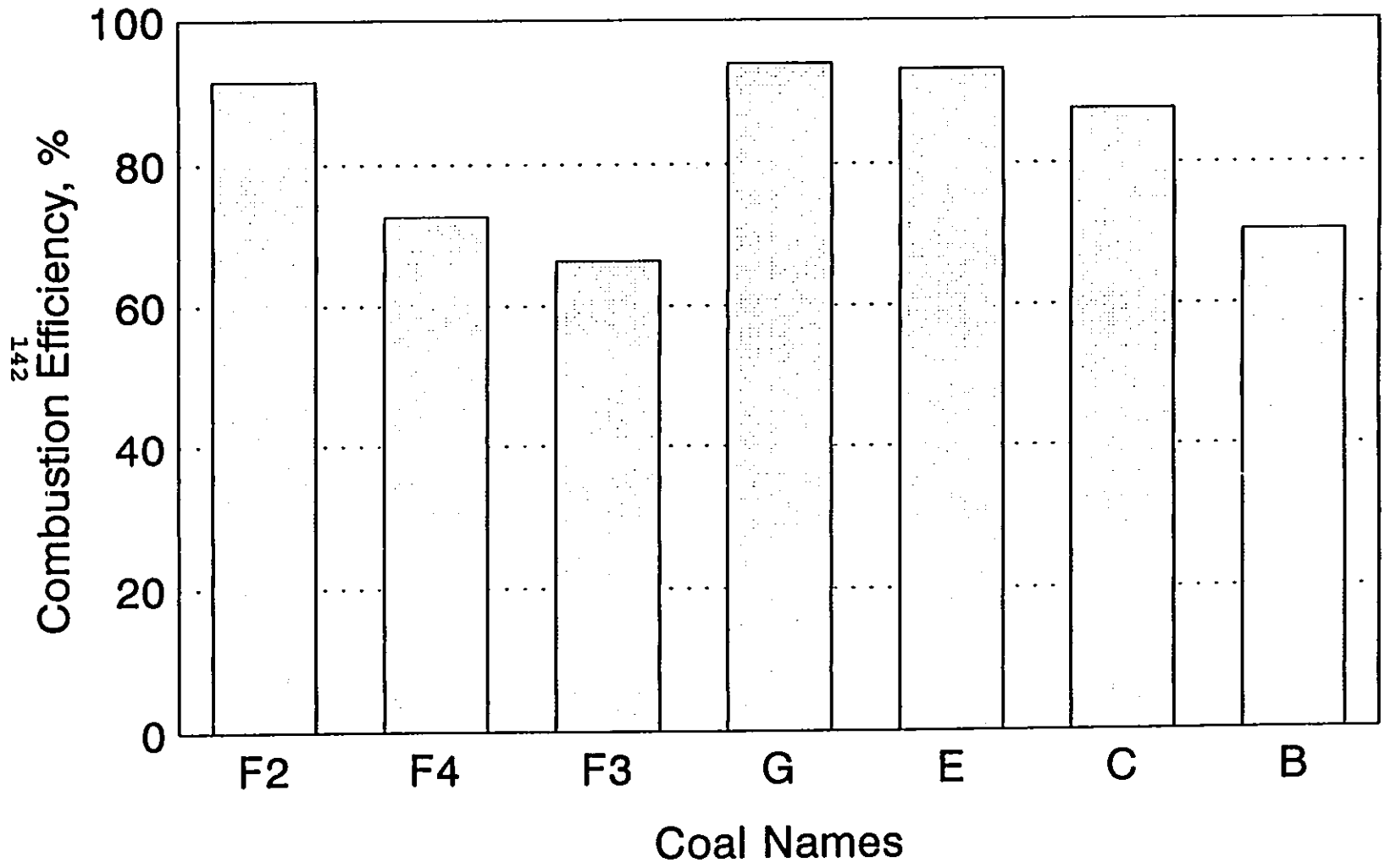

Fig. 6.3: Comparison of combustion efficiency of various coal chars

the size range 4 to 8 mm, the results become 8.32% and 4.6% for t_c and η respectively. It is noted that the results of 2.44 and 4.6% in efficiency mean a much larger standard deviation in the carbon loss fraction, 40.1 and 49.5% respectively.

These large deviations are not surprising considering the nature of the batch combustion experiments. Coals are heterogeneous substances, and their properties may be different from one sample to another although they are produced from the same mine. For repeated experiments, it is impossible to have char particle sizes and shapes, which are important factors affecting the present results, exactly similar among different batch samples. Other sources of variation may come from operation, gas sampling, gas and char analysis, but they should be small compared to that of the char sample differences. Because of the small quantity of experiments and the statistical analysis of their results, the conclusions obtained from the present experimental work should be treated as tentative and require further studies for verification.

6.1.2 Particle size and operating condition effects

Fig. 6.4 shows that both t_c and combustion efficiency increase with char particle size. In plotting this figure,

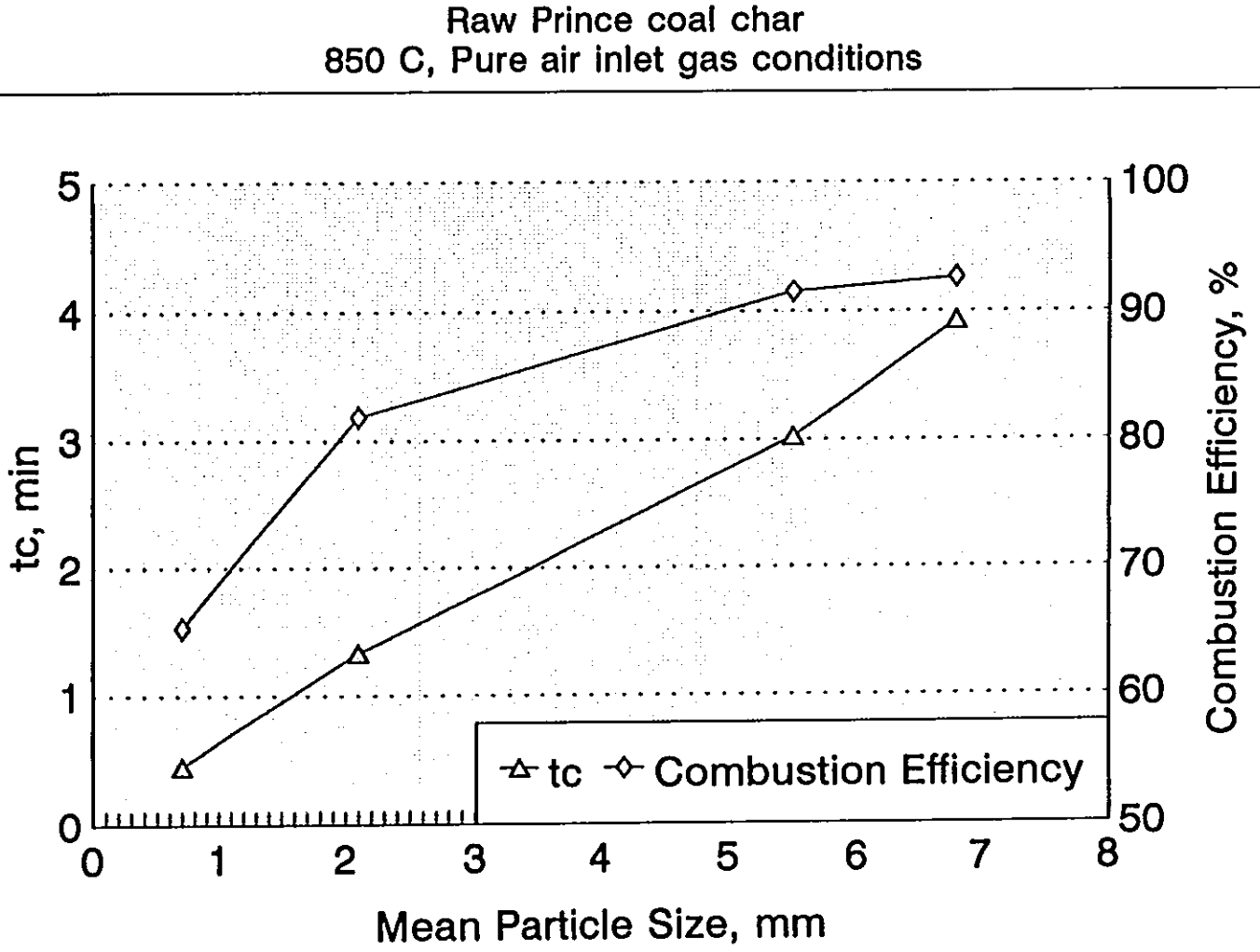

Fig. 6.4: Particle size effect on tc and combustion efficiency

arithmetic mean sizes are used for the char particles of the two large size fractions. For the two small size fractions, size measurement of a large number of particles is impractical, thus the intermediate value between size range limits was used. In general, since increasing particle size affects the mass transfer coefficient adversely, reactions burning small char particles approach the kinetic regime, while those burning large particles approach the diffusion regime. Assuming t_c directly proportional to t_B, so that the relationships in Table 2.1, or $t_c \propto d_o^{3/n}$, can be used, the value of n can be roughly estimated. The two data points of the small size fractions indicate that t_c is nearly directly proportional to particle size (close to linear when joining these two points with the origin), a reasonable kinetic regime result (n=3). However, the large size data show a lower t_c dependence on particle size than expected (n=2.36 instead of close to 1.5). Probably secondary fragmentation occurred during the combustion of large char particles, reducing the size effect. The particle size effect on combustion efficiency is obviously reduced when using large sized char particles, indicating that carbon loss due to elutriation of mother particles is diminishing.

Probably due to the fact that large sized particles were used in the experiments, the bed temperature has a mild effect on both t_c and efficiency, except at the lowest temperature

condition, 750°C, as shown in Fig. 6.5. The results suggest that diffusion is more important than kinetics for combustion of these large sized reactive char particles under normal FBC conditions. When chemical kinetics becomes important at low bed temperature conditions, mechanical attrition may also turn significant, resulting relatively in higher carbon losses.

In contrast, Fig. 6.6 shows that the oxygen concentration affects both t_c and the combustion efficiency markedly. In this study, a reactive bituminous coal, Prince, was used and was burnt under 850°C conditions with air diluted with nitrogen. When burning unreactive coal in low oxygen concentration conditions, the combustion rate is so low that the effect of pure mechanical attrition may become comparable to that of chemical attrition. Thus an even higher oxygen concentration influence on combustion efficiency is expected if an unreactive coal char is used. Also, when chemical attrition becomes relatively unimportant so that the attrition rate no longer depends on combustion, the combustion efficiency may become largely dominated by char reactivity.

6.1.3 Evaluation of the exponent n

Except for the two small particle size experiments, large size char particles were used in this experimental series. Therefore, Equ.(5.78), the simplified method for large

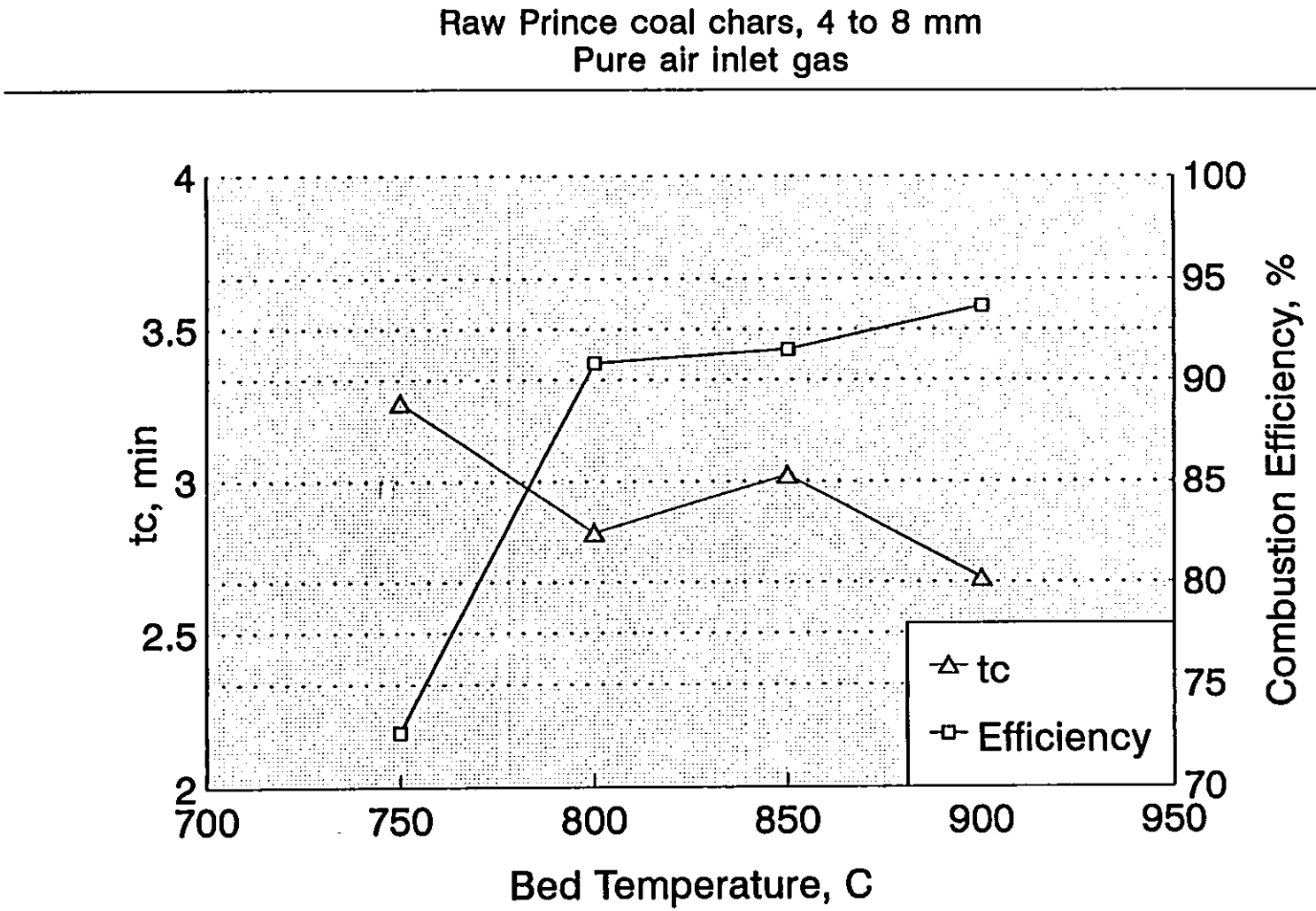

Fig. 6.5: Bed temperature effect on tc and combustion efficiency

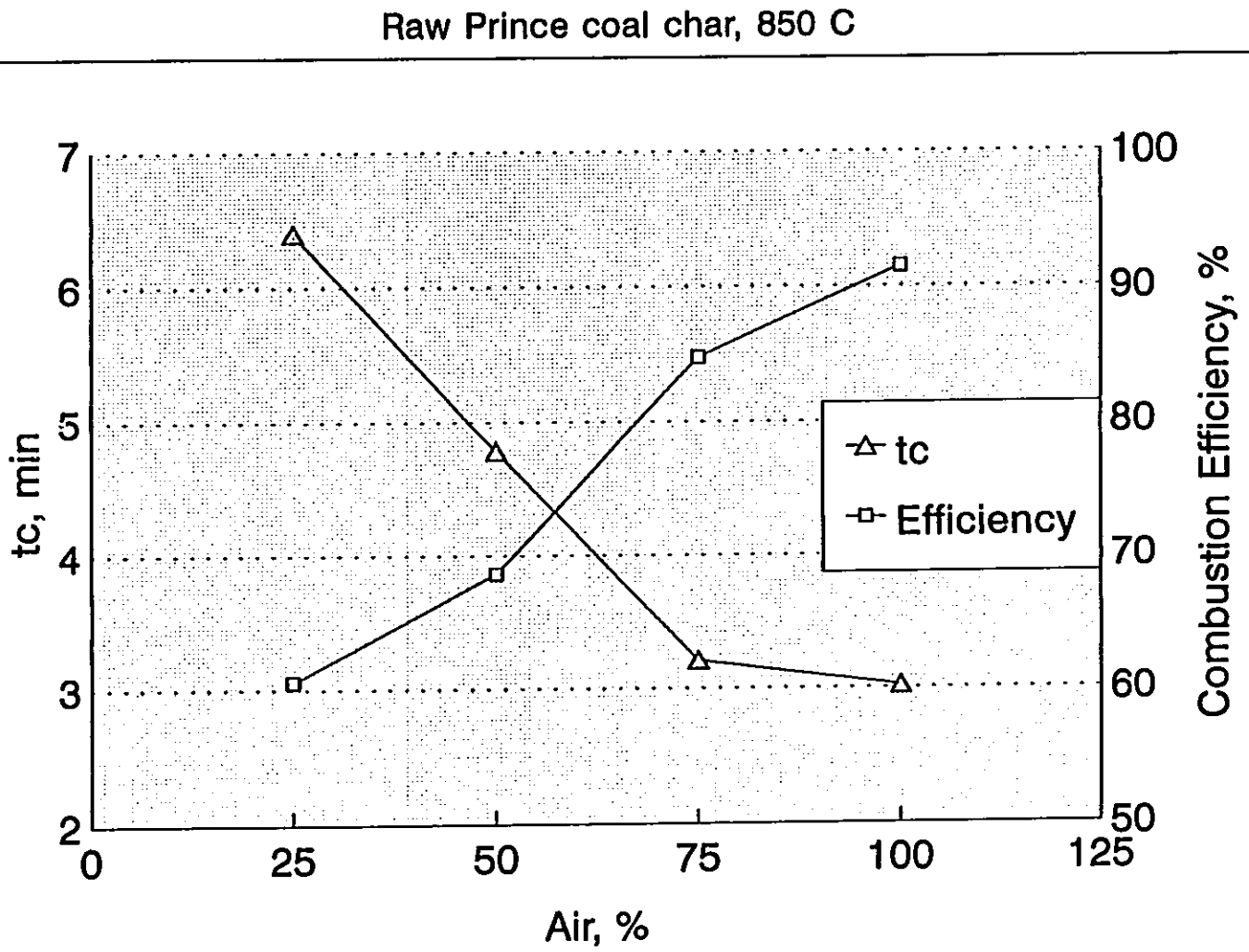

Fig. 6.6: Oxygen concentration effect on tc and combustion efficiency

particles, was used to evaluate the value of exponent n. The results are given in Table 6.1.

The value of exponent n should be between 1.5 and 3, the values for the diffusion and kinetic regimes respectively. Most results given in Table 6.1 are lower than expected and some of them even lower than the lower limit of 1.5. The unsuccessful attempt of evaluating n is probably due to the secondary fragmentation effect and the inaccurate burnout time measurement. Fragmentation during char combustion reduces both the t_c and t_{Bu} values. However, breakage of the largest particle, a high probability case, results in a greater effect on t_{Bu} than t_c, thus a lower n value. The exact burnout time is very difficult if not impossible to determine as the CO_2 concentration is very low in the final period of combustion. Most experiments in this series used the time when CO_2 concentration dropped to .005% as the end of combustion. Because of the effect of the instrumental noise, the measured burnout time may be too short, which can cause a significant error in n value evaluation. For example, a 10% reduction in t_{Bu} will typically yield an n-value about 15% lower.

6.2 Second Series Experiments

The main purpose of the second experimental series is to demonstrate the measurement of attrition related parameters.

TABLE 6.1: Evaluation of n values

Coal Name	AVE PART MASS(mg)	TEMP. (°C)	AIR %	t_c (min)	t_{Bu} (min)	n
F2	236.0	850	100	3.93	15.0	2.15
F2	131.5	900	100	2.68	8.0	1.06
F2	117.0	850	100	3.31	11.3	1.32
F2	145.8	850	100	2.87	9.9	1.99
F2	131.0	850	100	2.88	9.1	1.63
F2	142.0	800	100	2.83	9.3	1.38
F2	140.6	750	100	3.26	12.3	2.13
F2	144.5	850	75	3.21	10.7	1.64
F2	132.9	850	50	4.78	16.9	1.95
F2	135.1	850	25	6.4	18.4	--
F3	134.0	850	100	3.08	10.0	1.44
F4	171.5	850	100	3.11	10.4	1.4
E	114.0	850	100	2.18	6.8	1.46
C	130.6	850	100	3.12	9.8	1.58
B	136.8	850	100	3.84	15.8	2.51
G	121.2	850	100	3.14	11.2	1.98

According to the model development described in Chapter 3, these parameters are identical irrespective of which of the two models for attrition is applied. Gas dispersion corrections were applied to the data of the sub-tests but not the main tests.

In order to obtain information on the char particle size distribution after volatiles evolution, coal particles were used for experiments studying fragmentation. Devolatilized coal char was the only feed used for the rest of the experiments.

6.2.1 Shrinking particle model

Observing the char particles retrieved from different burning stages clearly shows that particles shrink in size during combustion. Except for the lignites (some of which were partly covered with white colour ash), ash deposits are hardly found on the char particles' surfaces. For the lignites, the ash layer is rather weak and porous, and easily broken when handling; it is therefore unlikely to provide any significant resistance to reaction.

To illustrate the validity of the application of the shrinking particle model, a couple of experimental series were conducted by burning the high ash content raw Prince coal, F2,

stagewise in fixed time periods until completion. Experimental procedures are similar to the consecutive runs described in Section 4.3.2., except that particles below the cut size were not removed, so that all the mother char particles remaining from the previous combustion stage were reburned in the next. Assuming carbon and ash are uniformly distributed in the char particles, the picture of ash deposit can be shown by comparing the ratio of the total amount of burnt carbon (from both the main test and sub-test) obtained from the flue gas concentration data, and the weight loss of the chars after various burning stages. Fig. 6.7 is a plot of the accumulated amount of burnt carbon against the accumulated weight loss in consecutive burning stages. The nearly linear relationship throughout the entire combustion period shows that no ash is deposited on char surfaces. If elutriation is very small, the slope of the curve approximately represents the carbon content of the char.

6.2.2 Particle size distribution and fragmentation

As described in Section 3.4.3, predicting the combustion efficiency for burning multi-sized char particles from the present models requires the original particle size distribution. Coals, not char, are used as feed for normal FBC operations. Chars are formed after evolution of volatiles but the particle size distribution has usually changed

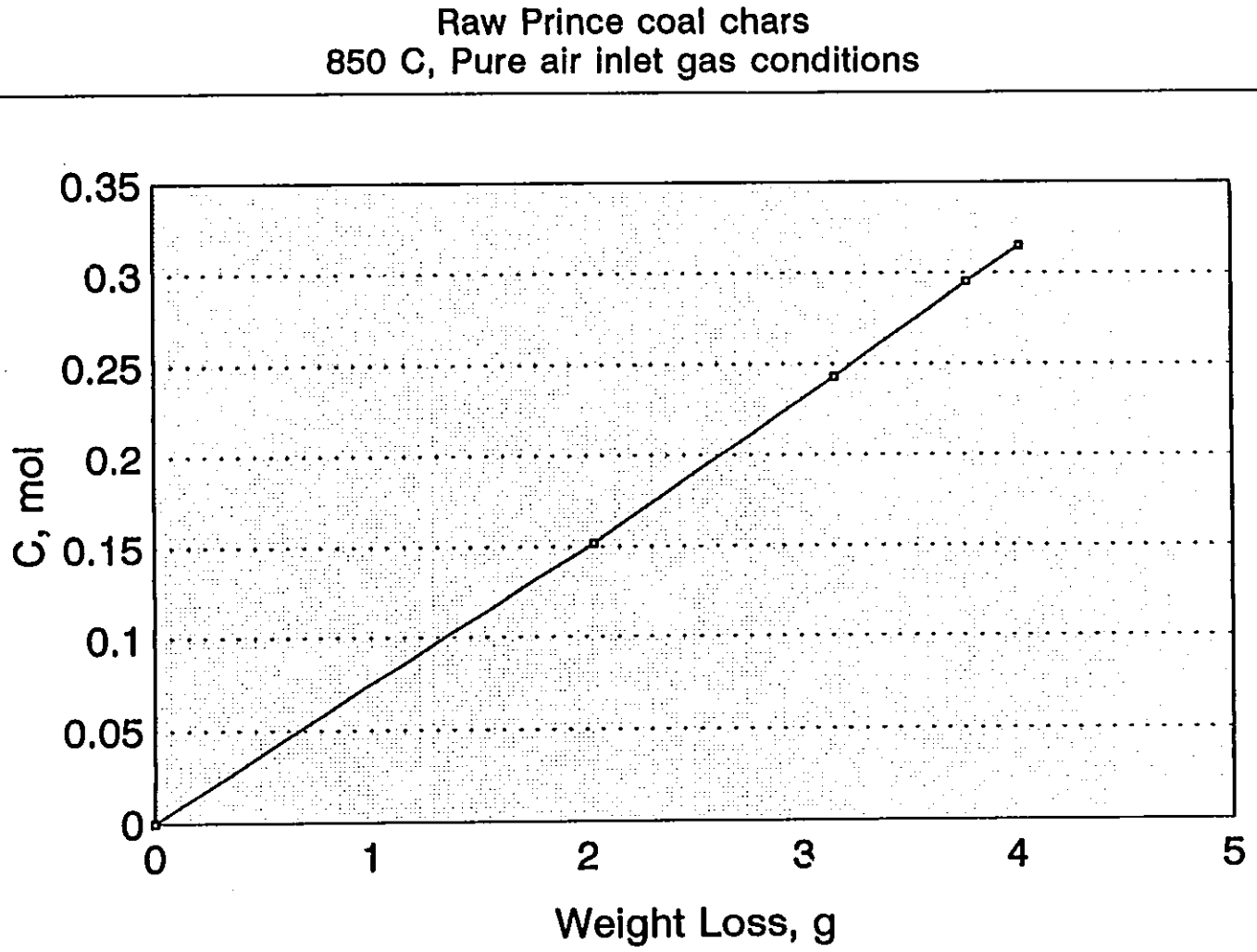

Fig. 6.7: Carbon conversion vs. weight loss

drastically from the feed coals. Information on the original char particle size distribution can be obtained only through primary fragmentation studies. In this work, the extent of primary fragmentation, simply represented by the ratio of particle numbers after and before devolatilization, N/N_o, has been investigated for various coals under different operating conditions. The present results show that primary fragmentation depends on coal type and particle size, but is a weak function of operating conditions. Within the ranges of bed temperature and oxygen concentration of the present work, no significant variation in primary fragmentation is found. When comparing coals of different sizes, Fig. 6.8 clearly shows that larger particles disintegrate more extensively than do smaller sizes. Fig. 6.8 also shows that primary fragmentation is more severe for a coal after deep cleaning than for coal in a raw form.

The coal type effect on fragmentation is given by Figs. 6.9 and 6.10, which show both primary and secondary fragmentation of various coals in two different sizes. As expected, the extent of primary fragmentation varies widely among coals. Burning coals with extensive primary fragmentation results in a large change in particle size distribution after devolatilization. Among the coals used in this study, the anthracite gives the highest extent of primary fragmentation. This contradicts the result of Jia (1991), who

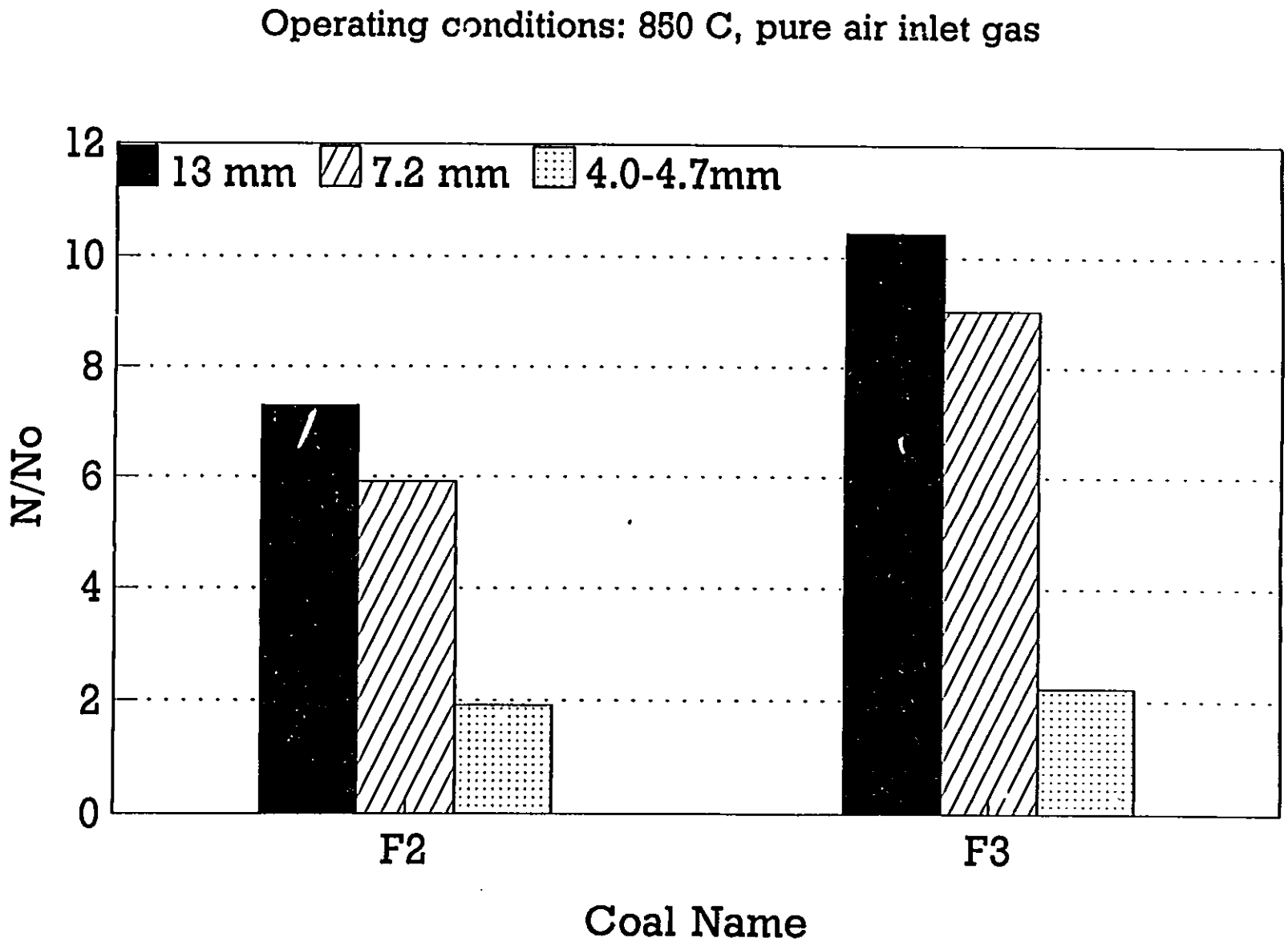

Fig. 6.8: Effect of coal size on fragmentation

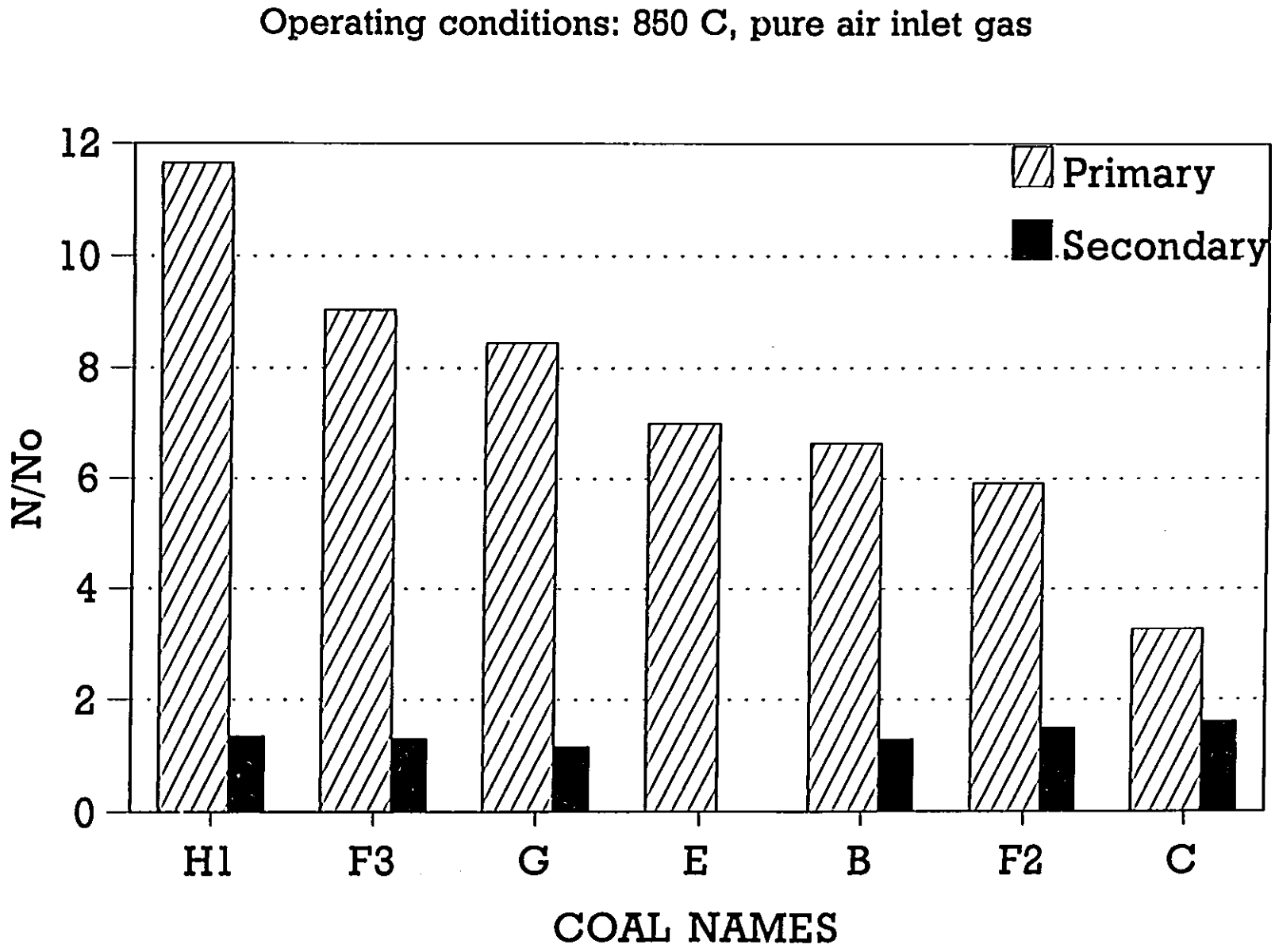

Fig. 6.9: Primary and scondary fragmentation (7.2 mm coal size)

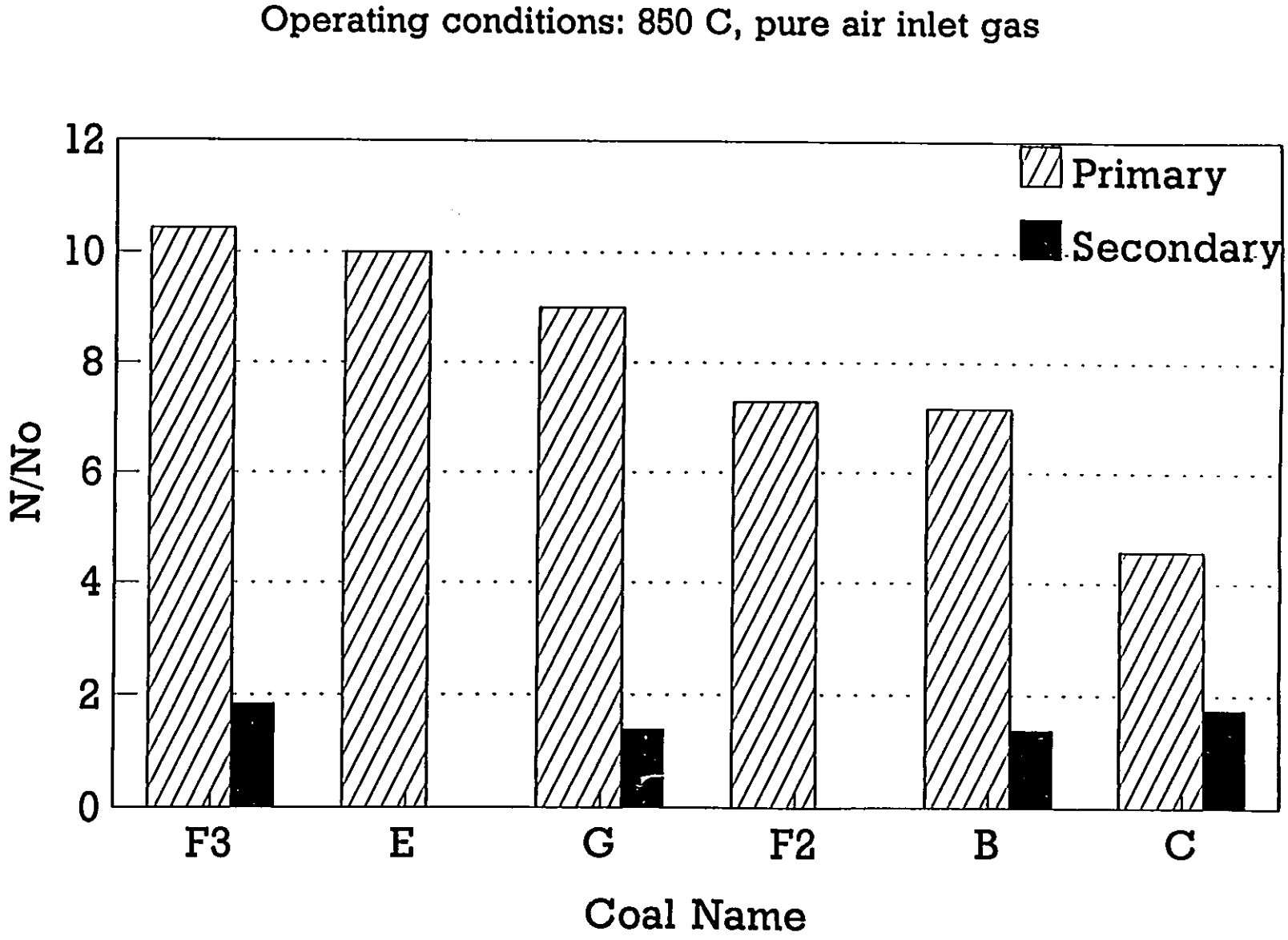

Fig. 6.10: Primary and secondary fragmentation (13 mm coal size)

found no fragmentation with anthracite. In this work, 128 fragments were retrieved after burning 11 large size anthracite particles in the combustor for one and a half minutes (the devolatilization time is difficult to determine for low volatile fuels). The retrieved chars have a wide size distribution with a large number of tiny pieces. However, two or three of the anthracite particles were found with little loss in weight or size, indicating no fragmentation for them at all. This means that even for the same kind of coal, particles may behave very differently. The study of fragmentation of coals obviously requires statistical analysis with large quantities. Since equipment size and type are not likely to influence primary fragmentation significantly, bench-scale units should perform well for this kind of study except for the difficulty in handling large quantities.

Repeated experiments for the present fragmentation studies were run with the Prince raw coal samples only. From the results of the experiments operating at 850°C bed temperature and 100% air inlet gas conditions, standard deviations for the results of N/N_o were calculated for those with original coal sizes of about 13 and 7.2 mm to yield 13.9 and 21.2% respectively (from data of 2 and 3 experiments respectively). The 7.2 mm coal samples were also used repeatedly for experiments with other operating conditions. By repeating the experiment once for the 900°C bed temperature

and for the 75% air inlet gas conditions, the standard deviation were estimated to be 17.6 and 5.43% respectively. This statistic represents mainly scatter due to the fracture variation of different coal samples.

Since all coals show that the extent of primary fragmentation increases with particle size, this process will bring the particle size distributions closer together when coal batches of different particle size are burnt. Therefore, particle size effects on FBC performance may appear mild especially for coals with large original particle size undergoing a high degree of fragmentation. To illustrate this, devolatilization experiments were conducted with two coal batches of original mean particle size 10 and 13 mm respectively under 850°C and pure air inlet gas conditions. The size of each particle before and after primary fragmentation was measured. The results are given in Fig. 6.11, which compares the cumulative particle size distributions of the product chars from the two different particle size coal samples.

During char combustion, particles may disintegrate further to a much lesser extent than in primary fragmentation. In this work, secondary fragmentation was studied by consecutive experiments using the same char particles but different degrees of conversion. Since only the char

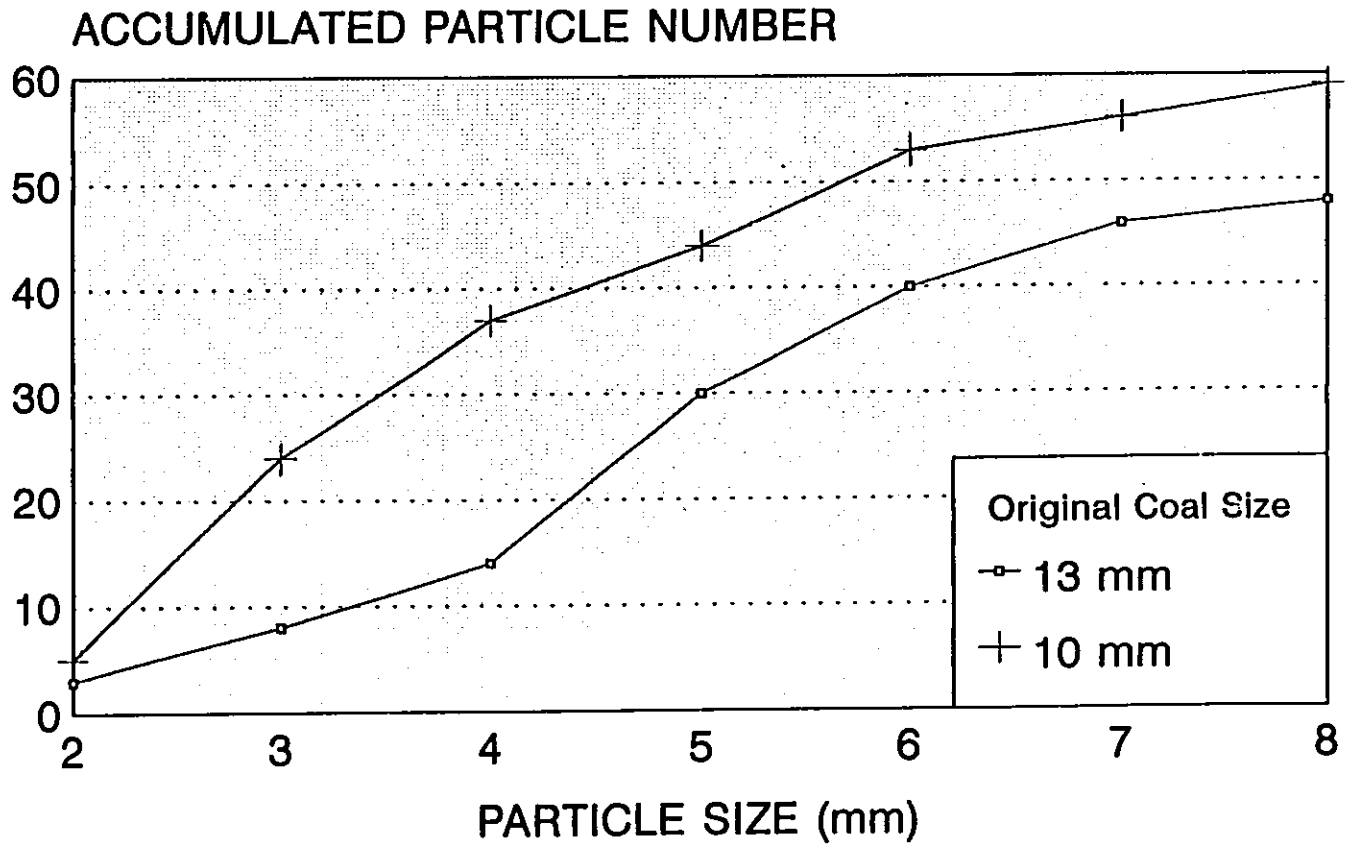

FIG. 6.11: PARTICLE SIZE DISTRIBUTIONS OF CHAR FRAGMENTS AT THE END OF COAL DEVOLATILIZATION

particles larger than the cut size were subjected to combustion, they should reappear on the screen after each char burning stage. It was assumed that the counted undersized particles would have burnt completely in the next combustion stage if they had not been removed. Thus the numbers of particles burnt and of new particles created by secondary fragmentation in each burning stage could be estimated and are shown typically in Fig. 6.12. The total extent of secondary fragmentation of some coals, accumulated from all char burning stages, are also given in Figs. 6.9 and 6.10, which shows little influence of coal type on secondary fragmentation.

Better statistics results are given by the secondary fragmentation data than those of the primary fragmentation studies; however, all the standard deviations calculated for the secondary fragmentation are based on only two experimental runs. For burning 7.2 mm Prince raw coals at 850°C and 100% air inlet gas conditions, the standard deviation of the secondary fragmentation data is 2.41%. With bed temperature changed to 900°C, and with inlet gas changed to 75% air, the results become 15.8 and 2.75% respectively. Similar to primary fragmentation, the variations in secondary fragmentation results are believed mainly caused by the coal sample differences.

Cracks on some chars are found by observation of the

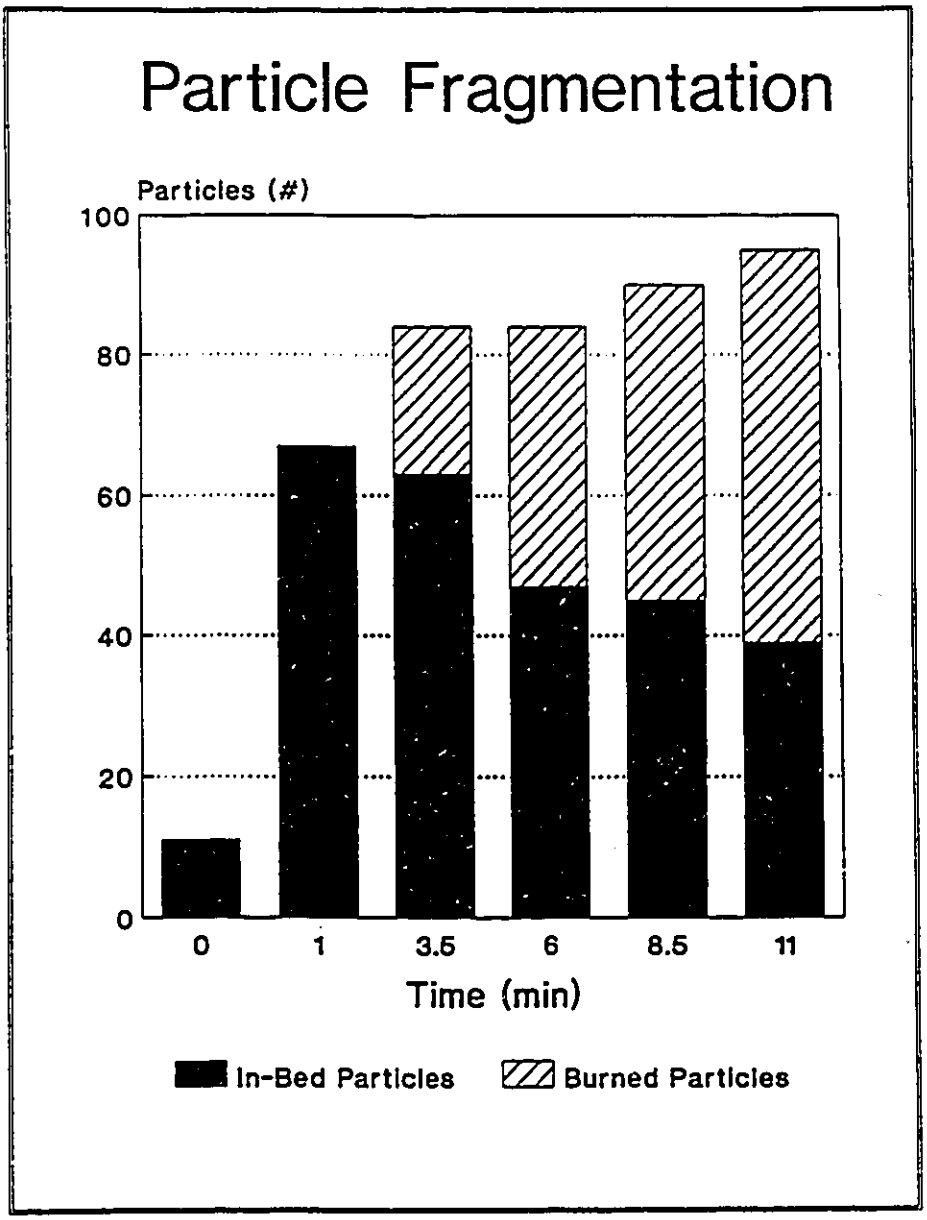

Fig. 6.12: Increase in particle numbers by fragmentation

particles after devolatilization. In a few cases, particles had broken but not separated, because an irregular crack shape held the separated fragments together. These particles, of course, are responsible for at least part of the secondary fragmentation during subsequent char combustion. Furthermore, primary fragmentation creates char particles of irregular shape from relatively round original coal particles. Char fragments with bridge portion are subject to be disintegrated as bridges are further weakened by combustion. Thus secondary fragmentation may be considered as a delay effect of primary fragmentation. Secondary fragmentation, with its phenomena not yet well known, causes more complications for combustion reaction modelling. Since unfinished primary fragmentation seems to play an important role in secondary fragmentation, one suggestion is to treat the extent of secondary fragmentation as included in the primary fragmentation as a simplified approximation for reaction modelling.

6.2.3 Attrition characteristics

As mentioned previously in Section 4.3.2, each experiment in this series includes a main test and a sub-test. During the experiment, the CO_2 concentration in the flue gas is recorded, and typical concentration curves resulting from a main-test and a sub-test are given respectively in Figs. 6.13a and 6.13b. The results of other experiments are given in

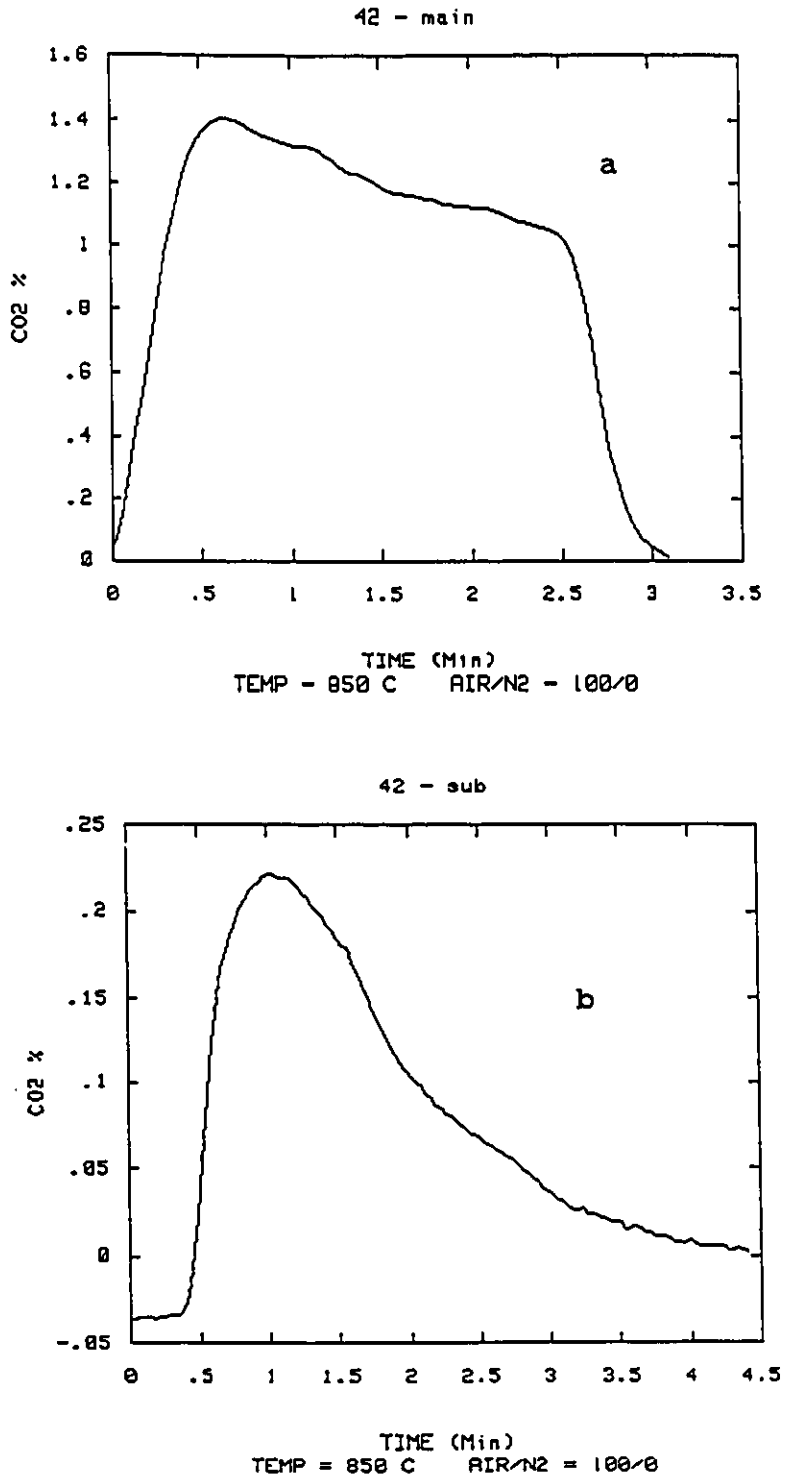

Fig. 6.13: Typical flue gas CO2 concentration curves

Appendix 2.

6.2.3.1 Particle size and extent of conversion effect

The main purpose of this experimental series is to demonstrate the measurement of the attrition-elutriation parameters, including t_{re}^*, t_{rs}^*, Y_a and $Q_a/(Q_a+R_m)$, which are required by the proposed models. The first two quantities characterize the sizes of the elutriated particles and the largest attrited particles, while the third and fourth give the elutriation fraction and attrition rate respectively. According to the model's assumptions, these parameters are independent of the extent of conversion and char particle size. As mentioned previously, many experiments were performed consecutively, beginning with devolatilizing the coal and followed by a number of runs burning the char in a fixed time period, usually 3 to 4 such char combustion periods being required to complete the combustion. In other words, the subsequent experiment used the residue char particles of the previous experiment as feedstock. Comparison of the results of these experiments can verify the previously stated assumptions. Unfortunately, the attrition results from the first of these consecutive experiments, devolatilization, are complicated by primary fragmentation, which may also generate a significant amount of fines. Parameter evaluations from many of these experimental data either reach no solution or

some obviously erroneous results; therefore, they are not used and not presented here. For the following char combustion experiments, since the original coal sample size for the first experiment is restricted to avoid significant upset to the operating conditions, such as bed temperature and oxygen concentration, the sample size becomes very small after a few combustion runs. Combustion of an extremely small amount of fines attrited from a small size char sample in the sub-test can generate only a very weak signal, so that effects from instrumental noise (up to about 30 ppm) and experimental errors become much exaggerated. Depending on the original coal particle size, char reactivity, and operating conditions, usually only the results from the first two or at most three char burning experiments can be used. A typical example is given in Table 6.2, which shows the results of three consecutive experiments burning the same char particles devolatilized from raw Prince coal under 850°C and 75% air/25% N_2 inlet gas conditions. Thus the table compares the attrition results at different degrees of char conversion, and with different mean feed char particle sizes d_o. The table shows that the results from the first two char burning periods are close. The third char burning experiment, using only 2.33 g char feed, results in more variations by comparison.

Fig. 6.14, which results from burning another type of coal, Quintette, a medium-volatile bituminous B, under 850°C

TABLE 6.2: Comparison of various burning stages

Prince raw coal char

850°C and 75% air/25% N_2 inlet gas

CHAR BURNING EXPERIMENTS	FIRST	SECOND	THIRD
$\bar{d}_o$ (mm)	5.64	4.99	4.38
$w_a \times 10^3$ (mole)	0.74	0.66	0.38
t_{re}^* (min)	0.65	0.64	0.77
t_{rs}^* (min)	1.14	1.21	2.0
λ_e	0.57	0.53	0.38
$\bar{t}_{ra}$ (min)	0.30	0.39	1.04
$R_a \times 10^3$ (mole/min)	0.72	0.63	0.26
$R_m \times 10^3$ (mole/min)	43.56	32.86	25.9
$Q_a \times 10^3$ (mole/min)	2.43	1.68	0.37
$Q_a/(Q_a+R_m)$ (%)	5.29	4.86	1.41
Y_a	0.70	0.62	0.30

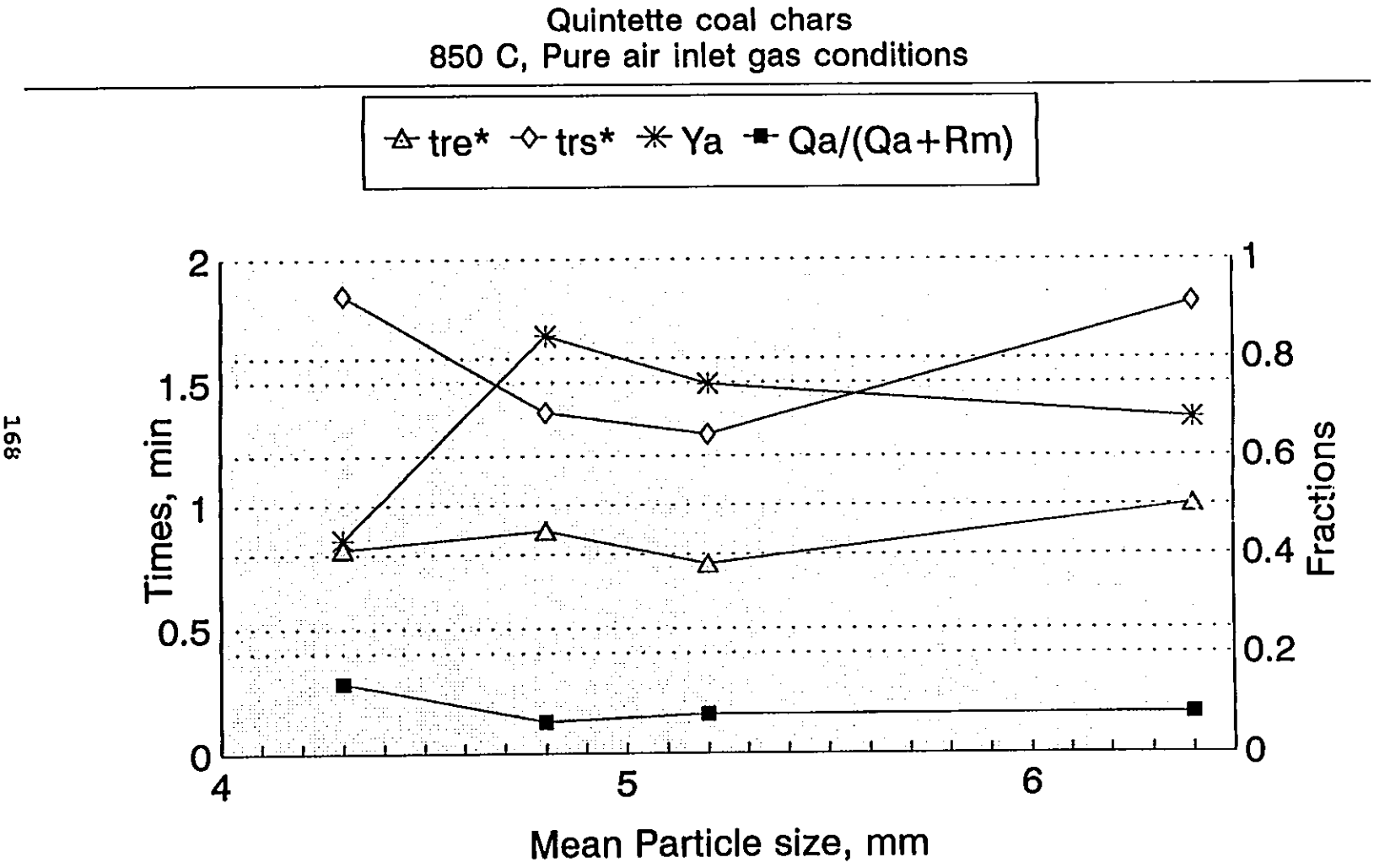

Fig. 6.14: Particle size effect on attrition characteristics

and 100 % air inlet gas conditions (not consecutive runs), further illustrates that the attrition-elutriation parameters are not strong functions of particle size. Large variations of these parameters with particle size usually appear only from the experimental results of burning chars at the final burning stages, where very small sample sizes are provided. Therefore, the following will present results averaged from experiments burning various particle sizes.

6.2.3.2 Comparison among various coals

Since the elutriated sizes of various coal chars fluidizing with similar gas velocity conditions are not expected to be highly different, a comparison of t_{re}^* between chars burning under the same operating conditions physically indicates char reactivity, while t_{rs}^* reflects both effects from kinetics and attrited particle size. Fig. 6.15 compares these parameters among coals and indicates that the lignite E is more reactive, and the medium-volatile bituminous coal B is less reactive, than the rest of the high-volatile bituminous coals. Thus the conclusions about char reactivity here are the same as those reached in the first experimental series. When comparing coals with the same origin but different cleaning histories, F2, F3, and F4, the figure indicates that the raw coal is a little more reactive than the clean coals - this agrees with Fig. 6.2; in fact, all trends for t_{re}^* agree

850 C, Pure air inlet gas conditions

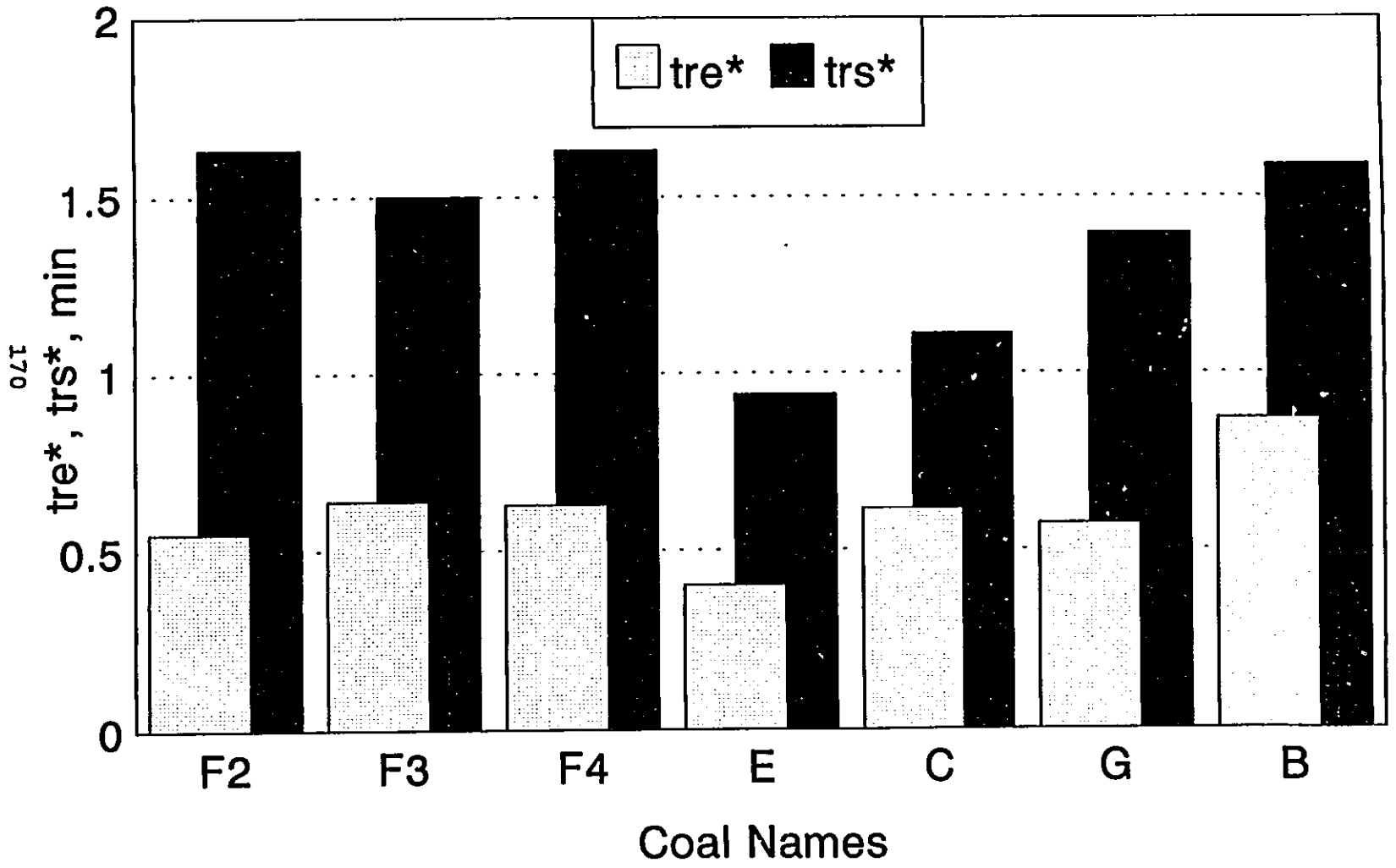

Fig. 6.15: Characteristic times comparison of various coal chars

with those for t_c.

Since t_{re}^* is the ideal mean residence time of carbon burnt under kinetic regime, its value can be approximately estimated from char reactivity correlations given in literature. For an elutriated particle, Re<0.4, its size can be evaluated from its terminal velocity u_t (Kunii and Levenspiel, 1969):

$$d_e=\left(\frac{18\mu u_t}{\rho_c g}\right)^{\frac{1}{2}} \qquad (6.1)$$

Under present experimental conditions, the freeboard temperature was about 600°C, thus μ and u_t are approximately equal to $3.8*10^{-5}$ kg/ms and 0.7 m/s respectively. By considering no large pores in the attrited fines, ρ_c is taken to be 1300 kg/m^3. Applying the above equation gives $d_e\approx200$ μm. The particle size so evaluated represents the size of the largest elutriated particle, and can be used to estimate its ideal burnout time with the following kinetic control expression (Levenspiel, 1972):

$$t_{Be}^*=\frac{\rho_c d_e}{2M_c r} \qquad (6.2)$$

From Field's correlation (1967), the reaction rate can be approximately calculated by:

$$M_c r=860 p_{o2} e^{(-18000/T_s)} \qquad (6.3)$$

When $T_s(=T_b)=850^{\circ}C$, $t_{Be}^*=61$ s, and $t_{re}^*=t_{Be}^*/4=15.2$ s or 0.25 min. Although of the same order, this value is smaller than those presented in Fig. 6.15 in spite of the largest elutriated size used. This may not be unexpected since the reaction kinetics of the attrited fines should be different to that of the fresh char particles used in the studies of Field (1967) for char reactivity correlations. The low reactivity of attrited carbons, due to lack of large pores and likely containing higher proportion of less reactive macerals, probably is part of the reason that ultra-fine char particles are generally found difficult to burn off in practice.

Besides the rate competition between the processes of reaction and attrition, combustion efficiency is determined also by the burnout degree of the attrited fines, a large fraction of which are considered larger than the elutriable size. Thus the relative particle size between attrition and elutriation is of primary importance for elutriation carbon loss. The mean value of the elutriation fraction of attrited fines, Y_a, depends, according to the model, only on λ (a ratio of t_{re}^* and t_{rs}^*), or on the relative particle sizes between elutriation and attrition. Therefore, Fig. 6.16 is the direct result of Fig. 6.15 and shows coals B and C (with higher t_{re}^*/t_{rs}^* ratio) having higher elutriation fractions for their attrited particles than the others. In other words, burning chars from coals B and C produces attrition fines with their

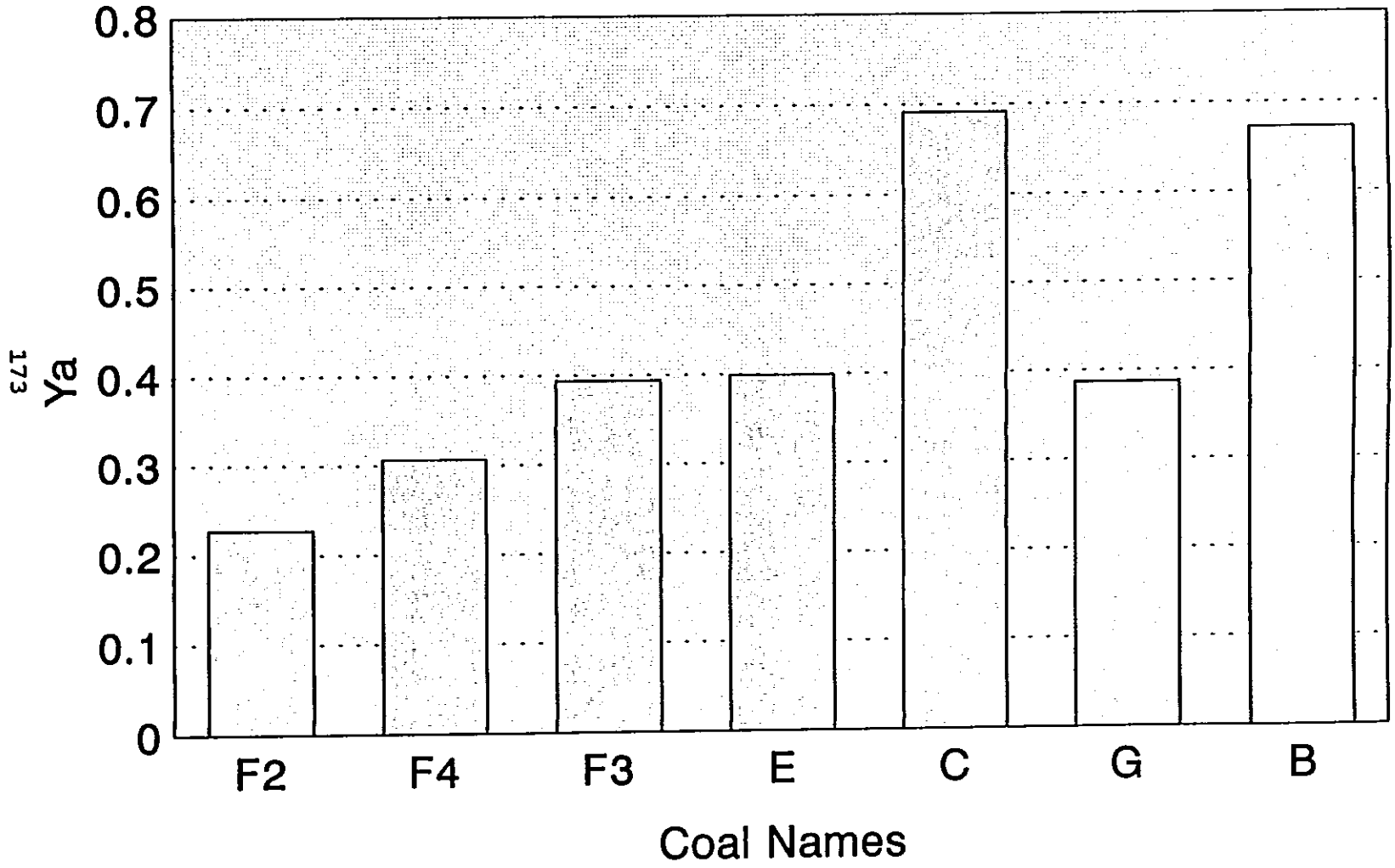

Fig. 6.16: Comparison of Ya for various coal chars

sizes relatively closer to the elutriable size, thus resulting in a higher fractional loss for the attrited fines than in burning other coal chars. Among the Prince coals, the higher the ash content, the lower the elutriation fraction for the attrited fines.

The attrition fraction, $Q_a/(Q_a+R_m)$, represents the rate competition between attrition and reaction. Fig. 6.17 shows that coal B has the highest attrition fraction among these coals, and the deep cleaned Prince coal F3 attrites more extensively than those in high ash form. The medium cleaned coal, F4, which is expected to perform in between the raw and deep cleaned coals, results in the lowest attrition fraction.

Since the attrition-elutriation parameters are not altered with particle size and conversion, the statistics of their measured values were calculated based on the results of the experiments using various particle sizes but otherwise the same operating conditions. Table 6.3 shows the standard deviations given in percentage, s, for all four parameters. Results are presented with various coals, various operating conditions, and the overall average values. For various coal chars running under 850°C and 100% air inlet gas conditions, the statistics were evaluated based on three experimental results, except coals F4, B, and F2, for which 2, 4, and 6 runs were used. No repeated experiments were performed for

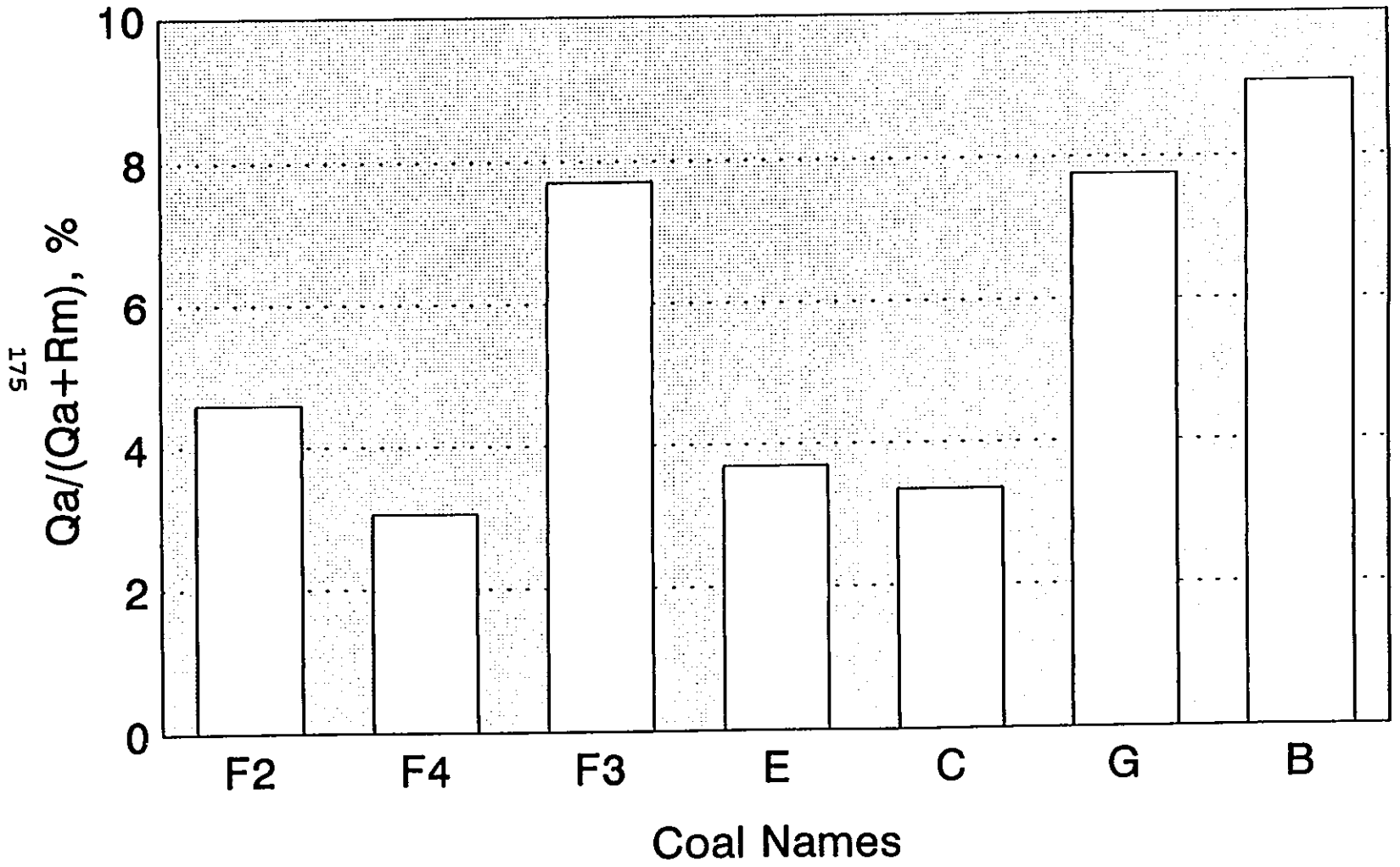

Fig. 6.17: Comparison of attrition % of various coal chars

TABLE 6.3: Standard deviation in percentage of the measured attrition-elutriation parameters

Coal Type O.C.	t_{re}^*		t_{rs}^*		Y_a		Q_a (Q_a+R_m)	
	s	s'	s	s'	s	s'	s	s'
B	12.1	13.8	18.6	19.3	26.4	11.8	37.6	11.9
C	8.71	7.19	22.1	13.0	21.6	7.95	20.5	25.2
G	5.76	0.72	21.1	3.98	42.5	12.6	18.5	0.33
F4	14.5	-	1.43	-	33.2	-	69.7	-
F3	9.13	4.85	10.6	12.8	16.6	18.8	47.6	42.8
F2	7.39	9.01	17.9	20.8	33.7	31.3	45.2	53.8
900°C	4.27	4.64	25.9	11.9	60.7	41.6	91.3	42.2
800°C	1.47	-	12.4	-	26.3	-	57.3	-
750°C	12.4	-	2.94	-	14.1	-	40.3	-
75%	9.50	1.96	25.5	2.74	28.2	7.87	45.3	27.5
25%	3.23	-	5.96	-	2.10	-	7.40	-
Ave.	8.03	6.70	15.0	9.74	27.8	18.9	43.7	34.4

Note: Results were calculated from the data of 850°C, 100% air inlet gas experiments, except those, all using F2 char, specified with either temperature or inlet gas conditions.

coal E, thus, no statistical data for this coal is given in the table. For experiments on bed temperature effects, there were three separate runs for 900°C, but only two runs for 750°C and 800°C conditions. The statistics for the 75/25 and the 25/75 air/N_2 ratio inlet gas conditions were calculated based on 5 and 2 experiments respectively. For the 50/50 air/N_2 conditions, no repeated runs were done.

Again, the scatter is high, especially for the parameters y_a and $Q_a/(Q_a+R_m)$, and the reason is likely to be the difference in behaviour among coal char samples. High scatter may also be contributed by certain experiments with difficulty in following all the restrictions of the present experimental techniques. As discussed in the last sub-section, experiments using a small particle size and sample size may result in large error. When standard deviations were calculated excluding the data of these experiments (ie excluding 8 experiments which used chars with a mean particle weight of less than 80 mg), the statistics are generally improved and are presented as s' in Table 6.3.

The char particle size used in the present experiments is considered to be large, so that the combustion efficiency can be approximated by neglecting the elutriation portion of the mother char particles. With this simplification, the carbon loss is equal to the product of the elutriation fraction of

the attrited fines and the attrition fraction irrespective of which model is used (cf. Equs.(3.9) and (3.11)). The results, given in Fig. 6.18, show much lower values than those obtained from experiments of the first series, but, with a couple of exceptions, the efficiency order among coals generally agree with each other. The reason for the large discrepancy between the results of the two experimental series is not understood. For the attrition experiments, the parameter calculations are very sensitive to the experimental data, which in turn are sensitive to any operating error due to the low sample size and low flue gas concentration dealt with, especially for sub-test runs. The restricted sample size of mother char particles will generate only a small amount of attrited fines, whose sizes may deviate significantly from the normal particle size distribution assumption. This suggests that significant errors are likely created from the second series experiments. On the other hand, the first series runs may also contribute significant errors since the carbon loss is evaluated from the difference between the carbon in the char and the carbon in the flue gas - taking a small difference of large numbers, which is always prone to large error. In addition, evaluation of combustion efficiency by carbon balance relies on analytical data which is obtained from a coal char sample statistically not necessarily identical to the char sample in use. For commercial units, high volatile bituminous coals are usually reported as burning with combustion efficiency over 98

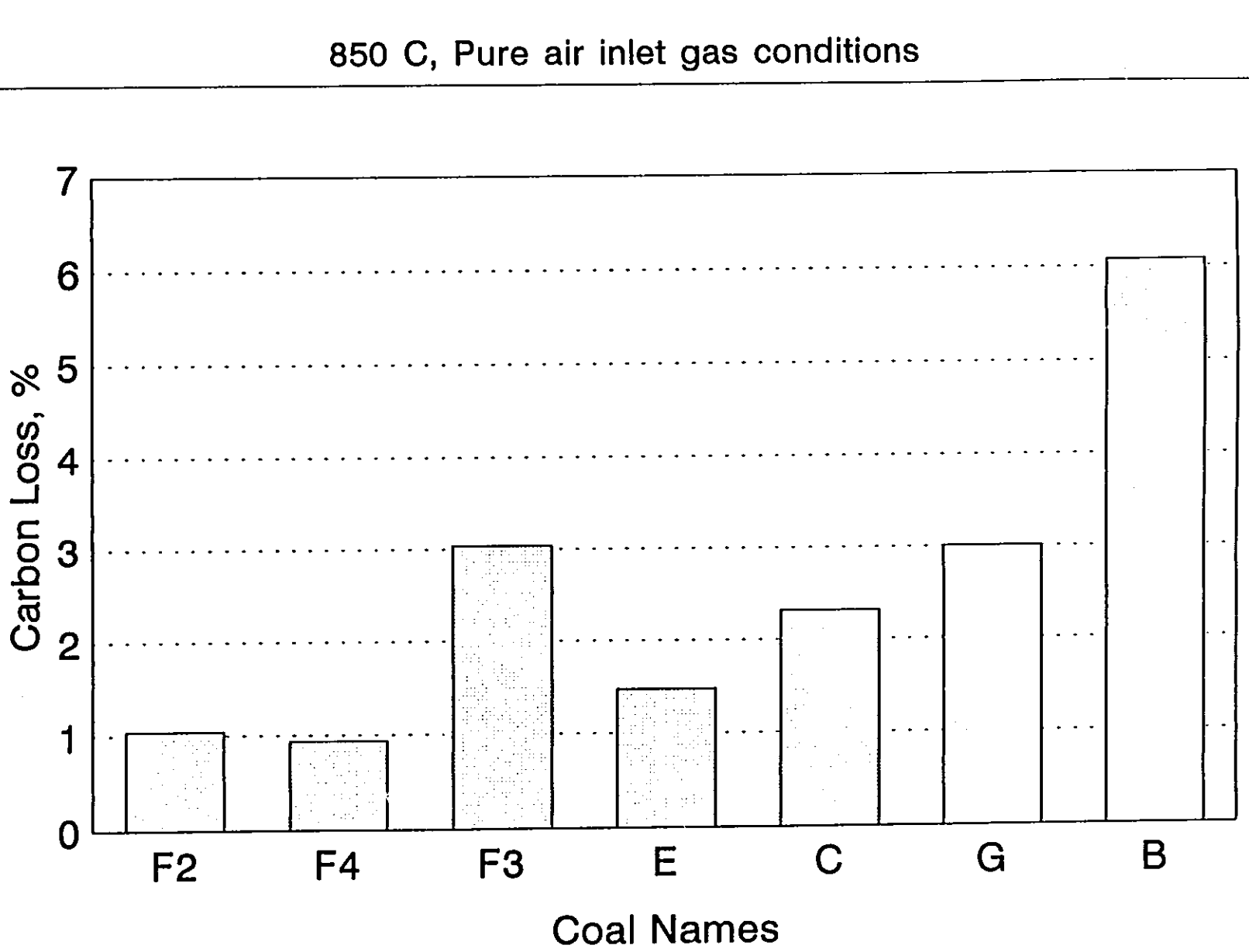

Fig. 6.18: Carbon loss comparison of various coal chars

or 99%. In comparison, large units provide long residence times for attrited fines to burn more completely; on the other hand, experiments of this work used higher oxygen concentration conditions. Thus it is difficult to judge the source of major error simply by such comparison.

6.2.3.3 Operating condition effects

The raw Prince coal char was chosen to study the bed temperature and the oxygen concentration effects on attrition parameters. Fig. 6.19 shows that t_{re}^* decreases with increasing bed temperature as expected from the kinetic point of view. The temperature effects on both t_{re}^* and t_{rs}^* become larger when bed temperature becomes lower than 800°C. When using the kinetic correlation data from literature for estimating t_{re}^* as described in the last sub-section, we obtained a value for 800°C operating conditions of 31.9 s, or 0.53 min, closed to the experimental measurement.

Fig. 6.20 shows that Y_a decreases with bed temperature while the results for attrition fraction are uncertain with widely scattered data. The Y_a result seems to suggest that larger size particles are generated by attrition processes at higher bed temperature conditions. Although oxygen may penetrate deeper into char particles at lower temperatures, the reaction is probably not rapid enough to produce

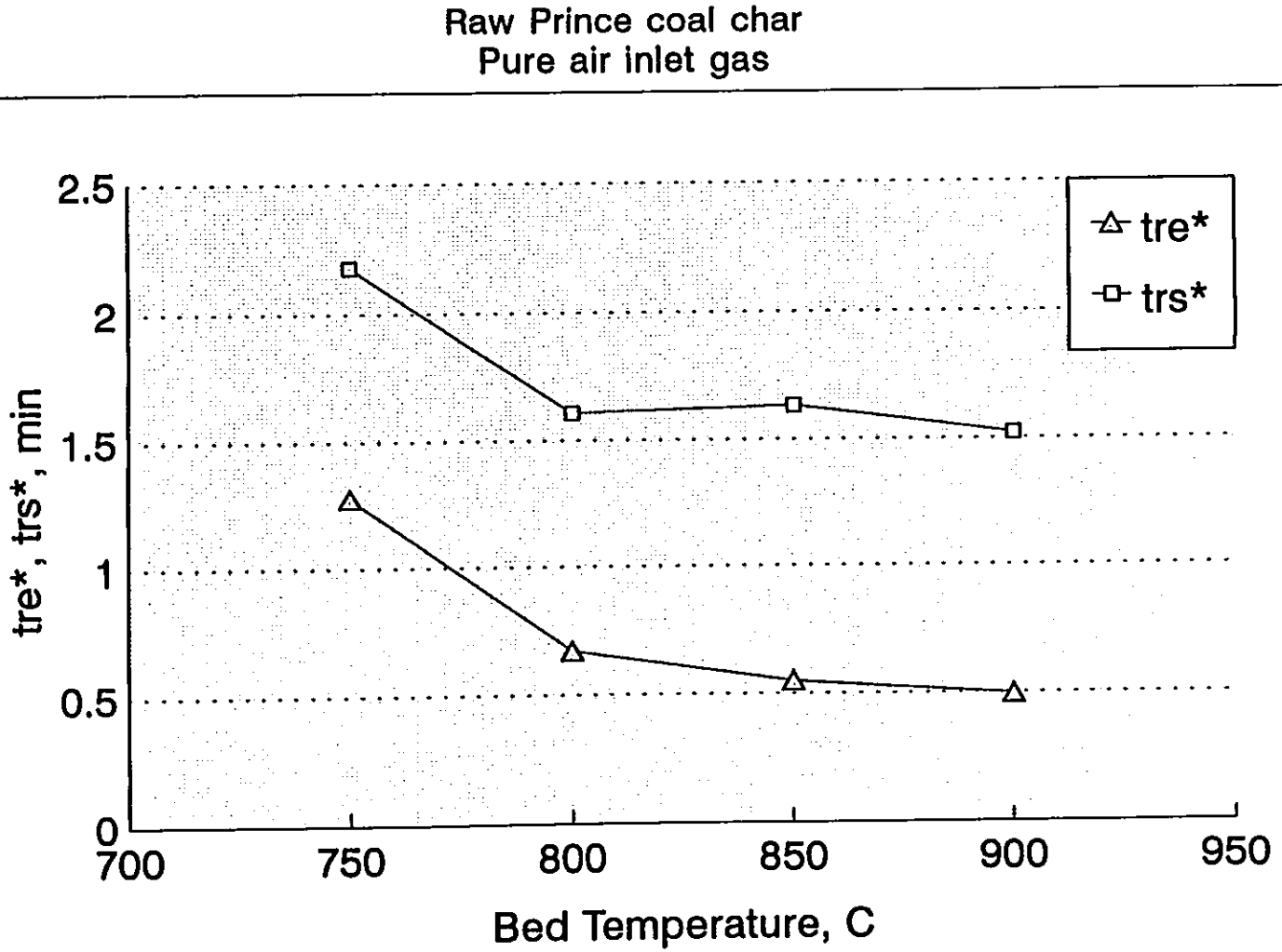

Fig. 6.19: Bed temperature effect on characteristic times

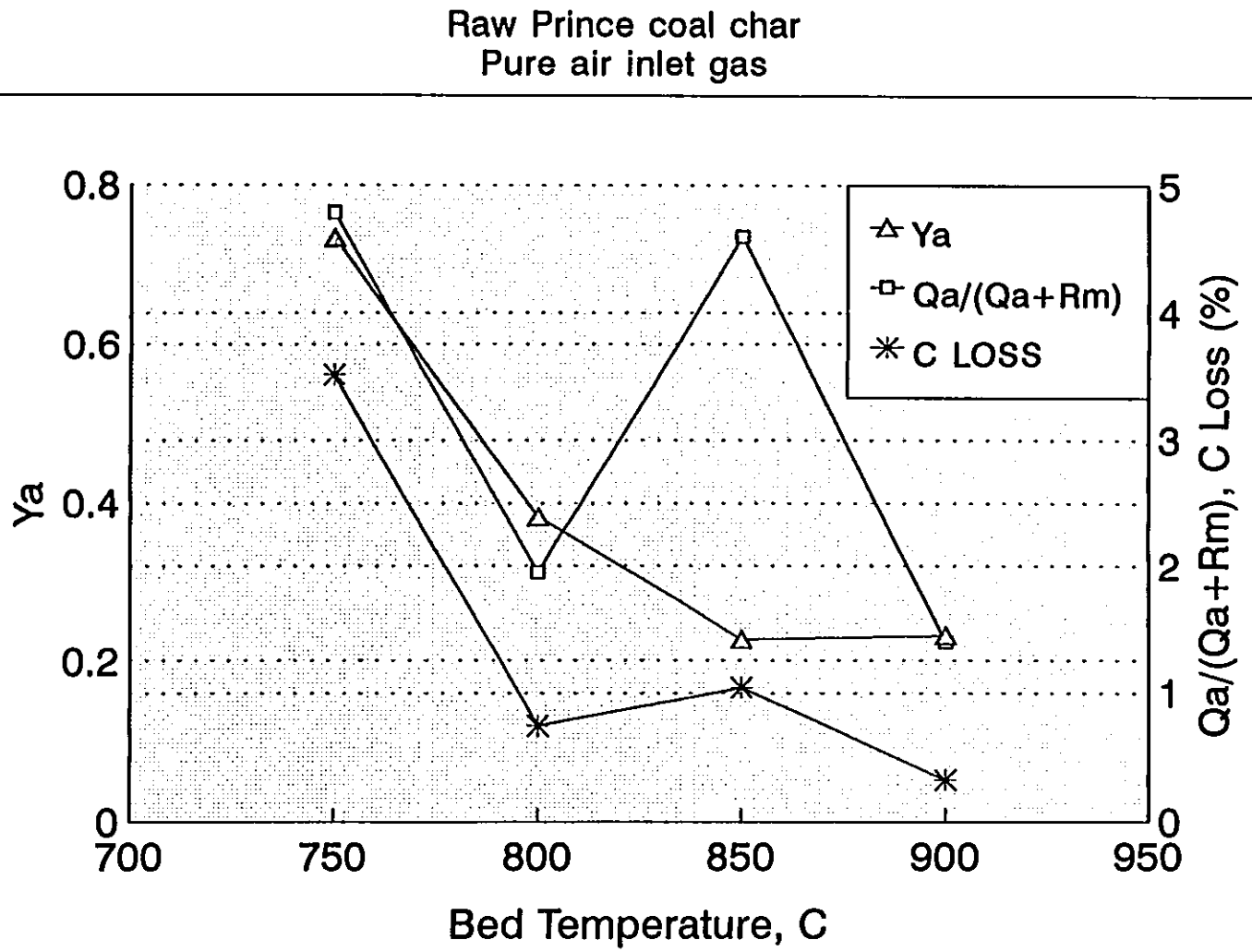

Fig. 6.20: Bed temperature effect on carbon loss

significant structural damage at the deep level. Another explanation is that mechanical attrition, which generates finer particles than chemical attrition, becomes important at low temperature conditions. Again, by applying the assumption of large particles, the carbon losses are estimated and also given in Fig. 6.20.

The results for t_{re}^* and t_{rs}^* have opposite trends with oxygen concentration conditions as shown in Fig. 6.21. Higher oxygen concentration means a higher reaction rate, for which lower values of both t_{re}^* and t_{rs}^* are expected. However, oxygen can penetrate deep into the char pores and generates large attrited particles at high oxygen concentration conditions. The larger attrited particles may burn with longer mean residence times despite the fact that reaction rate is higher. This probably is the reason why t_{rs}^* increases, instead of decreasing, with oxygen concentration.

With increasing t_{rs}^* and decreasing t_{re}^*, the elutriation fraction Y_a is undoubtedly decreasing with oxygen concentration as indicated in Fig. 6.22. The same graph also shows that oxygen concentration has little effect on attrition fraction except at the lowest oxygen level, 25% air/75% N_2 inlet gas, conditions of this work. At this point, the attrition rate is relatively high, resulting also in a higher carbon loss.

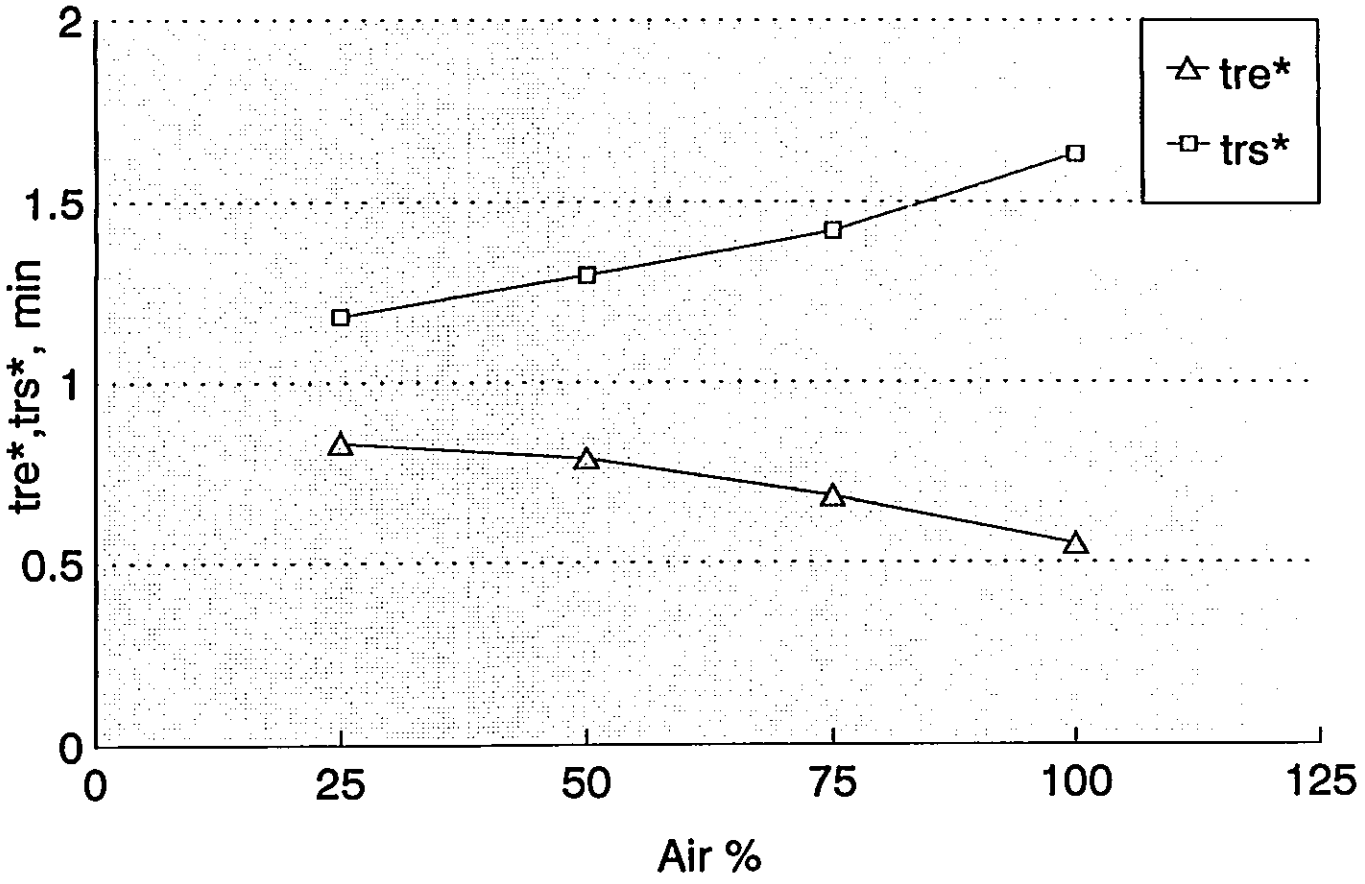

Fig. 6.21: Oxygen concentration effect on characteristic times

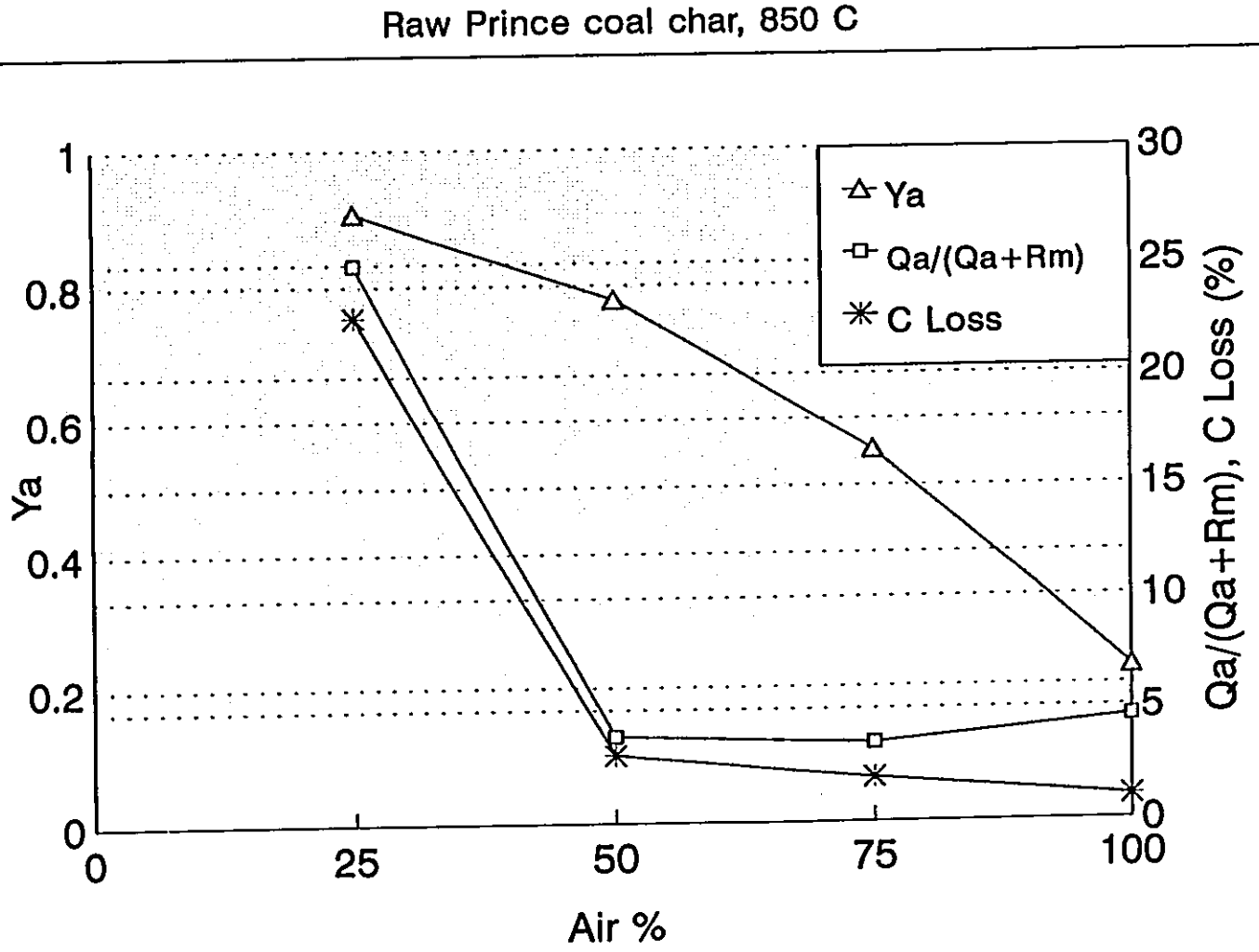

Fig. 6.22: Oxygen concentration effect on carbon loss

7. CONCLUSIONS AND RECOMMENDATIONS

7.1 Conclusions

Acknowledging the difficulties in FBC modelling by the conventional method, a fresh approach is attempted here which has the potential of being a useful way to predict combustion efficiency from bench-scale tests. Two slightly different models are developed based on fundamental gas-solid reaction kinetics and mean residence time concepts involving no complicated mechanisms or difficult mathematics.

New model parameters are introduced to characterize the reaction and attrition kinetics and the particle size in question. Experimental techniques for quantitative measurement of these parameters are developed. By applying this novel method, difficult to measure variables such as the extent of secondary fragmentation, attrition rate, post-attrition combustion rate, and elutriation fraction of attrited particles can be estimated.

The parameter measuring techniques were demonstrated by experiments, which may also be used to examine certain proposed features in the models. Most of the resulting values of the model parameters are within reasonable ranges. The results suggest that the attrited particle size and the ratio

between reaction rate and attrition rate are independent of char particle size and conversion as the models assumed. The burnout times of elutriated particles estimated from measurements in this work are longer than those predicted from correlations in the literature, which agrees with the model assumption that there is a lack of large pores in attrited fines, resulting in low reactivity. The coal type and operating condition effects agree generally with past experience and with the proposed model of the chemical attrition mechanism. The application of the shrinking particle model is also shown to be justified.

On the other hand, the difficulty of precise burnout time determination and the effect of secondary fragmentation may introduce errors in parameter measurements and create discrepancies in the results. Most results evaluated for the power of the dependence of conversion on time are lower than expected, and the results of carbon loss estimated from the second series runs are generally smaller than those estimated from the first series experiments. The experimental results seem to suggest that under slow combustion conditions mechanical attrition, which is assumed insignificant in the present models, may become important. The experimental techniques developed here also have difficulty in measuring attrition quantities during devolatilization periods. Thus future developments and modifications are certainly required

both for the model itself and the parameter measuring techniques.

In-bed carbon inventory is considered to be of great importance in determining not only combustion efficiency but also the transient response of the bed and hence its controllability. To characterize carbon inventory, which in turn indicates bed behaviour following step changes in air or fuel rates, the mean carbon residence time introduced in this work is a better choice to use than the burnout time. The burnout time obtained from a batch coal combustion experiment is the result of the largest particle after fragmentation. The MCRT is more meaningful in statistically representing the burning rate of the whole batch of fuel particles and more directly indicating the carbon inventory of practical continuous FBC systems than the burnout time. Studies on the relationship between bed transient response and MCRT may provide a better control of FBC operations. In another application, the mean carbon conversion time t_c is probably a good choice as a standard reactivity index for solid fuel comparison, since it is easy to obtain and represents the entire burning history of the particle.

The only difference between the two models developed is the handling of the final combustion stage, which is unlikely to have a large influence on combustion efficiency. Especially

for large size char particles, the difference is insignificant, thus the two models become identical. The restriction of using only large size char particles in the second series experiments simplifies the model parameter evaluation procedure. However, a comparison between the two models developed from the experimental results presented here is not possible.

7.2. Recommendations

Most of the results presented are obtained based on the novel developed model and measuring techniques, thus further verifications on the conclusions are required. Studies are needed to look at error propagation through the systems of equations set up in the models. For scale-up purposes and to provide better statistical analysis, experimental studies with larger units are preferred. Since the present work concerns only in-bed combustion, a well- developed free-board combustion model is required when comparing predicted combustion efficiency with that of a fluid bed boiler. For future experimental work, burning attrited fines in the sub-tests should be performed in a small diameter combustor to enrich the CO_2 concentration in the flue gas. Errors may also be minimized with the apparatus designed so as to make the residence times in the gas inlet and in the sampling system as short as possible. Better experimental techniques are

required to be developed to deal with the effect of secondary fragmentation and the attrition rate measurement during devolatilization period. Studies in relative contribution of mechanical attrition especially for slow combustion conditions and attrited fines reaction kinetics may further improve the models.

Although the models are developed for predicting combustion performance of coal chars burning in bubbling fluidized bed combustors, with proper modifications, they could be applied to a circulating bed or other combustion mode as well. Furthermore, the approach developed here is not necessarily restricted to coal char combustion, and may be extended to other gas-solid reaction systems having similar problems.

8. REFERENCES

Abdel-Hafez, A. H., "Simplified Overall Rate Expression for Shrinking-Core Bituminous Char Combustion", Chem. Eng. Sci. **43**, 839-845 (1988).

Andrei, M. A., A. F. Sarofim and J. M. Beér, "Time-resolved Burnout of Coal Particles in a Fluidized Bed", Combust. and Flame **61**, 17-27 (1985).

Arasstoopour H. and C-Y. Chen, "Attrition of Char Agglomerates", Powder Tech. **36**, 99-106 (1983).

Arena, U., M. D'Amore and L. Massimilla, "Carbon Attrition During the Fluidized Combustion of a Coal", AIChE J. **29**, 40-49 (1983).

Arena, A., R. Chirone, M. D'Amore and L. Massimilla, "Carbon Attrition in the Fluidized Combustion of a Metallurgical Coke", Combust. and Flame **57**, 123-125 (1984).

Arena, U., M. D'Amore, L. Massimilla, S. Meo and M. Miccio, "Evaluation of Attrition Rate Constants of Char Burning in Fluidized Beds by Means of Laboratory-Scale Combustors", AIChE J. **32**, 869-871 (1986).

Atimtay, A. T., "Combustion of Volatile Matter in Fluidized Beds", Ind. Eng. Chem. Res., 26, 452-456 (1987).

Avedesian, M. M. and J. F. Davidson, "Combustion of Carbon Particles in a Fluidized Bed", Trans. Inst. Chem. Engrs. 51, 121-131 (1973).

Basu P., "Burning Rate of Carbon in Fluidized Beds", Fuel 56, 390-392 (1977).

Becker, H. A. and R. K. Code, "Pilot Scale Trials on Atmospheric Fluidized Bed Combustion of High-Sulphur Eastern Canadian Coals (Minto and Devco) with Limestone Addition for Sulphur Capture", Report QFBC.TR.83.1, Queen's University, Kingston, Canada (1983).

Becker, H. A. and R. K. Code, "Pilot Plant Studies of Fluidized Coal Combustion", Report QFBC.TR.85.1, Queen's University, Kingston, Canada (1985).

Beér, J. M., L. Massimilla, A. F. Sarofim, "Fluidized Coal Combustion: The Effect of Coal Type on Carbon Load and Carbon Elutriation", in "Fluidized Combustion: Systems and Applications", Inst. of Energy Symp. Ser. 4, Paper IV-5, (1980) pp. 1-10.

Bemrose, C. R. and J. Bridgwater, "A Review of Attrition and Attrition Test Methods", Power Tech. **49**, 97-126 (1987).

Blinichev, V. N., V. V. Strel'tsov and E. S. Lebedeva, Int. Chem. Eng. **8**, 615 (1968).

Botterill, J. S. M., "Fluid-Bed Heat Transfer", Academic Press, London, (1975).

Bukur, D. B. and N. R. Amundson, "Fluidized Bed Char Combustion Diffusion Limited Models", Chem. Eng. Sci. **36**, 1239-1256 (1981).

Bywater, R.J., "The Effects of Devolatilization Kinetics on the Injector Region of Fluidized Beds", Proc. 6th Int. Conf. on FBC, Vol 3, Atlanta (1980), pp. 1092-1101.

Campbell, E. K. and J. F. Davidson, "The Combustion of Coal in Fluidised Beds", Inst. Fuel Symp. Ser. No. **1** : Fluidized Combustion, A2 (1975).

Caram H. S. and N. R. Amundson, "Diffusion and Reaction in a Stagnant Boundary Layer about a Carbon Particle", Ind. Eng. Fundam. **16**, 171-181 (1977).

Catipovic, N.M., Jovanovic, G.N. and Fitgerald, T.J., "Regimes

of Fluidization for Large Particles", AIChE J. **24**, 543-547 (1978).

Chakraborty, R. K. and J. R. Howard, "Burning Rates and Temperatures of Carbon Particles in a Shallow Fluidized-bed Combustor", J. Inst. Fuel **51**, 220-224 (1978).

Chakraborty, R. K. and J. R. Howard, "An Experimental Study of Mechanism of Combustion of Carbon in Shallow Fluidized Beds", Proc. 3rd Int. Fluidization Conf., New Hampshire (1980), pp 167-174.

Chakraborty, R. K. and J. R. Howard, "Combustion of Char in Shallow Fluidized Bed Combustors: Influence of Some Design and Operating Parameters", J. Inst. Energy **54**, 48-54 (1981).

Chandran, R.R., J. N. Duqum, M. A. Perna, D. D. Sutherland and D. R. Rowley, "Ranking Fuels for Utility-Scale AFBC Application", Proceeding of the 10th Int. Conf. on FBC, 313 - 322 (1989).

Chirone, R., A. Cammarota, M. D'Amore and L. Massimilla, "Fragmentation and Attrition in the Fluidized Combustion of a Coal", Proc. 6th Int. Conf. on FBC, Washington (1982), pp. 1023-1029.

Chirone, R., M. D'Amore, L. Massimilla and A. Mazza, "Char Attrition During the Batch Fluidized Bed Combustion of a Coal", AIChE J. **31**, 812-820 (1985).

Chirone, R. and L. Massimilla, Proc. 22nd Sypm. (Int.) on Combustion, (1988), p.267.

Chirone, R. and L. Massimilla, Powder Tech. **57**, 197 (1989).

Chirone, R. and L. Massimilla, "Primary Fragmentation in Fluidized Bed Combustion of Anthracites", Powder Tech. **64**, 249-258 (1991).

Chirone, R., P. Salatino and L. Massimilla, Combust. and Flame **77**, 79 (1989).

Congalidis, J. P. and C. Georgakis, "Multiplicity Patterns in Atmospheric Fluidized Bed Coal Combustors", Chem. Eng. Sci. **36**, 1529-1546 (1981).

Dakić, D., G. van der Honing and B. Grubor, "Mathematical Simulation of Coal Fragmentation During Devolatilization in Fluidized Bed", Paper presented at the IEA-AFBC Mathematical Modelling Meeting, Göteborg, Sweden (1989).

Davidson, J. F. and D. Harrison," Fluidized Particles",

Cambridge University Press, Cambridge, (1963).

Daw, C. S. and R. P. Krishnan, "Combustion Kinetics of Western Kentucky No. 9 Coal", Oak Ridge National Lab. Report ORNL/TM-8604 (1983).

Durão, D. F. G., P. Ferrão, I. Gulyurtlu and M. V. Heitor, "Combustion Kinetics of High-Ash Coals in Fluidized Beds", Combust. and Flame **79**, 162-174 (1990).

Fan, L. T., K. Tojo and C. C. Chang, "Modelling of Shallow Fluidized Bed Combustion of Coal Particles", Ind. Eng. Chem. Proc. Des. Dev. **18**, 333-337 (1979).

Field, M. A., D. W. Gill, G. G. Morgan and P. G. W. Hawksley, "Combustion of Pulverised Coal", BCURA, Leatherhead (1967), pp. 186-210.

Forsyth, W. L. and W. R. Herting, Ind. Eng. Chem. **6**, 1200 (1949).

Frössling, N., "The Evaporation of Falling Drops", Gerlands Beitr. Geophys. **52**, 107-216 (1938).

Fuertes, A. B., J. J. Pis, A. Suárez, V. Artos and F. Rubiera, "Coal Ash Attrition in a Fluidized Bed", Proc. 10th Int. Conf.

on FBC, Vol. 2, San Francisco (1989), pp. 1225-1230.

Gibbs, B. M., " A Mechanistic Model for Predicting the Performance of a Fluidized Bed Coal Combustor", Inst. Fuel Symp. Ser. 1: Fluidized Combustion, Vol.I, A5.1 (1975).

Gordon, A. L. and N. R. Amundson, "Modelling of Fluidized Bed Reactors-IV, Combustion of Carbon Particles", Chem. Eng. Sci. 31, 1163-1178 (1976).

Gordon, A. L., H. S. Caram and N. R. Amundson, "Modelling of Fluidized Bed Reactors-V, Combustion of Carbon Particles-an Extension", Chem. Eng. Sci. 33, 713-722 (1978).

Hayhurst, A. N., "Does Carbon Monoxide Burn Inside a Fluidized Bed? A New Model for the Combustion of Coal Char Particles in Fluidized Beds", Combust. and Flame 85, 155-168 (1991).

Hirama, T., H. Hosoda, H. Nishizaki, T. Chiba and H. Kobayashi, "Effect of the Size Distribution of Coal on Fluidized-Bed Combustion", Int. Chem. Eng. 24, 502-510 (1984).

Howard, J. B. and R. H. Essenhigh, "Mechanism of Solid-Particle Combustion with Simultaneous Gas-Phase Volatiles Combustion", 11th Symp. (Int.) on Combustion, The Combustion Institute, 399 (1967).

Howard, J. B., G. C. Williams and D. H. Fine, Proc. 14th Sypm. (Int.) Combust., The Combust. Inst., Pittsburgh, (1973), pp. 975-985.

Hustad, J. E., D. Vareide and O. K. Sønju, "Burning Ratesof Coke Particles in the Freeboard Above a Fluidized Bed Reactor", Combust. and Flame 85, 232-240 (1991).

Jia, L., "Burning and Devolatilization of Large Coal Particles in Fluidized Bed", PhD thesis, Queen's University, Kingston, Canada (1991).

Khraisha, Y. H. and D. R. Dugwell, "Coal Combustion and Limestone Calcination in a Suspension Reactor", Chem. Eng. Sci. 47, 993-1006 (1992).

Kono, H., AIChE Symp. Ser. No. 205, 77, 96 (1981).

La Nauze, R. D., "Fundamentals of Coal Combustion in Fluidised Beds", Chem. Eng. Res. Des. 63, 3-33 (1985).

Levenspiel, O., "Chemical Reaction Engineering", 2nd Ed., John Wiley & Sons, New York (1972).

Merrick, D. and J. Highley, AIChE Symp. Ser. 70, 366 (1972).

Olander, D.R., Sickhaus, W., Jones, R. and Schwarz, J.A., J. Chem. Phys. 57, 408 (1981).

Park, D., O. Levenspiel and T. J. Fitzgerald, "A Comparison of the Plume Model with Currently Used Model for Atmospheric Fluidized Bed Combustion", Chem. Eng. Sci. 35, 295-301 (1980).

Patel, M.S., "Fluidized Bed Gasification and Combustion", Ph.D. Dissertation, University of Cambridge, Cambridge, UK, (1979).

Patel, K., A. W. Nienow and I. P. Milne, "Attrition of Urea in a Gas-Fluidized Bed", Powder Tech. 47, 257-261 (1986).

Peeler, J. P. K. and H. J. Poynton, "Devolatilization of Large Coal Particles Under Fluidized Bed Conditions", Fuel, 71, 425-430 (1992).

Pillai, K. K., "The Influence of Coal Type on Devolatilization and Combustion in Fluidized Beds", J. Inst. of Energy 54, 142-150 (1981).

Pis, J. J., A. B. Fuertes, V. Artos, A. Suárez and F. Rubiera, "Attrition of Coal Ash Particles in a Fluidized Bed", Powder Tech. 66, 41-46 (1991).

Ragland, K. W. and F. A. Pecson, 22nd Sypm. (Int.) on Combust., The Combust.Inst. (1988), p. 259.

Ray, Y. C., T. S. Jiang and C. Y. Wen, "Particle Attrition Phenomena in a Fluidized Bed", Powder Tech. **49**, 193-206 (1987).

Roscoe, J. C., A. R. Witkowski and D. Harrison, "The Temperature of Coke Particles in a Fluidized Combustor", Trans. Inst. Chem. Eng. **58**, 69-72 (1980).

Ross, I. B. and J. F. Davidson, "The Combustion of Carbon Particles in a Fluidized Bed", Trans. Inst. Chem. Eng. **59**, 108-114 (1981).

Ross, I. B., M. S. Patel and J. F. Davidson, "The Temperature of Burning Carbon Particles in Fluidized Beds", Trans. Inst. Chem. Eng. **59**, 83-88 (1981).

Rowe, P. N., K. T. Claxton and J. B. Lewis, "Heat and Mass Transfer from a Single Sphere in an Extensive Flow Fluid", Trans. Inst. Chem. Eng. **43**, T14-T31 (1965).

Salatino, P. and Massimilla, L. "A Descriptive Model of Carbon Attrition in the Fluidized Combustion of a Coal Char", Chem. Eng. Sci. **40**, 1905-1916 (1985).

Saxena, S.C. and A. Rehmat, "A Mathematical Model for Char Combustion in a Fluidized Bed", Proc. 6th Int. Conf. on FBC, Atlanta (1980), pp. 1138-1150.

Shamlou, P. A., Liu, Z. and J. G. Yates, "Hydrodynamic Influences on Particle Breakage in Fluidized Beds", Chem. Eng. Sci. 45, 809-817 (1990).

Sishtla, C., I. Chan, J. Findlay and T. M. Knowlton, "The Effect of System Parameters on Fines Generation in Fluidized Limestone/Coal-Char Mixtures", Paper presented at the 1988 AIChE Annual Meeting, Washington (1988).

Sishtla, C., J. Findlay, I. Chan and T. M. Knowlton, "The Effect of Temperature and Gas Velocity on Fines Generation in Non-Reactive Fluidized Bed of Coal Char", in "Fluidization VI", J. R. Grace, L. W. Shemilt and M. A. Bergougnou, Eds., Engineering Foundation, New York (1989), p. 581.

Smith, I. W., Fuel 57, 409 (1978).

Spalding, D. B., "Some Fundamentals of Combustion, Gas Turbine Ser. Vol. 2", Butterworths, London, (1955).

Stach, E., M.-Th. Mackowsky, M. Teichmüller, G. H. Taylor, D. Chandra and R. Teichmüller, Eds., Gebrüder Borntraeger,

Berlin, Stuttgart (1982), P. 87-139.

Stubington, J. F. and T. M. Linjewile, "The Effect of Fragmentation on Devolatilization of Large Coal Particles", Fuel, **68**, 155 (1989).

Sundback, C. A., J. M. Beer and A. F. Sarofim. "Fragmentation Behaviour of Single Coal Particles in a Fluidized Bed", Proc. 20th Symp. (Int.) on Combust., The Combust. Inst. (1984), p. 1495-1503.

Turnbull, E., " Fluidized Combustion of Char and Volatiles from Coal", Ph.D. Dissertation, University of Cambridge, U.K. (1983).

Turnbull, E. and J. F. Davidson, "Fluidized Combustion of Char and Volatiles from Coal", AIChE J. **30**, 881-889 (1984).

Vaux, W. G. and D. L. Keairns, "Particle Attrition in Fluid-Bed Processes", in "Fluidization", J. R. Grace and J. M. Matsen, Eds., Engineering Foundation, New York (1980), p. 437.

Yagi, S. and Kunii, D., Chem. Eng. (Japan), **19**, 500 (1955).

Young, B. C. and I. W. Smith, Proc. 18th Symp. (Int.) on Combust., The Combust. Inst., Pittsburgh, (1981), pp. 1249-

1254.

Zhang, J. Q., "Devolatilization and Combustion of Large Coal Particles in Fluidized Sand Beds", PhD thesis, Queen's University, Kingston, Canada (1987).

APPENDIX 1

First Series Experimental Results

Each page gives the experimental CO_2 concentration and total carbon conversion versus time curves together with a summary of the operating conditions and the principal results for the first series experiments.

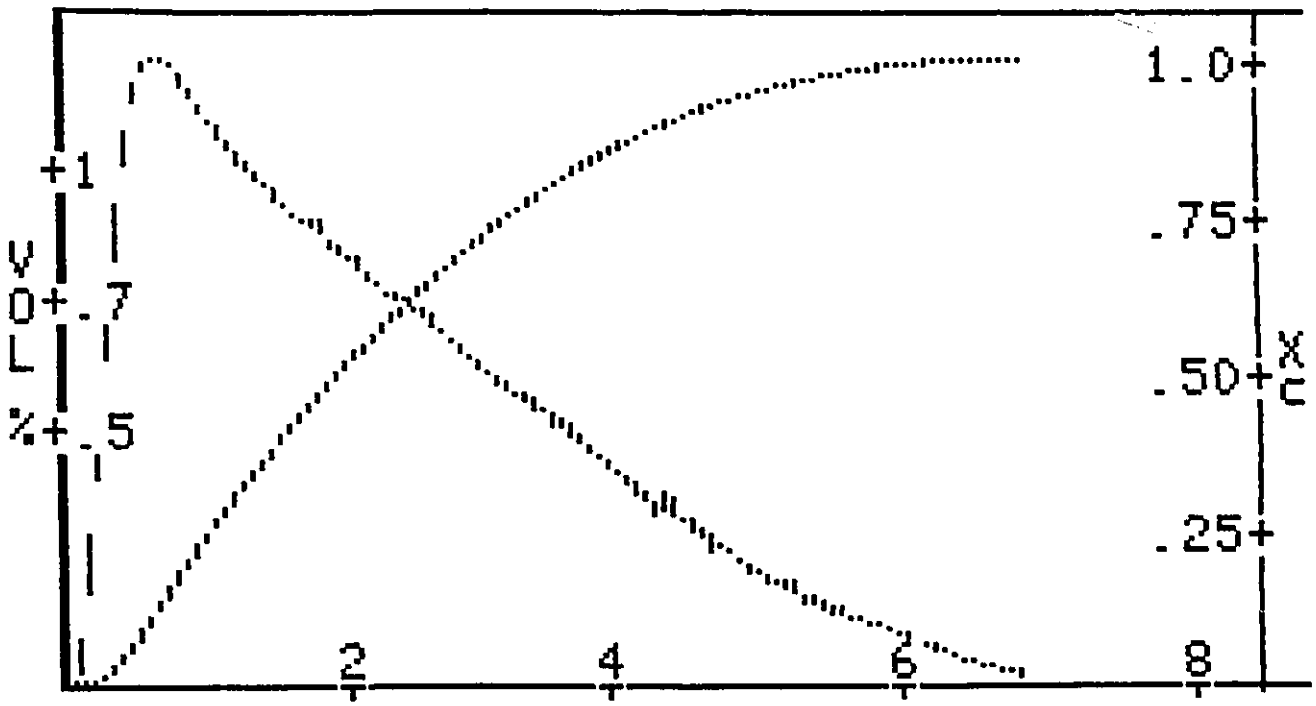

CO2 CONC. & ACC. C CONVERSION

EXP NO. 117
FUEL: E
SAMPLE AMOUNT= 2.74 g
PARTICLE SIZE RANGE= 4 TO 8 mm
BED TEMPERATURE= 850 C
FLUIDIZATION VELOCITY= .92 M/S
INLET GAS OXYGEN %= 21
BURNOUT TIME= 6.8 MIN
MEAN CARBON RESIDENCE TIME= 2.18 MIN
TOTAL CARBON BURNT= .18 MOLE
COMBUSTION EFFICIENCY= 93.08 %

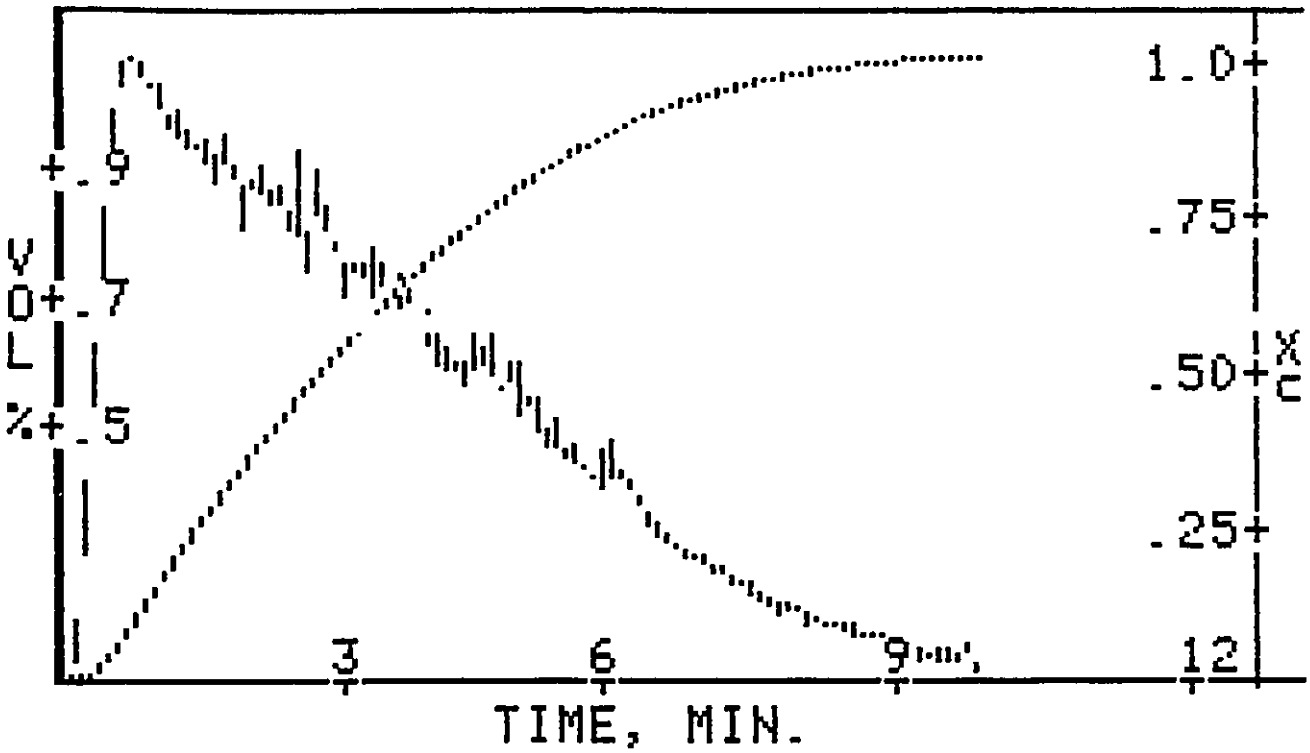

CO2 CONC. & ACC. C CONVERSION

EXP NO. 122
FUEL: C
SAMPLE AMOUNT= 3.79 g
PARTICLE SIZE RANGE= 4 TO 8 mm
BED TEMPERATURE= 850 C
FLUIDIZATION VELOCITY= .92 M/S
INLET GAS OXYGEN %= 21
BURNOUT TIME= 9.8 MIN
MEAN CARBON RESIDENCE TIME= 3.12 MIN
TOTAL CARBON BURNT= .24 MOLE
COMBUSTION EFFICIENCY= 87.51 %

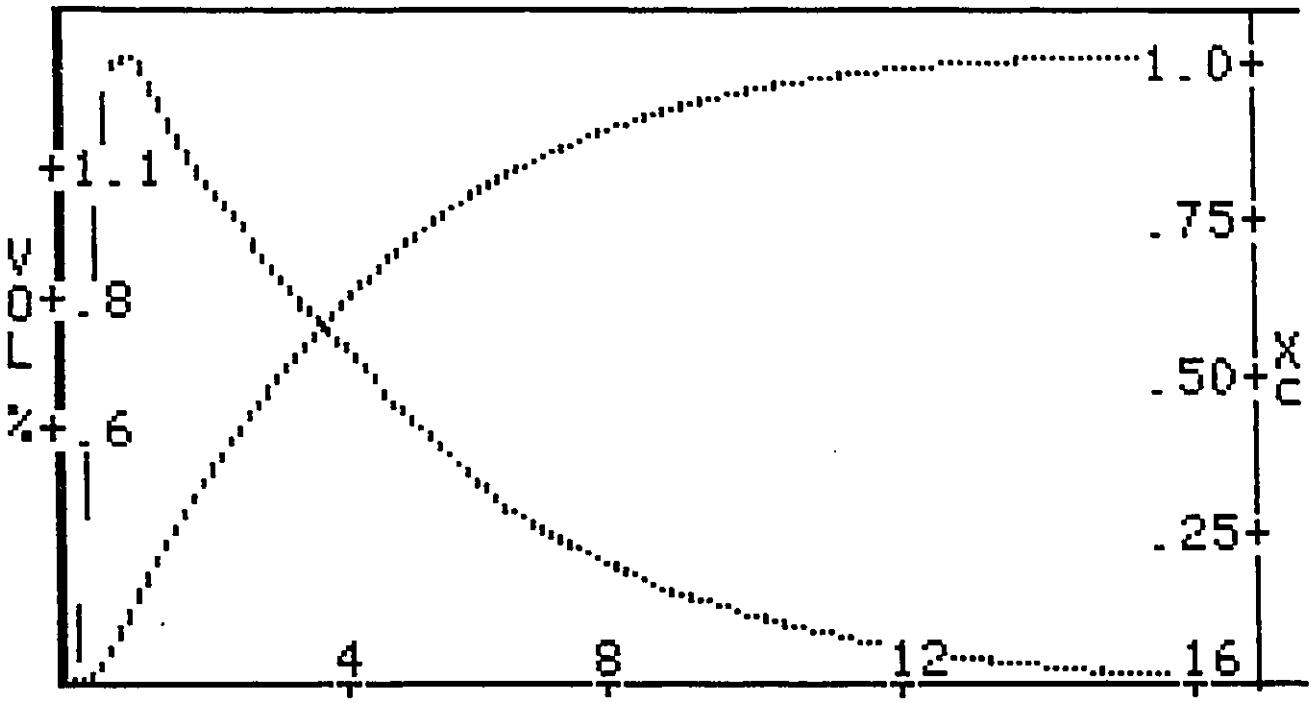

CO2 CONC. & ACC. C CONVERSION

EXP NO. 138
FUEL: B
SAMPLE AMOUNT= 6.15 g
PARTICLE SIZE RANGE= 4 TO 8 mm
BED TEMPERATURE= 850 C
FLUIDIZATION VELOCITY= .92 M/S
INLET GAS OXYGEN %= 21
BURNOUT TIME= 15.8 MIN
MEAN CARBON RESIDENCE TIME= 3.84 MIN
TOTAL CARBON BURNT= .33 MOLE
COMBUSTION EFFICIENCY= 70.42 %

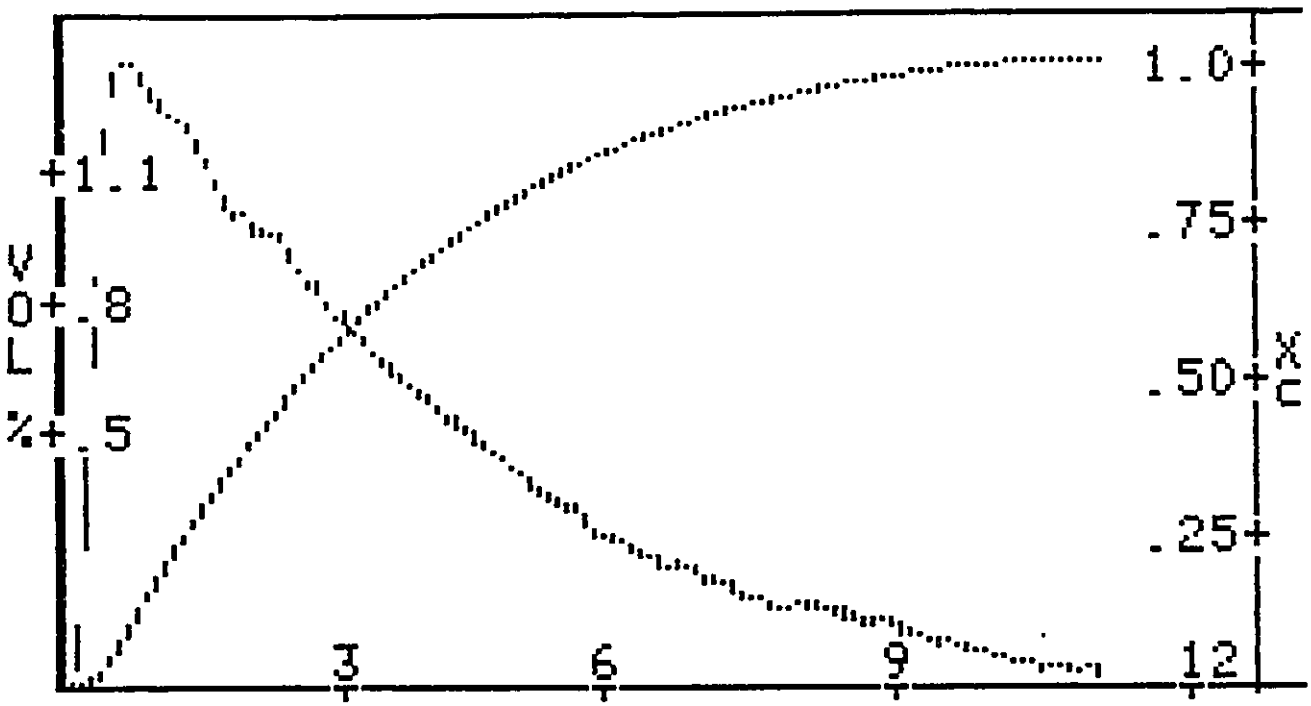

CO2 CONC. & ACC. C CONVERSION

EXP NO. 157
FUEL: G
SAMPLE AMOUNT= 2.18 g
PARTICLE SIZE RANGE= 4 TO 8 mm
BED TEMPERATURE= 850 C
FLUIDIZATION VELOCITY= .53 M/S
INLET GAS OXYGEN %= 21
BURNOUT TIME= 11.2 MIN
MEAN CARBON RESIDENCE TIME= 3.14 MIN
TOTAL CARBON BURNT= .15 MOLE
COMBUSTION EFFICIENCY= 93.92 %

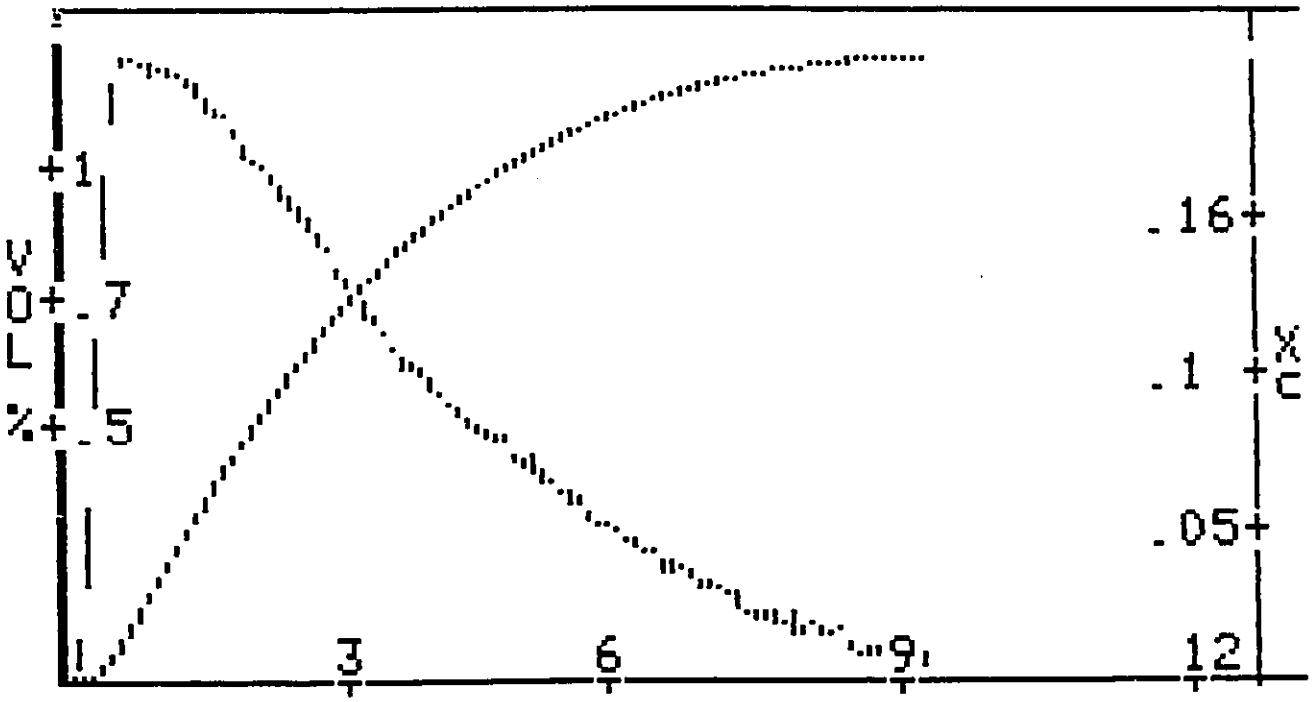

CO2 CONC. & ACC. C CONVERSION

EXP NO. 279
FUEL: F2
SAMPLE AMOUNT= 4.26 g
PARTICLE SIZE RANGE= 4 TO 8 mm
BED TEMPERATURE= 800 C
FLUIDIZATION VELOCITY= .81 M/S
INLET GAS OXYGEN %= 21
BURNOUT TIME= 9.3 MIN
MEAN CARBON RESIDENCE TIME= 2.83 MIN
TOTAL CARBON BURNT= .21 MOLE
COMBUSTION EFFICIENCY= 90.84 %

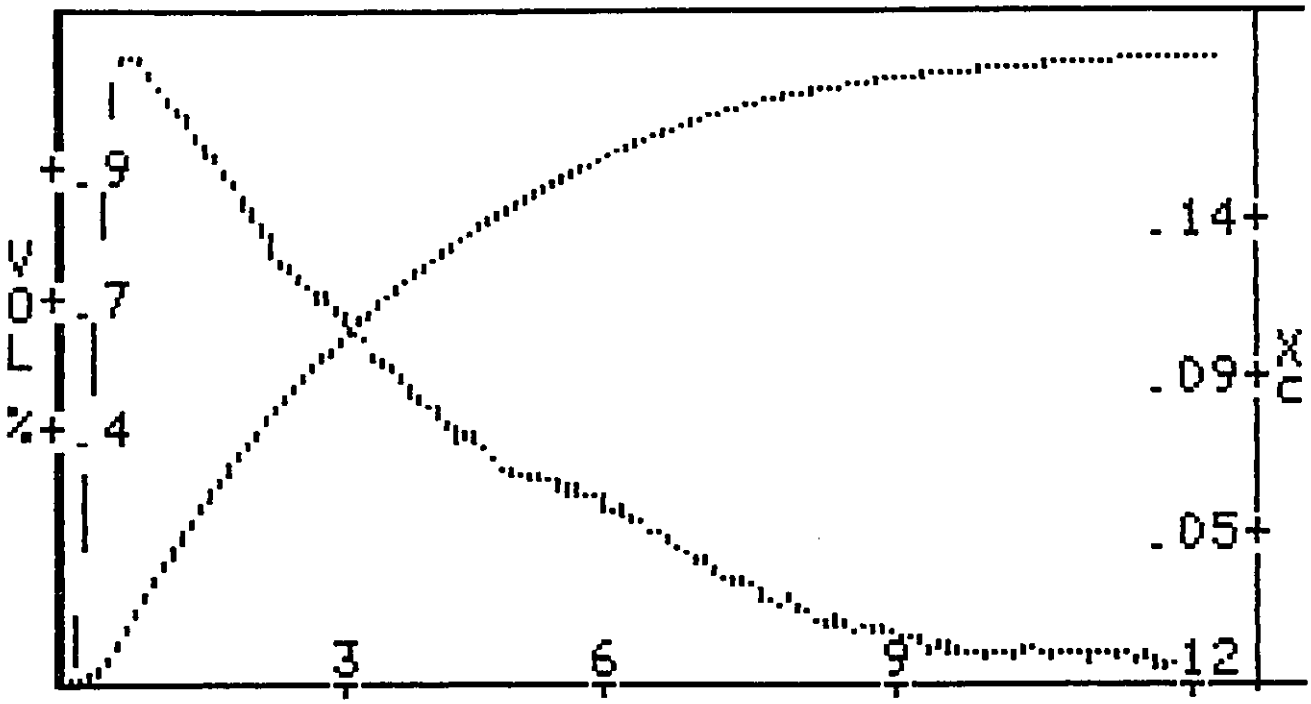

CO2 CONC. & ACC. C CONVERSION

EXP NO. 312
FUEL: F2
SAMPLE AMOUNT= 4.78 g
PARTICLE SIZE RANGE= 4 TO 8 mm
BED TEMPERATURE= 750 C
FLUIDIZATION VELOCITY= .8 M/S
INLET GAS OXYGEN %= 21
BURNOUT TIME= 12.3 MIN
MEAN CARBON RESIDENCE TIME= 3.26 MIN
TOTAL CARBON BURNT= .19 MOLE
COMBUSTION EFFICIENCY= 72.67 %

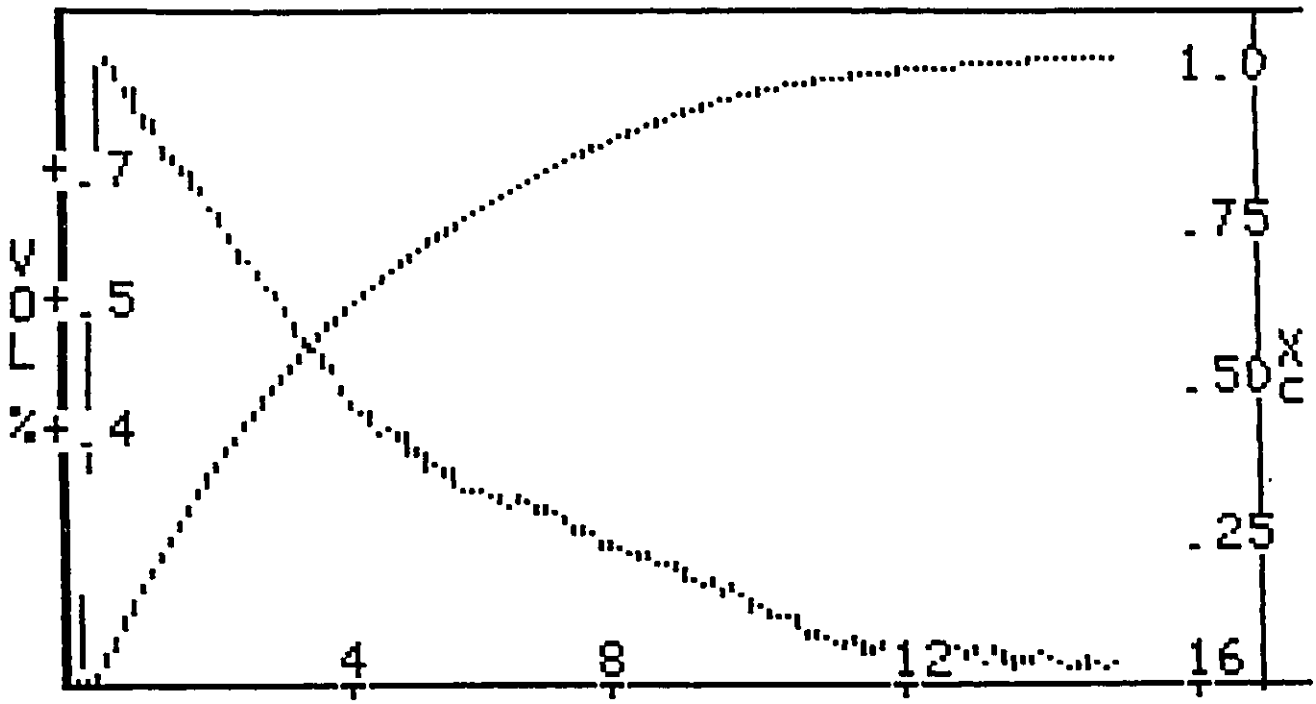

CO2 CONC. & ACC. C CONVERSION

EXP NO. 314
FUEL: F2
SAMPLE AMOUNT= 3.54 g
PARTICLE SIZE RANGE= 5.7 TO 12.7 mm
BED TEMPERATURE= 850 C
FLUIDIZATION VELOCITY= .85 M/S
INLET GAS OXYGEN %= 21
BURNOUT TIME= 15 MIN
MEAN CARBON RESIDENCE TIME= 3.93 MIN
TOTAL CARBON BURNT= .18 MOLE
COMBUSTION EFFICIENCY= 92.64 %

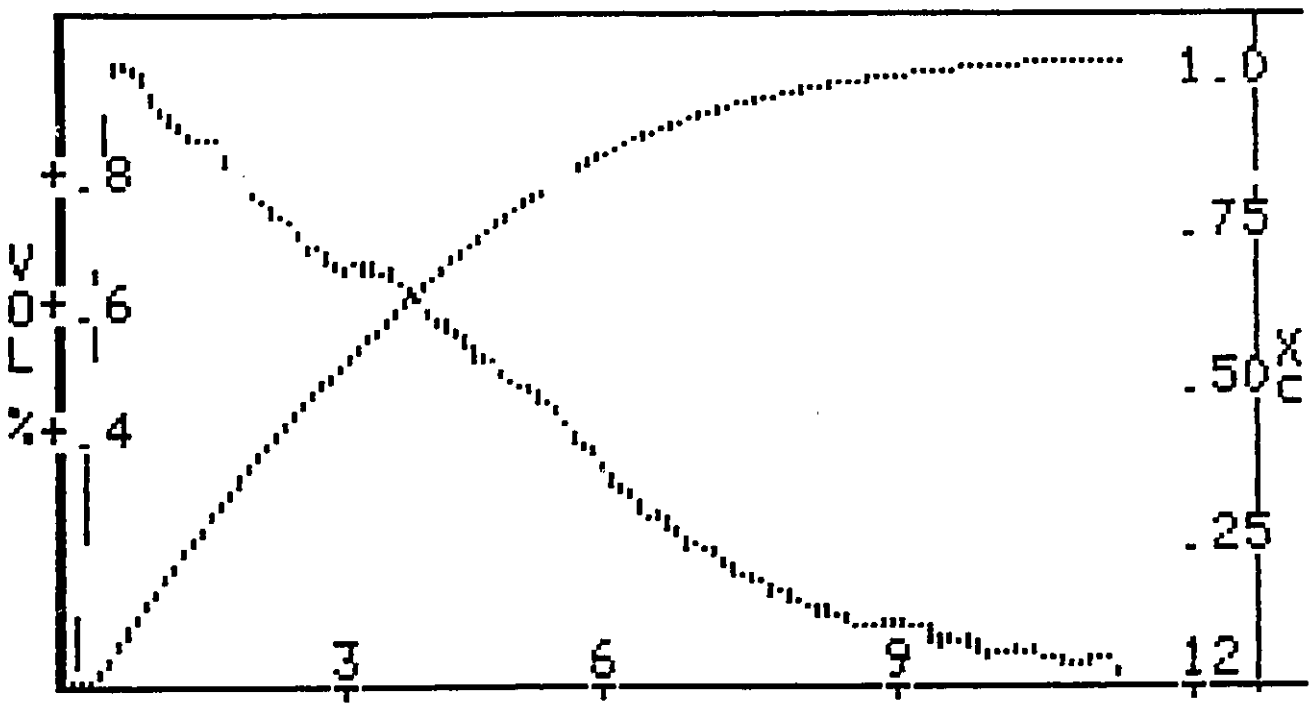

CO2 CONC. & ACC. C CONVERSION

EXP NO. 324
FUEL: F2
SAMPLE AMOUNT= 3.86 g
PARTICLE SIZE RANGE= 4 TO 8 mm
BED TEMPERATURE= 850 C
FLUIDIZATION VELOCITY= .81 M/S
INLET GAS OXYGEN %= 21
BURNOUT TIME= 11.3 MIN
MEAN CARBON RESIDENCE TIME= 3.31 MIN
TOTAL CARBON BURNT= .18 MOLE
COMBUSTION EFFICIENCY= 86.8 %

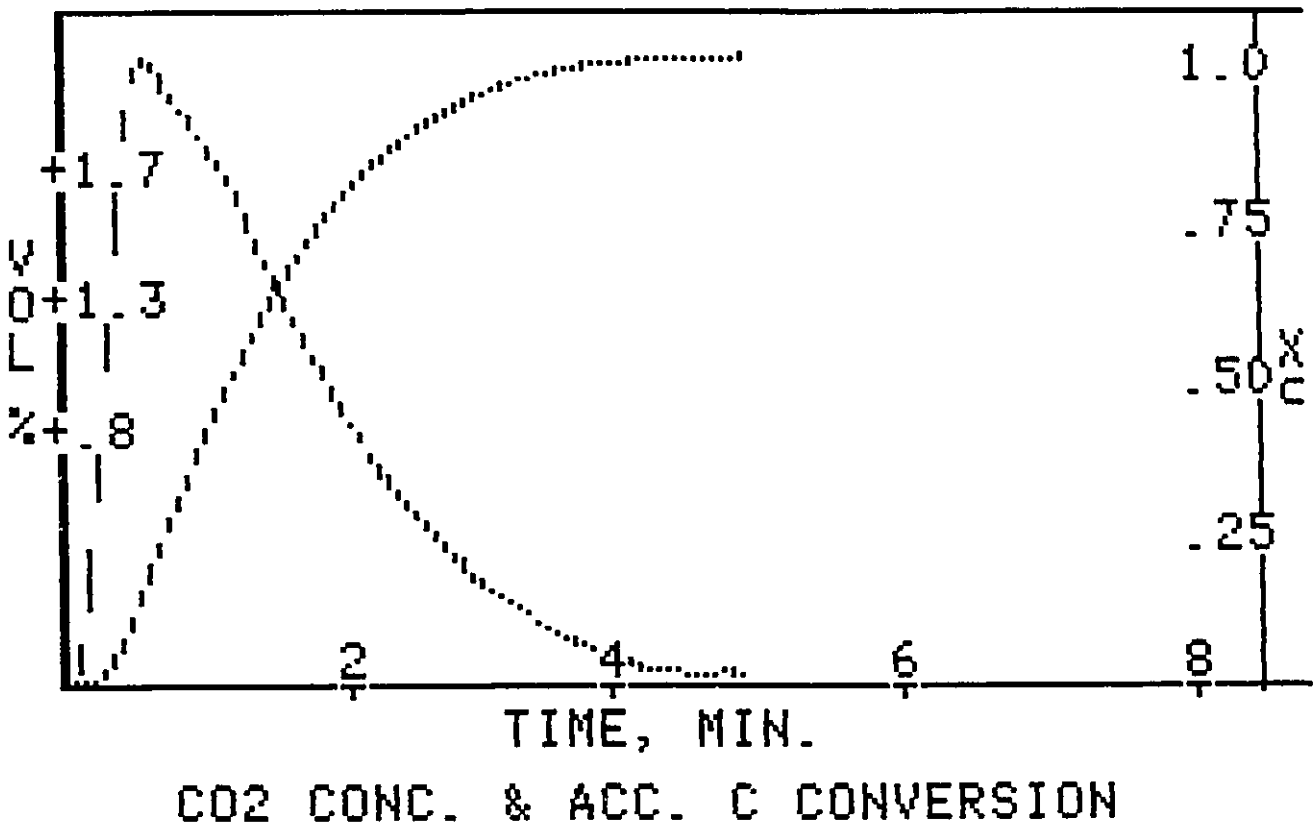

CO2 CONC. & ACC. C CONVERSION

EXP NO. 327
FUEL: F2
SAMPLE AMOUNT= 3.37 g
PARTICLE SIZE RANGE= .84 TO 4 mm
BED TEMPERATURE= 850 C
FLUIDIZATION VELOCITY= .81 M/S
INLET GAS OXYGEN %= 21
BURNOUT TIME= 4.8 MIN
MEAN CARBON RESIDENCE TIME= 1.33 MIN
TOTAL CARBON BURNT= .15 MOLE
COMBUSTION EFFICIENCY= 81.83 %

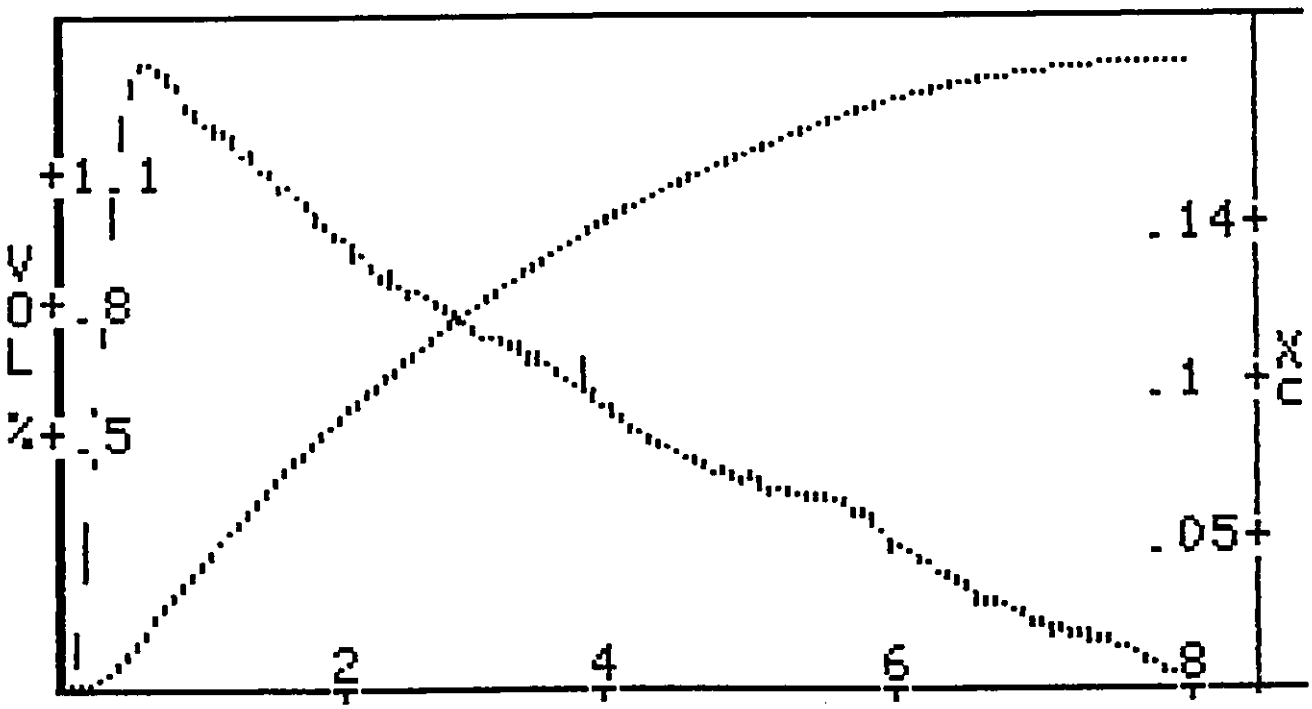

CO2 CONC. & ACC. C CONVERSION

EXP NO. 345
FUEL: F2
SAMPLE AMOUNT= 3.81 g
PARTICLE SIZE RANGE= 4 TO 8 mm
BED TEMPERATURE= 900 C
FLUIDIZATION VELOCITY= .83 M/S
INLET GAS OXYGEN %= 21
BURNOUT TIME= 8 MIN
MEAN CARBON RESIDENCE TIME= 2.68 MIN
TOTAL CARBON BURNT= .19 MOLE
COMBUSTION EFFICIENCY= 93.65 %

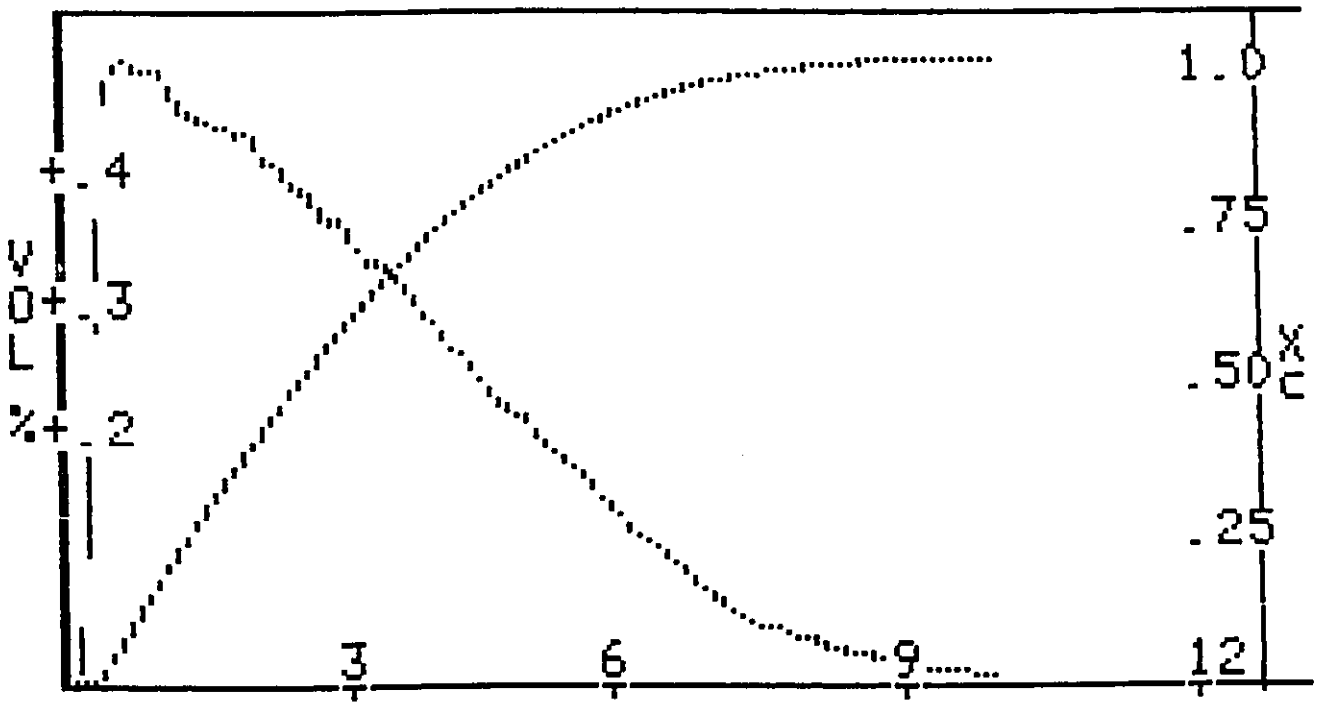

CO2 CONC. & ACC. C CONVERSION

EXP NO. 379
FUEL: F2
SAMPLE AMOUNT= 2.77 g
PARTICLE SIZE RANGE= 4 TO 8 mm
BED TEMPERATURE= 850 C
FLUIDIZATION VELOCITY= .89 M/S
INLET GAS OXYGEN %= 21
BURNOUT TIME= 9.9 MIN
MEAN CARBON RESIDENCE TIME= 2.87 MIN
TOTAL CARBON BURNT= .14 MOLE
COMBUSTION EFFICIENCY= 92.86 %

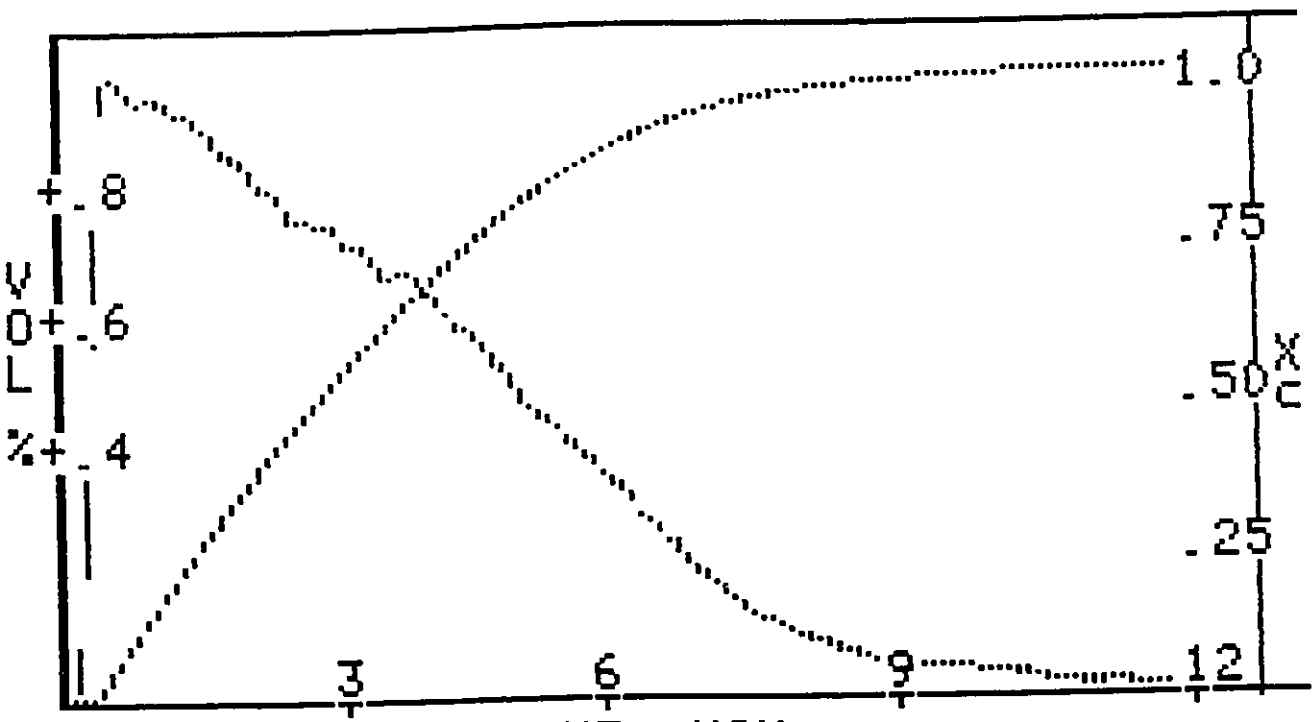

CO2 CONC. & ACC. C CONVERSION

EXP NO. 505
FUEL: F2
SAMPLE AMOUNT= 5.29 g
PARTICLE SIZE RANGE= 5.7 TO 12.7 mm
BED TEMPERATURE= 850 C
FLUIDIZATION VELOCITY= .89 M/S
INLET GAS OXYGEN %= 21
BURNOUT TIME= 11.8 MIN
MEAN CARBON RESIDENCE TIME= 3.17 MIN
TOTAL CARBON BURNT= .27 MOLE
COMBUSTION EFFICIENCY= 95.89 %

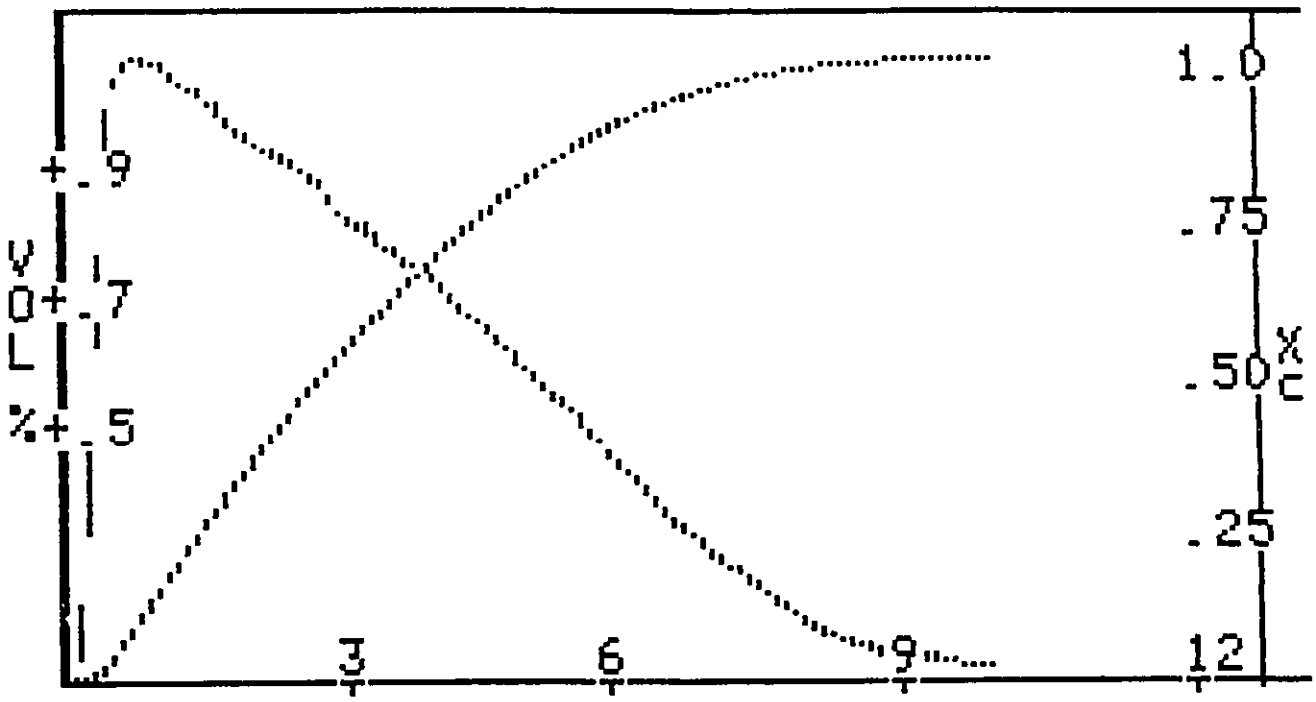

CO2 CONC. & ACC. C CONVERSION

EXP NO. 511
FUEL: F3
SAMPLE AMOUNT= 6.03 g
PARTICLE SIZE RANGE= 4 TO 8 mm
BED TEMPERATURE= 850 C
FLUIDIZATION VELOCITY= .89 M/S
INLET GAS OXYGEN %= 21
BURNOUT TIME= 10 MIN
MEAN CARBON RESIDENCE TIME= 3.08 MIN
TOTAL CARBON BURNT= .3 MOLE
COMBUSTION EFFICIENCY= 66.38 %

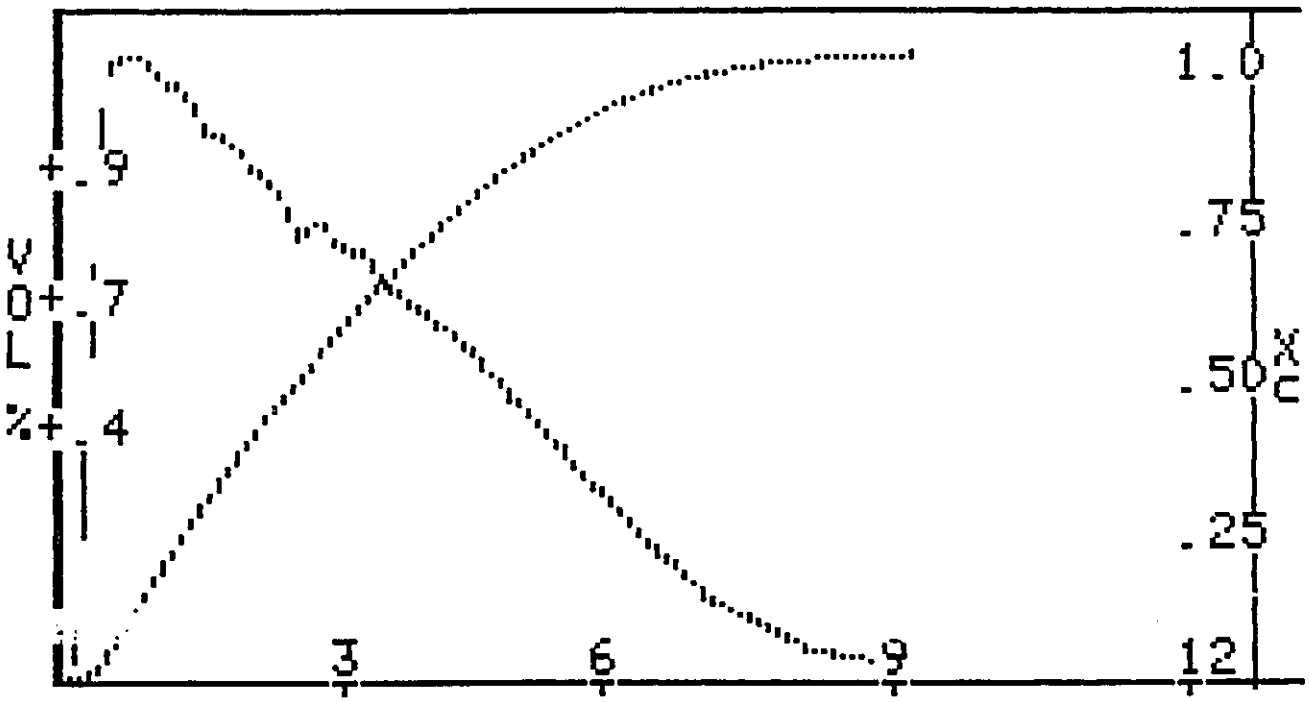

CO2 CONC. & ACC. C CONVERSION

EXP NO. 513
FUEL: F2
SAMPLE AMOUNT= 5.24 g
PARTICLE SIZE RANGE= 4 TO 8 mm
BED TEMPERATURE= 850 C
FLUIDIZATION VELOCITY= .89 M/S
INLET GAS OXYGEN %= 21
BURNOUT TIME= 9.1 MIN
MEAN CARBON RESIDENCE TIME= 2.88 MIN
TOTAL CARBON BURNT= .27 MOLE
COMBUSTION EFFICIENCY= 94.88 %

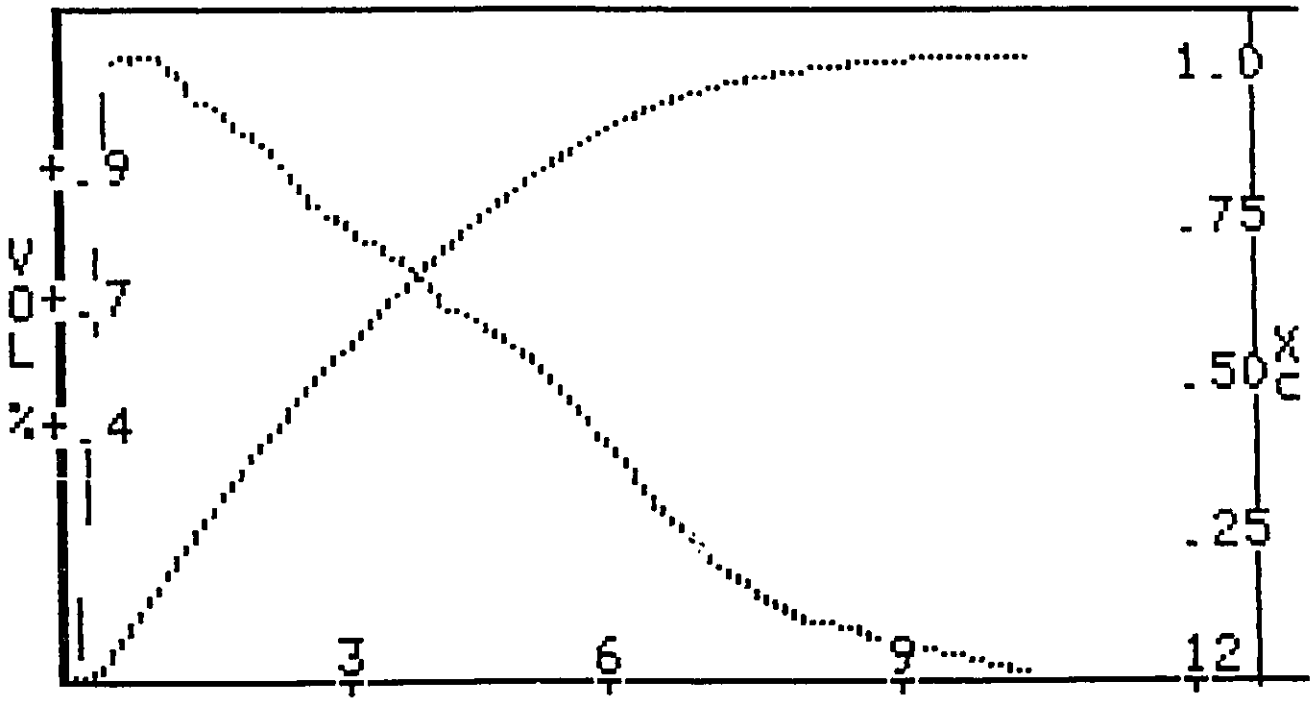

CO2 CONC. & ACC. C CONVERSION

EXP NO. 514
FUEL: F4
SAMPLE AMOUNT= 6 g
PARTICLE SIZE RANGE= 4 TO 8 mm
BED TEMPERATURE= 850 C
FLUIDIZATION VELOCITY= .89 M/S
INLET GAS OXYGEN %= 21
BURNOUT TIME= 10.4 MIN
MEAN CARBON RESIDENCE TIME= 3.11 MIN
TOTAL CARBON BURNT= .29 MOLE
COMBUSTION EFFICIENCY= 72.63 %

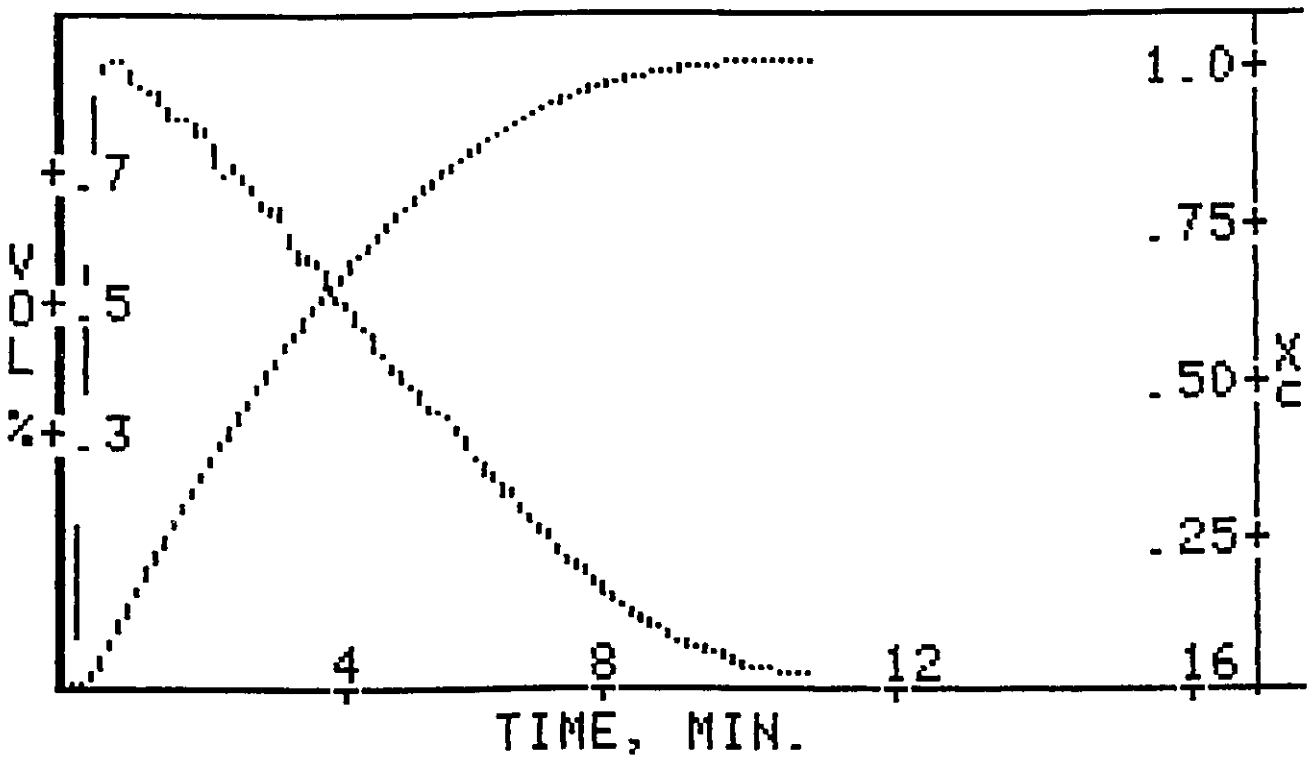

CO2 CONC. & ACC. C CONVERSION

EXP NO. 612
FUEL: F2-2
SAMPLE AMOUNT= 4.91 g
PARTICLE SIZE RANGE= 4 TO 8 mm
BED TEMPERATURE= 850 C
FLUIDIZATION VELOCITY= .89 M/S
INLET GAS OXYGEN %= 15.8
BURNOUT TIME= 10.7 MIN
MEAN CARBON RESIDENCE TIME= 3.21 MIN
TOTAL CARBON BURNT= .22 MOLE
COMBUSTION EFFICIENCY= 84.78 %

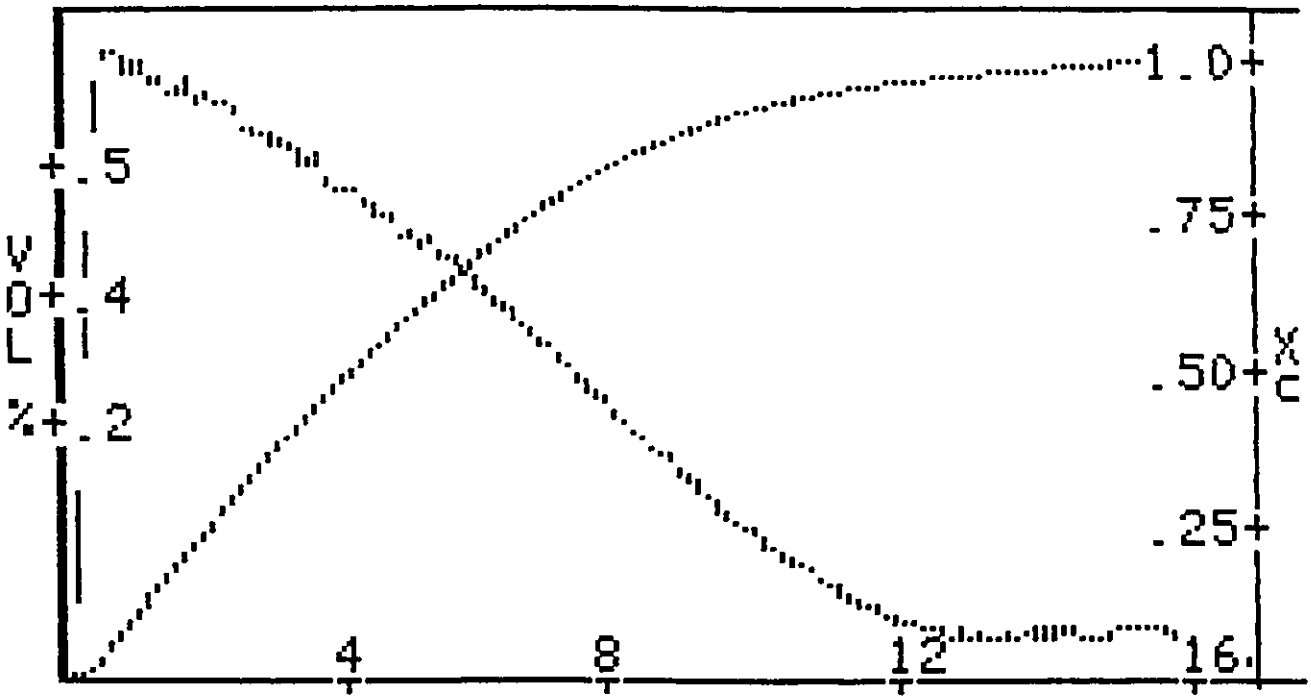

CO2 CONC. & ACC. C CONVERSION

EXP NO. 631
FUEL: F2-2
SAMPLE AMOUNT= 6.51 g
PARTICLE SIZE RANGE= 4 TO 8 mm
BED TEMPERATURE= 850 C
FLUIDIZATION VELOCITY= .88 M/S
INLET GAS OXYGEN %= 10.5
BURNOUT TIME= 16.9 MIN
MEAN CARBON RESIDENCE TIME= 4.78 MIN
TOTAL CARBON BURNT= .24 MOLE
COMBUSTION EFFICIENCY= 68.63 %

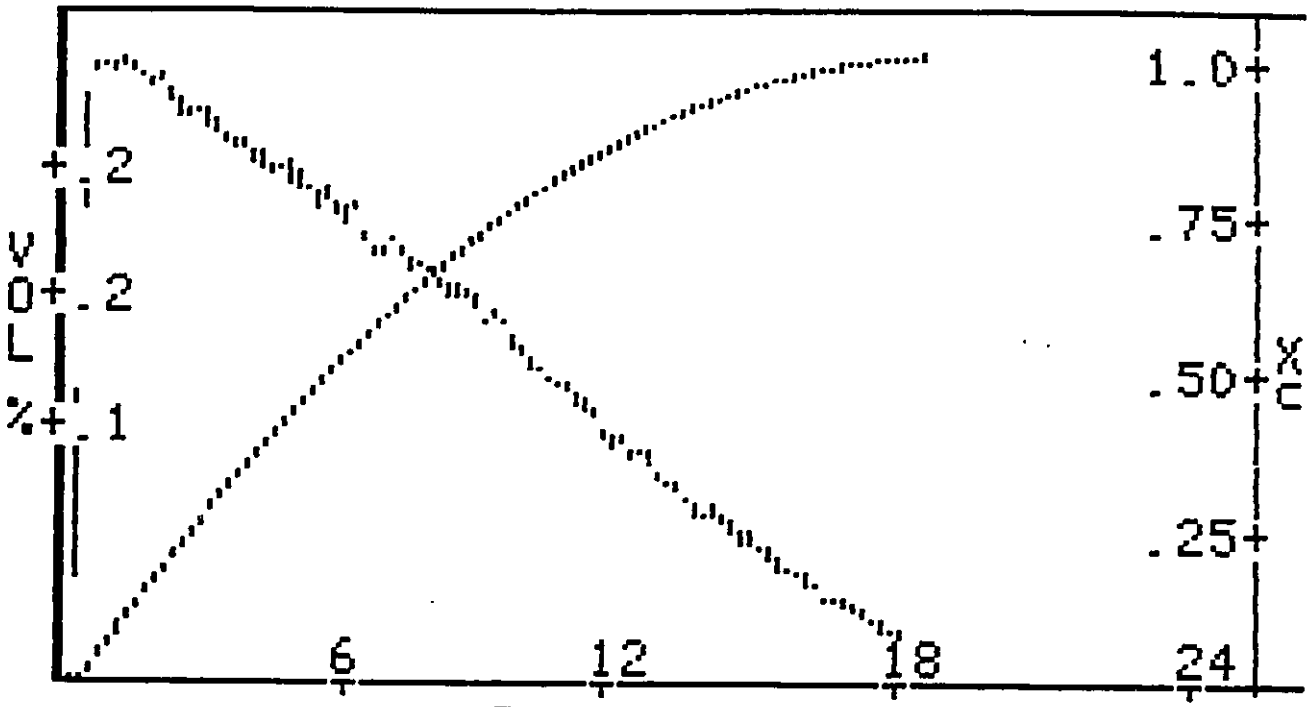

CO2 CONC. & ACC. C CONVERSION

EXP NO. 646
FUEL: F2-2
SAMPLE AMOUNT= 5.13 g
PARTICLE SIZE RANGE= 4 TO 8 mm
BED TEMPERATURE= 850 C
FLUIDIZATION VELOCITY= .89 M/S
INLET GAS OXYGEN %= 5.3
BURNOUT TIME= 18.4 MIN
MEAN CARBON RESIDENCE TIME= 6.4 MIN
TOTAL CARBON BURNT= .17 MOLE
COMBUSTION EFFICIENCY= 60.56 %

APPENDIX 2

Second Series Experimental Results

For each experiment two pages are presented. The first summarizes operating conditions and gives the CO_2 versus time curve of the main test, while the second page presents the CO_2 versus time curve for the subsequent sub-test.

SER2 - 12 :F2
BED TEMPERATURE = 850 C
OXYGEN CONCENTRATION = 21 %
MOTHER CHAR BURNING RATE Rm = 11.58 E-6 kg/s
ATTRITED FINES BURNING RATE Ra = 72.36 E-8 kg/s
RETRIEVED ATTRITED CARRBON Wa = 47.75 E-6 kg
MCRT OF BURNING FINES IN SUB-TEST Tria = 51.8 s
MCRT OF ATTRITED PARTICLES (MAIN TEST) Tra = 48.3 s
IDEAL MCRT OF ELUTRATED SIZE PARTICLE Tre* = 32.9 s
IDEAL MCRT OF THE LARGEST ATTRITED PARTICLE Trs* = 89.7 s
ELUTRIATED FRACTION OF ATTRITED PARTICLES Ya = .267
ATTRITION RATE Qa = 98.8 E-8 kg/s
RATIO Qa/(Qa+Rm) = 7.87 %

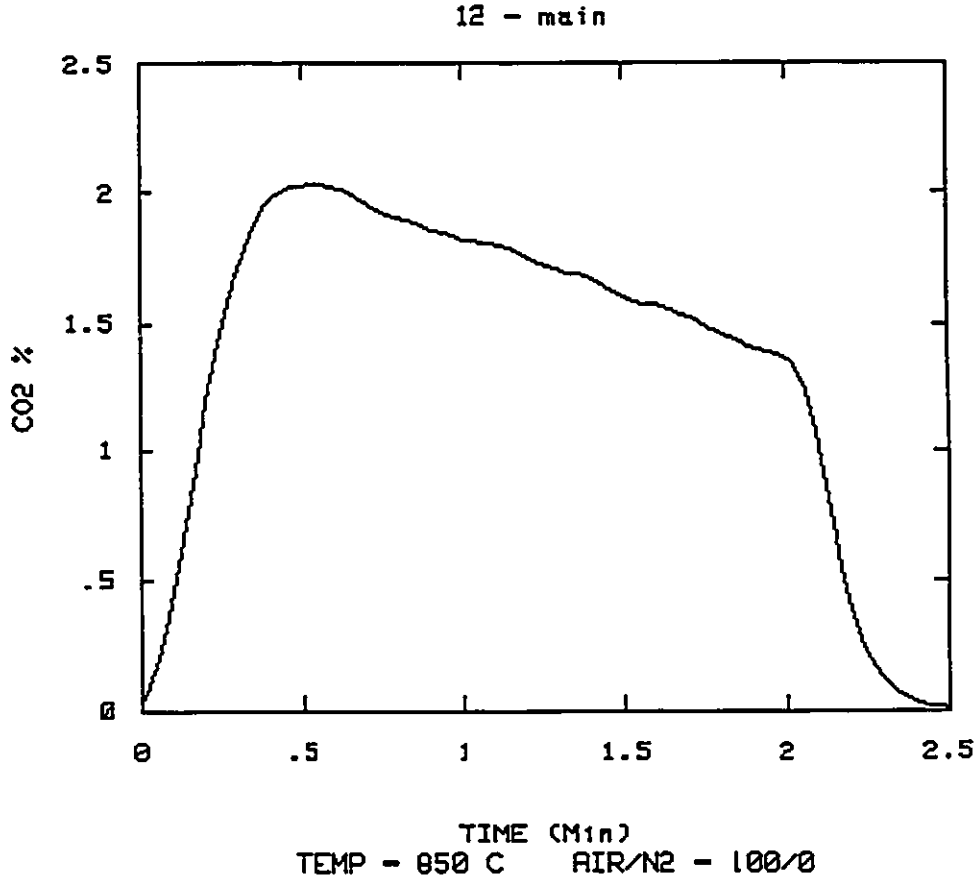

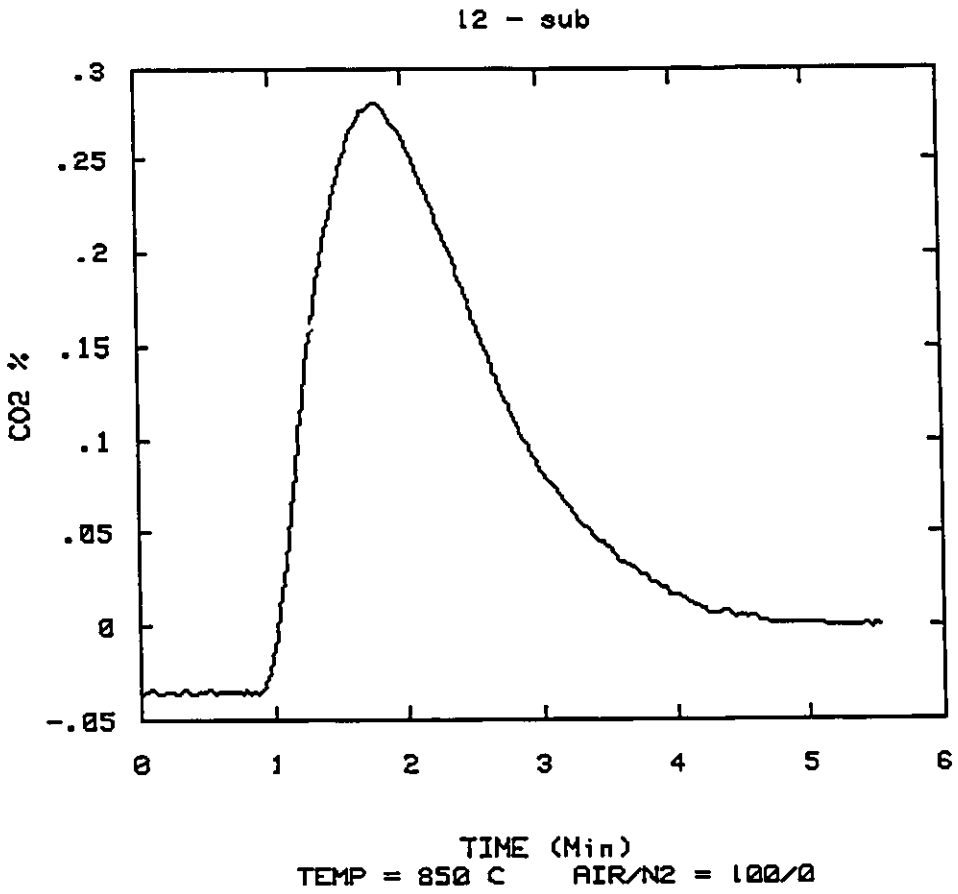
12 - sub
.3
.25
.2
.15
.1
.05
0
-.05
CO2 %
0
1
2
3
4
5
6
TIME (Min)
TEMP = 850 C
AIR/N2 = 100/0

SER2 - 13 :F2
BED TEMPERATURE = 850 C
OXYGEN CONCENTRATION = 21 %
MOTHER CHAR BURNING RATE Rm = 7.18 E-6 kg/s
ATTRITED FINES BURNING RATE Ra = 20.42 E-8 kg/s
RETRIEVED ATTRITED CARRBON Wa = 15.91 E-6 kg
MCRT OF BURNING FINES IN SUB-TEST Tria = 62.2 s
MCRT OF ATTRITED PARTICLES (MAIN TEST) Tra = 64.8 s
IDEAL MCRT OF ELUTRATED SIZE PARTICLE Tre* = 34.4 s
IDEAL MCRT OF THE LARGEST ATTRITED PARTICLE Trs* = 111.1 s
ELUTRIATED FRACTION OF ATTRITED PARTICLES Ya = .169
ATTRITION RATE Qa = 24.6 E-8 kg/s
RATIO Qa/(Qa+Rm) = 3.31 %

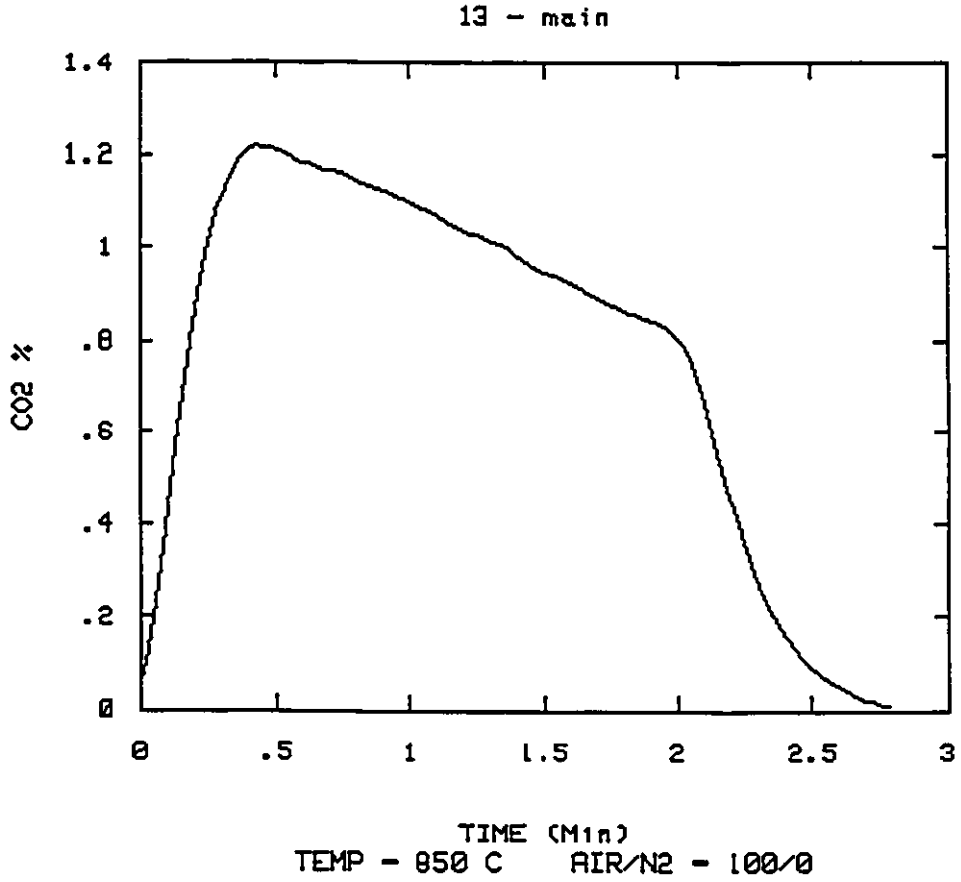

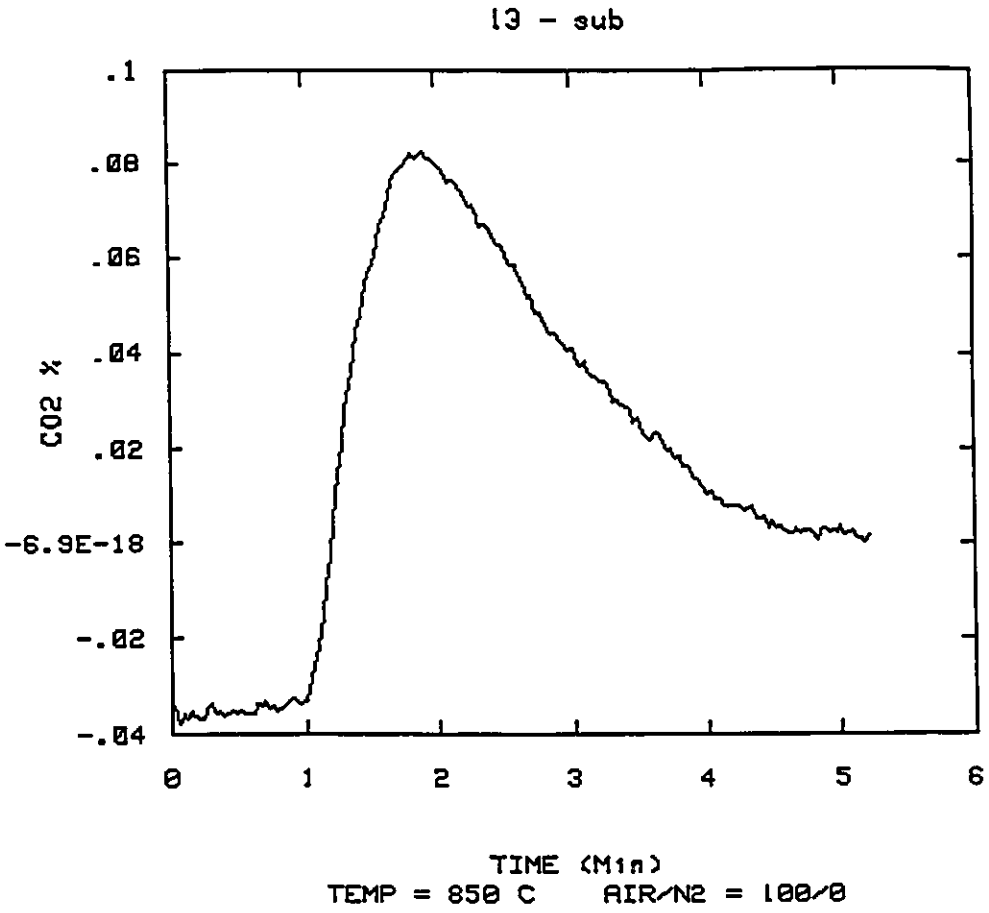
13 - sub
.1
.08
.06
.04
.02
-6.9E-18
-.02
-.04
CO2 %
0
1
2
3
4
5
6
TIME (Min)
TEMP = 850 C
AIR/N2 = 100/0

SER2 - 15 :F2
BED TEMPERATURE = 850 C
OXYGEN CONCENTRATION = 21 %
MOTHER CHAR BURNING RATE Rm = 10.87 E-6 kg/s
ATTRITED FINES BURNING RATE Ra = 35.84 E-8 kg/s
RETRIEVED ATTRITED CARRBON Wa = 23.77 E-6 kg
MCRT OF BURNING FINES IN SUB-TEST Tria = 52.6 s
MCRT OF ATTRITED PARTICLES (MAIN TEST) Tra = 50.9 s
IDEAL MCRT OF ELUTRATED SIZE PARTICLE Tre* = 32.2 s
IDEAL MCRT OF THE LARGEST ATTRITED PARTICLE Trs* = 91.8 s
ELUTRIATED FRACTION OF ATTRITED PARTICLES Ya = .235
ATTRITION RATE Qa = 46.8 E-8 kg/s
RATIO Qa/(Qa+Rm) = 4.12 %

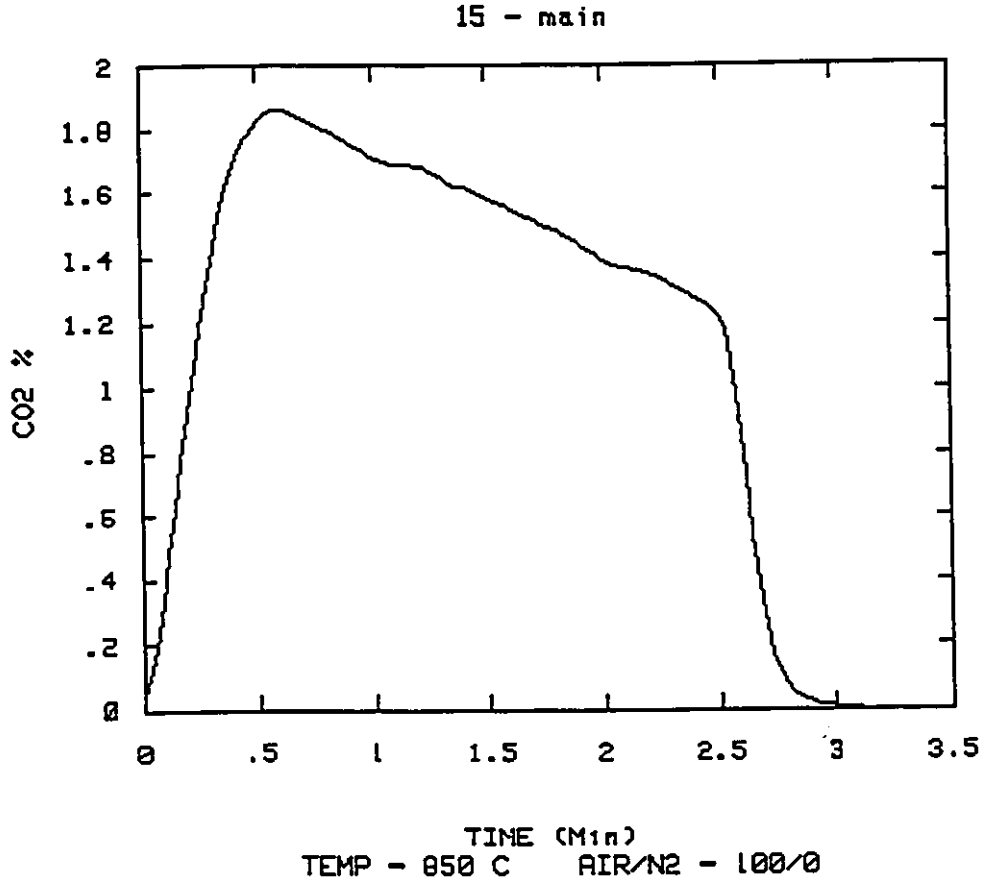

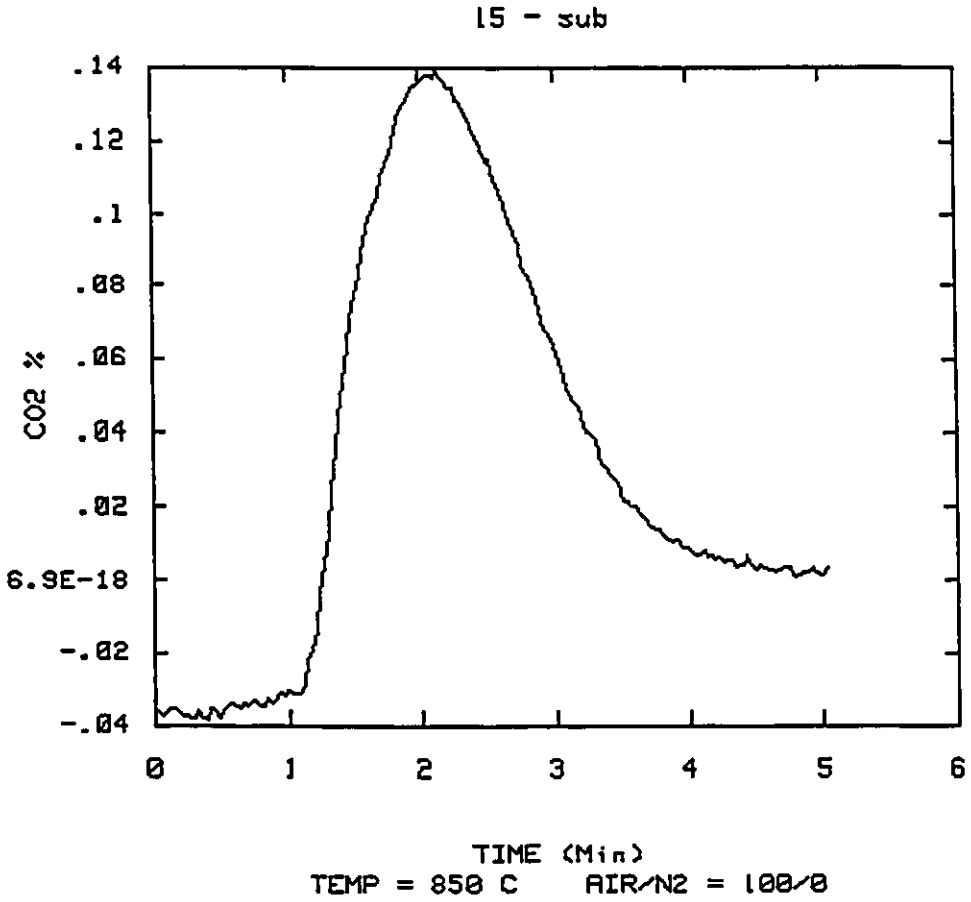
15 - sub
.14
.12
.1
.08
.06
.04
.02
6.9E-18
-.02
-.04
CO2 %
0
1
2
3
4
5
6
TIME (Min)
TEMP = 850 C
AIR/N2 = 100/0

SER2 - 16 :F2
BED TEMPERATURE = 850 C
OXYGEN CONCENTRATION = 21 %
MOTHER CHAR BURNING RATE Rm = 5.56 E-6 kg/s
ATTRITED FINES BURNING RATE Ra = 27.96 E-8 kg/s
RETRIEVED ATTRITED CARRBON Wa = 21.35 E-6 kg
MCRT OF BURNING FINES IN SUB-TEST Tria = 60.8 s
MCRT OF ATTRITED PARTICLES (MAIN TEST) Tra = 63.3 s
IDEAL MCRT OF ELUTRATED SIZE PARTICLE Tre* = 33.7 s
IDEAL MCRT OF THE LARGEST ATTRITED PARTICLE Trs* = 108.6 s
ELUTRIATED FRACTION OF ATTRITED PARTICLES Ya = .169
ATTRITION RATE Qa = 33.8 E-8 kg/s
RATIO Qa/(Qa+Rm) = 5.72 %

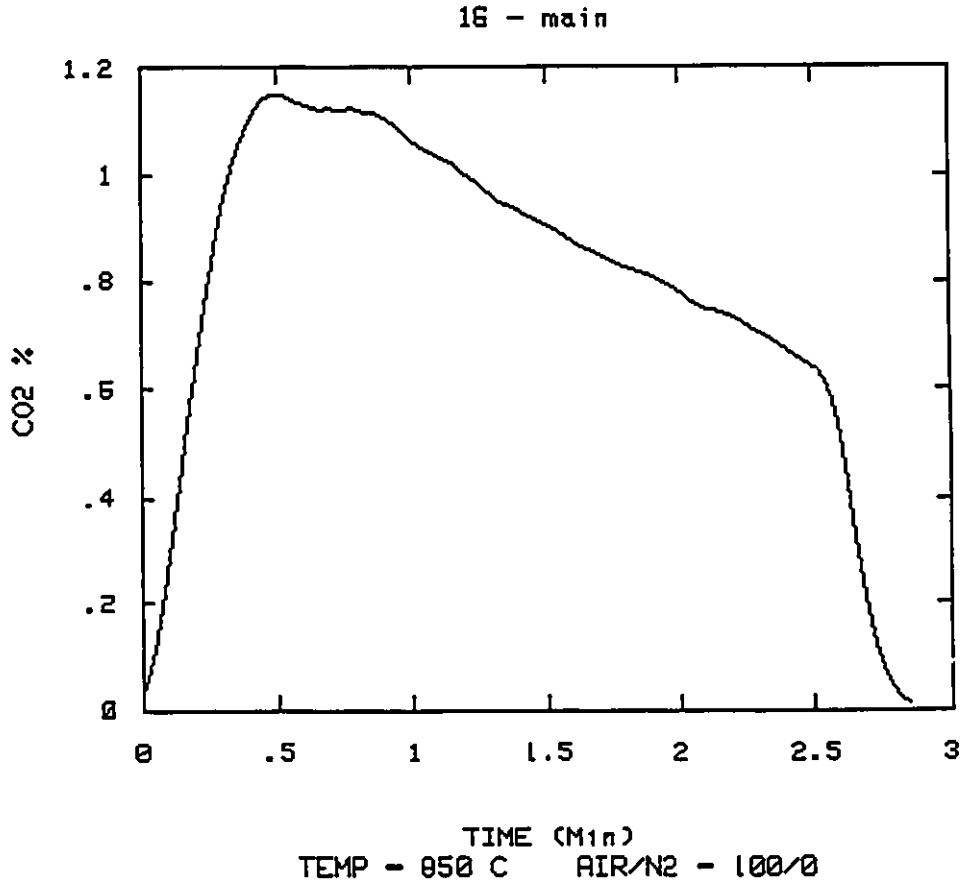

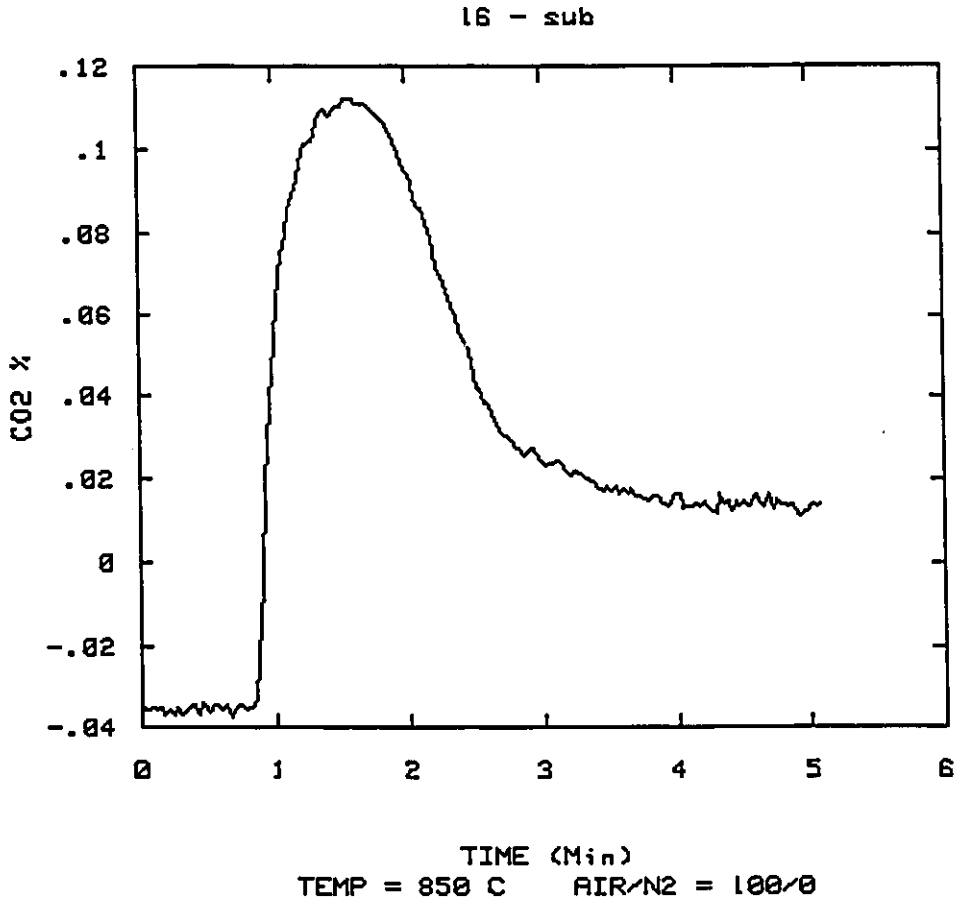
16 - sub
.12
.1
.08
.06
.04
.02
0
-.02
-.04
CO2 %
0
1
2
3
4
5
6
TIME (Min)
TEMP = 850 C
AIR/N2 = 100/0

SER2 - 17 :F2
BED TEMPERATURE = 850 C
OXYGEN CONCENTRATION = 21 %
MOTHER CHAR BURNING RATE Rm = 4.63 E-6 kg/s
ATTRITED FINES BURNING RATE Ra = 19.3 E-8 kg/s
RETRIEVED ATTRITED CARRBON Wa = 15.68 E-6 kg
MCRT OF BURNING FINES IN SUB-TEST Tria = 65 s
MCRT OF ATTRITED PARTICLES (MAIN TEST) Tra = 68 s
IDEAL MCRT OF ELUTRATED SIZE PARTICLE Tre* = 35.7 s
IDEAL MCRT OF THE LARGEST ATTRITED PARTICLE Trs* = 116.2 s
ELUTRIATED FRACTION OF ATTRITED PARTICLES Ya = .164
ATTRITION RATE Qa = 23 E-8 kg/s
RATIO Qa/(Qa+Rm) = 4.75 %

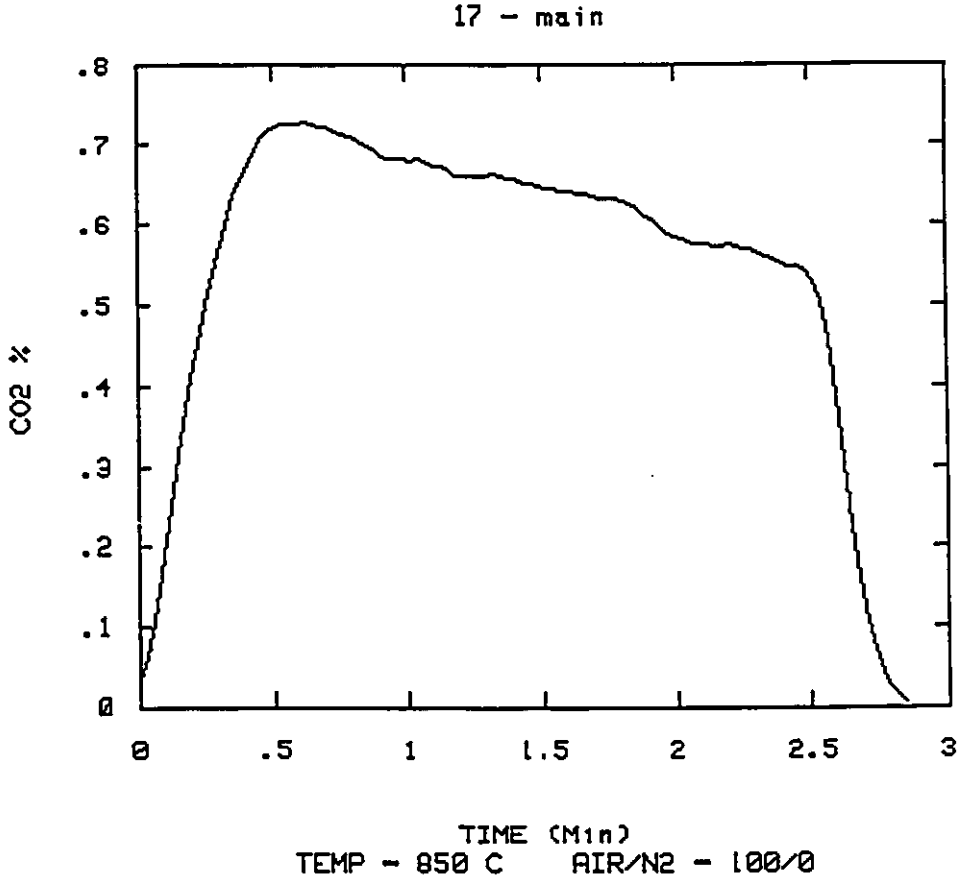

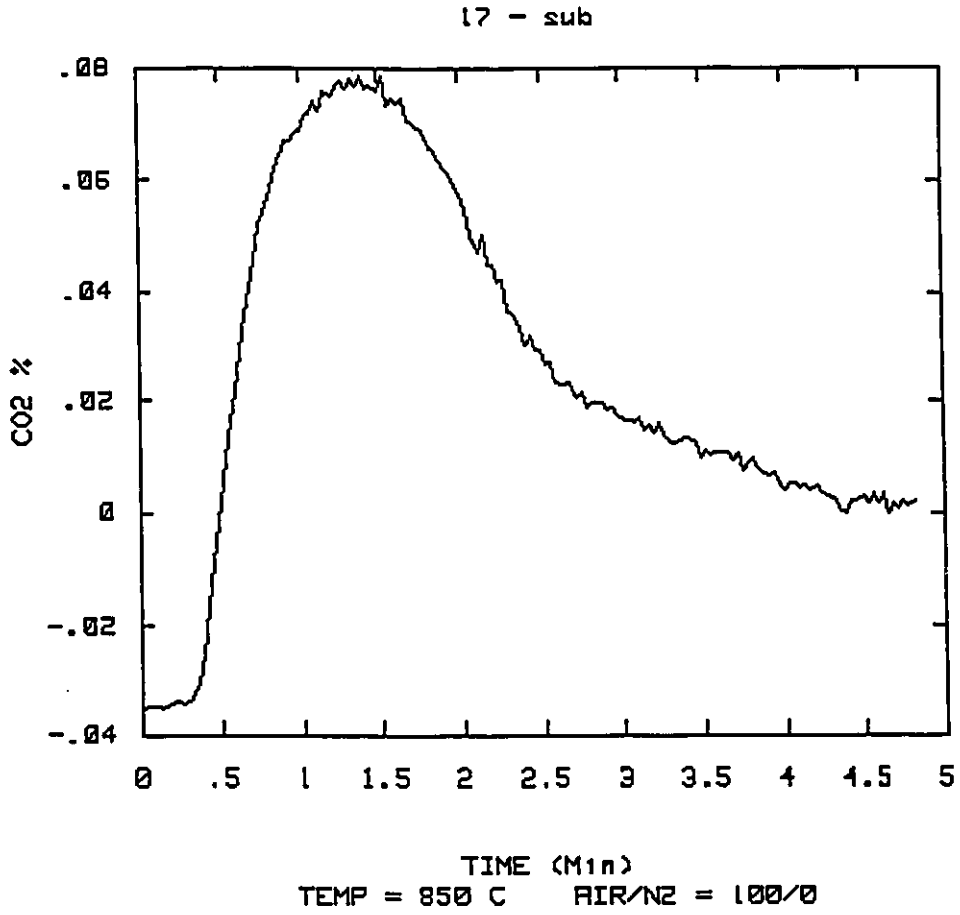
17 - sub
.08
.06
.04
.02
0
-.02
-.04
CO2 %
0
.5
1
1.5
2
2.5
3
3.5
4
4.5
5
TIME (Min)
TEMP = 850 C
AIR/N2 = 100/0

SER2 - 18 :F2
BED TEMPERATURE = 850 C
OXYGEN CONCENTRATION = 21 %
MOTHER CHAR BURNING RATE Rm = 13.45 E-6 kg/s
ATTRITED FINES BURNING RATE Ra = 16.08 E-8 kg/s
RETRIEVED ATTRITED CARRBON Wa = 8.51 E-6 kg
MCRT OF BURNING FINES IN SUB-TEST Tria = 41.5 s
MCRT OF ATTRITED PARTICLES (MAIN TEST) Tra = 34.2 s
IDEAL MCRT OF ELUTRATED SIZE PARTICLE Tre* = 28.6 s
IDEAL MCRT OF THE LARGEST ATTRITED PARTICLE Trs* = 69.6 s
ELUTRIATED FRACTION OF ATTRITED PARTICLES Ya = .357
ATTRITION RATE Qa = 24.8 E-8 kg/s
RATIO Qa/(Qa+Rm) = 1.82 %

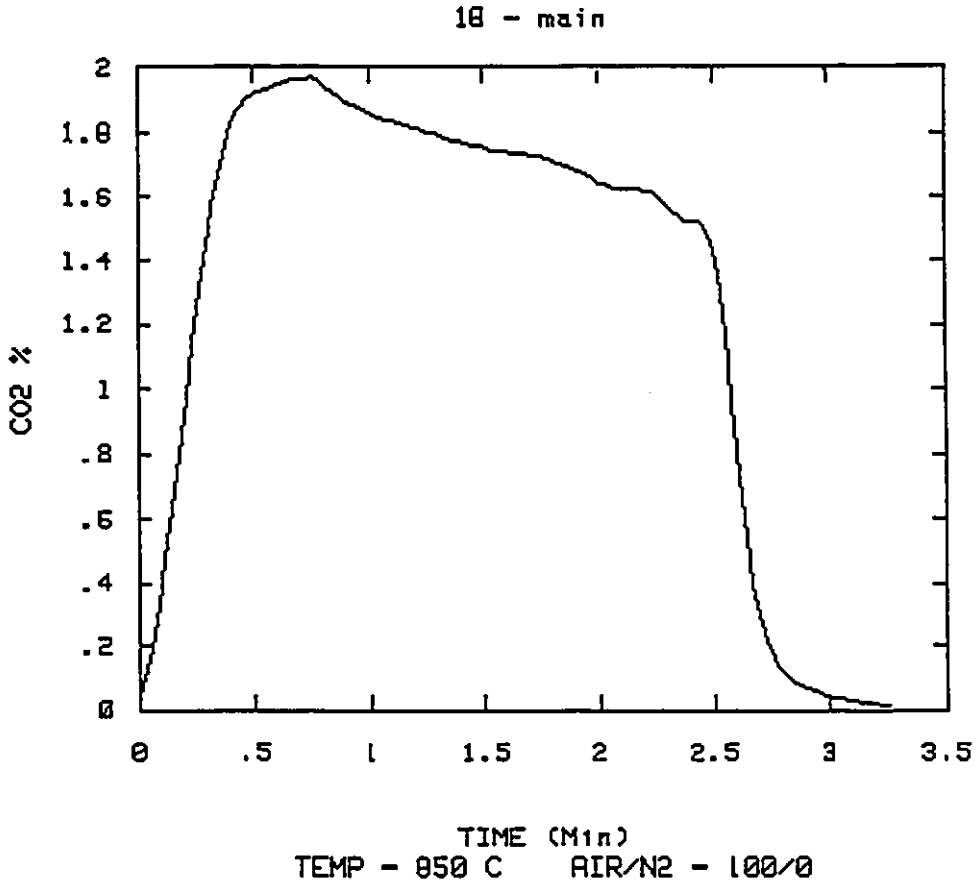

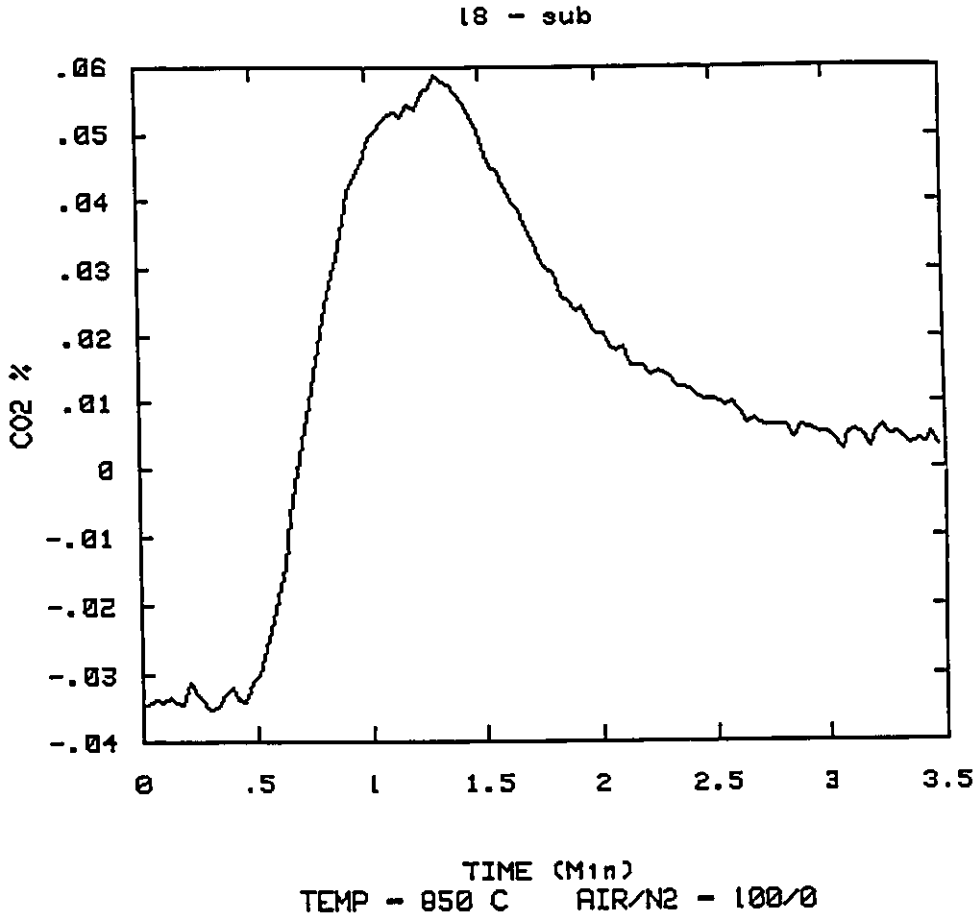
18 - sub
.06
.05
.04
.03
.02
.01
0
-.01
-.02
-.03
-.04
CO2 %
0
.5
1
1.5
2
2.5
3
3.5
TIME (Min)
TEMP - 850 C
AIR/N2 - 100/0

SER2 - 19 :F3
BED TEMPERATURE = 850 C
OXYGEN CONCENTRATION = 21 %
MOTHER CHAR BURNING RATE Rm = 10.43 E-6 kg/s
ATTRITED FINES BURNING RATE Ra = 28.5 E-8 kg/s
RETRIEVED ATTRITED CARRBON Wa = 22 E-6 kg
MCRT OF BURNING FINES IN SUB-TEST Tria = 60.2 s
MCRT OF ATTRITED PARTICLES (MAIN TEST) Tra = 49.5 s
IDEAL MCRT OF ELUTRATED SIZE PARTICLE Tre* = 41.6 s
IDEAL MCRT OF THE LARGEST ATTRITED PARTICLE Trs* = 101 s
ELUTRIATED FRACTION OF ATTRITED PARTICLES Ya = .359
ATTRITION RATE Qa = 44.4 E-8 kg/s
RATIO Qa/(Qa+Rm) = 4.08 %

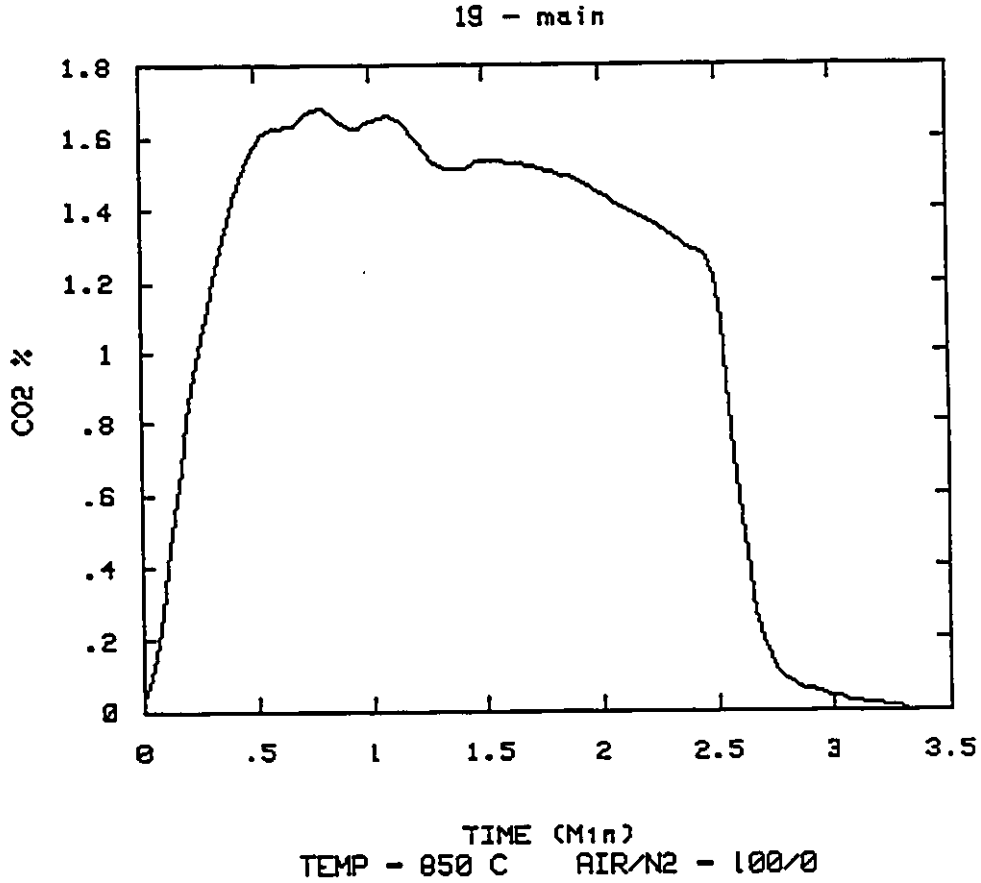

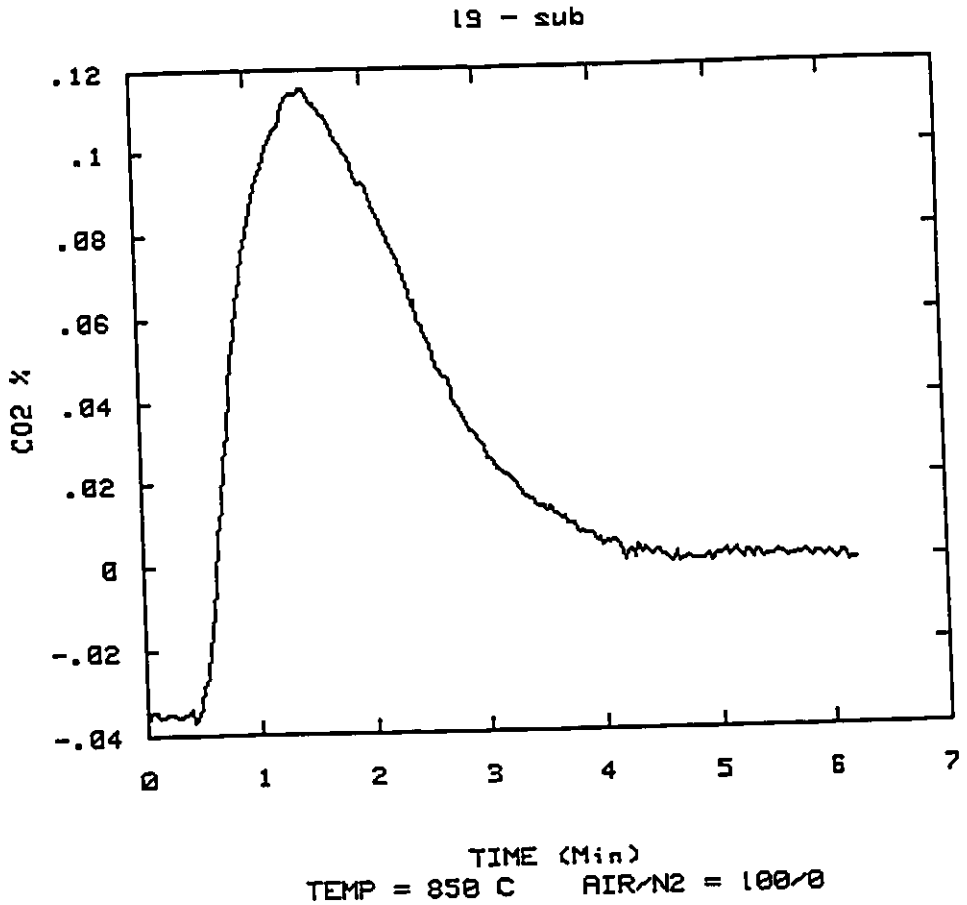
19 - sub
.12
.1
.08
.06
.04
.02
0
-.02
-.04
CO2 %
0
1
2
3
4
5
6
7
TIME (Min)
TEMP = 850 C
AIR/N2 = 100/0

SER2 - 21 :F3
BED TEMPERATURE = 850 C
OXYGEN CONCENTRATION = 21 %
MOTHER CHAR BURNING RATE Rm = 12.53 E-6 kg/s
ATTRITED FINES BURNING RATE Ra = 54.84 E-8 kg/s
RETRIEVED ATTRITED CARRBON Wa = 37.15 E-6 kg
MCRT OF BURNING FINES IN SUB-TEST Tria = 52.3 s
MCRT OF ATTRITED PARTICLES (MAIN TEST) Tra = 36 s
IDEAL MCRT OF ELUTRATED SIZE PARTICLE Tre* = 38.9 s
IDEAL MCRT OF THE LARGEST ATTRITED PARTICLE Trs* = 84.3 s
ELUTRIATED FRACTION OF ATTRITED PARTICLES Ya = .469
ATTRITION RATE Qa = 103.2 E-8 kg/s
RATIO Qa/(Qa+Rm) = 7.62 %

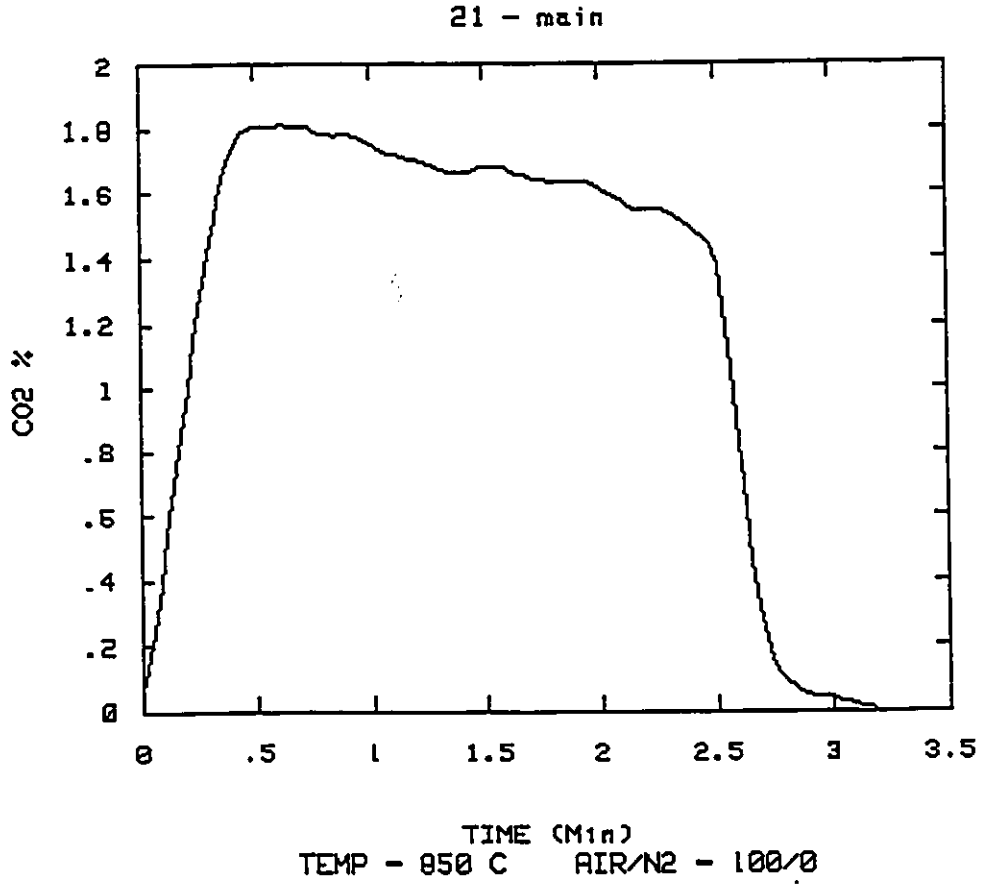

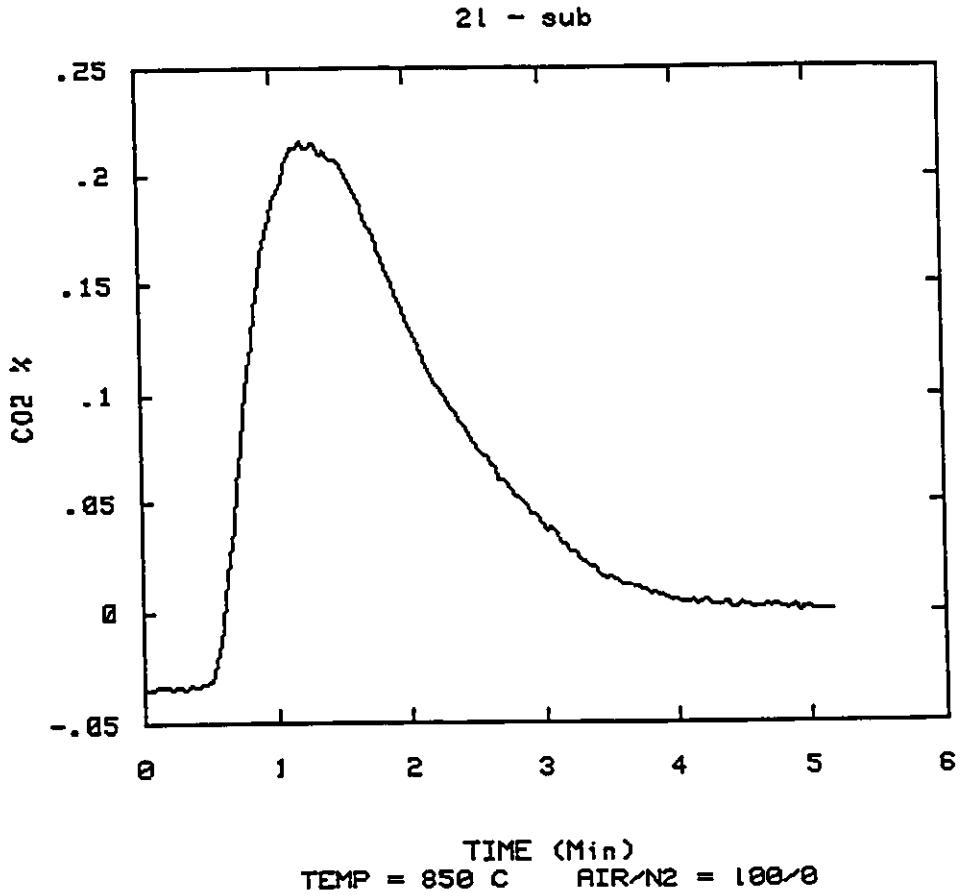
21 - sub
.25
.2
.15
.1
.05
0
-.05
CO2 %
0
1
2
3
4
5
6
TIME (Min)
TEMP = 850 C
AIR/N2 = 100/0

SER2 - 22 :F3
BED TEMPERATURE = 850 C
OXYGEN CONCENTRATION = 21 %
MOTHER CHAR BURNING RATE Rm = 4.52 E-6 kg/s
ATTRITED FINES BURNING RATE Ra = 37.6 E-8 kg/s
RETRIEVED ATTRITED CARRBON Wa = 24.34 E-6 kg
MCRT OF BURNING FINES IN SUB-TEST Tria = 50.4 s
MCRT OF ATTRITED PARTICLES (MAIN TEST) Tra = 41.8 s
IDEAL MCRT OF ELUTRATED SIZE PARTICLE Tre* = 34.7 s
IDEAL MCRT OF THE LARGEST ATTRITED PARTICLE Trs* = 84.6 s
ELUTRIATED FRACTION OF ATTRITED PARTICLES Ya = .353
ATTRITION RATE Qa = 58.2 E-8 kg/s
RATIO Qa/(Qa+Rm) = 11.41 %

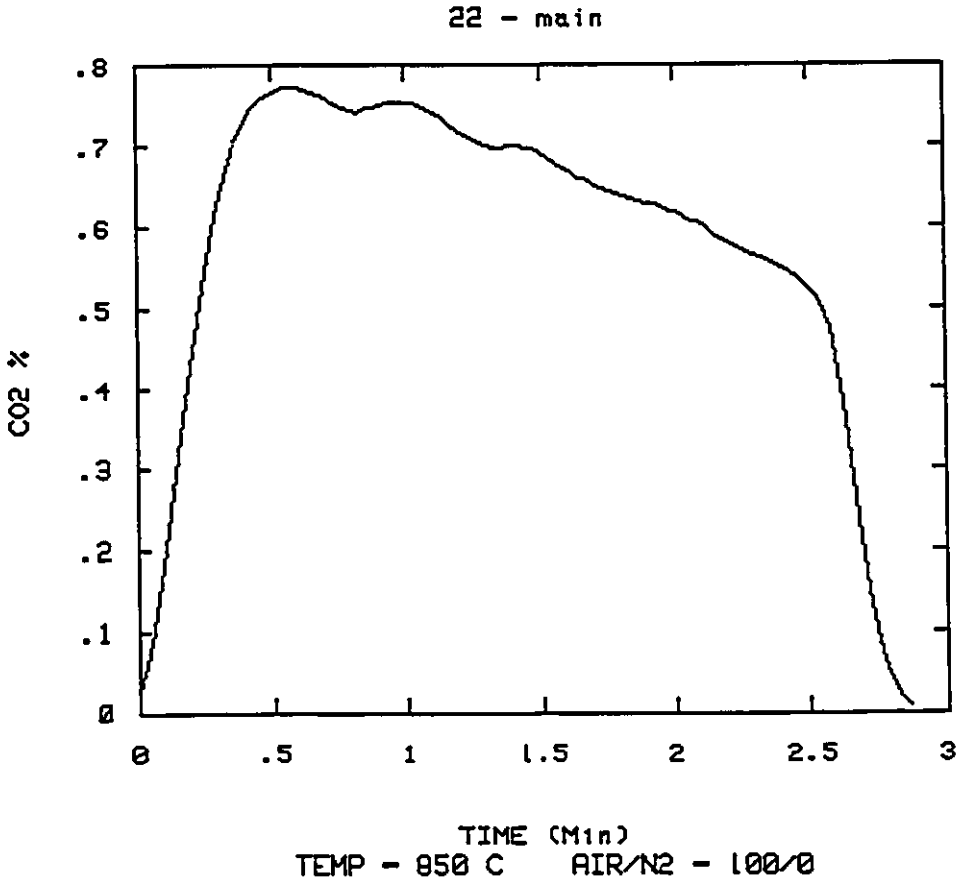

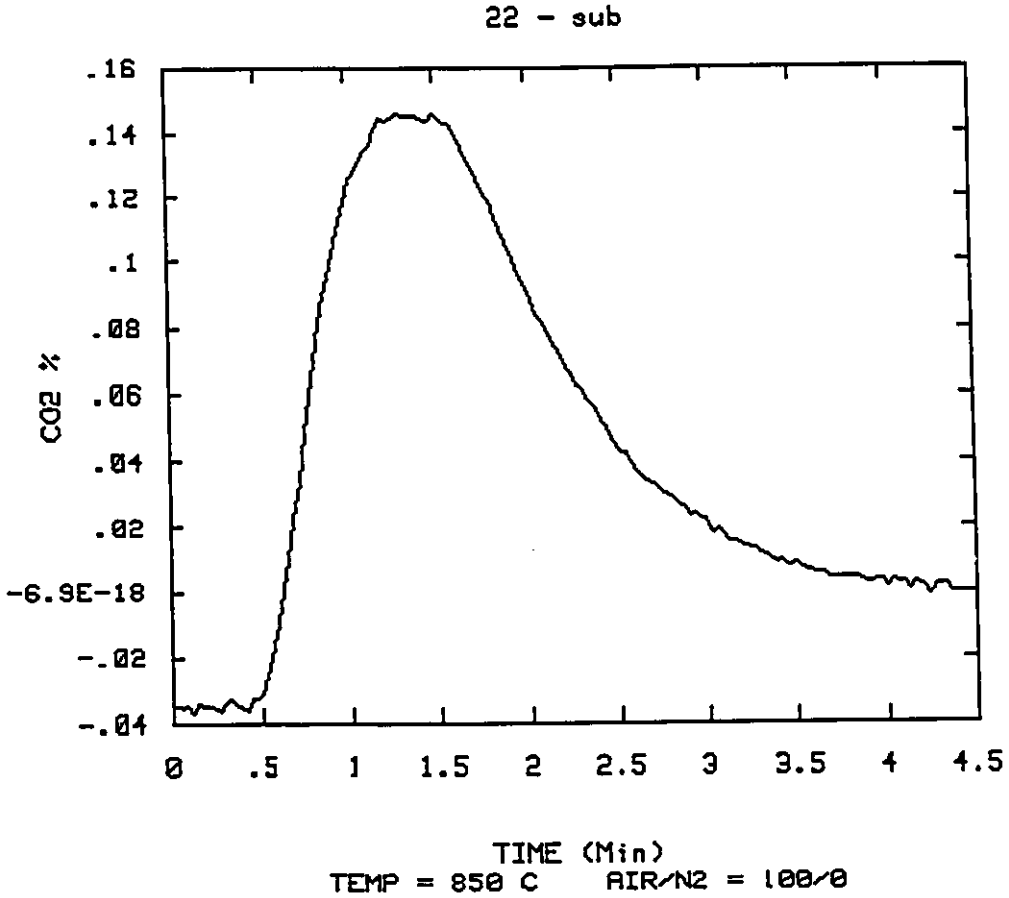
22 - sub
.16
.14
.12
.1
.08
.06
.04
.02
-6.9E-18
-.02
-.04
CO2 %
0
.5
1
1.5
2
2.5
3
3.5
4
4.5
TIME (Min)
TEMP = 850 C
AIR/N2 = 100/0

SER2 - 24 :F4
BED TEMPERATURE = 850 C
OXYGEN CONCENTRATION = 21 %
MOTHER CHAR BURNING RATE Rm = 12.13 E-6 kg/s
ATTRITED FINES BURNING RATE Ra = 11.92 E-8 kg/s
RETRIEVED ATTRITED CARRBON Wa = 9.07 E-6 kg
MCRT OF BURNING FINES IN SUB-TEST Tria = 59.3 s
MCRT OF ATTRITED PARTICLES (MAIN TEST) Tra = 47.4 s
IDEAL MCRT OF ELUTRATED SIZE PARTICLE Tre* = 41.6 s
IDEAL MCRT OF THE LARGEST ATTRITED PARTICLE Trs* = 98.7 s
ELUTRIATED FRACTION OF ATTRITED PARTICLES Ya = .379
ATTRITION RATE Qa = 19.2 E-8 kg/s
RATIO Qa/(Qa+Rm) = 1.55 %

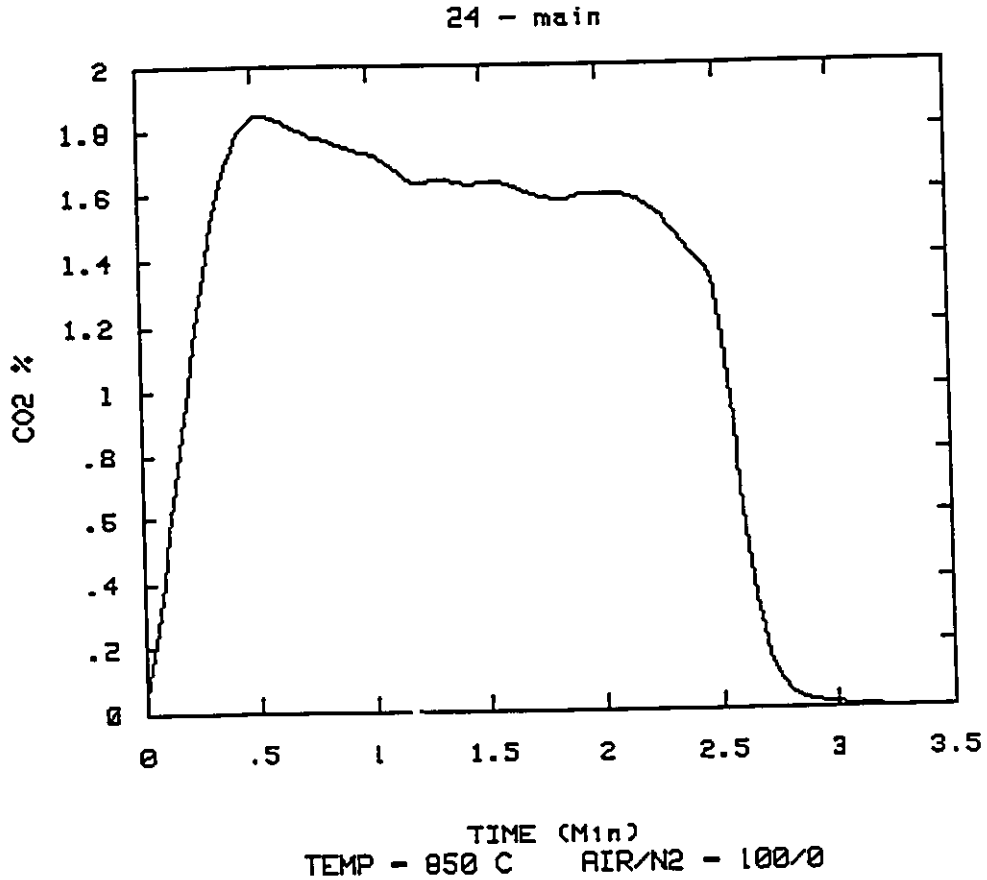

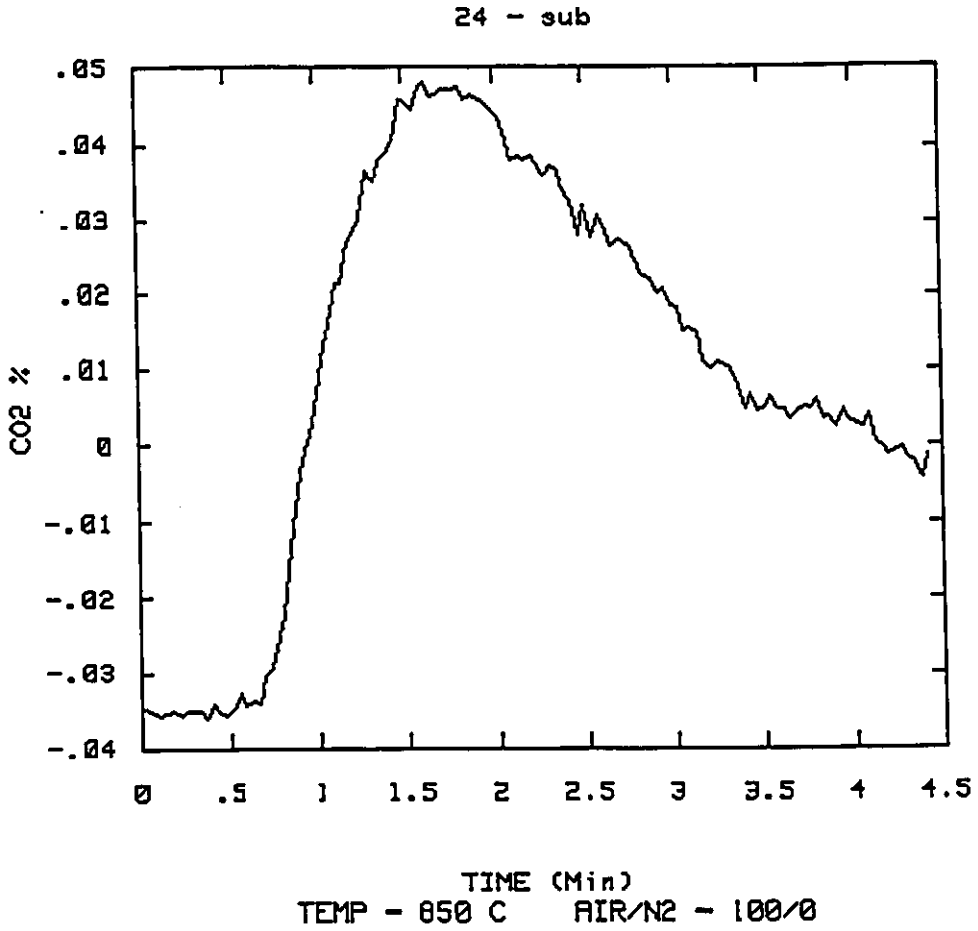
24 - sub
.05
.04
.03
.02
.01
0
-.01
-.02
-.03
-.04
CO2 %
0
.5
1
1.5
2
2.5
3
3.5
4
4.5
TIME (Min)
TEMP - 850 C
AIR/N2 - 100/0

SER2 - 25 :F4
BED TEMPERATURE = 850 C
OXYGEN CONCENTRATION = 21 %
MOTHER CHAR BURNING RATE Rm = 6.28 E-6 kg/s
ATTRITED FINES BURNING RATE Ra = 22.96 E-8 kg/s
RETRIEVED ATTRITED CARRBON Wa = 16.06 E-6 kg
MCRT OF BURNING FINES IN SUB-TEST Tria = 55.3 s
MCRT OF ATTRITED PARTICLES (MAIN TEST) Tra = 53.6 s
IDEAL MCRT OF ELUTRATED SIZE PARTICLE Tre* = 33.8 s
IDEAL MCRT OF THE LARGEST ATTRITED PARTICLE Trs* = 96.7 s
ELUTRIATED FRACTION OF ATTRITED PARTICLES Ya = .235
ATTRITION RATE Qa = 30 E-8 kg/s
RATIO Qa/(Qa+Rm) = 4.56 %

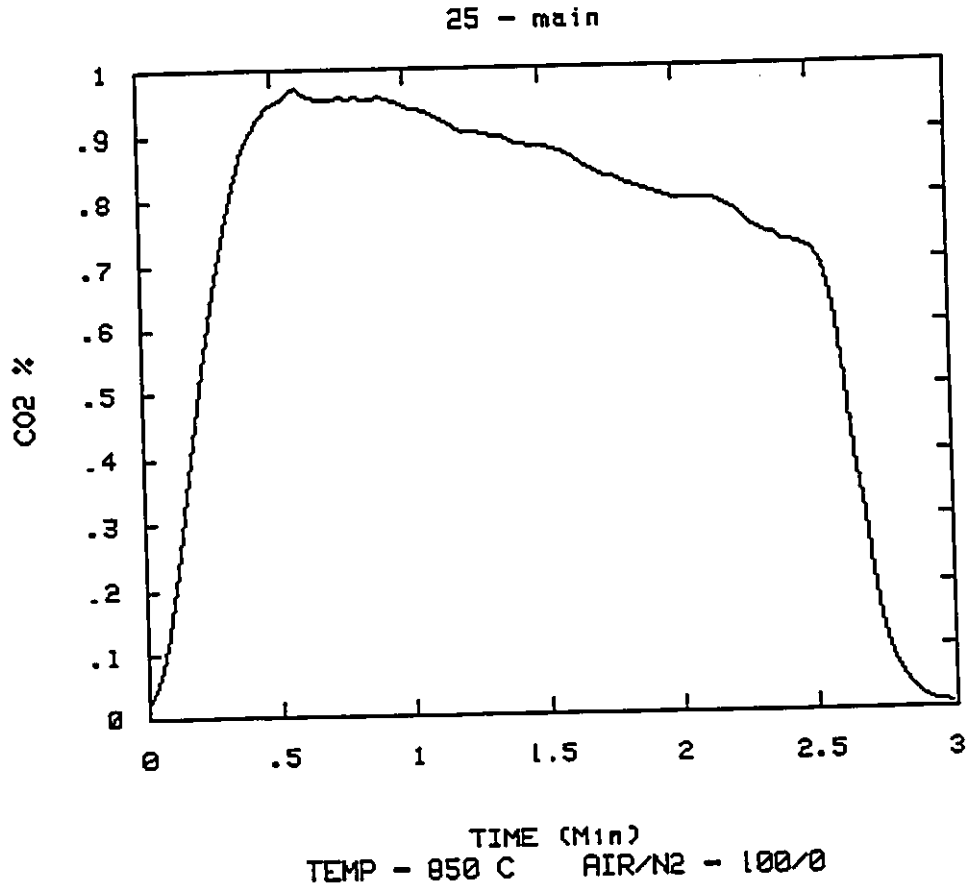

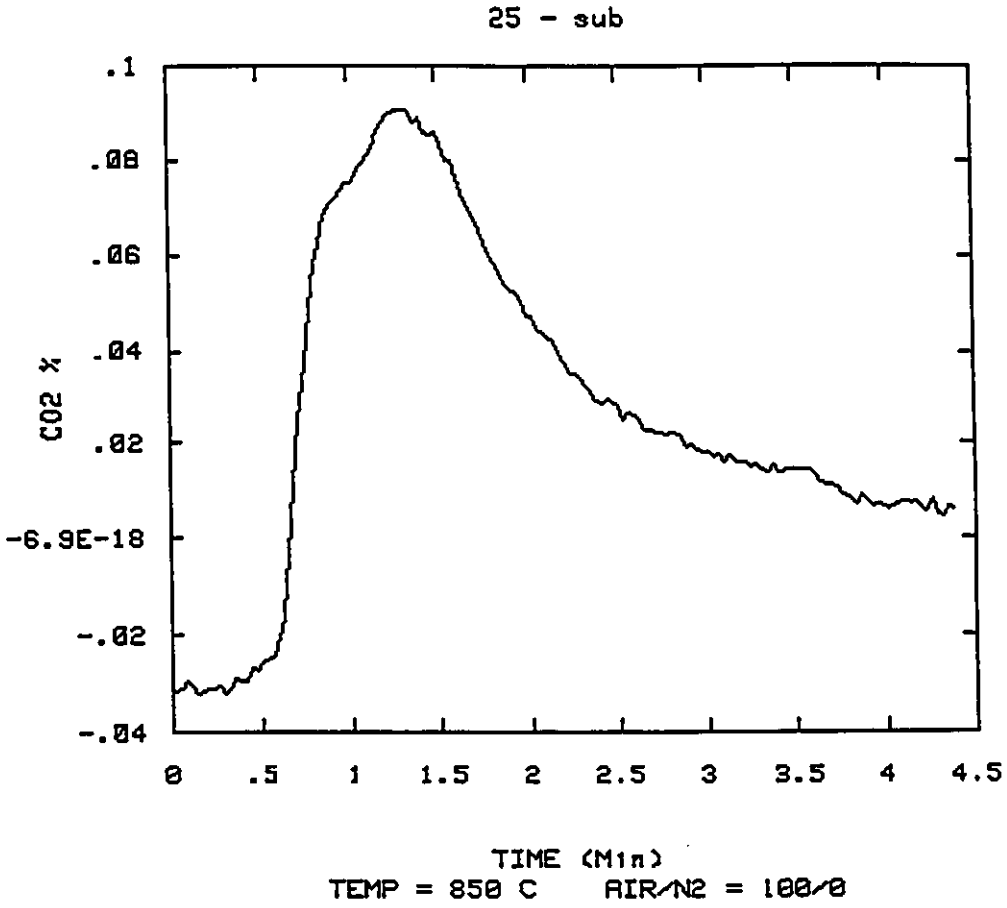
25 - sub
.1
.08
.06
.04
.02
-6.9E-18
-.02
-.04
CO2 %
0
.5
1
1.5
2
2.5
3
3.5
4
4.5
TIME (Min)
TEMP = 850 C
AIR/N2 = 100/0

SER2 - 27 :B
BED TEMPERATURE = 850 C
OXYGEN CONCENTRATION = 21 %
MOTHER CHAR BURNING RATE Rm = 8.17 E-6 kg/s
ATTRITED FINES BURNING RATE Ra = 23.64 E-8 kg/s
RETRIEVED ATTRITED CARRBON Wa = 22.75 E-6 kg
MCRT OF BURNING FINES IN SUB-TEST Tria = 73.6 s
MCRT OF ATTRITED PARTICLES (MAIN TEST) Tra = 32.1 s
IDEAL MCRT OF ELUTRATED SIZE PARTICLE Tre* = 60.2 s
IDEAL MCRT OF THE LARGEST ATTRITED PARTICLE Trs* = 109.5 s
ELUTRIATED FRACTION OF ATTRITED PARTICLES Ya = .667
ATTRITION RATE Qa = 70.8 E-8 kg/s
RATIO Qa/(Qa+Rm) = 7.98 %

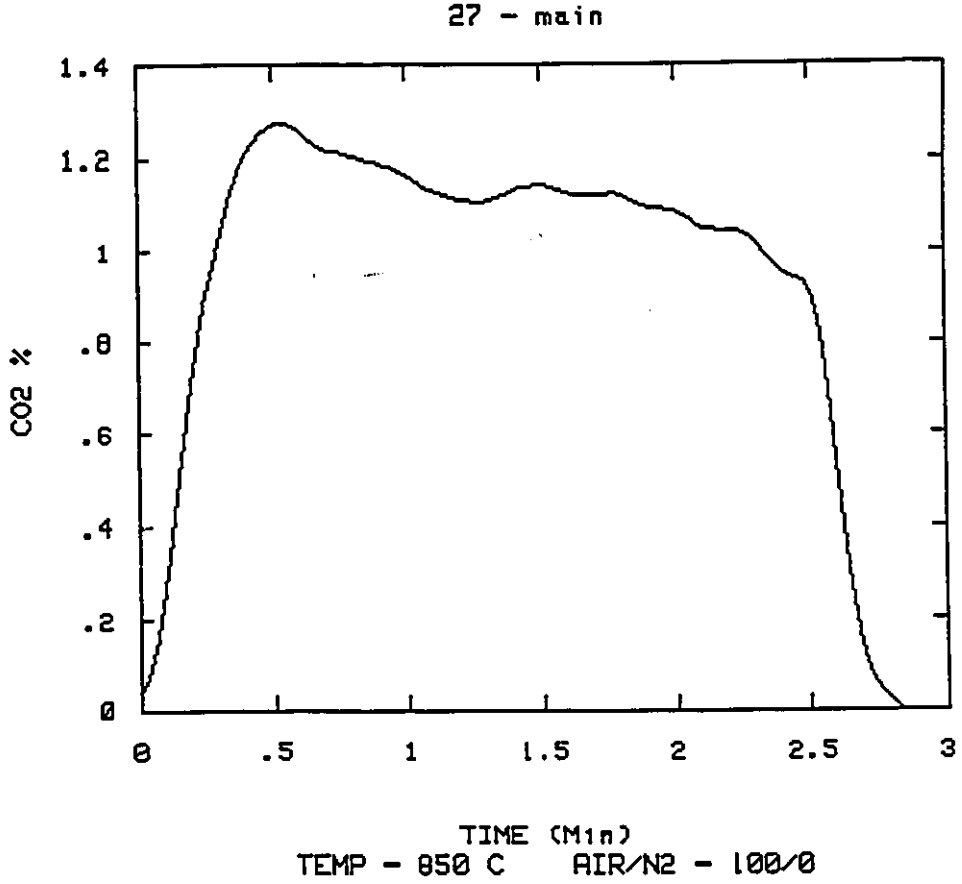

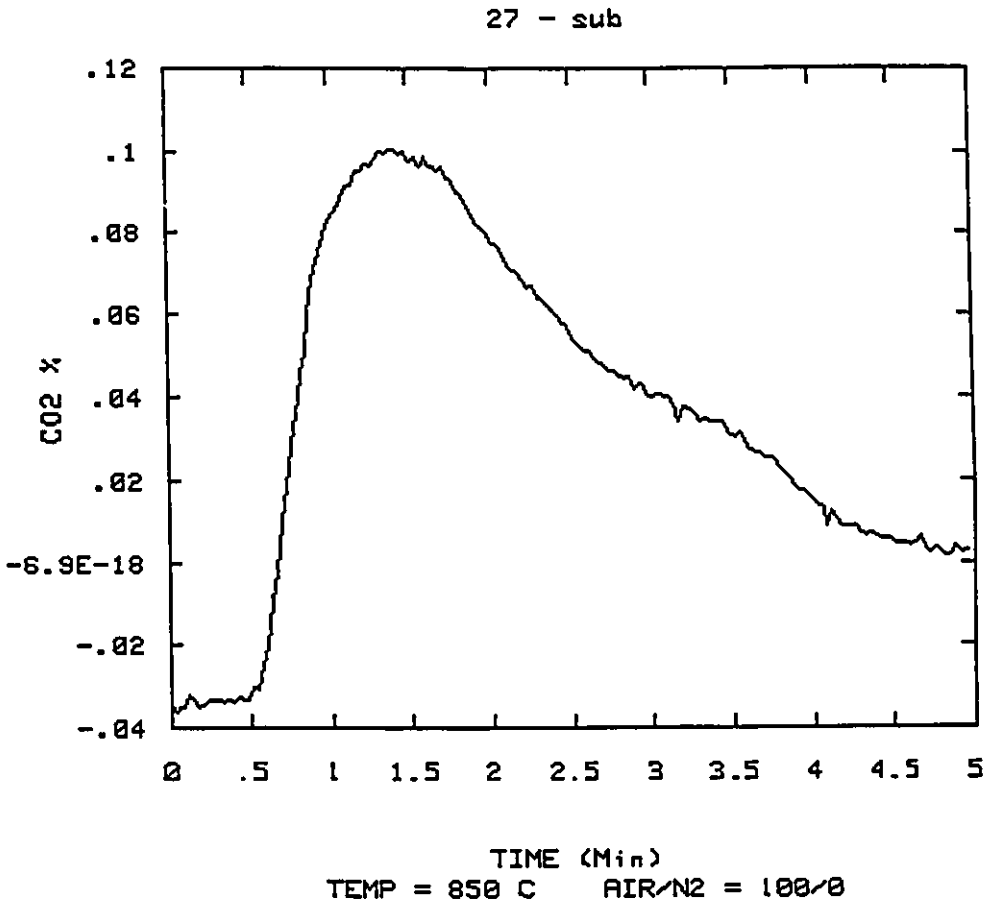
27 - sub
.12
.1
.08
.06
.04
.02
-6.9E-18
-.02
-.04
CO2 %
0
.5
1
1.5
2
2.5
3
3.5
4
4.5
5
TIME (Min)
TEMP = 850 C
AIR/N2 = 100/0

SER2 - 29 :B
BED TEMPERATURE = 850 C
OXYGEN CONCENTRATION = 21 %
MOTHER CHAR BURNING RATE Rm = 5.67 E-6 kg/s
ATTRITED FINES BURNING RATE Ra = 12.1 E-8 kg/s
RETRIEVED ATTRITED CARRBON Wa = 8.63 E-6 kg
MCRT OF BURNING FINES IN SUB-TEST Tria = 54 s
MCRT OF ATTRITED PARTICLES (MAIN TEST) Tra = 18 s
IDEAL MCRT OF ELUTRATED SIZE PARTICLE Tre* = 45.6 s
IDEAL MCRT OF THE LARGEST ATTRITED PARTICLE Trs* = 77.3 s
ELUTRIATED FRACTION OF ATTRITED PARTICLES Ya = .747
ATTRITION RATE Qa = 48 E-8 kg/s
RATIO Qa/(Qa+Rm) = 7.79 %

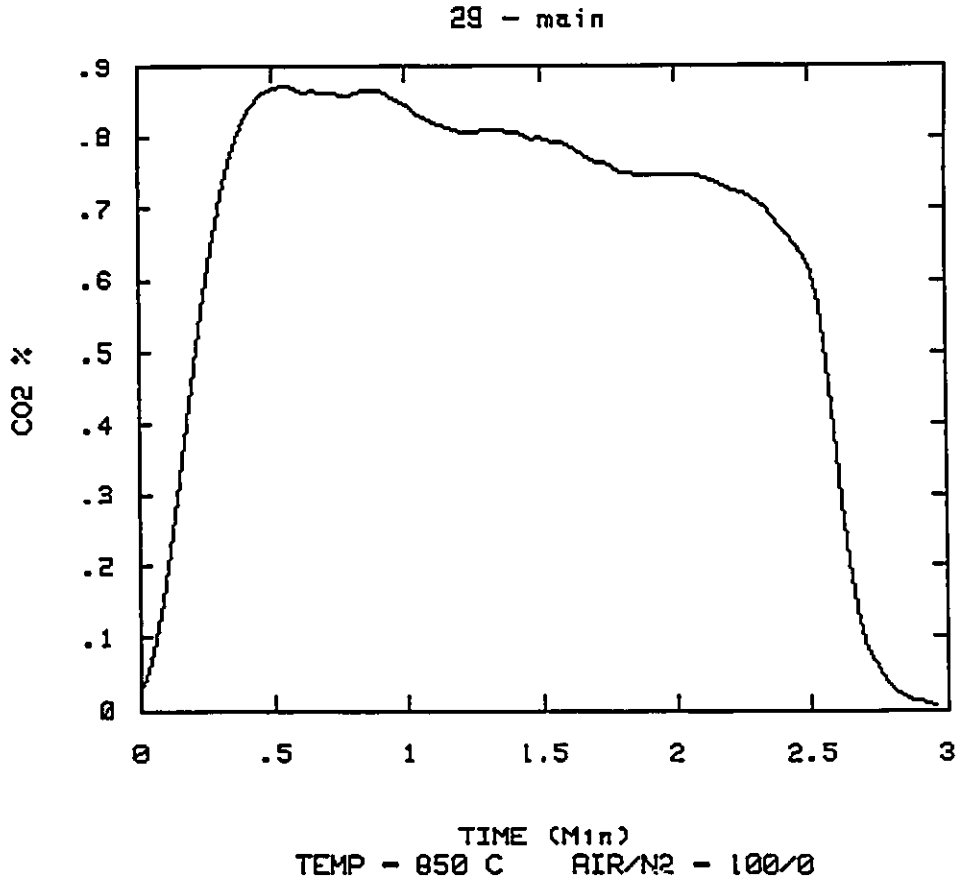

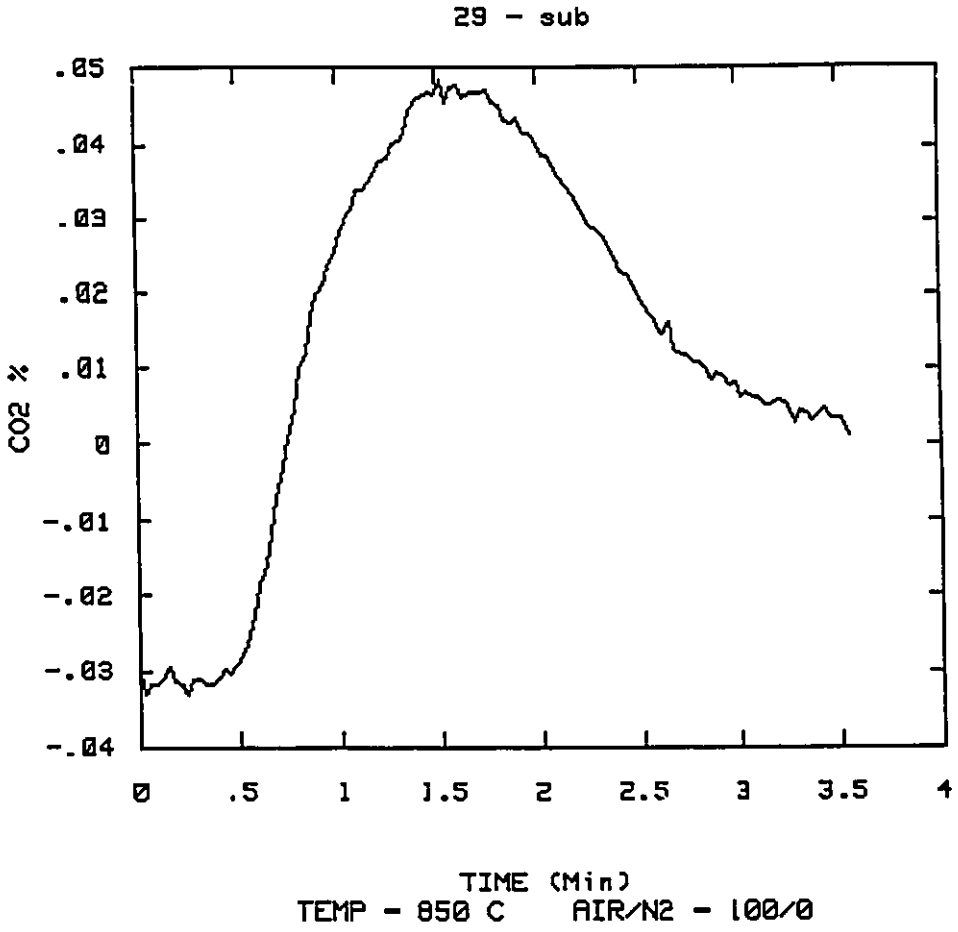
29 - sub
.05
.04
.03
.02
.01
0
-.01
-.02
-.03
-.04
CO2 %
0
.5
1
1.5
2
2.5
3
3.5
4
TIME (Min)
TEMP - 850 C
AIR/N2 - 100/0

SER2 - 31 :B
BED TEMPERATURE = 850 C
OXYGEN CONCENTRATION = 21 %
MOTHER CHAR BURNING RATE Rm = 6.58 E-6 kg/s
ATTRITED FINES BURNING RATE Ra = 6.96 E-8 kg/s
RETRIEVED ATTRITED CARRBON Wa = 5.63 E-6 kg
MCRT OF BURNING FINES IN SUB-TEST Tria = 61.2 s
MCRT OF ATTRITED PARTICLES (MAIN TEST) Tra = 12.6 s
IDEAL MCRT OF ELUTRATED SIZE PARTICLE Tre* = 53.7 s
IDEAL MCRT OF THE LARGEST ATTRITED PARTICLE Trs* = 82.6 s
ELUTRIATED FRACTION OF ATTRITED PARTICLES Ya = .845
ATTRITION RATE Qa = 44.8 E-8 kg/s
RATIO Qa/(Qa+Rm) = 6.37 %

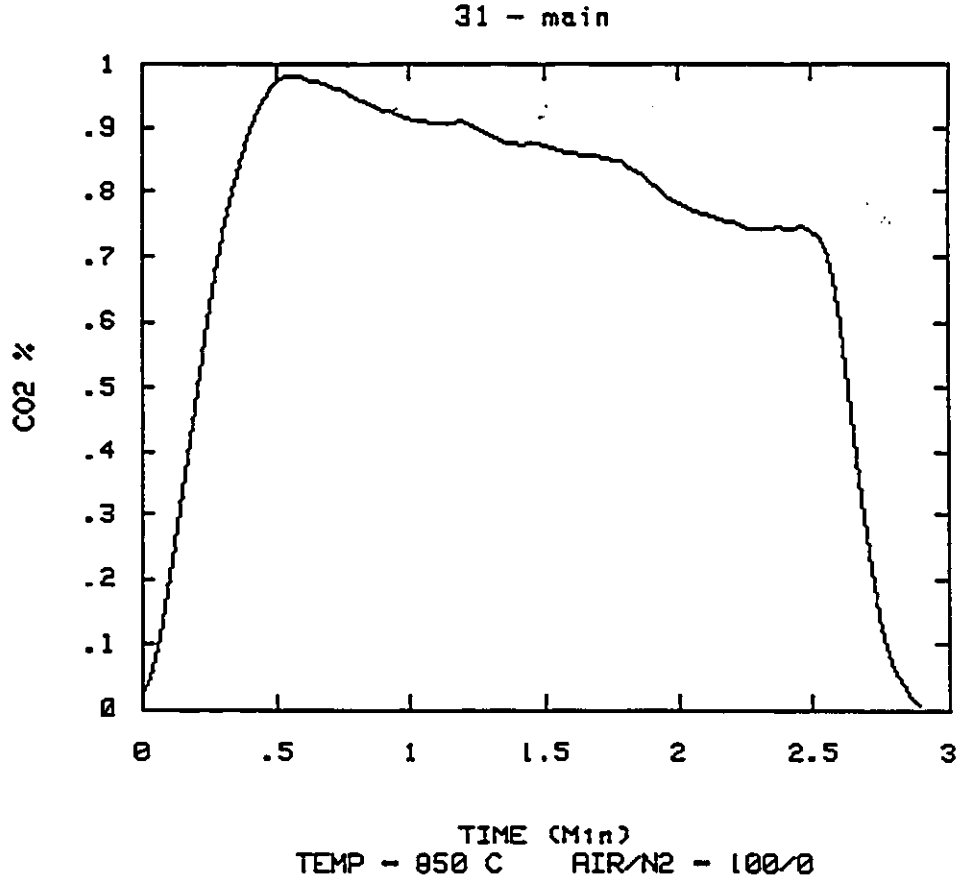

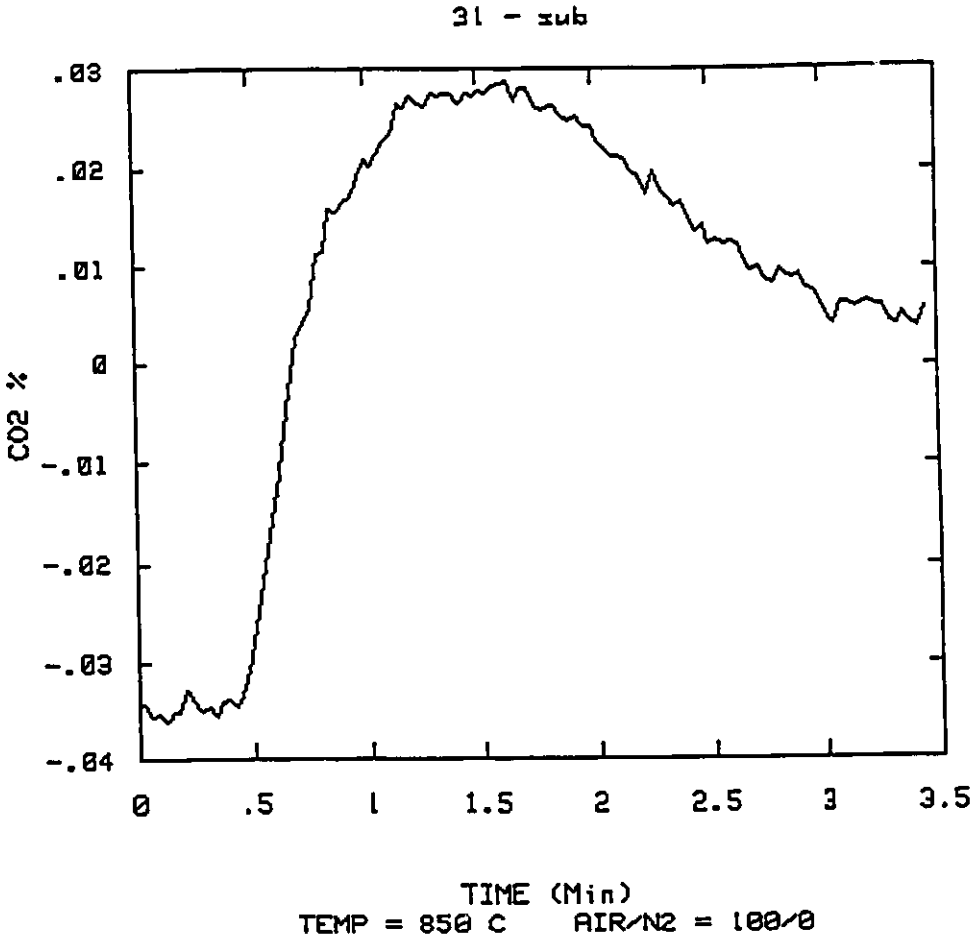
31 - sub
.03
.02
.01
0
-.01
-.02
-.03
-.04
CO2 %
0
.5
1
1.5
2
2.5
3
3.5
TIME (Min)
TEMP = 850 C
AIR/N2 = 100/0

SER2 - 32 :B
BED TEMPERATURE = 850 C
OXYGEN CONCENTRATION = 21 %
MOTHER CHAR BURNING RATE Rm = 2.33 E-6 kg/s
ATTRITED FINES BURNING RATE Ra = 21.66 E-8 kg/s
RETRIEVED ATTRITED CARRBON Wa = 19.03 E-6 kg
MCRT OF BURNING FINES IN SUB-TEST Tria = 68 s
MCRT OF ATTRITED PARTICLES (MAIN TEST) Tra = 50.1 s
IDEAL MCRT OF ELUTRATED SIZE PARTICLE Tre* = 49.3 s
IDEAL MCRT OF THE LARGEST ATTRITED PARTICLE Trs* = 111.2 s
ELUTRIATED FRACTION OF ATTRITED PARTICLES Ya = .43
ATTRITION RATE Qa = 38 E-8 kg/s
RATIO Qa/(Qa+Rm) = 14.02 %

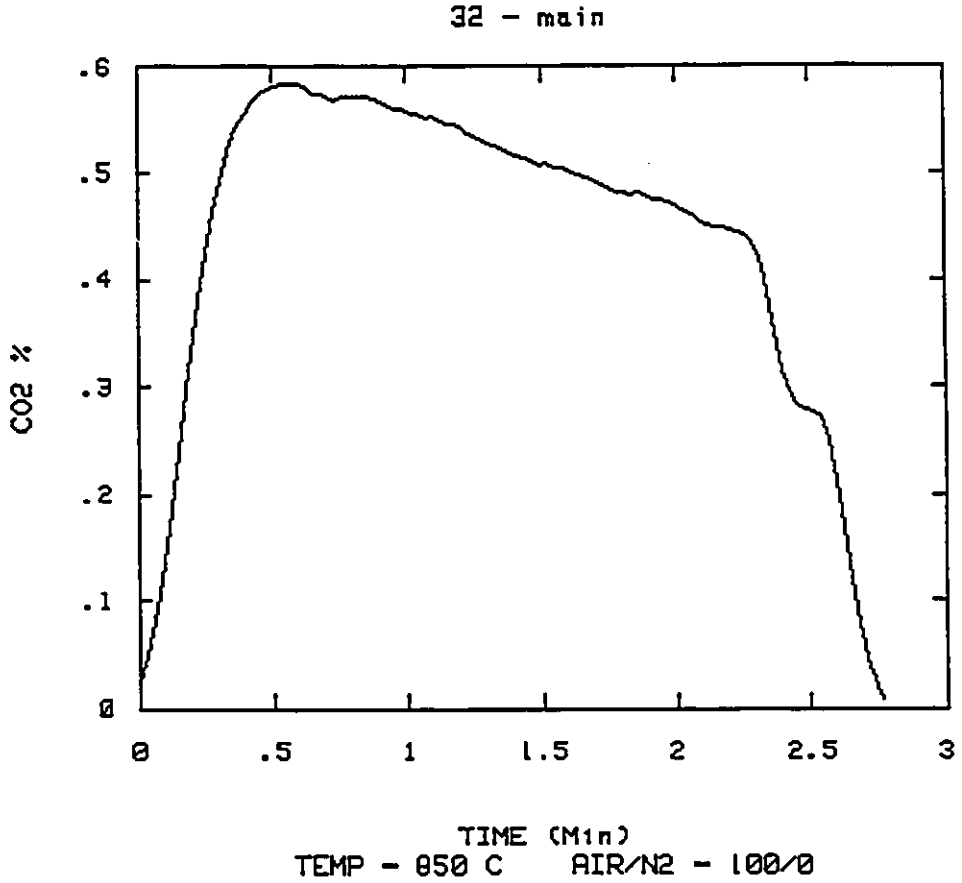

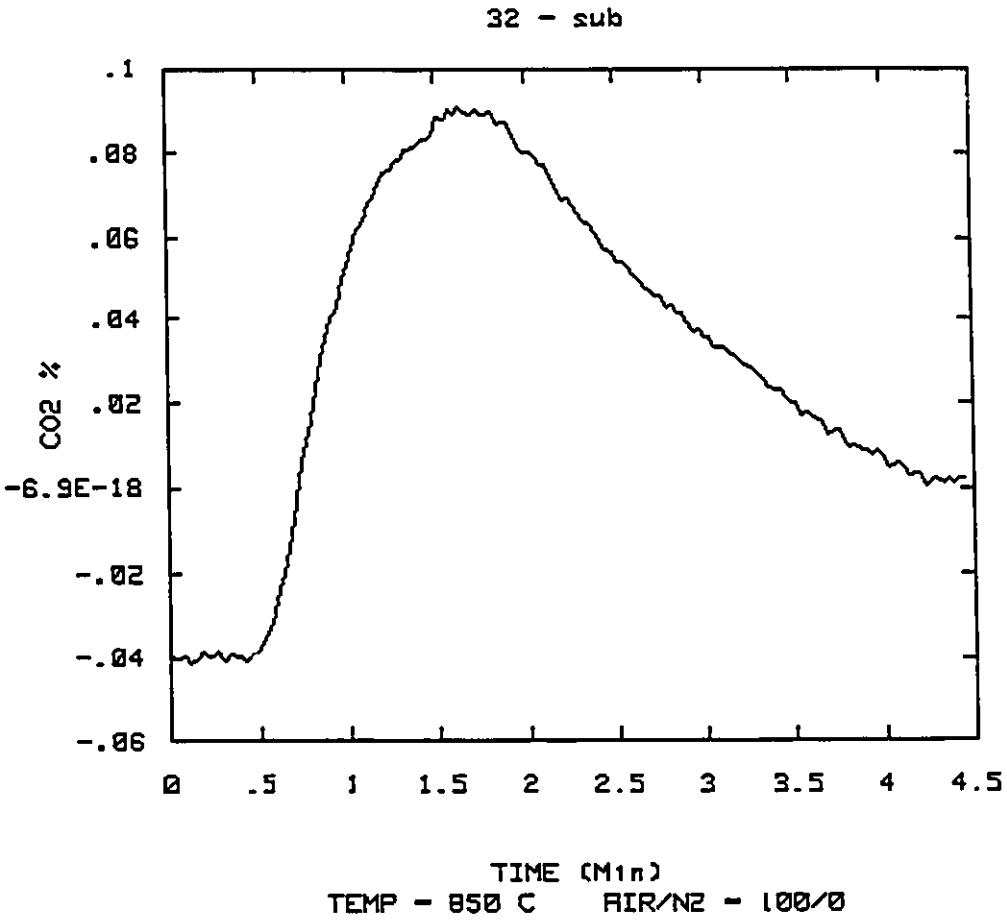
32 - sub
.1
.08
.06
.04
.02
-6.9E-18
-.02
-.04
-.06
CO2 %
0
.5
1
1.5
2
2.5
3
3.5
4
4.5
TIME (Min)
TEMP - 850 C
AIR/N2 - 100/0

SER2 - 33 :C
BED TEMPERATURE = 850 C
OXYGEN CONCENTRATION = 21 %
MOTHER CHAR BURNING RATE Rm = 11.33 E-6 kg/s
ATTRITED FINES BURNING RATE Ra = 7.94 E-8 kg/s
RETRIEVED ATTRITED CARRBON Wa = 4.04 E-6 kg
MCRT OF BURNING FINES IN SUB-TEST Tria = 38.8 s
MCRT OF ATTRITED PARTICLES (MAIN TEST) Tra = 9.4 s
IDEAL MCRT OF ELUTRATED SIZE PARTICLE Tre* = 33.6 s
IDEAL MCRT OF THE LARGEST ATTRITED PARTICLE Trs* = 53.2 s
ELUTRIATED FRACTION OF ATTRITED PARTICLES Ya = .817
ATTRITION RATE Qa = 43.2 E-8 kg/s
RATIO Qa/(Qa+Rm) = 3.67 %

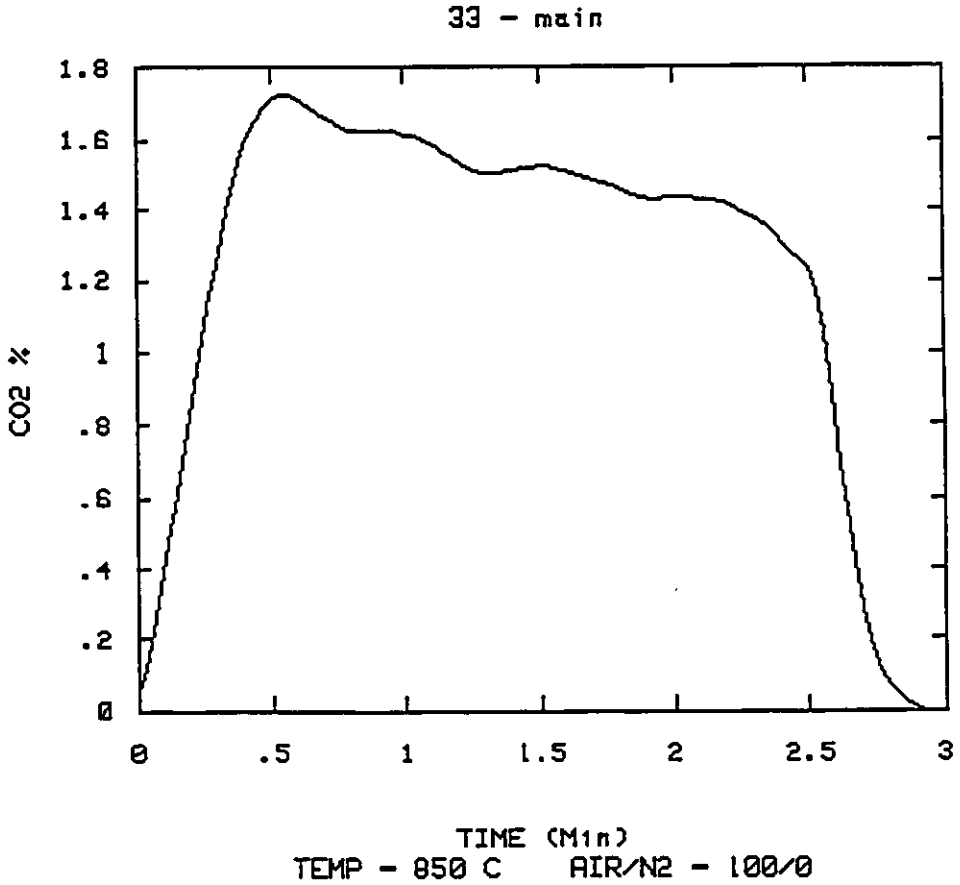

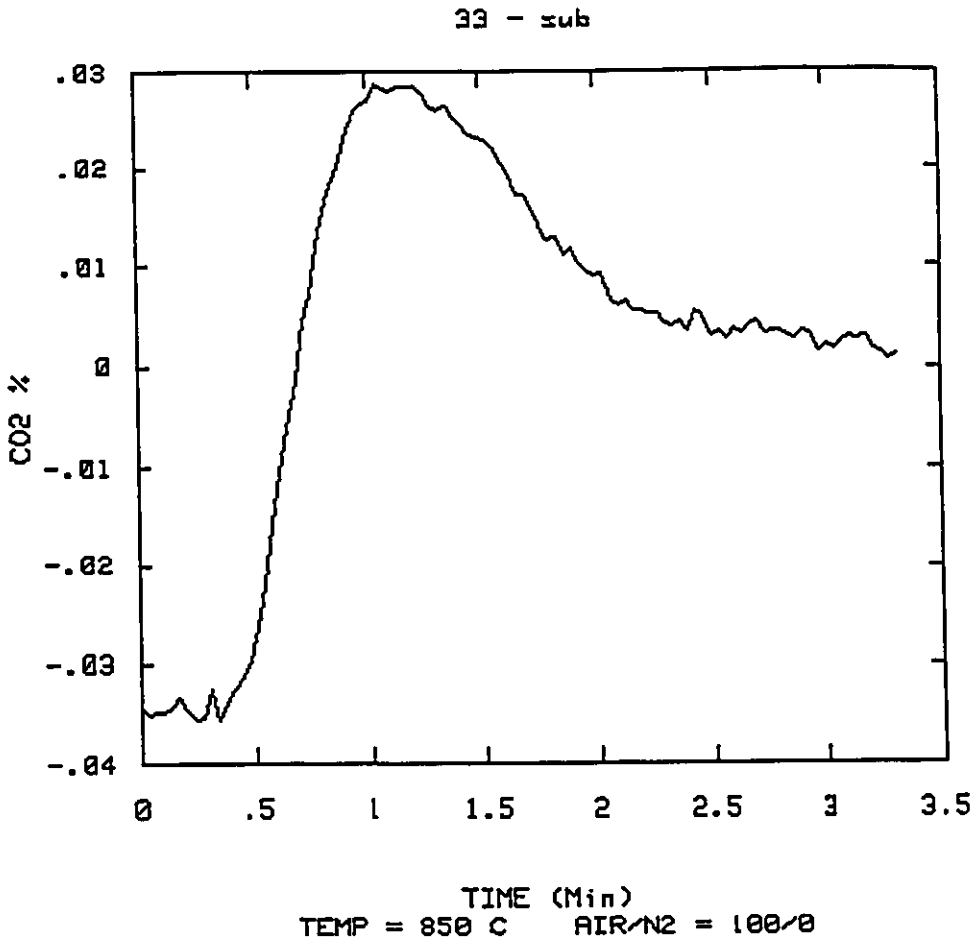
33 - sub
.03
.02
.01
0
-.01
-.02
-.03
-.04
CO2 %
0
.5
1
1.5
2
2.5
3
3.5
TIME (Min)
TEMP = 850 C
AIR/N2 = 100/0

SER2 - 35 :C
BED TEMPERATURE = 850 C
OXYGEN CONCENTRATION = 21 %
MOTHER CHAR BURNING RATE Rm = 12.65 E-6 kg/s
ATTRITED FINES BURNING RATE Ra = 9 E-8 kg/s
RETRIEVED ATTRITED CARRBON Wa = 5.26 E-6 kg
MCRT OF BURNING FINES IN SUB-TEST Tria = 44.4 s
MCRT OF ATTRITED PARTICLES (MAIN TEST) Tra = 15.8 s
IDEAL MCRT OF ELUTRATED SIZE PARTICLE Tre* = 37.2 s
IDEAL MCRT OF THE LARGEST ATTRITED PARTICLE Trs* = 64 s
ELUTRIATED FRACTION OF ATTRITED PARTICLES Ya = .73
ATTRITION RATE Qa = 33.2 E-8 kg/s
RATIO Qa/(Qa+Rm) = 2.56 %

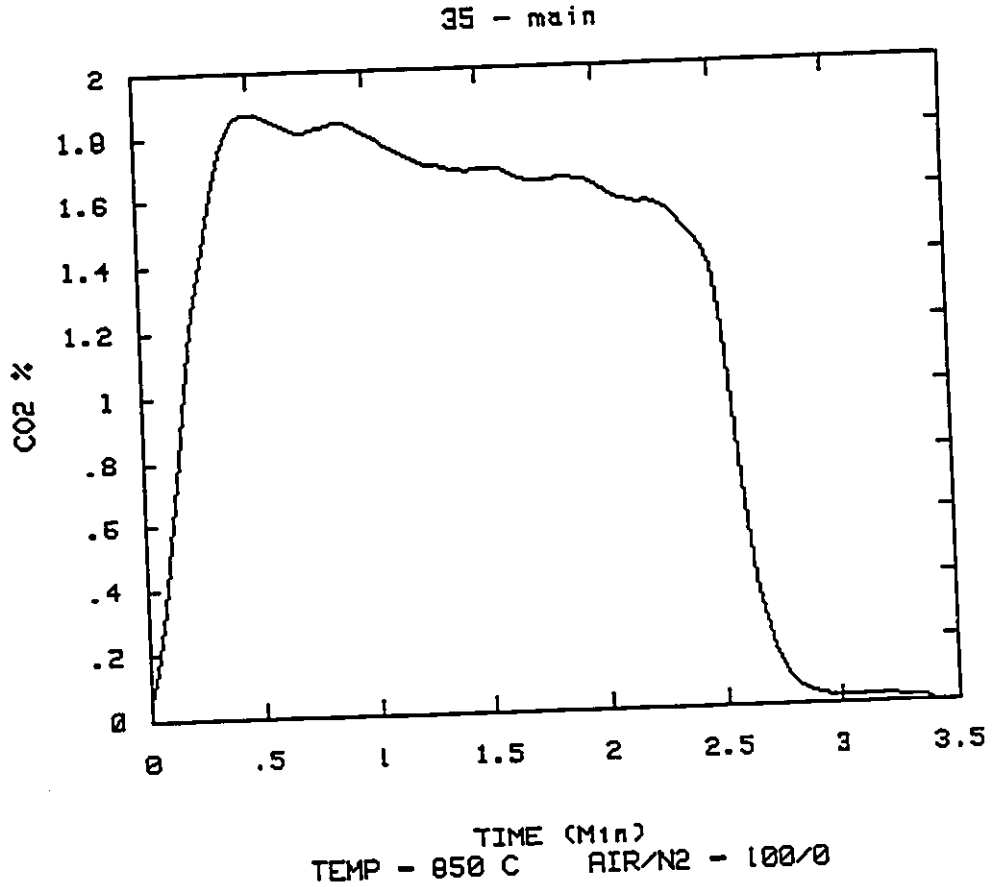

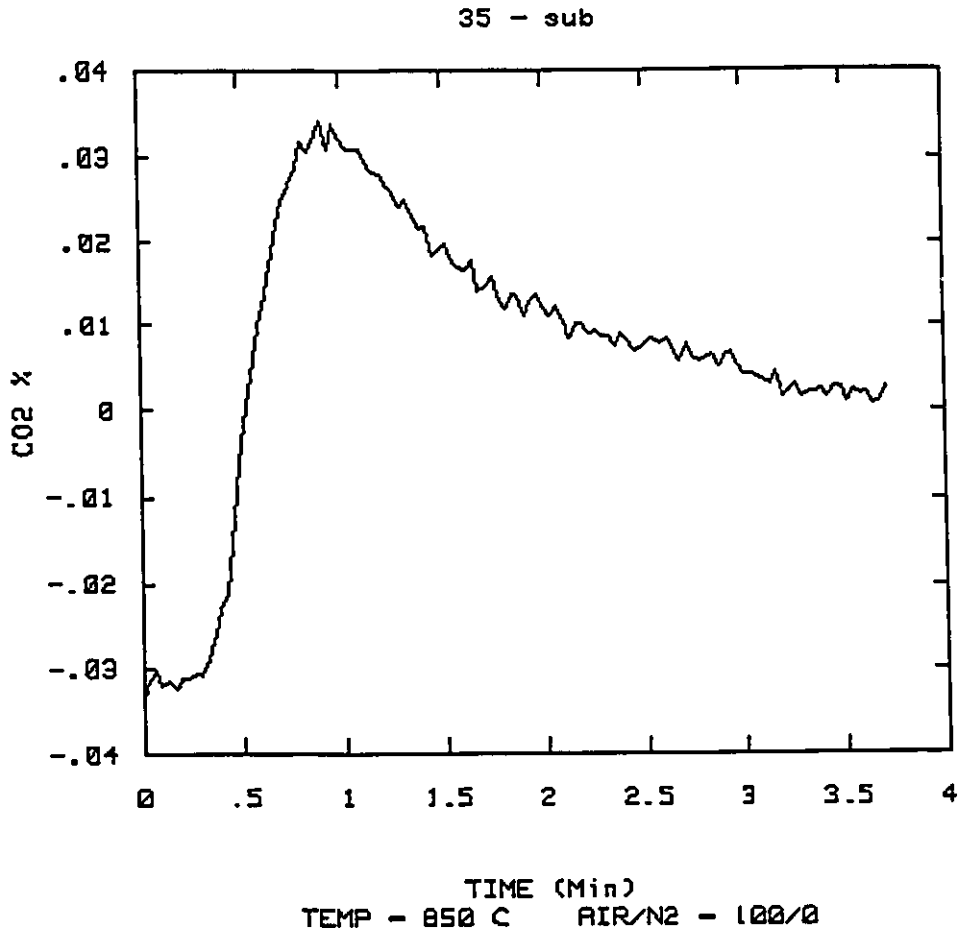
35 - sub
.04
.03
.02
.01
0
-.01
-.02
-.03
-.04
CO2 %
0
.5
1
1.5
2
2.5
3
3.5
4
TIME (Min)
TEMP - 850 C
AIR/N2 - 100/0

SER2 - 37 :C
BED TEMPERATURE = 850 C
OXYGEN CONCENTRATION = 21 %
MOTHER CHAR BURNING RATE Rm = 3.48 E-6 kg/s
ATTRITED FINES BURNING RATE Ra = 6.48 E-8 kg/s
RETRIEVED ATTRITED CARRBON Wa = 4.42 E-6 kg
MCRT OF BURNING FINES IN SUB-TEST Tria = 52.2 s
MCRT OF ATTRITED PARTICLES (MAIN TEST) Tra = 32.2 s
IDEAL MCRT OF ELUTRATED SIZE PARTICLE Tre* = 40 s
IDEAL MCRT OF THE LARGEST ATTRITED PARTICLE Trs* = 82.4 s
ELUTRIATED FRACTION OF ATTRITED PARTICLES Ya = .526
ATTRITION RATE Qa = 13.8 E-8 kg/s
RATIO Qa/(Qa+Rm) = 3.81 %

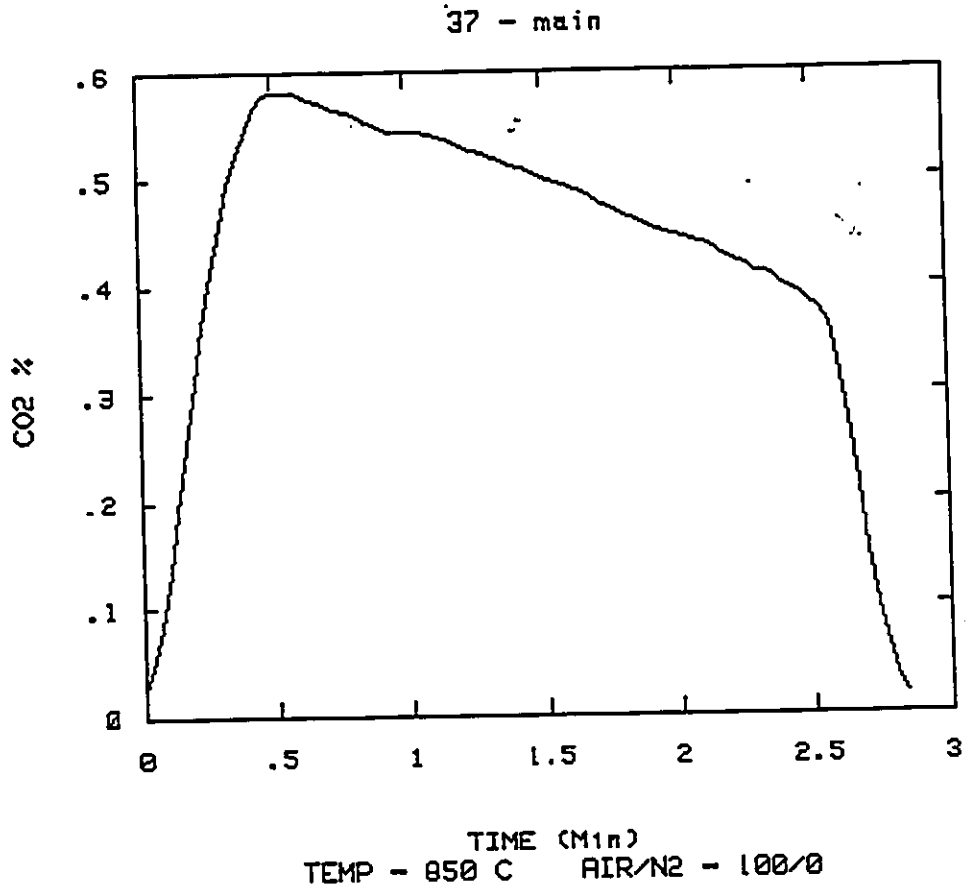

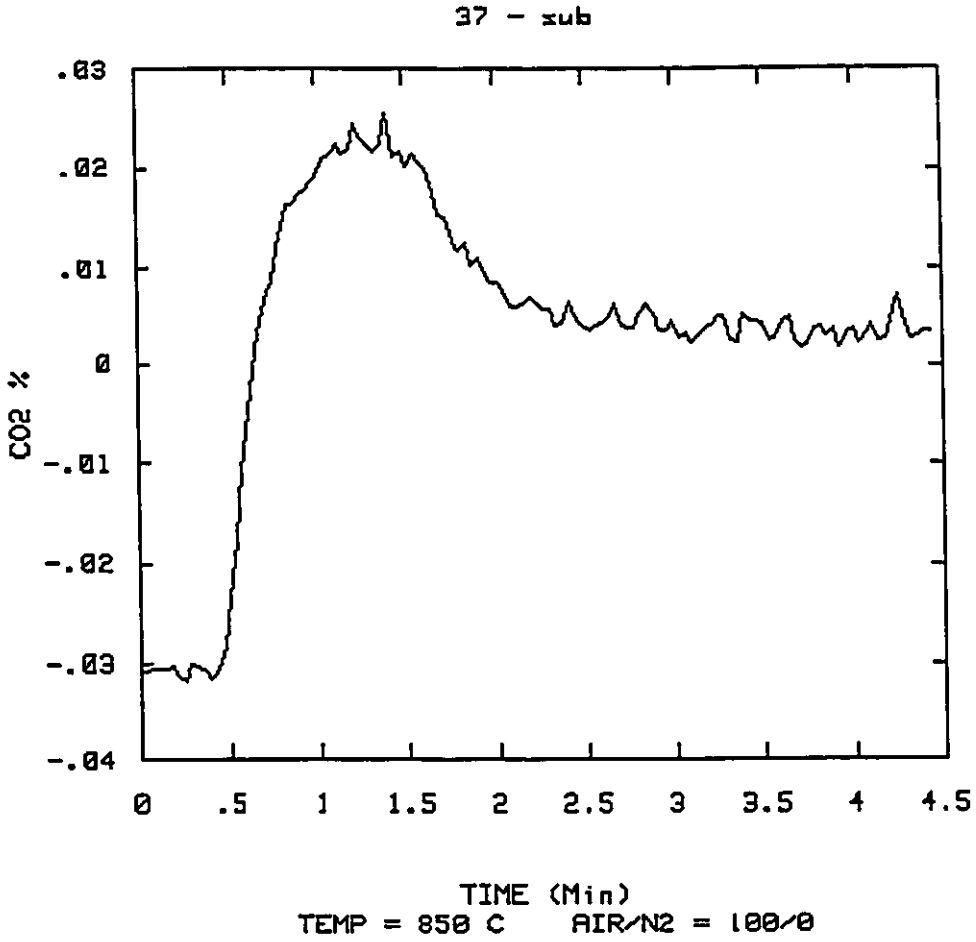
37 - sub
.03
.02
.01
0
-.01
-.02
-.03
-.04
CO2 %
0
.5
1
1.5
2
2.5
3
3.5
4
4.5
TIME (Min)
TEMP = 850 C
AIR/N2 = 100/0

SER2 - 38 :E
BED TEMPERATURE = 850 C
OXYGEN CONCENTRATION = 21 %
MOTHER CHAR BURNING RATE Rm = 9.73 E-6 kg/s
ATTRITED FINES BURNING RATE Ra = 22.32 E-8 kg/s
RETRIEVED ATTRITED CARRBON Wa = 9.83 E-6 kg
MCRT OF BURNING FINES IN SUB-TEST Tria = 34 s
MCRT OF ATTRITED PARTICLES (MAIN TEST) Tra = 26.4 s
IDEAL MCRT OF ELUTRATED SIZE PARTICLE Tre* = 24.2 s
IDEAL MCRT OF THE LARGEST ATTRITED PARTICLE Trs* = 56.3 s
ELUTRIATED FRACTION OF ATTRITED PARTICLES Ya = .399
ATTRITION RATE Qa = 37.2 E-8 kg/s
RATIO Qa/(Qa+Rm) = 3.69 %

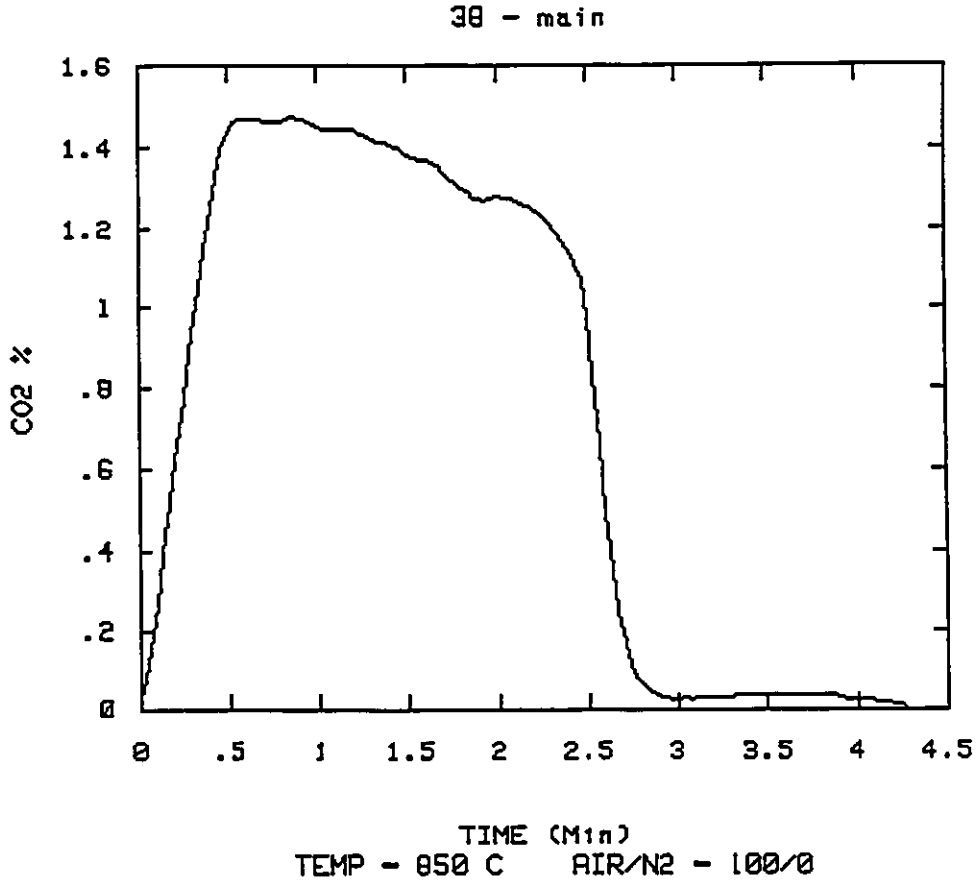

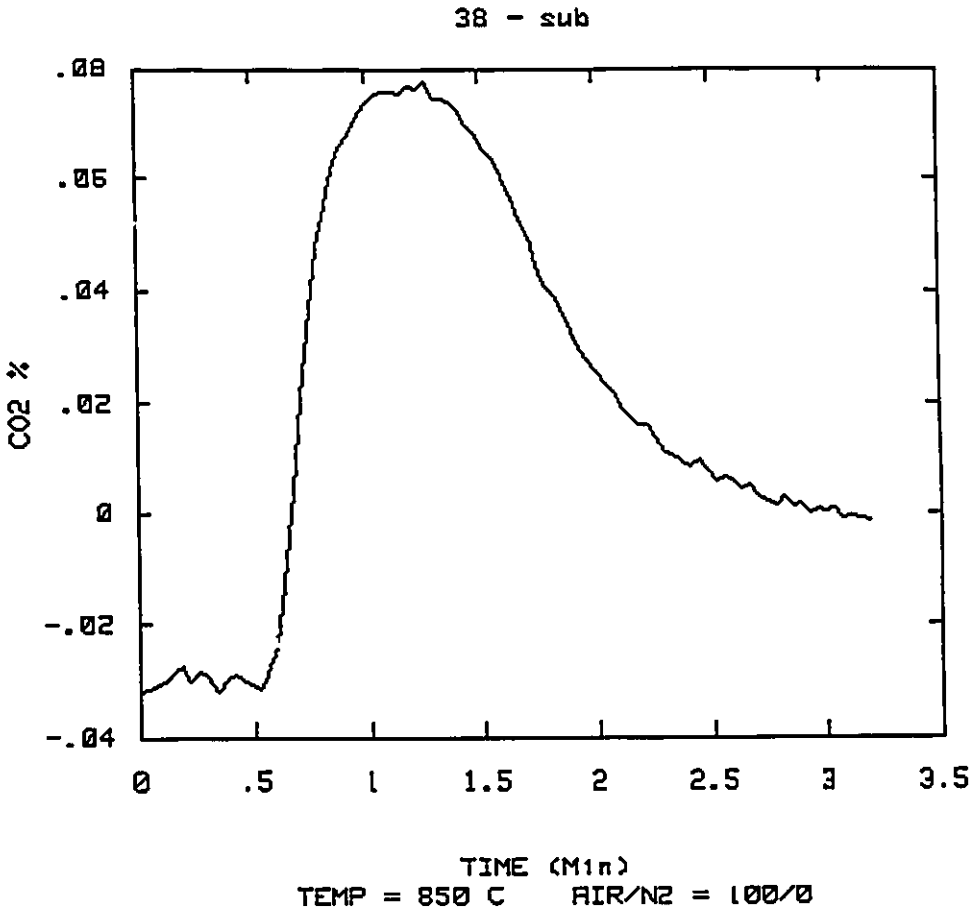
38 - sub
.08
.06
.04
.02
0
-.02
-.04
CO2 %
0
.5
1
1.5
2
2.5
3
3.5
TIME (Min)
TEMP = 850 C
AIR/N2 = 100/0

SER2 - 41 :G
BED TEMPERATURE = 850 C
OXYGEN CONCENTRATION = 21 %
MOTHER CHAR BURNING RATE Rm = 14.72 E-6 kg/s
ATTRITED FINES BURNING RATE Ra = 101.88 E-8 kg/s
RETRIEVED ATTRITED CARRBON Wa = 71.99 E-6 kg
MCRT OF BURNING FINES IN SUB-TEST Tria = 55.7 s
MCRT OF ATTRITED PARTICLES (MAIN TEST) Tra = 51.9 s
IDEAL MCRT OF ELUTRATED SIZE PARTICLE Tre* = 35.4 s
IDEAL MCRT OF THE LARGEST ATTRITED PARTICLE Trs* = 96.4 s
ELUTRIATED FRACTION OF ATTRITED PARTICLES Ya = .267
ATTRITION RATE Qa = 138.6 E-8 kg/s
RATIO Qa/(Qa+Rm) = 8.61 %

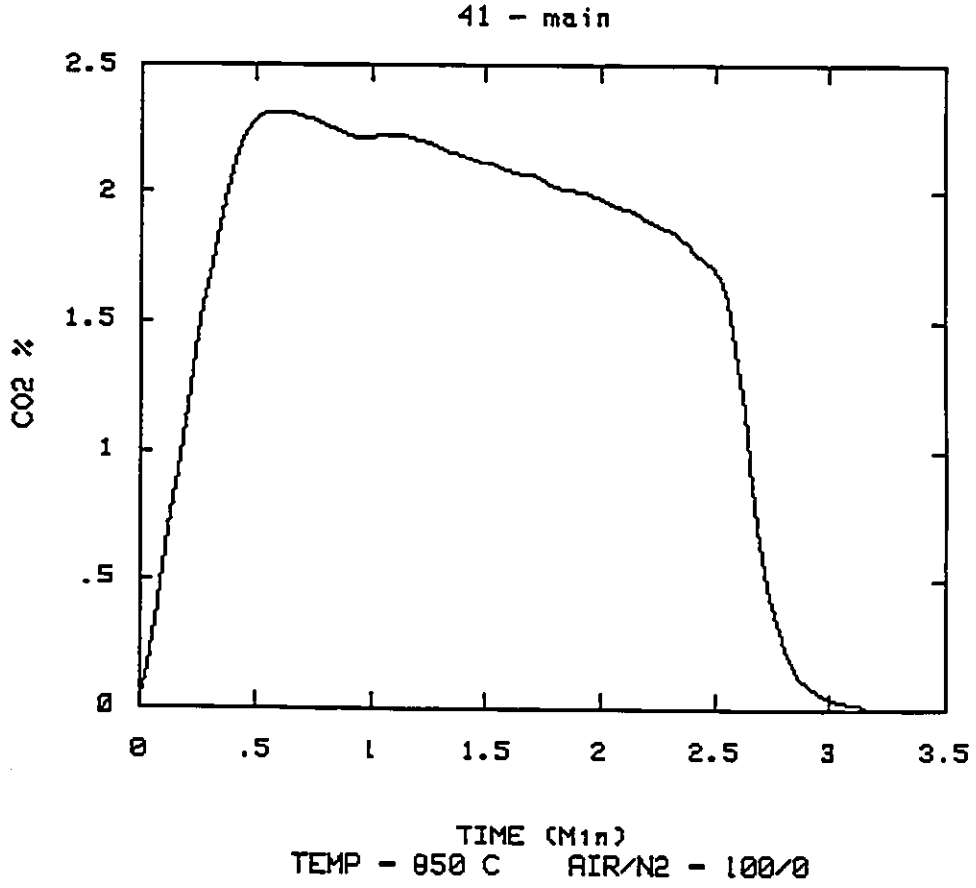

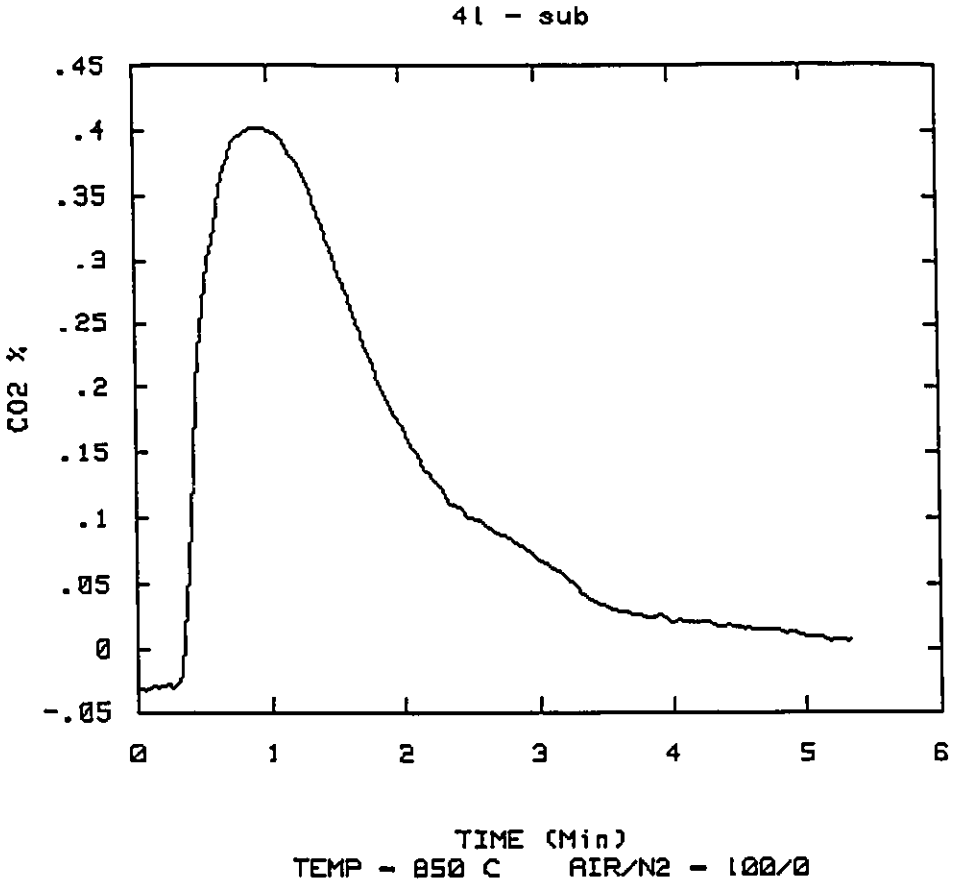
4l - sub
.45
.4
.35
.3
.25
.2
.15
.1
.05
0
-.05
CO2 %
0
1
2
3
4
5
6
TIME (Min)
TEMP - 850 C
AIR/N2 - 100/0

SER2 - 42 :G
BED TEMPERATURE = 850 C
OXYGEN CONCENTRATION = 21 %
MOTHER CHAR BURNING RATE Rm = 8.83 E-6 kg/s
ATTRITED FINES BURNING RATE Ra = 56.62 E-8 kg/s
RETRIEVED ATTRITED CARRBON Wa = 38.64 E-6 kg
MCRT OF BURNING FINES IN SUB-TEST Tria = 53.6 s
MCRT OF ATTRITED PARTICLES (MAIN TEST) Tra = 46.7 s
IDEAL MCRT OF ELUTRATED SIZE PARTICLE Tre* = 35.8 s
IDEAL MCRT OF THE LARGEST ATTRITED PARTICLE Trs* = 91.1 s
ELUTRIATED FRACTION OF ATTRITED PARTICLES Ya = .319
ATTRITION RATE Qa = 82.8 E-8 kg/s
RATIO Qa/(Qa+Rm) = 8.57 %

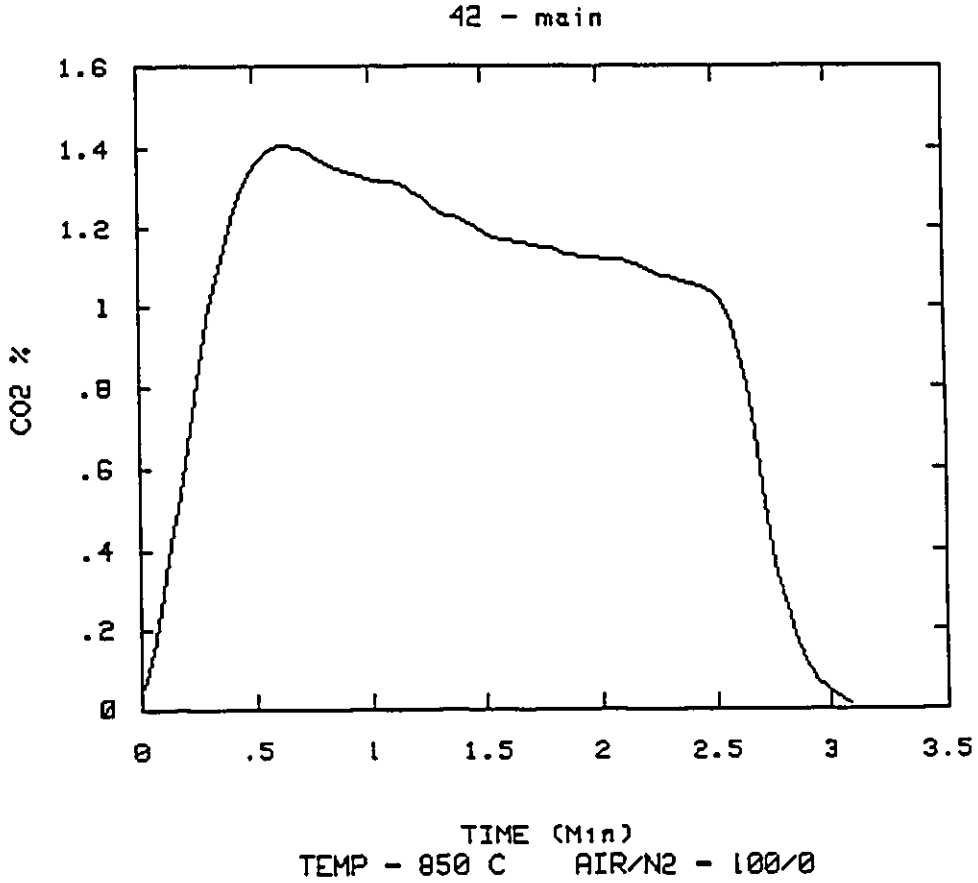

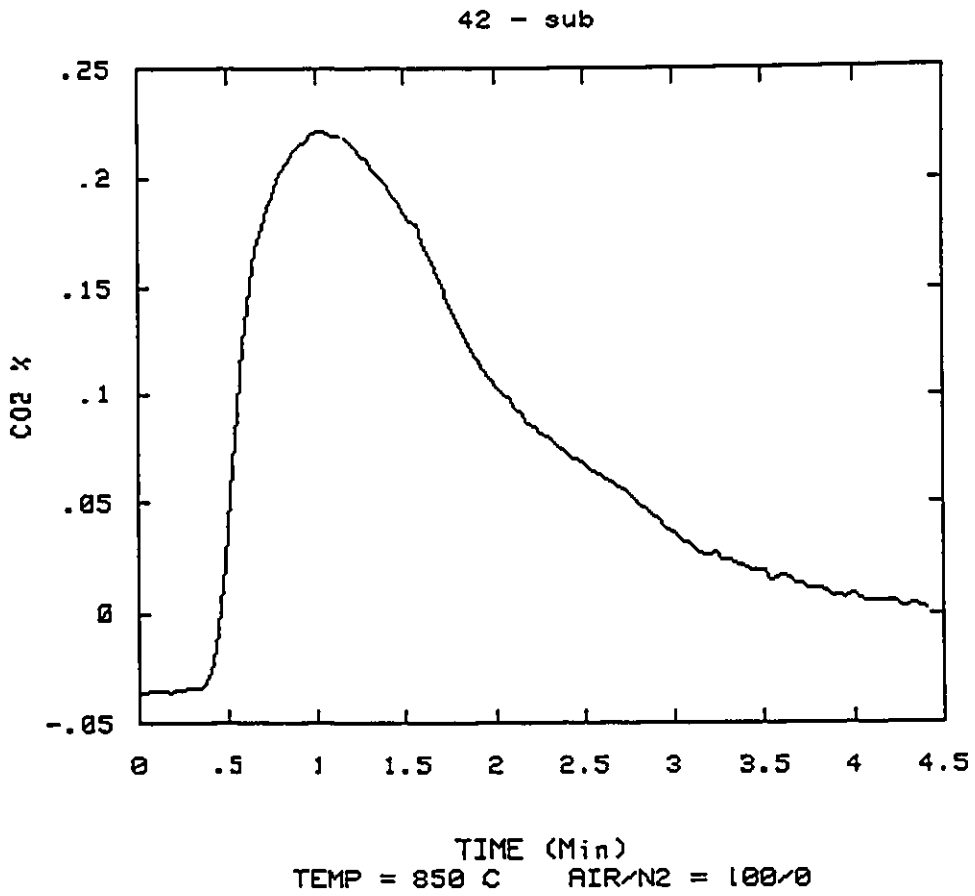
42 - sub
.25
.2
.15
.1
.05
0
-.05
CO2 %
0
.5
1
1.5
2
2.5
3
3.5
4
4.5
TIME (Min)
TEMP = 850 C
AIR/N2 = 100/0

SER2 - 43 :G
BED TEMPERATURE = 850 C
OXYGEN CONCENTRATION = 21 %
MOTHER CHAR BURNING RATE Rm = 5.48 E-6 kg/s
ATTRITED FINES BURNING RATE Ra = 15.24 E-8 kg/s
RETRIEVED ATTRITED CARRBON Wa = 8.12 E-6 kg
MCRT OF BURNING FINES IN SUB-TEST Tria = 41 s
MCRT OF ATTRITED PARTICLES (MAIN TEST) Tra = 22.8 s
IDEAL MCRT OF ELUTRATED SIZE PARTICLE Tre* = 32.2 s
IDEAL MCRT OF THE LARGEST ATTRITED PARTICLE Trs* = 63.5 s
ELUTRIATED FRACTION OF ATTRITED PARTICLES Ya = .574
ATTRITION RATE Qa = 35.6 E-8 kg/s
RATIO Qa/(Qa+Rm) = 6.1 %

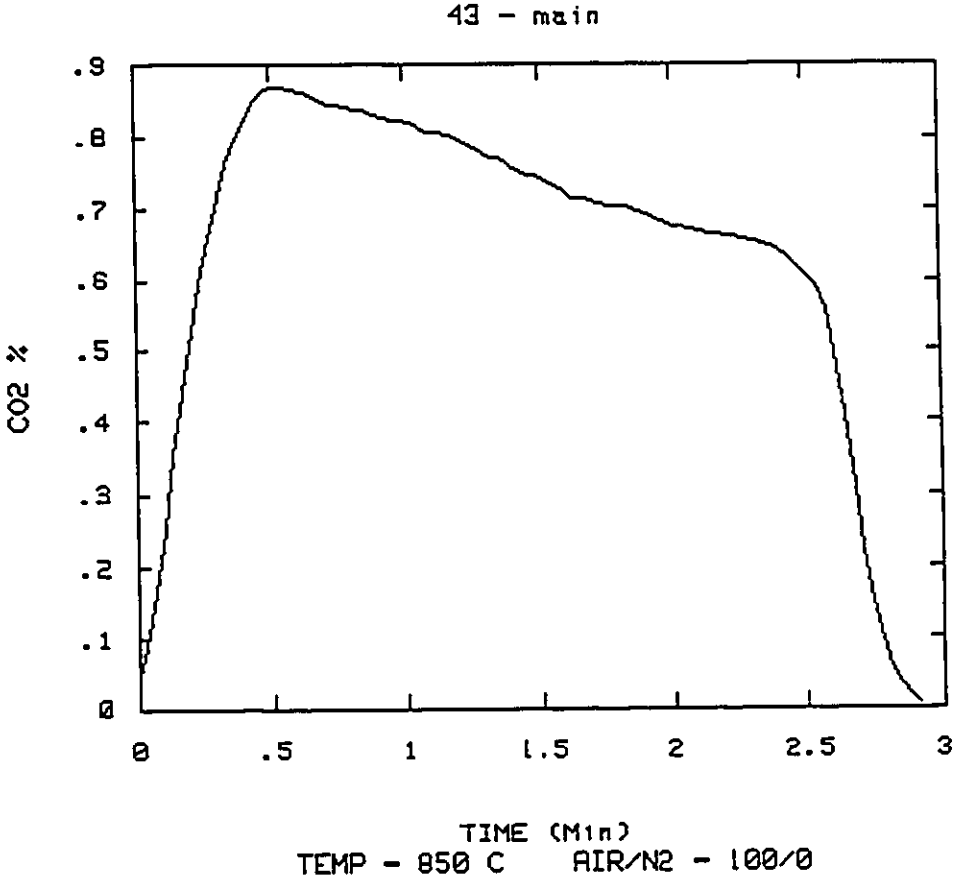

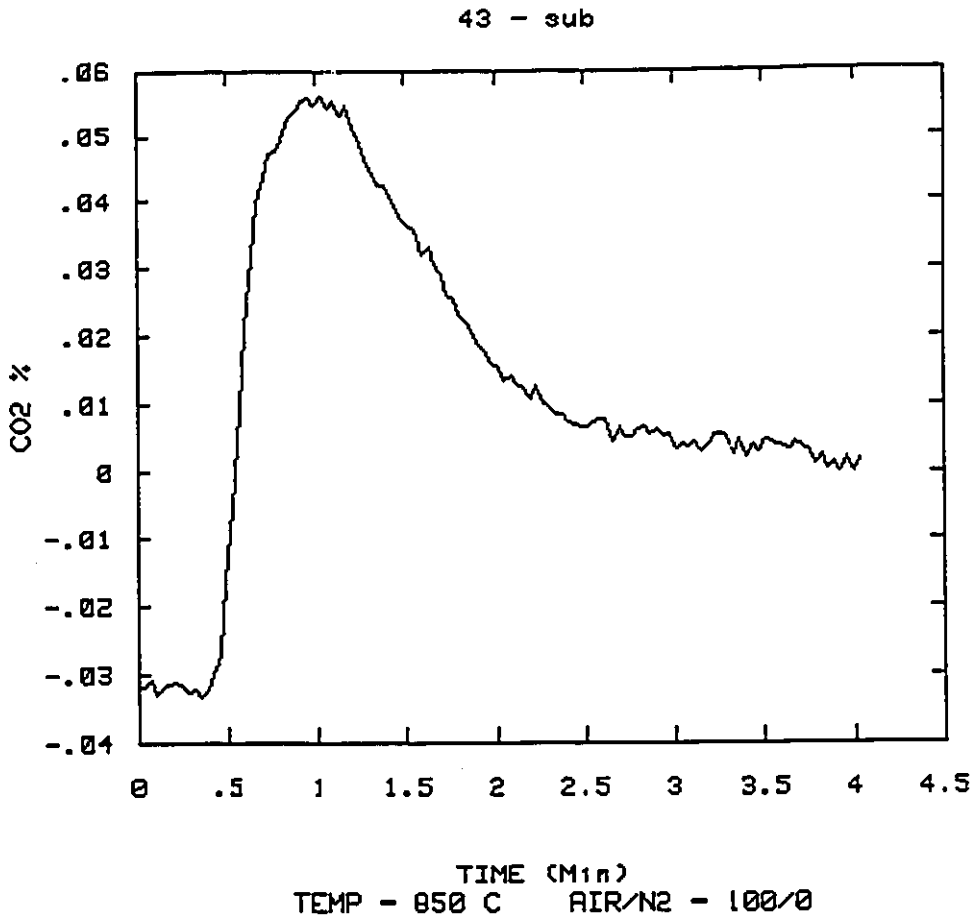
43 - sub
.06
.05
.04
.03
.02
.01
0
-.01
-.02
-.03
-.04
CO2 %
0
.5
1
1.5
2
2.5
3
3.5
4
4.5
TIME (Min)
TEMP - 850 C
AIR/N2 - 100/0

SER2 - 45 :F2
BED TEMPERATURE = 750 C
OXYGEN CONCENTRATION = 21 %
MOTHER CHAR BURNING RATE Rm = 11.26 E-6 kg/s
ATTRITED FINES BURNING RATE Ra = 7.68 E-8 kg/s
RETRIEVED ATTRITED CARRBON Wa = 9.78 E-6 kg
MCRT OF BURNING FINES IN SUB-TEST Tria = 96.3 s
MCRT OF ATTRITED PARTICLES (MAIN TEST) Tra = 24.5 s
IDEAL MCRT OF ELUTRATED SIZE PARTICLE Tre* = 83.2 s
IDEAL MCRT OF THE LARGEST ATTRITED PARTICLE Trs* = 133.2 s
ELUTRIATED FRACTION OF ATTRITED PARTICLES Ya = .807
ATTRITION RATE Qa = 39.8 E-8 kg/s
RATIO Qa/(Qa+Rm) = 3.42 %

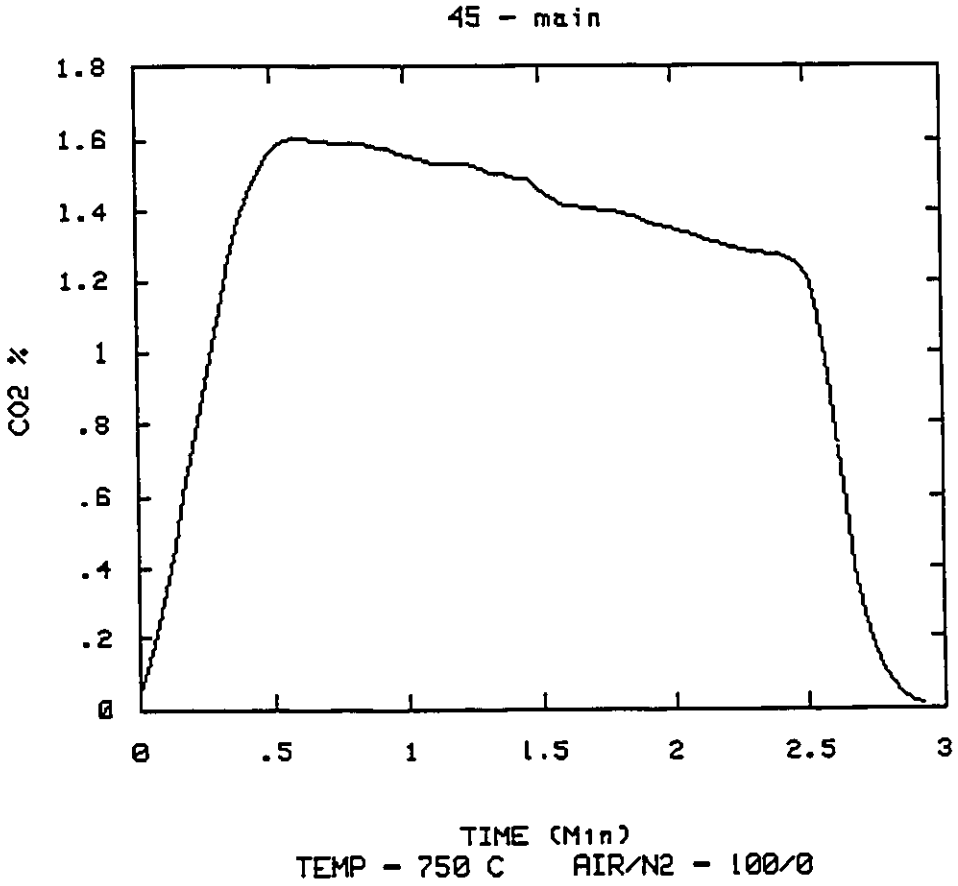

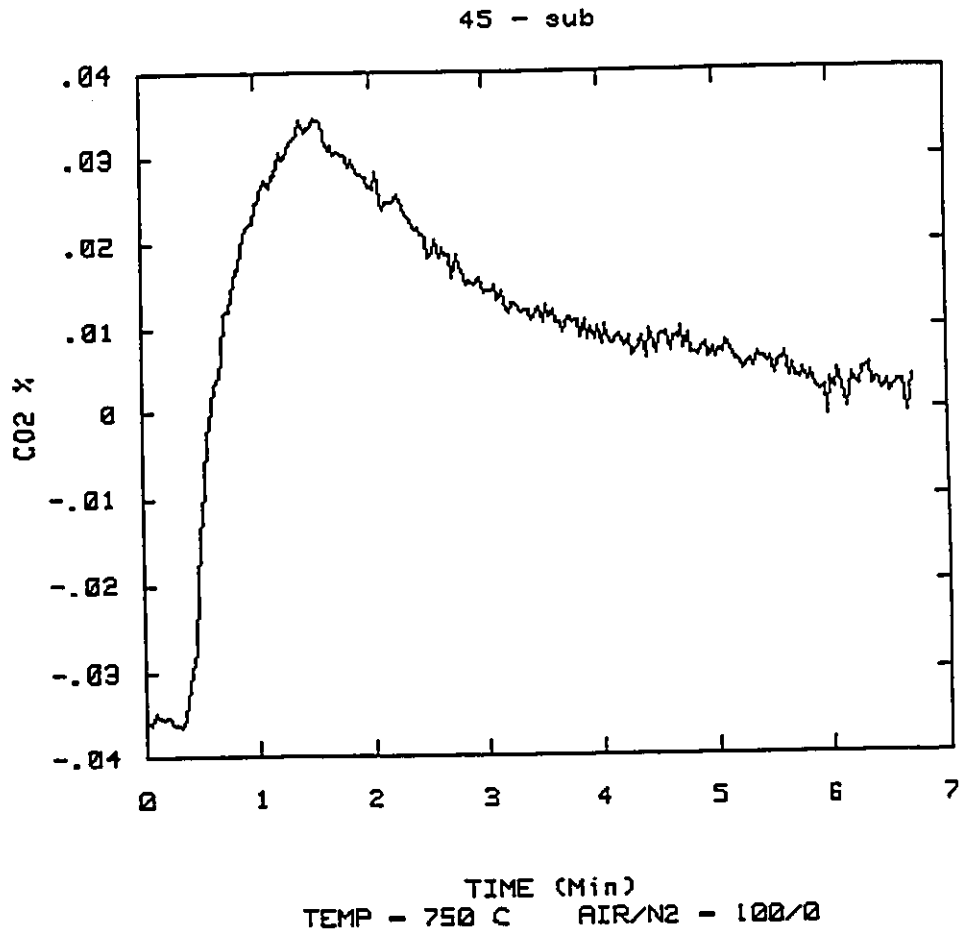
45 - sub
.04
.03
.02
.01
0
-.01
-.02
-.03
-.04
CO2 %
0
1
2
3
4
5
6
7
TIME (Min)
TEMP - 750 C
AIR/N2 - 100/0

SER2 - 47 :F2
BED TEMPERATURE = 750 C
OXYGEN CONCENTRATION = 21 %
MOTHER CHAR BURNING RATE Rm = 2.08 E-6 kg/s
ATTRITED FINES BURNING RATE Ra = 4.6 E-8 kg/s
RETRIEVED ATTRITED CARRBON Wa = 5.16 E-6 kg
MCRT OF BURNING FINES IN SUB-TEST Tria = 85.7 s
MCRT OF ATTRITED PARTICLES (MAIN TEST) Tra = 38.1 s
IDEAL MCRT OF ELUTRATED SIZE PARTICLE Tre* = 69.8 s
IDEAL MCRT OF THE LARGEST ATTRITED PARTICLE Trs* = 127.8 s
ELUTRIATED FRACTION OF ATTRITED PARTICLES Ya = .661
ATTRITION RATE Qa = 13.6 E-8 kg/s
RATIO Qa/(Qa+Rm) = 6.15 %

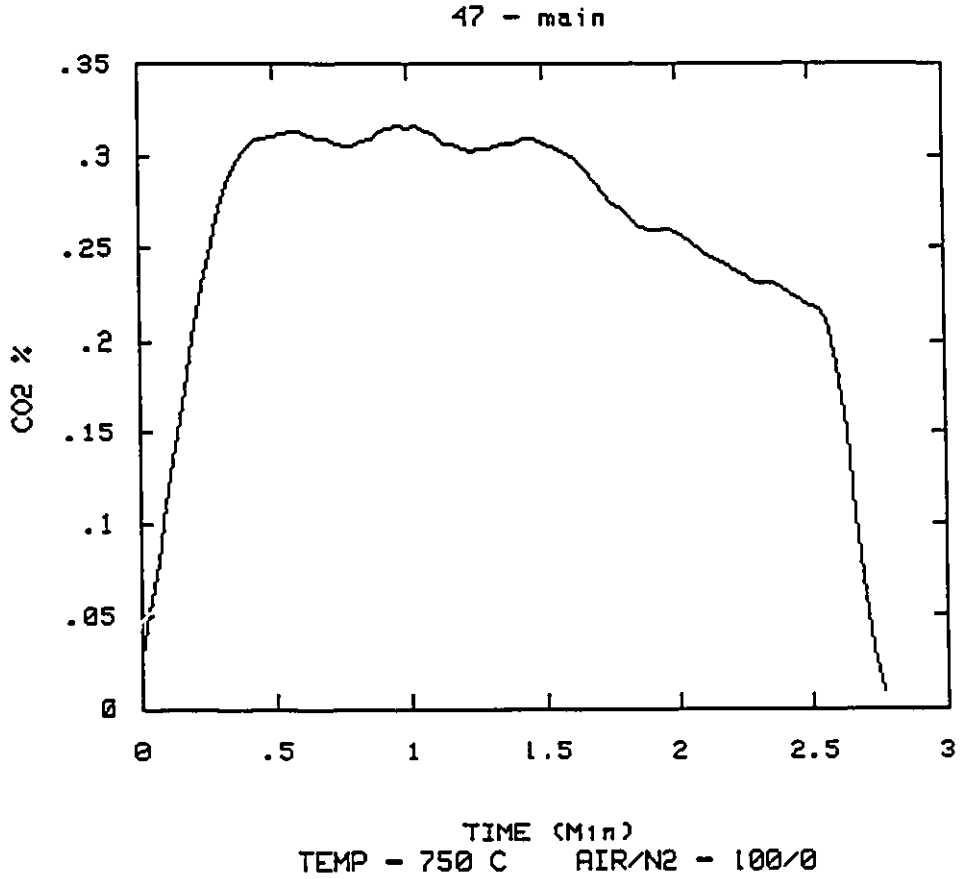

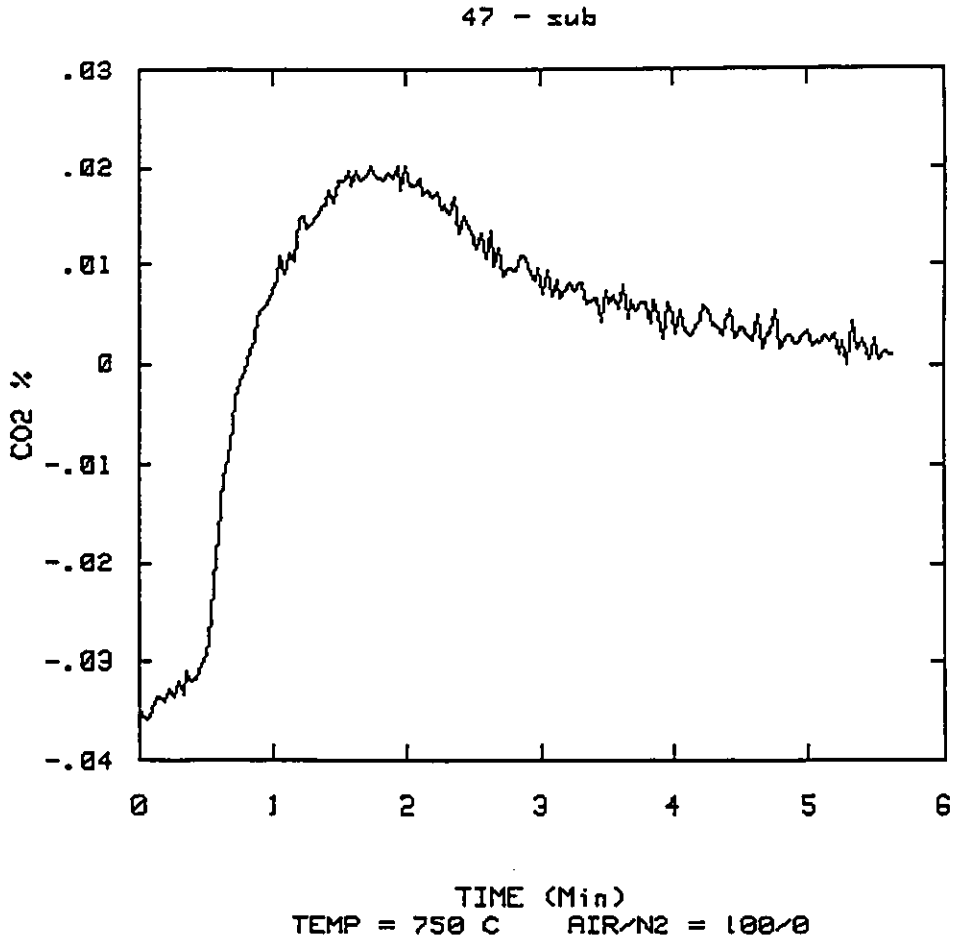
47 - sub
.03
.02
.01
0
-.01
-.02
-.03
-.04
CO2 %
0
1
2
3
4
5
6
TIME (Min)
TEMP = 750 C
AIR/N2 = 100/0

SER2 - 49 :F2
BED TEMPERATURE = 800 C
OXYGEN CONCENTRATION = 21 %
MOTHER CHAR BURNING RATE Rm = 11.54 E-6 kg/s
ATTRITED FINES BURNING RATE Ra = 17.86 E-8 kg/s
RETRIEVED ATTRITED CARRBON Wa = 12.48 E-6 kg
MCRT OF BURNING FINES IN SUB-TEST Tria = 54.2 s
MCRT OF ATTRITED PARTICLES (MAIN TEST) Tra = 38.4 s
IDEAL MCRT OF ELUTRATED SIZE PARTICLE Tre* = 39.9 s
IDEAL MCRT OF THE LARGEST ATTRITED PARTICLE Trs* = 87.9 s
ELUTRIATED FRACTION OF ATTRITED PARTICLES Ya = .453
ATTRITION RATE Qa = 32.6 E-8 kg/s
RATIO Qa/(Qa+Rm) = 2.74 %

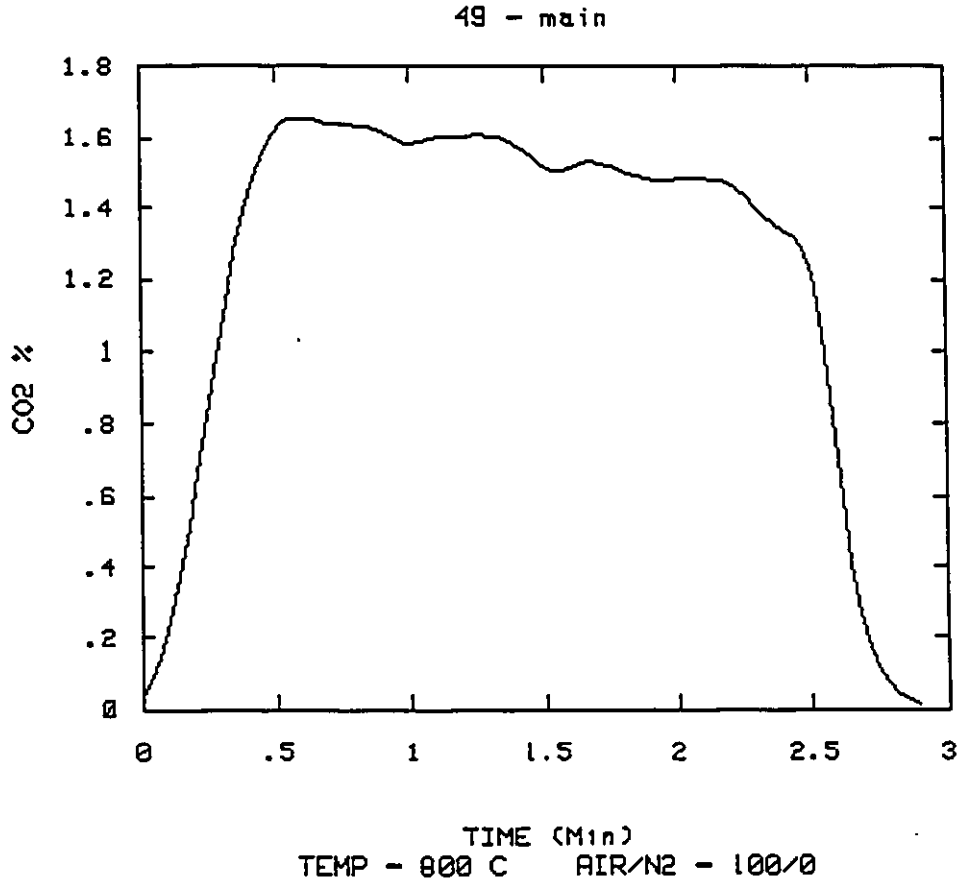

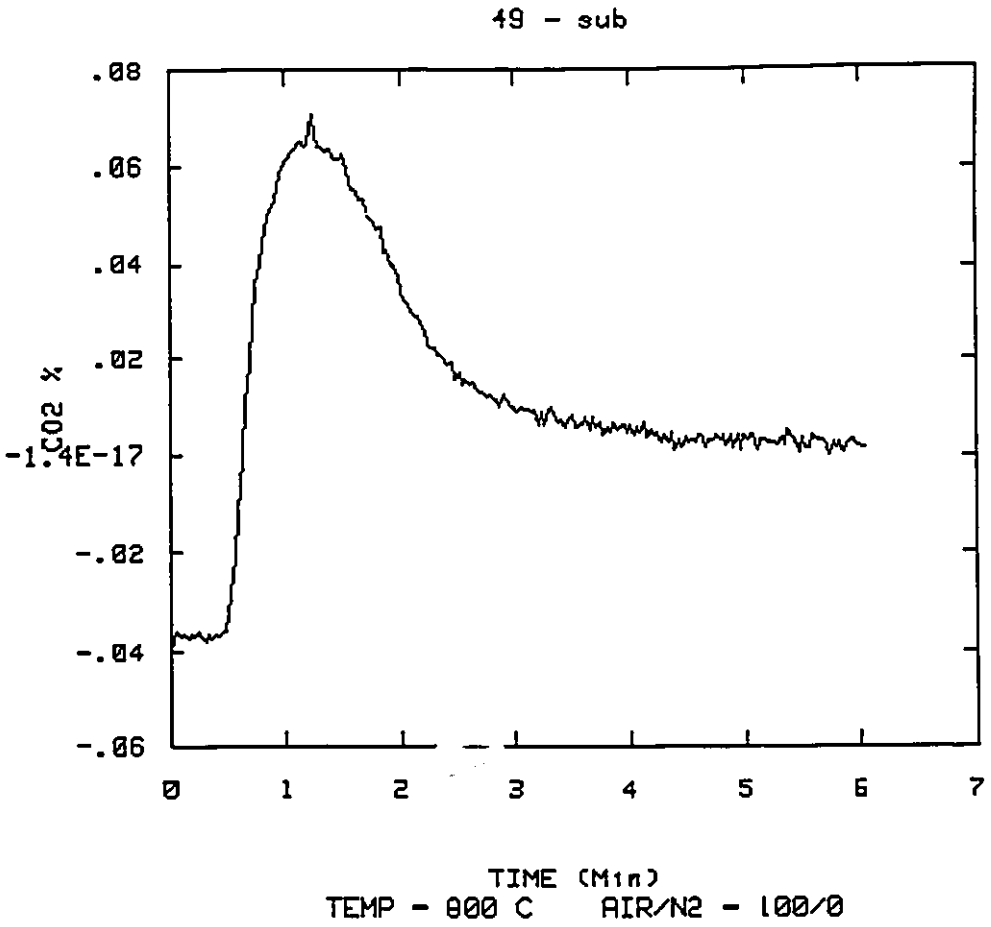
49 - sub
.08
.06
.04
.02
-1.4E-17
-.02
-.04
-.06
CO2 %
0
1
2
3
4
5
6
7
TIME (Min)
TEMP - 800 C
AIR/N2 - 100/0

SER2 - 50 :F2
BED TEMPERATURE = 800 C
OXYGEN CONCENTRATION = 21 %
MOTHER CHAR BURNING RATE Rm = 5.29 E-6 kg/s
ATTRITED FINES BURNING RATE Ra = 4.28 E-8 kg/s
RETRIEVED ATTRITED CARRBON Wa = 3.37 E-6 kg
MCRT OF BURNING FINES IN SUB-TEST Tria = 61.5 s
MCRT OF ATTRITED PARTICLES (MAIN TEST) Tra = 54.1 s
IDEAL MCRT OF ELUTRATED SIZE PARTICLE Tre* = 40.7 s
IDEAL MCRT OF THE LARGEST ATTRITED PARTICLE Trs* = 104.8 s
ELUTRIATED FRACTION OF ATTRITED PARTICLES Ya = .311
ATTRITION RATE Qa = 6.2 E-8 kg/s
RATIO Qa/(Qa+Rm) = 1.16 %

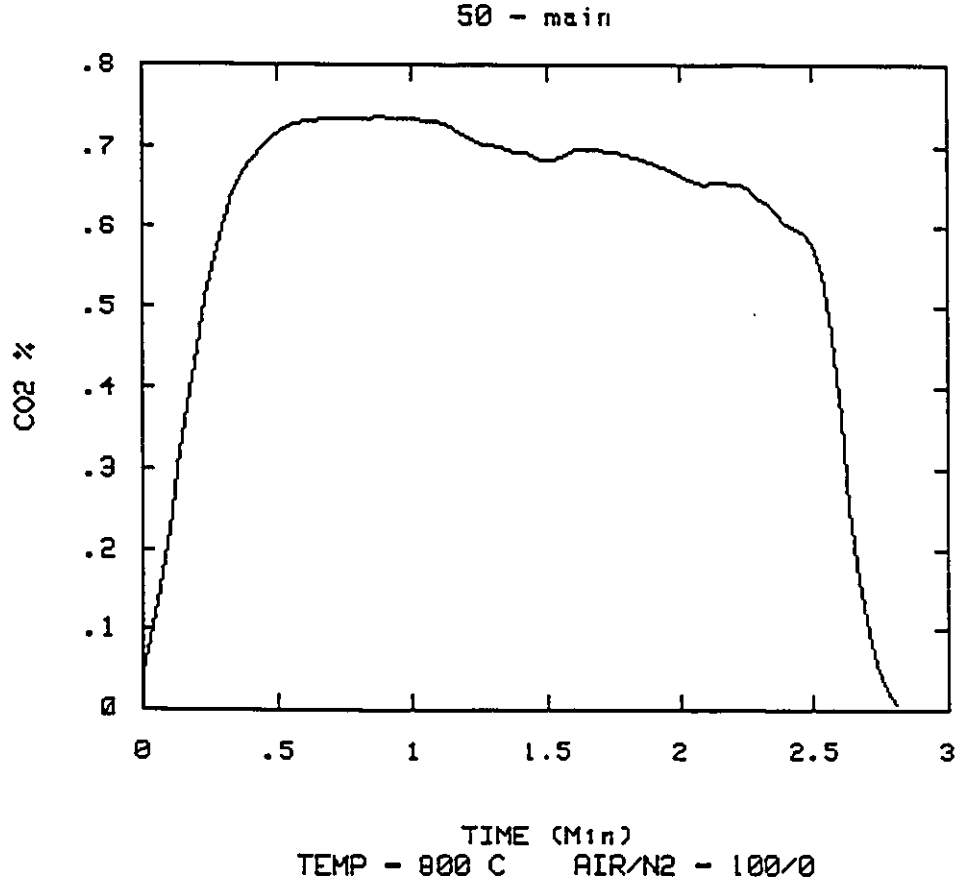

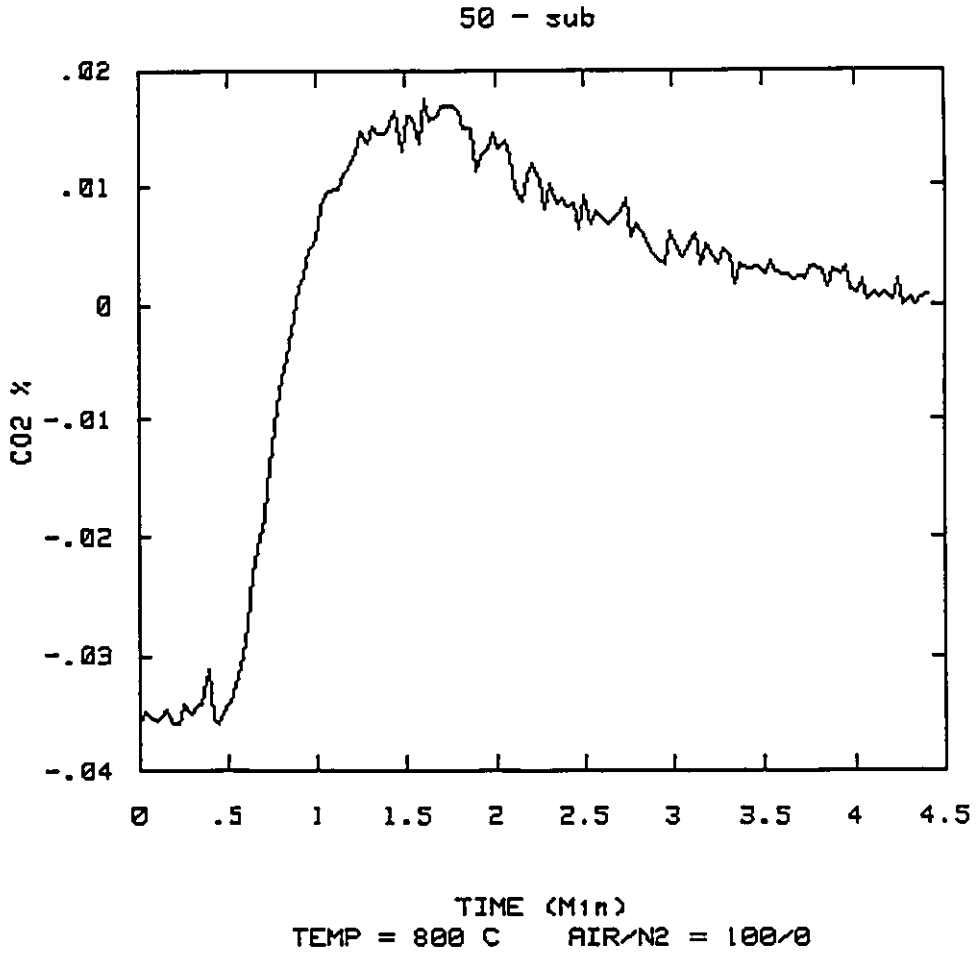
50 - sub
.02
.01
0
-.01
-.02
-.03
-.04
CO2 %
0
.5
1
1.5
2
2.5
3
3.5
4
4.5
TIME (Min)
TEMP = 800 C
AIR/N2 = 100/0

SER2 - 51 :F2
BED TEMPERATURE = 900 C
OXYGEN CONCENTRATION = 21 %
MOTHER CHAR BURNING RATE Rm = 10.6 E-6 kg/s
ATTRITED FINES BURNING RATE Ra = 3.98 E-8 kg/s
RETRIEVED ATTRITED CARRBON Wa = 2.41 E-6 kg
MCRT OF BURNING FINES IN SUB-TEST Tria = 48.1 s
MCRT OF ATTRITED PARTICLES (MAIN TEST) Tra = 47.9 s
IDEAL MCRT OF ELUTRATED SIZE PARTICLE Tre* = 28.3 s
IDEAL MCRT OF THE LARGEST ATTRITED PARTICLE Trs* = 84.7 s
ELUTRIATED FRACTION OF ATTRITED PARTICLES Ya = .209
ATTRITION RATE Qa = 5 E-8 kg/s
RATIO Qa/(Qa+Rm) = .47 %

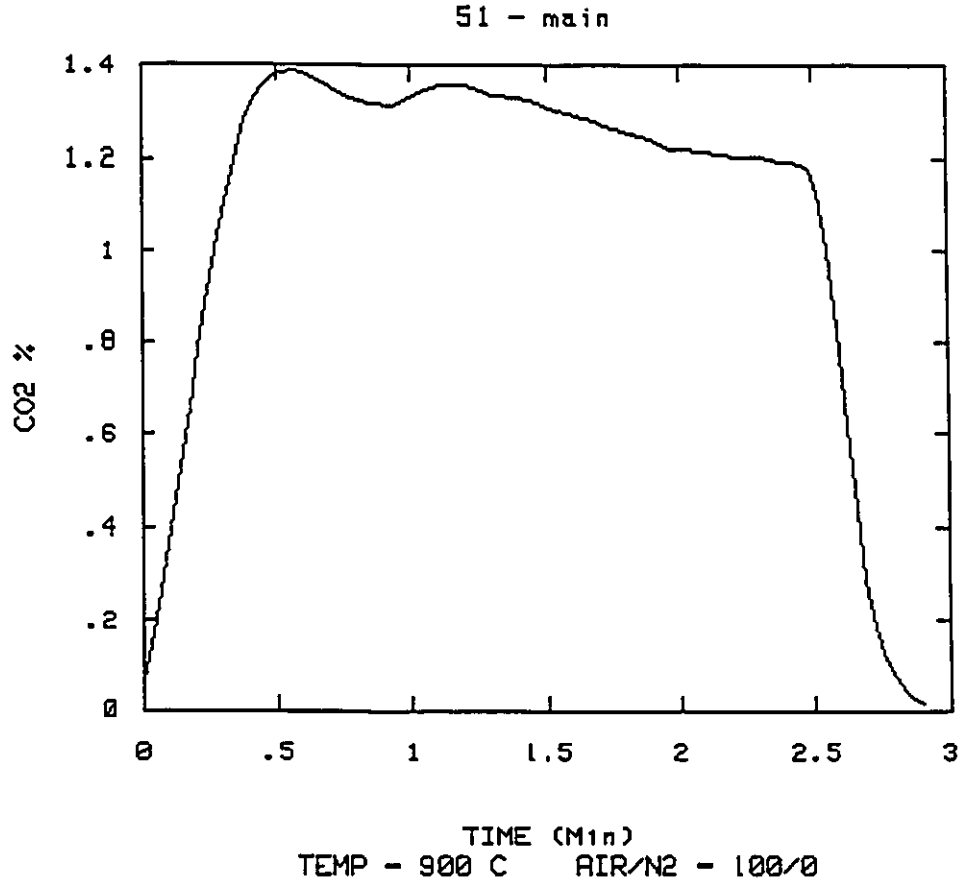

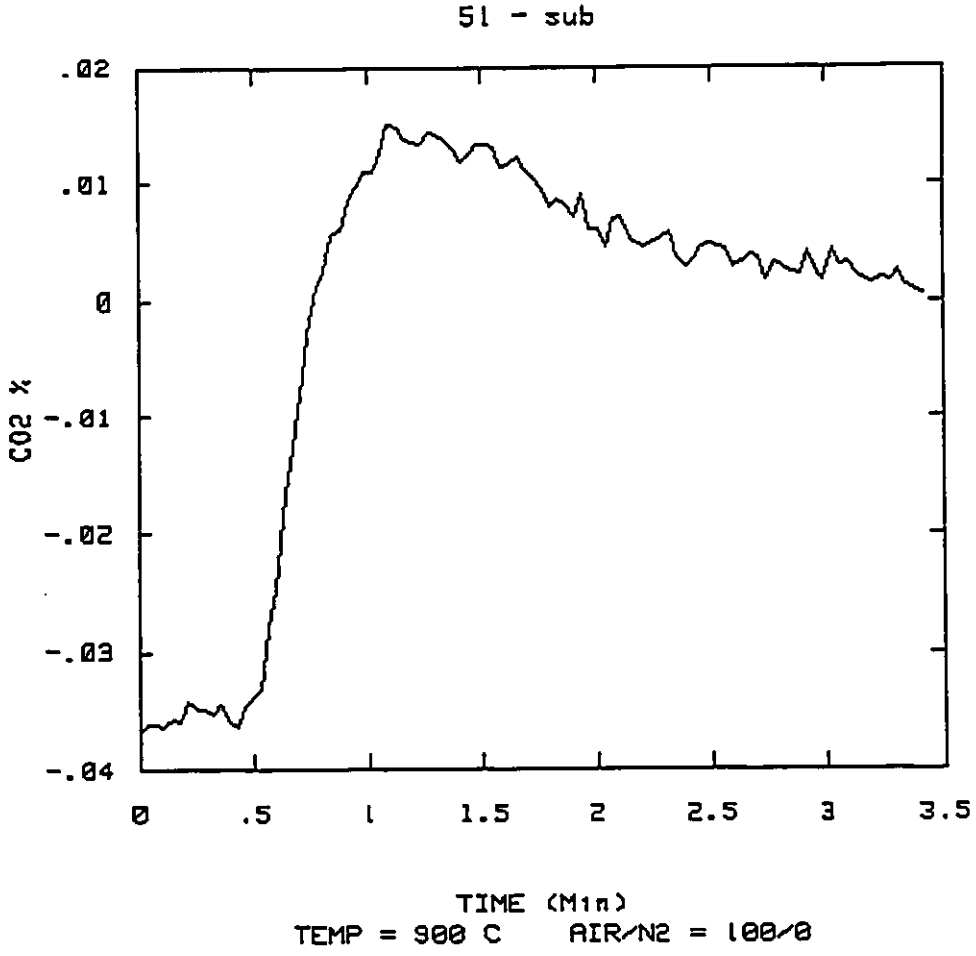
51 - sub
.02
.01
0
-.01
-.02
-.03
-.04
CO2 %
0
.5
1
1.5
2
2.5
3
3.5
TIME (Min)
TEMP = 900 C
AIR/N2 = 100/0

SER2 - 56 :F2
BED TEMPERATURE = 850 C
OXYGEN CONCENTRATION = 15.8 %
MOTHER CHAR BURNING RATE Rm = 9.51 E-6 kg/s
ATTRITED FINES BURNING RATE Ra = 11.54 E-8 kg/s
RETRIEVED ATTRITED CARRBON Wa = 7.06 E-6 kg
MCRT OF BURNING FINES IN SUB-TEST Tria = 47 s
MCRT OF ATTRITED PARTICLES (MAIN TEST) Tra = 23.9 s
IDEAL MCRT OF ELUTRATED SIZE PARTICLE Tre* = 37.5 s
IDEAL MCRT OF THE LARGEST ATTRITED PARTICLE Trs* = 71.6 s
ELUTRIATED FRACTION OF ATTRITED PARTICLES Ya = .611
ATTRITION RATE Qa = 29.6 E-8 kg/s
RATIO Qa/(Qa+Rm) = 3.02 %

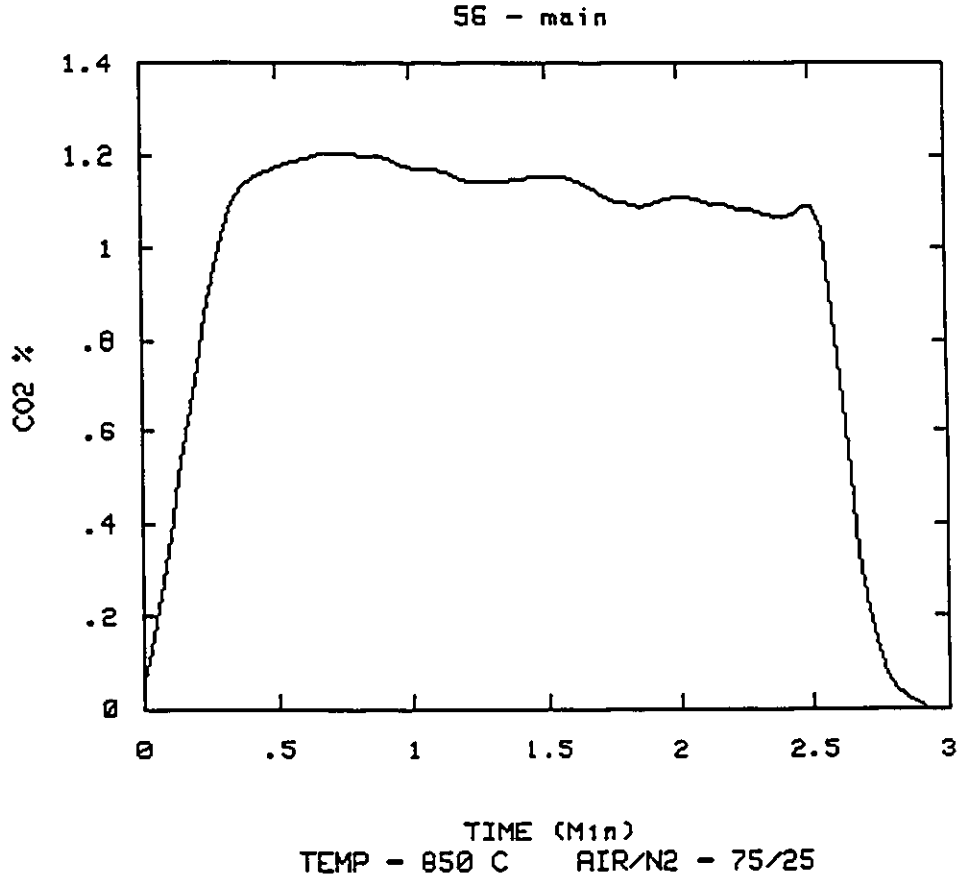

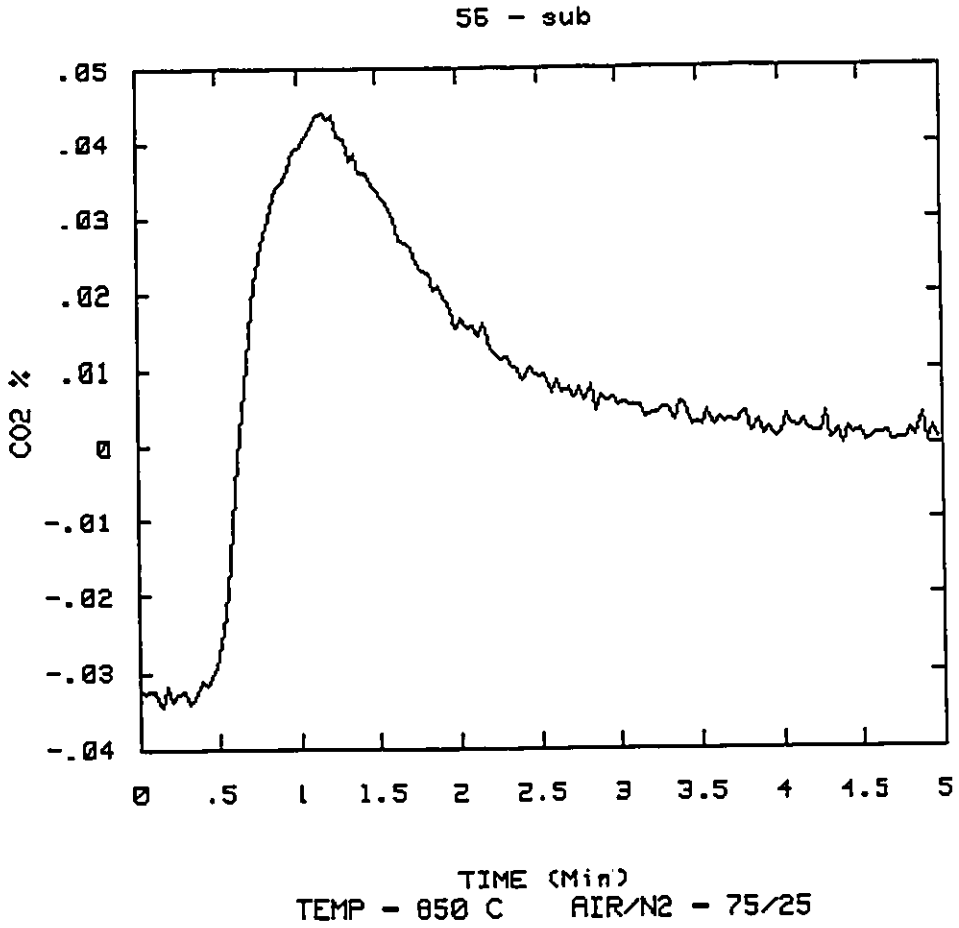
56 - sub
.05
.04
.03
.02
.01
0
-.01
-.02
-.03
-.04
CO2 %
0
.5
1
1.5
2
2.5
3
3.5
4
4.5
5
TIME (Min)
TEMP - 850 C
AIR/N2 - 75/25

SER2 - 57 :F2
BED TEMPERATURE = 850 C
OXYGEN CONCENTRATION = 15.8 %
MOTHER CHAR BURNING RATE Rm = 5.82 E-6 kg/s
ATTRITED FINES BURNING RATE Ra = 8.52 E-8 kg/s
RETRIEVED ATTRITED CARRBON Wa = 6.46 E-6 kg
MCRT OF BURNING FINES IN SUB-TEST Tria = 58.4 s
MCRT OF ATTRITED PARTICLES (MAIN TEST) Tra = 37.1 s
IDEAL MCRT OF ELUTRATED SIZE PARTICLE Tre* = 44.4 s
IDEAL MCRT OF THE LARGEST ATTRITED PARTICLE Trs* = 92.6 s
ELUTRIATED FRACTION OF ATTRITED PARTICLES Ya = .51
ATTRITION RATE Qa = 17.4 E-8 kg/s
RATIO Qa/(Qa+Rm) = 2.9 %

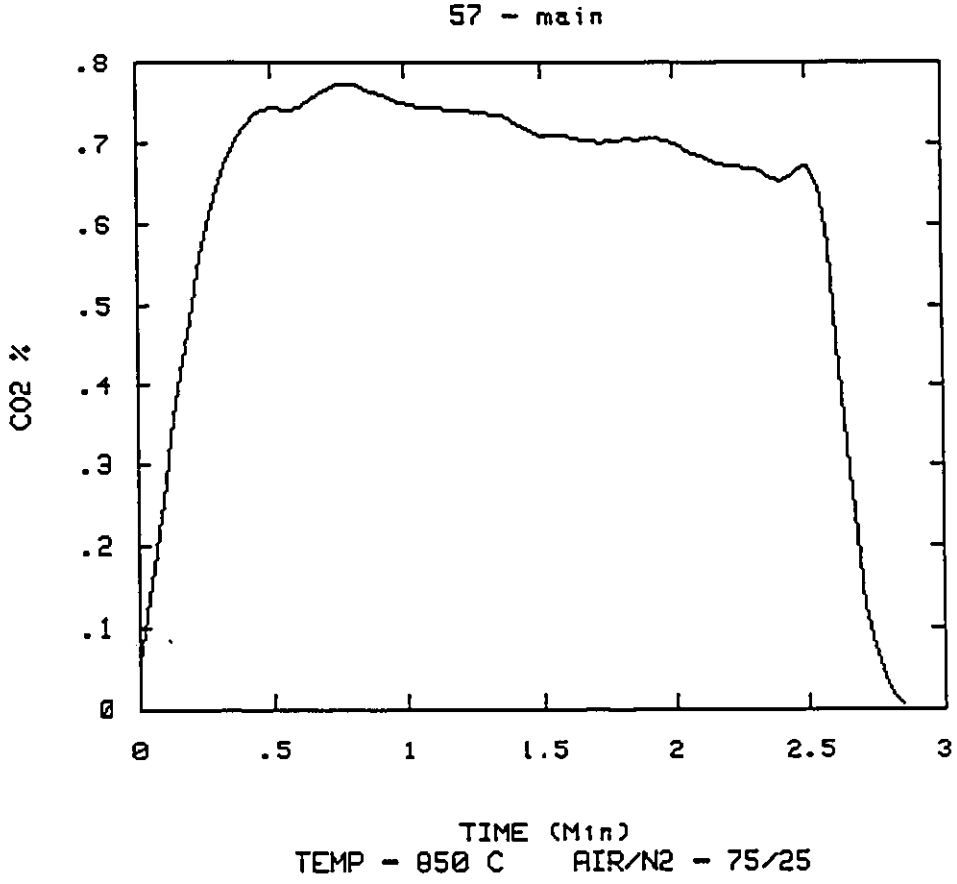

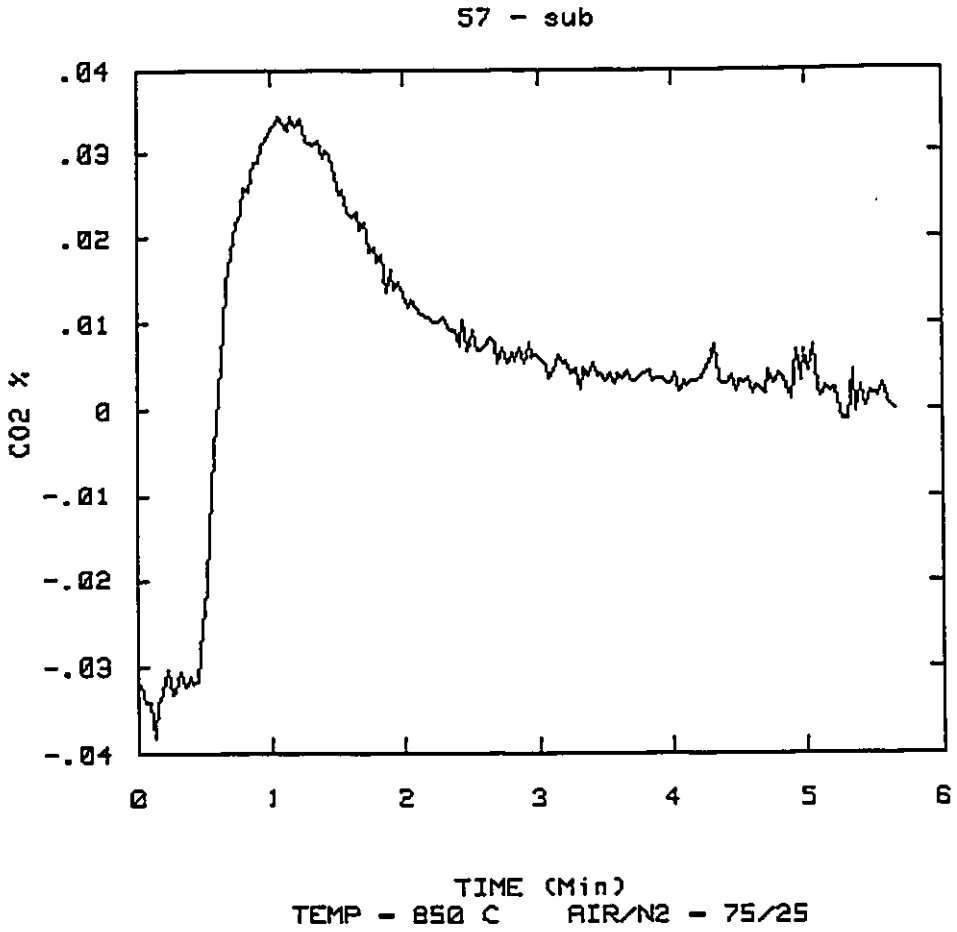
57 - sub
.04
.03
.02
.01
0
-.01
-.02
-.03
-.04
CO2 %
0
1
2
3
4
5
6
TIME (Min)
TEMP - 850 C
AIR/N2 - 75/25

SER2 - 59 :F2
BED TEMPERATURE = 900 C
OXYGEN CONCENTRATION = 21 %
MOTHER CHAR BURNING RATE Rm = 12.5 E-6 kg/s
ATTRITED FINES BURNING RATE Ra = 6.76 E-8 kg/s
RETRIEVED ATTRITED CARRBON Wa = 3.73 E-6 kg
MCRT OF BURNING FINES IN SUB-TEST Tria = 43 s
MCRT OF ATTRITED PARTICLES (MAIN TEST) Tra = 34.1 s
IDEAL MCRT OF ELUTRATED SIZE PARTICLE Tre* = 30.2 s
IDEAL MCRT OF THE LARGEST ATTRITED PARTICLE Trs* = 71.5 s
ELUTRIATED FRACTION OF ATTRITED PARTICLES Ya = .383
ATTRITION RATE Qa = 11 E-8 kg/s
RATIO Qa/(Qa+Rm) = .87 %

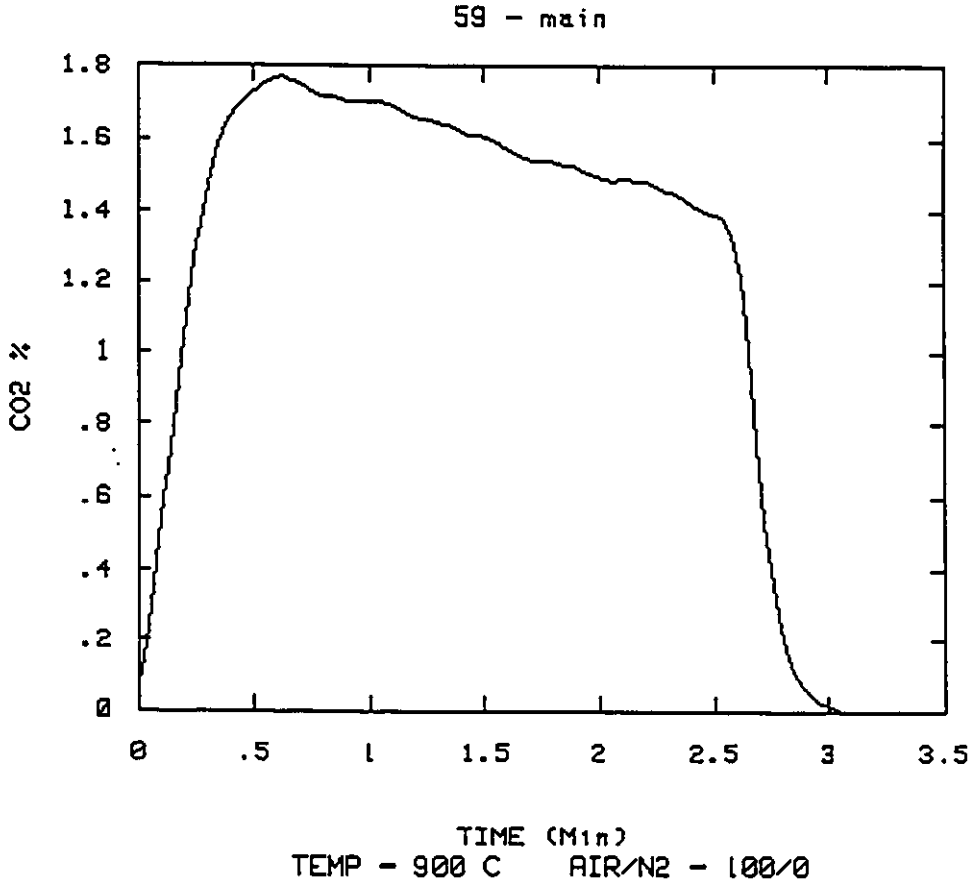

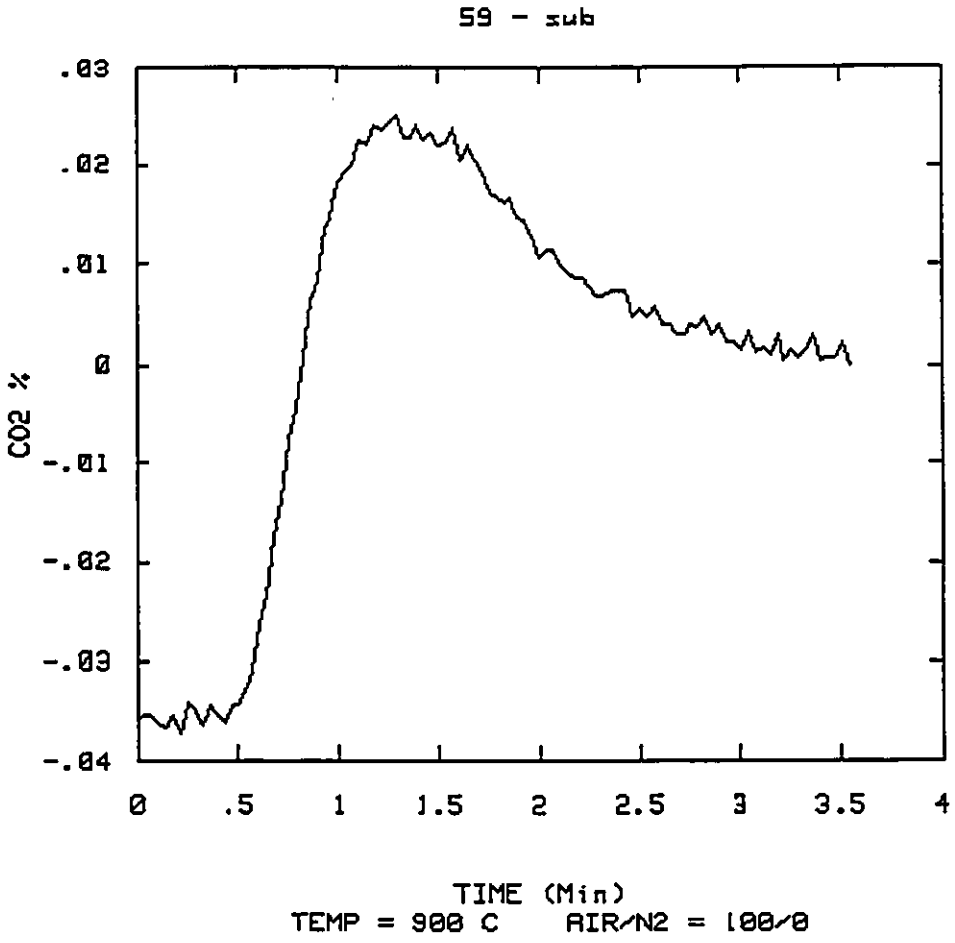
59 - sub
.03
.02
.01
0
-.01
-.02
-.03
-.04
CO2 %
0
.5
1
1.5
2
2.5
3
3.5
4
TIME (Min)
TEMP = 900 C
AIR/N2 = 100/0

SER2 - 60 :F2
BED TEMPERATURE = 900 C
OXYGEN CONCENTRATION = 21 %
MOTHER CHAR BURNING RATE Rm = 5.43 E-6 kg/s
ATTRITED FINES BURNING RATE Ra = 14.24 E-8 kg/s
RETRIEVED ATTRITED CARRBON Wa = 11.36 E-6 kg
MCRT OF BURNING FINES IN SUB-TEST Tria = 64.4 s
MCRT OF ATTRITED PARTICLES (MAIN TEST) Tra = 71.3 s
IDEAL MCRT OF ELUTRATED SIZE PARTICLE Tre* = 30.7 s
IDEAL MCRT OF THE LARGEST ATTRITED PARTICLE Trs* = 117.3 s
ELUTRIATED FRACTION OF ATTRITED PARTICLES Ya = .104
ATTRITION RATE Qa = 16 E-8 kg/s
RATIO Qa/(Qa+Rm) = 2.85 %

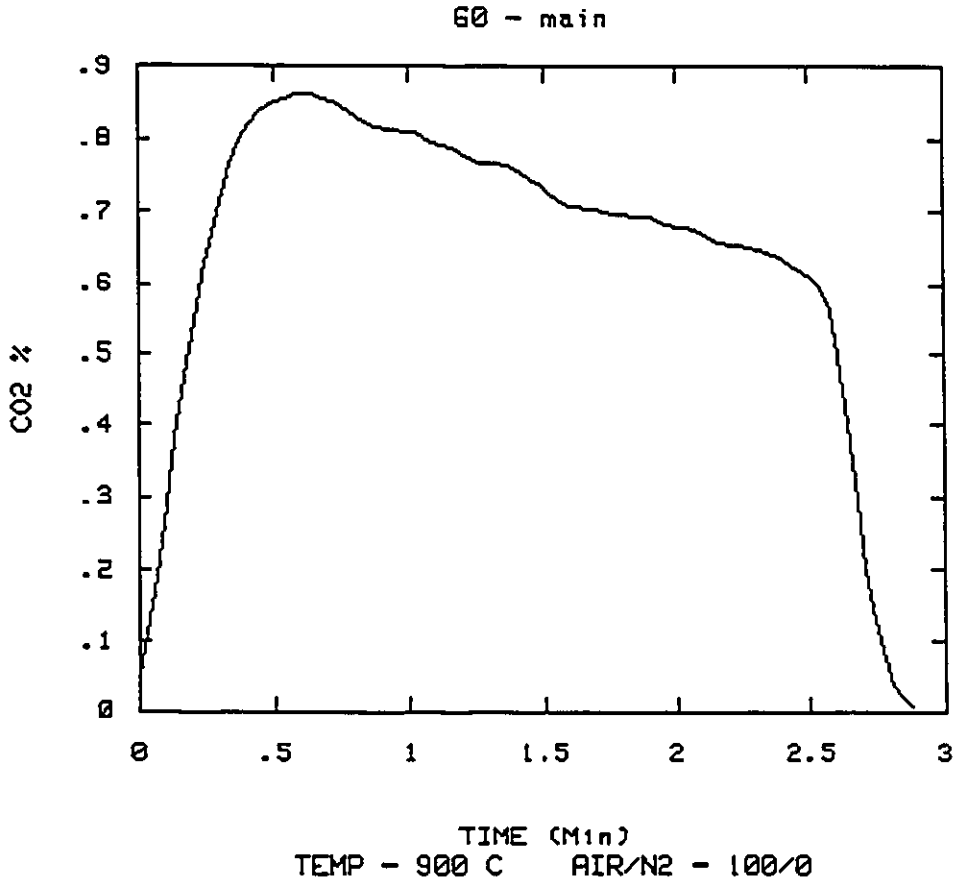

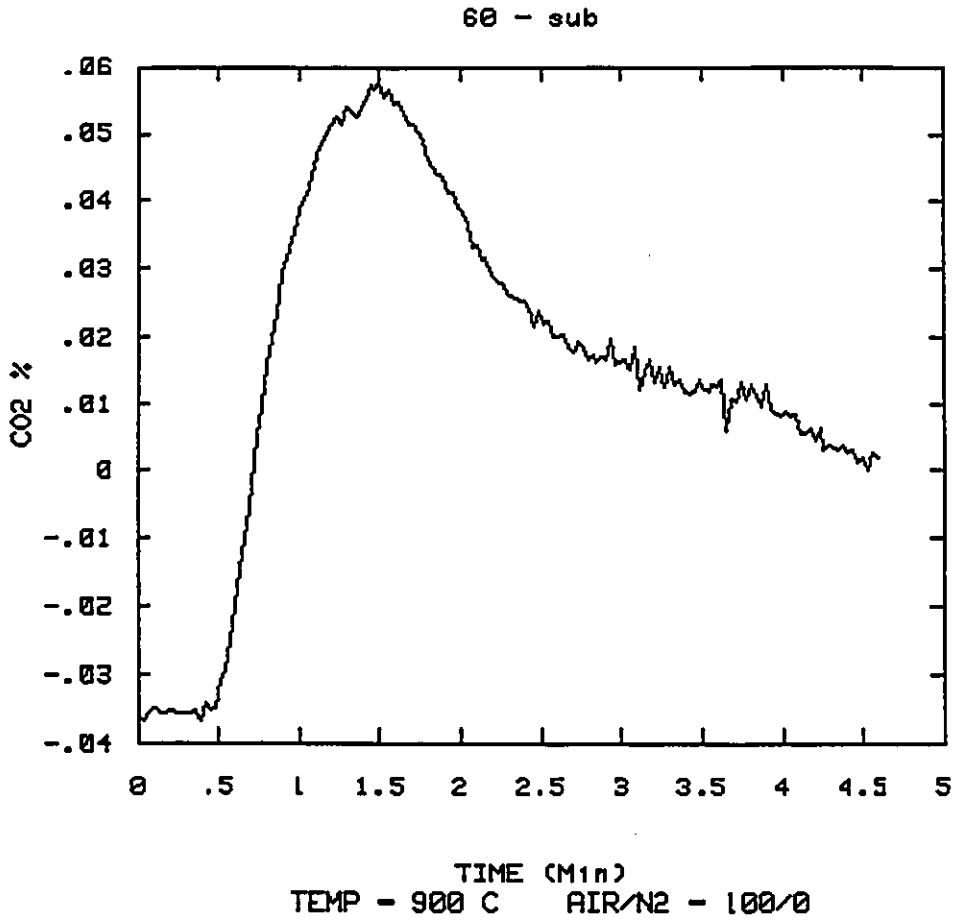
60 - sub
.06
.05
.04
.03
.02
.01
0
-.01
-.02
-.03
-.04
CO2 %
0
.5
1
1.5
2
2.5
3
3.5
4
4.5
5
TIME (Min)
TEMP - 900 C
AIR/N2 - 100/0

SER2 - 62 :F2
BED TEMPERATURE = 850 C
OXYGEN CONCENTRATION = 10.5 %
MOTHER CHAR BURNING RATE Rm = 3.91 E-6 kg/s
ATTRITED FINES BURNING RATE Ra = 3.48 E-8 kg/s
RETRIEVED ATTRITED CARRBON Wa = 2.53 E-6 kg
MCRT OF BURNING FINES IN SUB-TEST Tria = 55.3 s
MCRT OF ATTRITED PARTICLES (MAIN TEST) Tra = 16.1 s
IDEAL MCRT OF ELUTRATED SIZE PARTICLE Tre* = 47.3 s
IDEAL MCRT OF THE LARGEST ATTRITED PARTICLE Trs* = 77.8 s
ELUTRIATED FRACTION OF ATTRITED PARTICLES Ya = .779
ATTRITION RATE Qa = 15.6 E-8 kg/s
RATIO Qa/(Qa+Rm) = 3.85 %

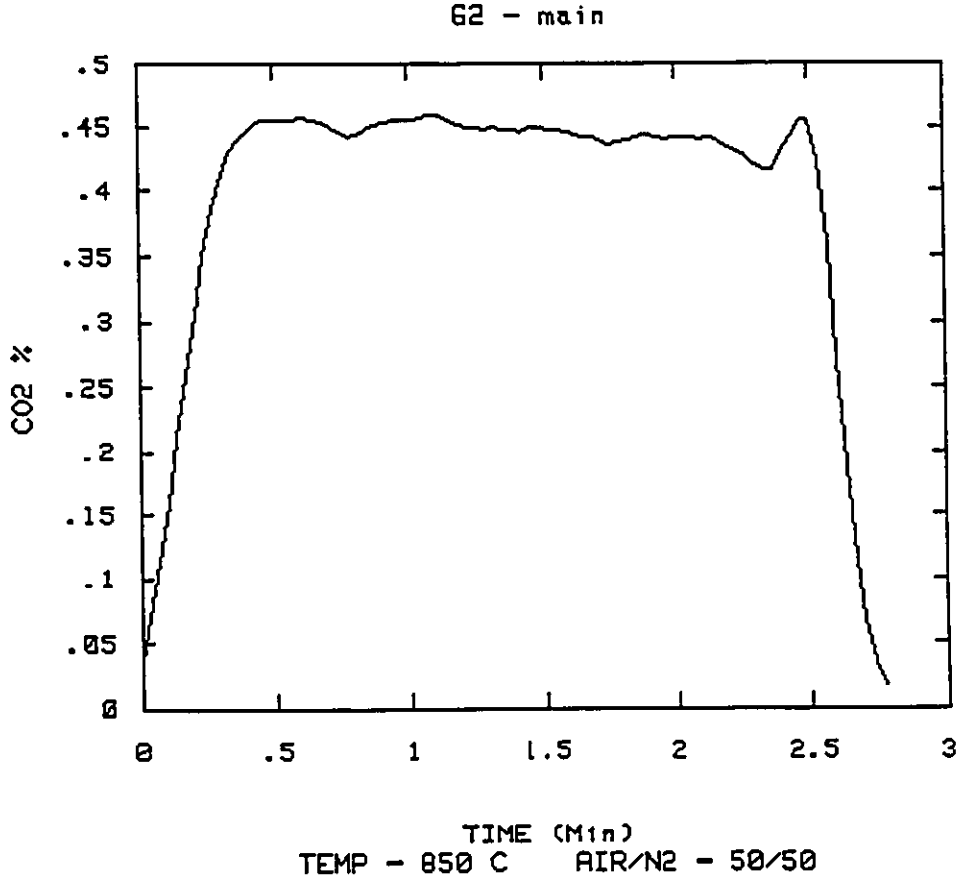

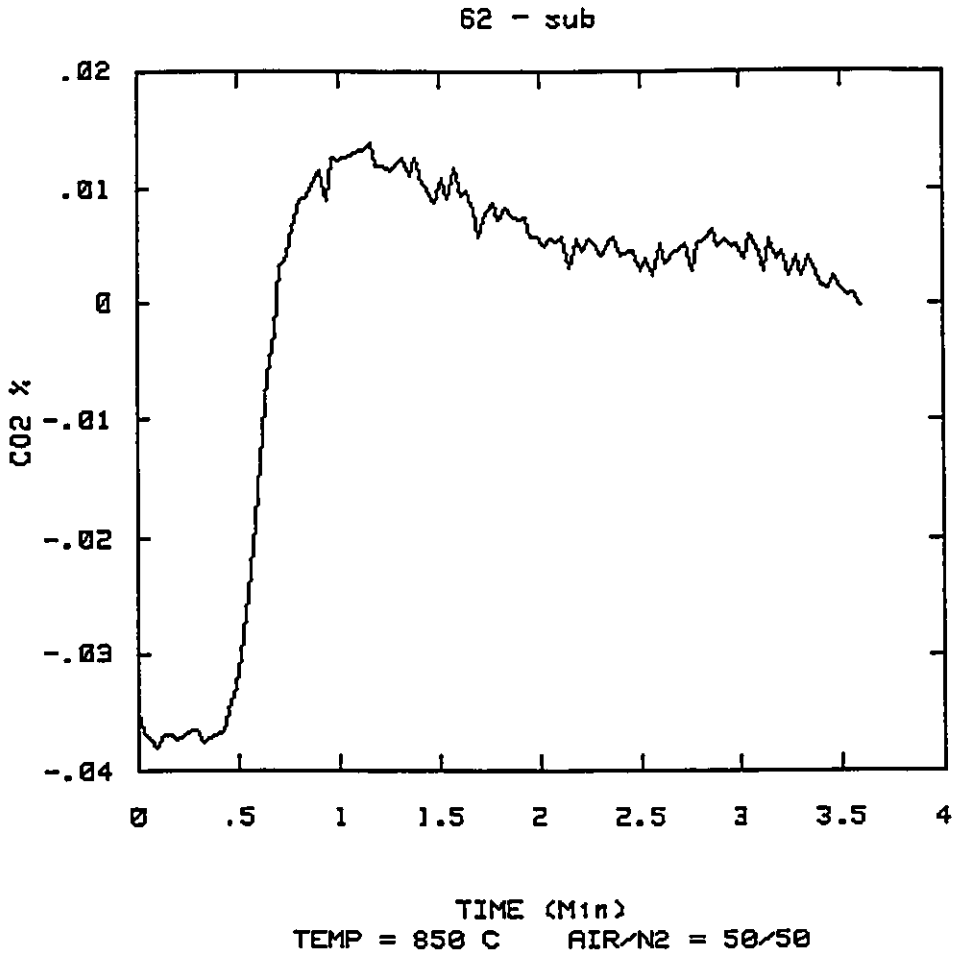
62 - sub
.02
.01
0
-.01
-.02
-.03
-.04
CO2 %
0
.5
1
1.5
2
2.5
3
3.5
4
TIME (Min)
TEMP = 850 C
AIR/N2 = 50/50

SER2 - 64 :F2
BED TEMPERATURE = 850 C
OXYGEN CONCENTRATION = 5.3 %
MOTHER CHAR BURNING RATE Rm = 3.53 E-6 kg/s
ATTRITED FINES BURNING RATE Ra = 9.94 E-8 kg/s
RETRIEVED ATTRITED CARRBON Wa = 7.08 E-6 kg
MCRT OF BURNING FINES IN SUB-TEST Tria = 53.8 s
MCRT OF ATTRITED PARTICLES (MAIN TEST) Tra = 5.6 s
IDEAL MCRT OF ELUTRATED SIZE PARTICLE Tre* = 48.8 s
IDEAL MCRT OF THE LARGEST ATTRITED PARTICLE Trs* = 68 s
ELUTRIATED FRACTION OF ATTRITED PARTICLES Ya = .921
ATTRITION RATE Qa = 125.6 E-8 kg/s
RATIO Qa/(Qa+Rm) = 26.26 %

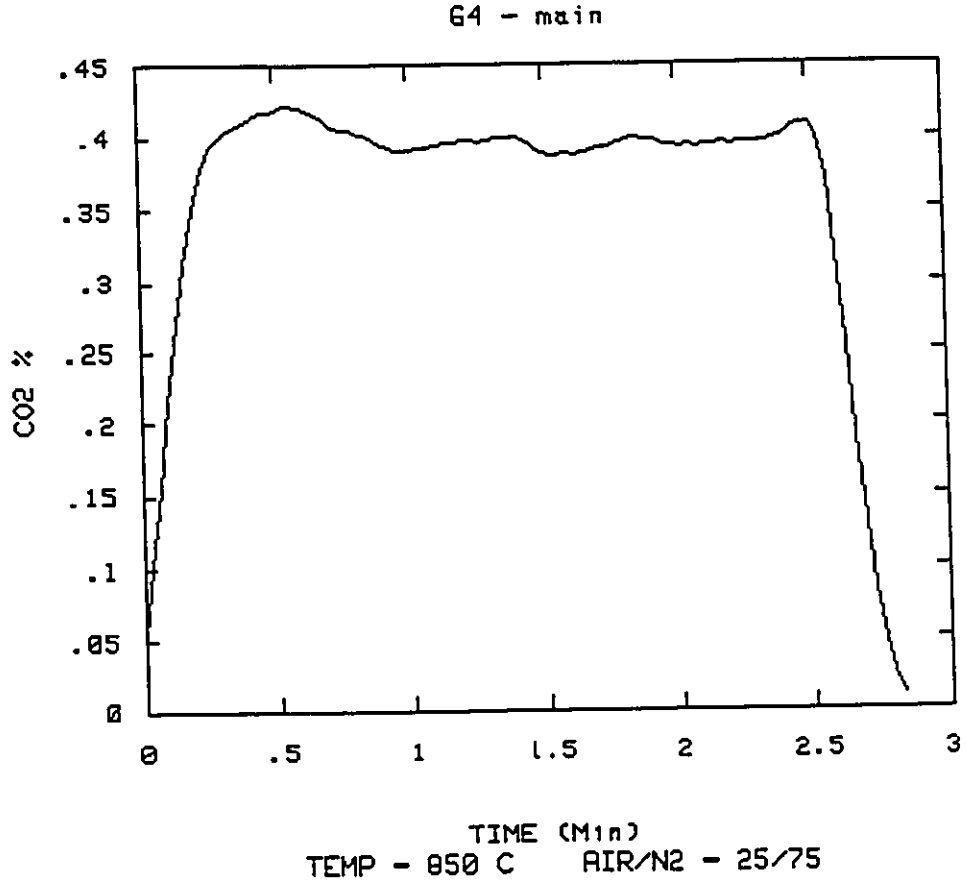

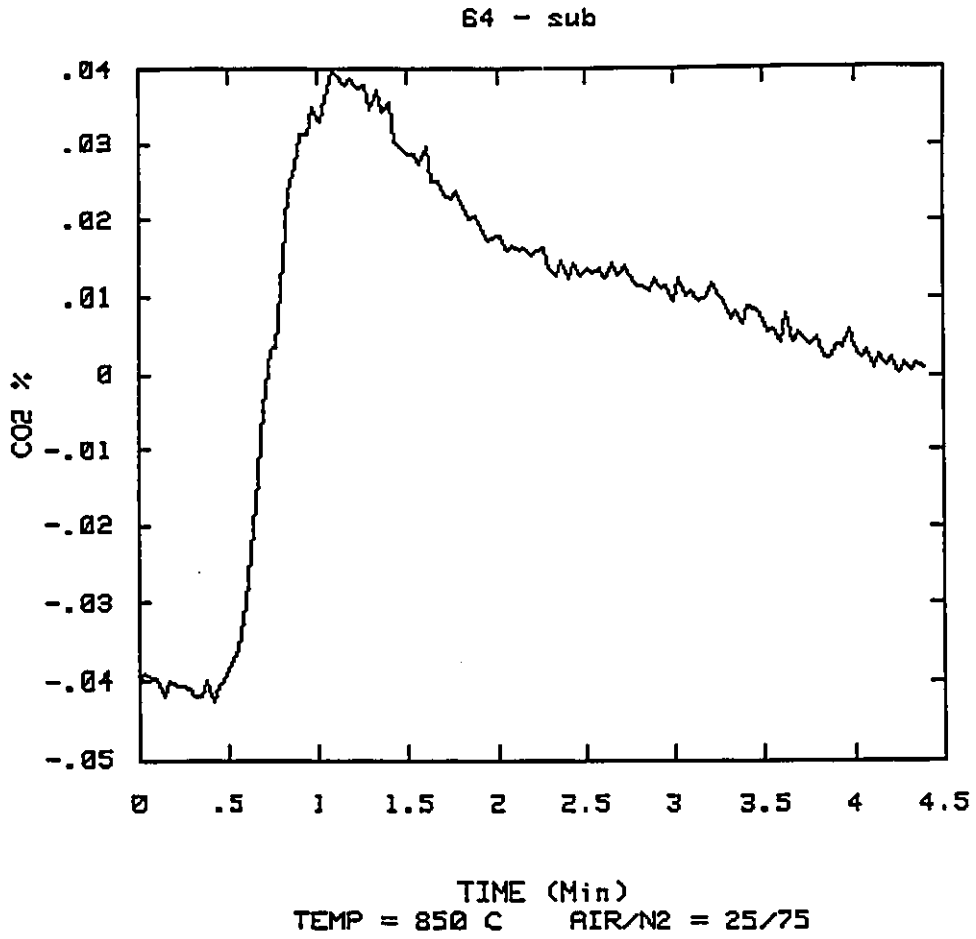
64 - sub
.04
.03
.02
.01
0
-.01
-.02
-.03
-.04
-.05
CO2 %
0
.5
1
1.5
2
2.5
3
3.5
4
4.5
TIME (Min)
TEMP = 850 C
AIR/N2 = 25/75

SER2 - 65 :F2
BED TEMPERATURE = 850 C
OXYGEN CONCENTRATION = 5.3 %
MOTHER CHAR BURNING RATE Rm = 1.99 E-6 kg/s
ATTRITED FINES BURNING RATE Ra = 6.52 E-8 kg/s
RETRIEVED ATTRITED CARRBON Wa = 4.91 E-6 kg
MCRT OF BURNING FINES IN SUB-TEST Tria = 57 s
MCRT OF ATTRITED PARTICLES (MAIN TEST) Tra = 8 s
IDEAL MCRT OF ELUTRATED SIZE PARTICLE Tre* = 51.1 s
IDEAL MCRT OF THE LARGEST ATTRITED PARTICLE Trs* = 74 s
ELUTRIATED FRACTION OF ATTRITED PARTICLES Ya = .894
ATTRITION RATE Qa = 61.6 E-8 kg/s
RATIO Qa/(Qa+Rm) = 23.65 %

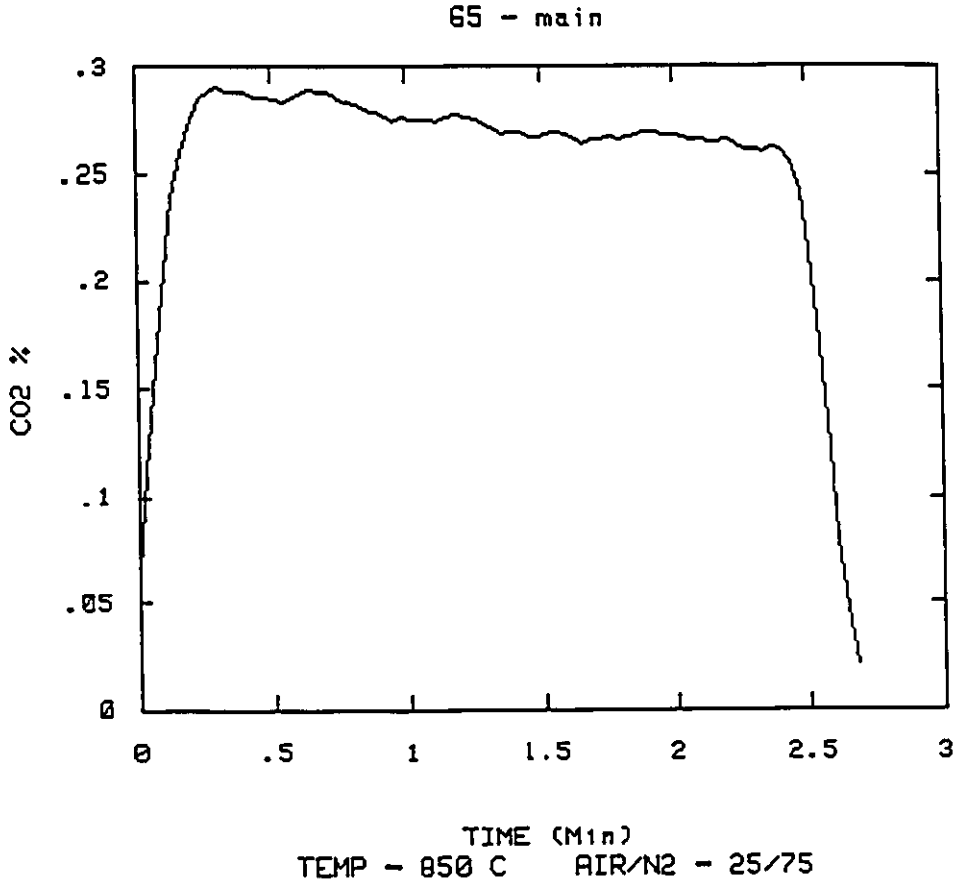

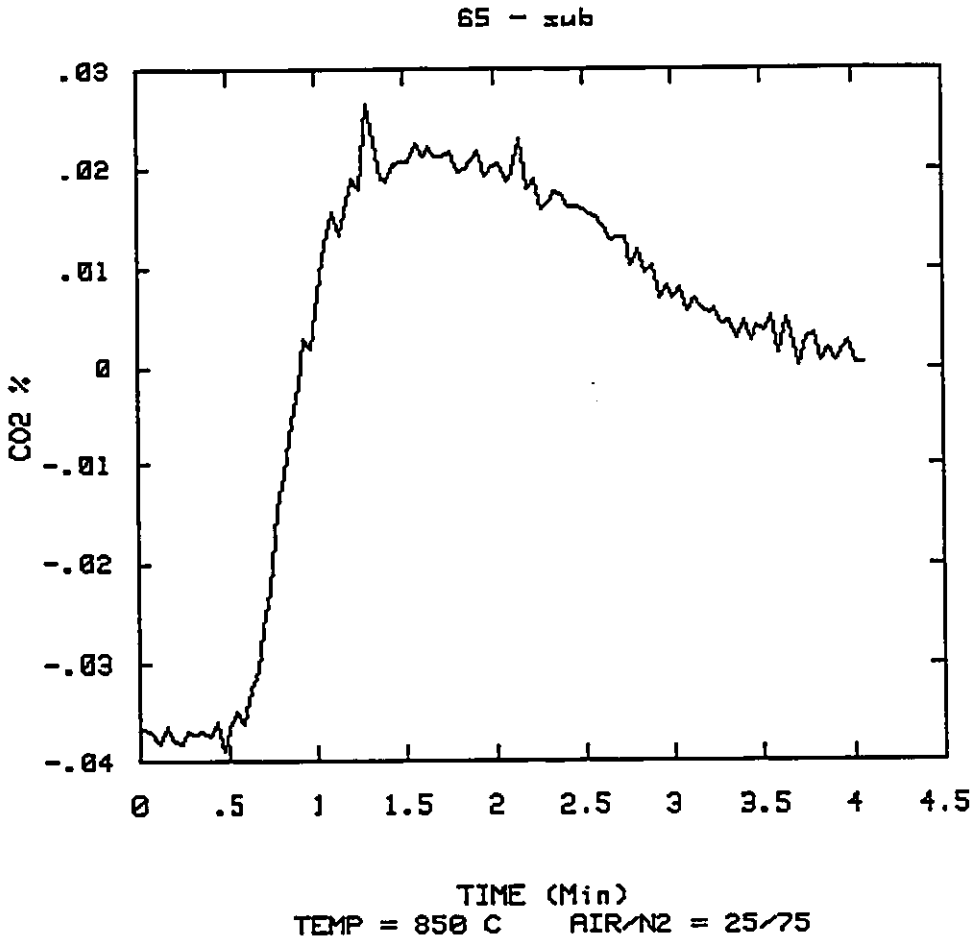
65 - sub
.03
.02
.01
0
-.01
-.02
-.03
-.04
CO2 %
0
.5
1
1.5
2
2.5
3
3.5
4
4.5
TIME (Min)
TEMP = 850 C
AIR/N2 = 25/75

SER2 - 67 :F2
BED TEMPERATURE = 850 C
OXYGEN CONCENTRATION = 15.8 %
MOTHER CHAR BURNING RATE Rm = 8.71 E-6 kg/s
ATTRITED FINES BURNING RATE Ra = 14.42 E-8 kg/s
RETRIEVED ATTRITED CARRBON Wa = 8.88 E-6 kg
MCRT OF BURNING FINES IN SUB-TEST Tria = 47 s
MCRT OF ATTRITED PARTICLES (MAIN TEST) Tra = 18.2 s
IDEAL MCRT OF ELUTRATED SIZE PARTICLE Tre* = 39 s
IDEAL MCRT OF THE LARGEST ATTRITED PARTICLE Trs* = 68.7 s
ELUTRIATED FRACTION OF ATTRITED PARTICLES Ya = .704
ATTRITION RATE Qa = 48.6 E-8 kg/s
RATIO Qa/(Qa+Rm) = 5.29 %

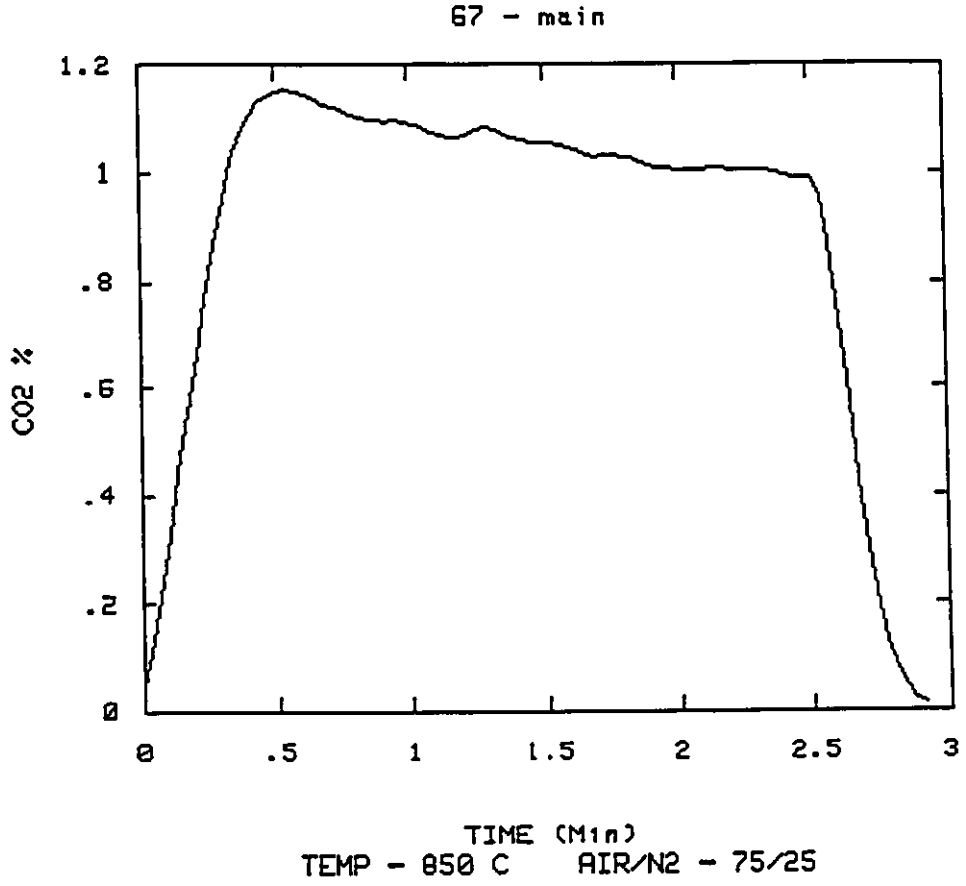

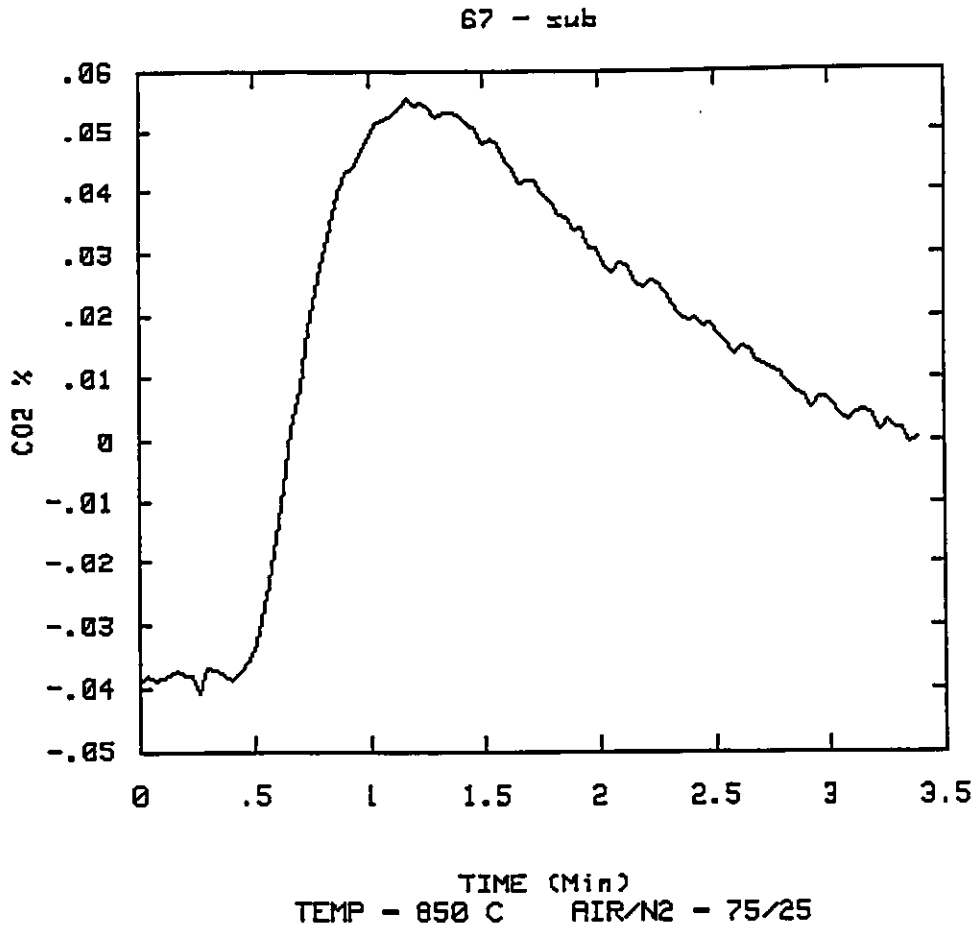
67 - sub
.06
.05
.04
.03
.02
.01
0
-.01
-.02
-.03
-.04
-.05
CO2 %
0
.5
1
1.5
2
2.5
3
3.5
TIME (Min)
TEMP - 850 C
AIR/N2 - 75/25

SER2 - 68 :F2
BED TEMPERATURE = 850 C
OXYGEN CONCENTRATION = 15.8 %
MOTHER CHAR BURNING RATE Rm = 6.57 E-6 kg/s
ATTRITED FINES BURNING RATE Ra = 12.68 E-8 kg/s
RETRIEVED ATTRITED CARRBON Wa = 7.92 E-6 kg
MCRT OF BURNING FINES IN SUB-TEST Tria = 47.6 s
MCRT OF ATTRITED PARTICLES (MAIN TEST) Tra = 23.6 s
IDEAL MCRT OF ELUTRATED SIZE PARTICLE Tre* = 38.2 s
IDEAL MCRT OF THE LARGEST ATTRITED PARTICLE Trs* = 72.3 s
ELUTRIATED FRACTION OF ATTRITED PARTICLES Ya = .622
ATTRITION RATE Qa = 33.6 E-8 kg/s
RATIO Qa/(Qa+Rm) = 4.86 %

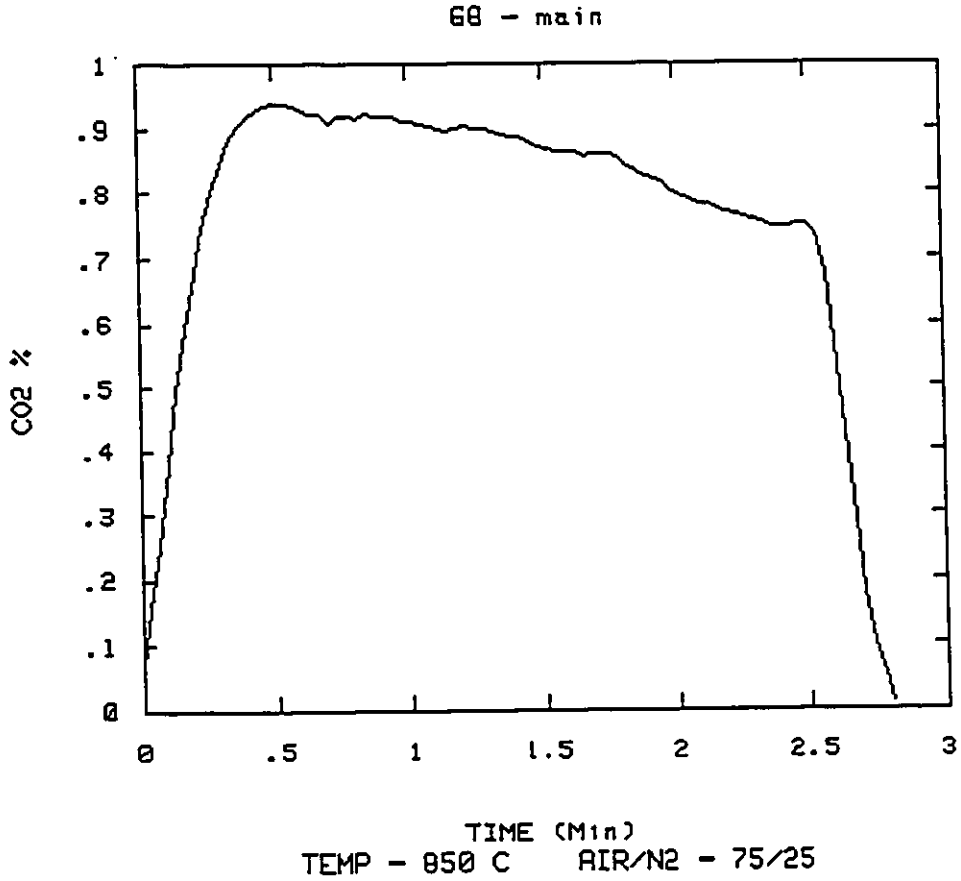

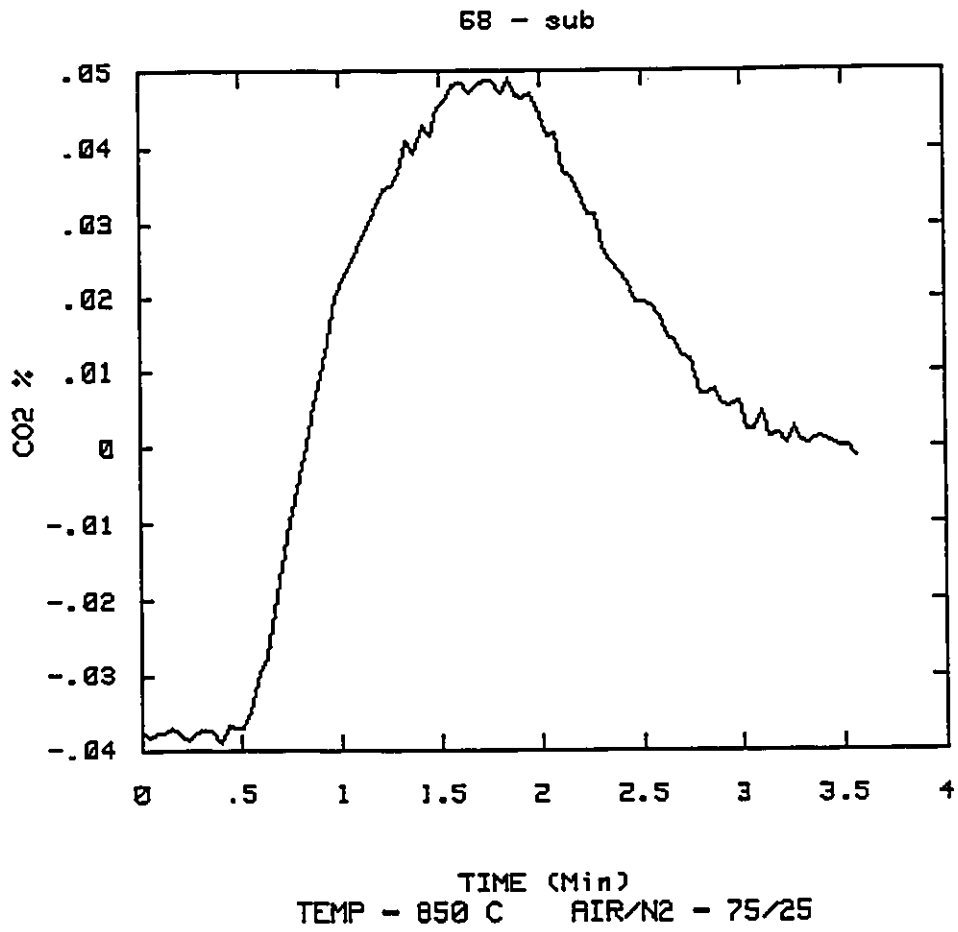
68 - sub
.05
.04
.03
.02
.01
0
-.01
-.02
-.03
-.04
CO2 %
0
.5
1
1.5
2
2.5
3
3.5
4
TIME (Min)
TEMP - 850 C
AIR/N2 - 75/25

SER2 - 69 :F2
BED TEMPERATURE = 850 C
OXYGEN CONCENTRATION = 15.8 %
MOTHER CHAR BURNING RATE Rm = 5.18 E-6 kg/s
ATTRITED FINES BURNING RATE Ra = 5.14 E-8 kg/s
RETRIEVED ATTRITED CARRBON Wa = 4.6 E-6 kg
MCRT OF BURNING FINES IN SUB-TEST Tria = 70.1 s
MCRT OF ATTRITED PARTICLES (MAIN TEST) Tra = 62.5 s
IDEAL MCRT OF ELUTRATED SIZE PARTICLE Tre* = 46 s
IDEAL MCRT OF THE LARGEST ATTRITED PARTICLE Trs* = 119.8 s
ELUTRIATED FRACTION OF ATTRITED PARTICLES Ya = .301
ATTRITION RATE Qa = 7.4 E-8 kg/s
RATIO Qa/(Qa+Rm) = 1.41 %

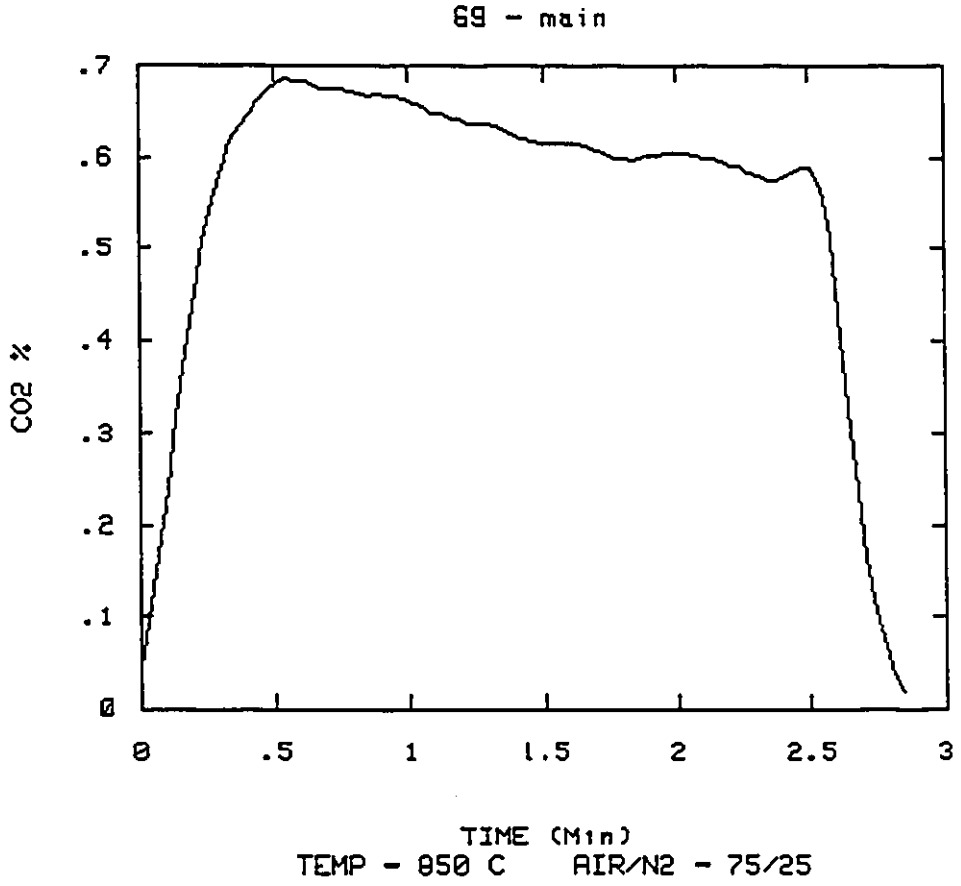

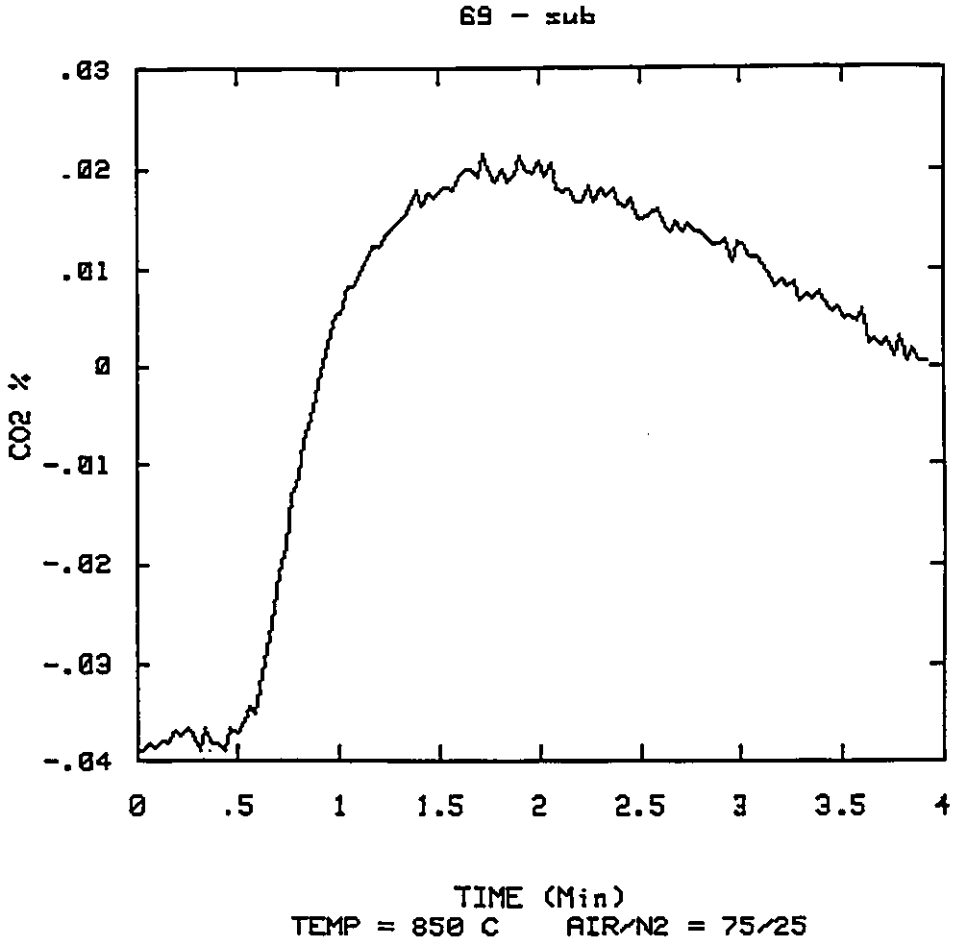
69 - sub
.03
.02
.01
0
-.01
-.02
-.03
-.04
CO2 %
0
.5
1
1.5
2
2.5
3
3.5
4
TIME (Min)
TEMP = 850 C
AIR/N2 = 75/25